4-2-2023

Analog Cosmology and Superfluidity in Atomic Gases and Electronic Materials

Anshuman Bhardwaj
Louisiana State University and Agricultural and Mechanical College

ANALOG COSMOLOGY AND SUPERFLUIDITY IN ATOMIC GASES AND ELECTRONIC MATERIALS

A Dissertation

Submitted to the Graduate Faculty of the
Louisiana State University and
Agricultural and Mechanical College
in partial fulfillment of the
requirements for the degree of
Doctor of Philosophy

in

The Department of Physics and Astronomy

by
Anshuman Bhardwaj
Integrated M.Sc., Indian Institute of Technology, Roorkee, 2014
M.Sc., University of Nottingham, 2015
M.Res., University of Nottingham, 2017
May 2023

To my parents

Sarita and Rakesh Kumar

ACKNOWLEDGMENTS

This thesis would not have been possible without the help of my advisor, Prof. Daniel Sheehy. I have benefited a lot from his open mindedness and support to work on different areas of physics. There have been times where I could not understand how to make progress. I would like to thank him for being patient with me and for his knowledge and experience, using which he could almost immediately clarify the problem or suggest alternatives to me. Before coming to LSU, I was specializing in gravity and therefore I had little idea of the research in condensed matter and ultracold atoms. His spending countless hours explaining me concepts on the whiteboard and on his iPad during the pandemic, his courses on solid state and statistical mechanics all helped bridge this gap for me. One important thing he taught me is that when you start solving a problem, there can be multiple routes to reaching the answer, and therefore one must explore as many of these as possible because this approach improves your understanding of that topic and eventually contributes to your experience. It is said that PhD is like a nursery where you get to play and re-learn things. I am very fortunate that I got to spend this academic childhood under Prof. Sheehy's guidance.

I would like to thank my thesis committee comprising Prof. Ilya Vekhter, Prof. Justin Wilson, Prof. Ravi Rau and Prof. Scott Baldridge for their feedback and help throughout my candidacy. I want to thank Prof. Ilya Vekhter for teaching me how to critically read papers and how to simplify your research problem to simple cases, before attacking the general case. Prof. Justin Wilson has been very supportive in terms of academic and career advice. Through him I got to meet with some of my heroes such as William Unruh, Stephen Fulling and Robert Wald, and recently got a chance to work with

Prof. Ian Spielman who is a leading cold atom experimentalist. I will always remember my discussion with him en route to Texas A&M University, where we talked about physics and careers in academia. I would like to thank Prof. Ravi Rau for his quantum mechanics classes which a pleasure to attend. In his weekly informal seminars one could discuss almost anything with him. These meetings have had a very positive impact on me as I learned how to find colors and joy in what other people are doing, whether it be research, playing games, reading novels etc. I would like to thank Prof. Scott Baldridge for asking me the question, "Suppose you enter an elevator with a famous entrepreneur. How would you explain your research topic such that by the time elevator doors open he is willing to fund you?" This one question has helped me understand how to develop and present my research to make it understandable to a wider audience.

I would like to thank my collaborators Prof. Ivan Agullo, Prof. Justin Wilson, Prof. Edmund Copeland, Prof. Jorma Louko, Prof. Ian Spielman, Andrew Allocca, Dimitrios Kranas and Dzmitry Vaido. I also want to extend my thanks to the many wonderful teachers and postdocs I've had the pleasure of learning from at LSU, Alvaro Jimenez-Galan, Prof. Francois Mauger, Prof. Mette Gaarde, Prof. Kenneth Schafer, Prof. Lai-Him Chan, Prof. Jorge Pullin, Prof. Gabriela Gonzalez, Prof. Robert Hynes, Prof. Kristina Launey, Prof. William MacElgin, Prof. Juana Moreno, Prof. Parampreet Singh, Jing-Han Chen, Lun Yue, Mahmoud Asmar, and Andrew Allocca. I am especially thankful to Prof. Ivan Agullo and Prof. Dana Browne. I attended Prof. Agullo's classes on quantum field theory and differential geometry which have deeply impacted my way of thinking. I have learned that on the surface one may see different topics of physics, but at a deeper level they are all connected, and this approach is very satisfying to me. Every time Prof. Ivan

Agullo stands from his chair and moves towards the board, I could feel that I am going to learn something amazing today. I am grateful to Prof. Dana Browne for showing me lot of support in tough situations. He is like a giant library of knowledge and I have had the pleasure of discussing with him topics in statistical mechanics, non-equilibrium physics, turbulence and chaos. I used to fear the word 'correlations', but when he told me that correlation is just conditional probability, that paved the foundation for me in understanding many topics in field theory and condensed matter.

I am also indebted to my teachers at the University of Nottingham, especially Prof. Jorma Louko who taught me black holes, and Prof. Copeland who taught me cosmology and inflation. They have always supported me through tough times and have played a huge role in my career. I would also like to thank my school teachers Mr. Satish Ahlawat, Mrs. Sneh Saini and Mrs. Gomti. They serve as an inspiration to me on how to teach and make classroom learning enjoyable.

I would like to thank Prof. Jonathan Dowling, may he rest in peace. He was an amazing person who shaped many lives, but unfortunately I never got a chance work with him. However he was so influential that even though he had left us, a conference was organized in his honor, where I got to me Prof. Marlan Scully which changed my life. I would also like to thank Prof. Marlan Scully who saw my presentation that day and then decided to invite me to the Casper Summer School in Wyoming, and to the Fulling Fest at Texas A&M University, both of which were fully funded by him. I am also grateful that I got to meet Prof. Abhay Ashtekar, Prof. Rodolfo Gambini and Prof. Suhail Zubairy with whom I had very useful scientific discussions.

Many thanks to Paige Whittington, Arnell Nelson, Carol Duran, Stephanie Jones,

Laurie Rea, Kathryn Perry and other members of the administrative staff Department of Physics and Astronomy at LSU for their help during my Ph.D.

A friend in need is a friend indeed. There are some people I met at LSU that have helped me get through very rough times. I would like to express my gratitude to Himanshu Singh Mehra, Zac Gryb, Shengjie Guo, Dineep Thomas and Peng Loh. Peng and June are like my local guardians. They have made my journey at LSU full of happiness. Playing badminton, going out for shopping and spending time with their kids (Faith, Gabriel and Michael) has made me feel I have a family in US also.

I would like to thank all of my badminton buddies such as Guannan Wang, Jesil James Dsilva, Baoyue Zhou, Qing Chen, Ashwani Rai, Surabhi Jain, Gede Raditya, Ling Zhu, Anuja Pande, Prof. Harris Wang, Prof. Rui Lu, Yuxin Fang, Sai Shankar Ganesh, Huy Ngyuyenhuu, Nha Tran, Chao Dong, Stav Haldar, Anshumitra Baul, Akhil Bhardwaj, Siavash Sarrafan, Iswarya Sitiraju, Shaofu Du, Quynh Anh Nguyen and Katie Anh Nguyen. I would also like thank all my friends in my department such as Anthony Brady, Dimitrios Kranas, Karunya Shirali, Eklavya Thareja, Kunal Sharma, Sumeet Khatri, Mahmoud M. Asmar, Corey Austin, Siddharth Soni, Eneet Kaur, Vishal Katariya, Himanshu Singh Mehra, Vishakha Vishwakarma, Chenglong You, Sanjay Kumar, Muneera Mashkoor, Arshag Danageozian, Prateek Barge, Laalitya Uppalapati, David Alspaugh and Sudarshan Balakrishnan. This journey would be incomplete without them. I would like to thank my friends that I made in Nottingham with whom I correspond from time to time: Olawale Ogunrinde, Atirach Ritboon and Haozhang Gan. These people have shown me immense support both when I was in Nottingham and at LSU. I would like to thank my friends from school who never forget to wish me a happy birthday: Sahil Sahoo, Sahil

Singla, Ranjeet Singh Chaudhary, Akshay Suresh and Dipan Chatterjee.

Finally, I would like to quote a saying from my country that what our parents do for us is a debt that can never be paid back. After all how can one quantify their care, love, worry and unconditional support for us. However, since I am made from the same material as them, therefore the completion of this thesis is in a sense, their achievement. So instead of paying back or saying thanks, I would like to congratulate them, for they are the ones who are actually receiving this Ph.D. degree!

CONTENTS

ABSTRACT

I present a study of analog cosmological models in Bose-Einstein condensates (BEC) and in graphene, and superfluidity in a box-shaped traps. I start by examining the dynamics of a Bose-Einstein condensate (BEC) trapped inside an expanding toroid that can realize an analog inflationary universe. The expanding condensate forces phonons to undergo redshift and damping due to quantum pressure, owing to the thinness of the ring. I predict that such expanding BECs can exhibit spontaneous phonon creation from the vacuum state and show how it would manifest in the atom density and density correlations and discuss connections with the inflationary theory. I then extend this work to study entanglement of the spontaneously generated phonon pairs, for which I use the techniques of quantum continuous variables. I then develop a protocol to experimentally measure the correlations entering the covariance matrix, allowing an experimental quantification of the entanglement properties of the inflationary BEC. I then present a of how a spatially-varying quasiparticle velocity in honeycomb lattices, achievable using strained graphene or in engineered cold-atom optical lattices that have a spatial dependent tunneling amplitude, can yield the Rindler Hamiltonian embodying an observer accelerating in Minkowski spacetime. Within this setup, a sudden switch-on of the spatially-varying strain yields a spontaneous production of electron-hole pairs, an analog version of the Unruh effect characterized by the Unruh temperature. I discuss how this thermal behavior, along with Takagi's statistics inversion, can manifest themselves in photo-emission and scanning tunneling microscopy experiments. I show that the electronic conductivity grows linearly with frequency ω, vanishing in the DC limit. Finally, I find that the total electronic energy at zero environment temperature looks like Planck's blackbody result

for photons due to the aforementioned statistics inversion, whereas for an initial thermally excited state of fermions, the total internal energy undergoes stimulated particle reduction. Finally, I study ultracold Fermi gases trapped inside a three-dimensional box with vanishing boundary conditions, with interactions modeled using the Fermi-Huang pseudopotential. Taylor expanding the pairing to linear order in position, solves the gap equation yielding the transition temperature and local pairing amplitude that vanishes at the edges.

CHAPTER 1. INTRODUCTION

In this thesis, I will be exploring the area of analog gravity and superfluid properties in laser traps with toroidal and box geometries. Analog gravity is an arena, where gravitational phenomena can be mimicked, in particular the theory of how quantum fields behave in curved spacetimes, using condensed matter systems such as graphene, cold atom setups like a Bose-Einstein condensate (BEC) and fiber optical systems. In Chapter 2, our focus will be on mimicking the primordial inflationary universe inside a BEC, i.e., I establish an analogy between how a scalar field evolves in an exponentially expanding universe, with how phonon modes evolve in a rapidly expanding toroidal BEC. I will then look at how this BEC expansion leads to a spontaneous creation of entangled phonon pairs. In Chapter 3, I use the theory of continuous quantum variables to model the states of these phonons and thereby quantify their entanglement.

In Chapter 4, I will show that graphene with a certain spatial strain pattern can lead to spontaneous creation of electron and hole pairs with an emergent thermal distribution. This is the celebrated Unruh effect which predicts that an accelerating observer will see the Minkwoski vacuum as a thermal bath of particles. However, unlike their relativistic counterparts, the quasi-particle creation in the analog systems here (graphene and toroidal BEC) can manifest themselves in correlations and susceptibilities. Thus, by importing techniques from quantum field theory in curved spacetimes helps explore new and interesting physics in condensed matter and cold atom systems. In Chapter 5, I will use the Bogoliubov-de Gennes approach with the interactions being modeled by a pseudopotential to explore superfluid properties inside a box-shaped trap with hard-wall boundary

conditions, such as the transition temperature and the local pairing amplitude. I will end this thesis with some brief concluding remarks in Chapter 6. In the following subsections, I provide introductions to the material for each chapter.

1.1. Toroidal BEC

The theory of inflation is the most promising description of the early universe [1, 2, 3, 4, 5, 6, 7], although alternatives exist [8]. This theory is based on a field ϕ, the inflaton, propagating in a classical spacetime and moving under the influence of its own potential $V(\phi)$. The quantum fluctuations in the inflaton field couple with the spatial curvature of the universe, thus acting as seeds for the observed cosmic microwave background (CMB) anisotropies [9] and the large scale structure of our universe [10], although primordial gravitational waves are yet to be observed. The exact shape of the potential $V(\phi)$ is currently not known, although work has been done to reconstruct it [11]. Indeed, experiments have put stringent constraints on some of the candidates such as the quadratic and quartic inflationary potentials, though there remains a huge class of models that are able to explain observations [12]. In addition, the CMB observations have revealed possible anomalies on the largest scales with a 3σ significance, that hint towards new physics [13]. However, testing inflationary models using cosmological experiments is expensive and difficult.

A natural question, is if there exists an alternative setting to test the predictions of inflation. The answer is 'analog gravity' [14], where the aim is to come up with simple experimental setups that can be performed in a lab and which mimic the equations governing gravitational and cosmological phenomena such as inflation and black hole physics.

Early work in this direction came from Unruh who, in 1981, showed [15] that the Navier-Stokes' equations for fluid flow, such as in a draining bathtub, could mimic Hawking radiation [16, 17] coming from a black hole horizon. This showed that analog black holes can be constructed, allowing the study of near-horizon physics outside of an astrophysical setting. Several recent experiments have confirmed the existence of such analog Hawking radiation [18, 19, 20, 21], as well as other phenomena such as classical superradiance [22], the Casimir effect [23], and Sakharov oscillations [24]. Other analog gravity proposals test ideas like the Gibbons-Hawking effect [25], the vacuum decay [26, 27, 28, 29] and the Unruh effect [30].

Inflation in analog systems has been studied theoretically [31, 32, 33, 34, 35, 36, 37], and realized experimentally in Bose-Einstein condensates (BECs) [38] and in ion traps [74]. Here, our primary motivation is the BEC implementation of analog inflation realized by Eckel et al. [38]. The Eckel et al. experiments featured a BEC in a time-dependent trap with the shape of a thin toroid, with a rapid expansion of the toroid mimicking the inflationary era. Some of the analogs of cosmological phenomena observed by Eckel et al were the red-shifting of frequencies and damping of modes due to expansion. Vortex creation after halting of the ring expansion was also observed, an analog of reheating in the early universe.

1.2. Toroidal Entanglement

In 1966, L. Parker made a fascinating discovery [58, 59]: the expansion of the universe can create particles out of the vacuum (see [57] for a brilliant, earlier intuition about this phenomenon by E. Schrodinger). More precisely, Parker considered Friedman-

Lemaitre-Robertson-Walker (FLRW) spacetimes that are asymptotically Minkowskian in the future and past, and showed that (non-conformal invariant) quantum fields that at early times are prepared in the vacuum state, generically end up in an excited state. The underlying translational invariance of the gravitation field leads to momentum conservation for the quantum field, which in turns implies that particles are created in pairs, with wavenumber $\vec{k}$ and $-\vec{k}$.

Phrased in a modern language, Parker showed that, for each pair $(\vec{k}, -\vec{k})$, the initial vacuum evolves to a *two-mode squeezed vacuum*, with squeezing intensity and squeezing angle determined by the expansion history of the universe. This means, in particular, that the two particles in each created pair are *entangled*. This entanglement is of primary importance, since it constitute the quantum signature of the phenomenon of particle creation.

Parker's ideas were formulated in the theory of linearized quantum field propagating on a fixed gravitational background—the quantized fields are *test fields*, which do not disrupt or modify in any way the underling geometry— and the use of Bogoliubov transformations. This same formalism was later applied to black holes by S. Hawking in the mid seventies, leading to the celebrated Hawking effect [16, 17], and also to the paradigm of cosmic inflation in the early eighties [1, 2, 3, 4, 5, 6, 7]. These two phenomena probably constitute the most important predictions of quantum field theory in curved spacetimes. In particular, the later provides a possible explanation for the origin of the density perturbations in the early universe, which seeded the matter distribution I observed today. This is an outstanding statement, as it would imply that the structures in our universe have emerged from a process of squeezing of the quantum vacuum. Several investigations

have focused on envisaging ways of testing this extraordinary possibility. More concretely, important efforts have been dedicated to quantify the genuine quantum signature of the squeezing process predicted by inflation, namely the generation of quantum entanglement, and to discuss ways of observing it [60, 61, 62, 63, 64, 65, 66, 67, 69, 71].

On the other hand, in a seminal paper W. Unruh proved that the physics of quantum fields propagating on non-trivial geometries can be simulated in the lab, giving birth to the field of analog gravity [15]. Analog models offer an interesting test bank to recreate Parker's phenomenon of particle creation in the lab in a controlled manner, and to confirm its key predictions. In this chapter, I focus attention on one of the simplest analog systems leading to quasiparticle creation a la Parker—a toroidal Bose-Einstein condensate (BEC) whose radius is rapidly growing. This system has been recently recreated [38, 73], and used to simulate an effectively one-dimensional inflationary universe [36, 76, 77]. Experimental efforts have been able to observe the cosmological redshift that the expansion induces on density perturbations in the fluid, as well as damping. This is a promising platform to directly observe particle pair creation. Recent theoretical studies [76] have analyzed the spectrum of particles created in this system under a finite period of exponential expansion, and have computed the signatures that these particles produce on density-density correlation functions.

The focus of this chapter is on entanglement. As mentioned above, entanglement is the quantum hallmark of the process of two-mode squeezing behind pair-creation, and observing it would assist on identifying the physical origin of the observed correlations and in distinguishing them from other physical processes. Our goal is to contribute, from the theoretical side, to the observability of this key aspect of the pair-creation process. I first

quantify the entanglement generated in this process by using an entanglement measure well adapted to the physical setup. Next, this quantification allows us to analyze the way entanglement is affected by the presence of thermal noise and losses, ubiquitous in real experiments. Using the tools put forward in [81], I show that noise and losses *degrade* the entanglement in the final state, possibly eliminating it entirely, rendering the final state classical. This is important for experimental setups. I determine under what conditions the quantum signatures of the pair-creation process are washed away. Next, following the ideas in [87], I propose a way of amplifying the entanglement generated in this scenario, possibly compensating for the aforementioned deleterious effects. This is done by considering *stimulated* particle-creation using appropriate initial states—stimulated in the standard sense of atomic physics; to be contrasted with the spontaneous effects arising when the input is merely vacuum fluctuations. In particular, I study the use of single-mode squeezed inputs as a way of stimulating additional creation of entangled pairs, increasing the observability of this effect. Finally, I envisage an experimental protocol to reconstruct the final state and to measure the entanglement it contains between pairs $(\vec{k}, -\vec{k})$ of modes.

1.3. Unruh Effect in Graphene

As I discussed in the previous two subsections, quantum field theory in curved spacetime [45, 47, 48, 99, 46, 100] is an exciting arena in which two cornerstones of modern physics, quantum field theory and general relativity, merge to produce surprising results. One classic prediction at this crossroads is that a quantum field in an initial vacuum state, under the influence of spacetime curvature (or gravity), leads to a spontaneous gen-

eration of particles associated with that field. This was first realized by Schrodinger [57] in the context of relativistic quantum mechanics in an expanding universe and later by Parker [58, 59] who independently showed this in the context of general quantum fields in cosmological spacetimes. One such class of spacetimes is the one experienced by an accelerating observer: the Rindler spacetime [101]. However, this spacetime is special because it creates particles with a thermal spectrum [102, 103, 104], i.e., an accelerating (or Rindler) observer sees the Minkowski (or flat) spacetime vacuum as a thermal bath of particles. This phenomenon is called the Fulling-Davies-Unruh effect (also known as the Unruh effect). Here, the thermality emerges due to two reasons. The first is the appearance of a horizon that splits the entire spacetime into two mutually inaccessible regions (corresponding to observers accelerating in opposite directions) and thus vacuum expectation values in one region lead to tracing over the degrees of freedom of the other region, thus yielding a mixed state. The second reason is that the response function of an accelerating particle detector follows the principle of detailed balance, or in other words satisfies the Kubo-Martin-Schwinger (KMS) condition [105, 106], which is a sufficient condition for a spectrum to be called thermal.

Similar horizons and therefore their associated thermal behavior also emerge in other spacetimes, such as black holes [16, 17] where this behavior is known as Hawking radiation, and the Gibbons-Hawking effect in de-Sitter cosmologies [107]. A surprising result that appears here is that the power spectrum, which depends on the density of states and the statistics, is sensitive to the dimensions of spacetime. In odd spacetime dimensions, the power spectrum of fermions has a Bose-Einstein distribution, whereas bosons follow a Fermi-Dirac distribution. This is the well-known 'apparent inversion of statistics'

due to Takagi [108] which is linked to the violation of Huygens' principle in odd spacetime dimensions [109, 110, 111, 112, 113, 114, 115].

There have been various proposals to detect the Unruh effect in accelerating systems [116, 117, 118], for example using Bose-Einstein condensates [120, 119]. However, observing this effect is challenging as an acceleration of about $10^{21}\mathrm{m/s}^2$ is required to generate a temperature of 1K [46] which is likely beyond the reach of current technology. In such a situation, analog gravity [14] offers an alternative arena for observing relativistic phenomena, in which condensed matter or cold atom systems are engineered to mimic the behavior of relativistic systems. This area emerged in 1981 when Unruh showed [15] how water ripples in a draining bathtub can mimic the Klein-Gordon equation for a scalar field near a black hole horizon. This led to the prediction of analog Hawking radiation which was realized in a series of experiments [18, 19, 20, 21]. On the other hand, particle creation in the context of the inflationary early universe was recently observed in toroidal Bose-Einstein condensates [38, 73] and studied theoretically in Refs. [36, 76, 77].

Such analog platforms can be used to mimic the Unruh effect, as was recently observed in Bose-Einstein condensates [121] by modulating the scattering length that determines the interactions between ultracold bosonic atoms. Various proposals have also been made to detect the analog Unruh effect in ultracold Fermi gases in square lattices [123, 30, 122], in graphene [124, 126, 125], in quantum hall systems [127, 128], and in Weyl semi-metals [129].

Here our main interest is in exploring analog Rindler physics, and the analog Unruh effect, in graphene and related cold-atom systems (i.e., fermionic atoms in honeycomb lattices. Indeed, the status of graphene as an analog relativistic system has been

long recognized [130, 131], and the fact that graphene's low-energy excitations obey the Dirac equation was established even from the earliest experimental work on these systems [132, 133]. As is well known, the effective "speed of light" characterizing the Dirac quasiparticles in graphene takes a value $v \simeq c/300$ (with c the actual speed of light). To achieve the Rindler Hamiltonian in graphene requires engineering a spatial variation in v along one direction.

In this chapter, our aim is to discuss how the Unruh effect would be manifested in honeycomb systems such as mechanically strained graphene or in an appropriately engineered cold atom optical lattice system [137, 135, 136, 134, 138]. In either case, what is needed is a spatial variation in the local tunneling matrix elements between sites. The basic idea is to start with unstrained graphene, in equilibrium at low temperature T (that I will usually assume to be $T = 0$). As mentioned above, fermionic excitations in unstrained graphene obey the conventional Dirac equation, i.e., the Dirac equation in Minkowski (flat) spacetime. The next step is to suddenly switch on the strain field, changing the system Hamiltonian to the Rindler Hamiltonian, with excitations described by a Rindler Dirac equation. The Unruh effect emerges because a vacuum initial (Minkowski) state becomes, after the strain, an effective thermal distribution of Rindler quasiparticles characterized by the strain-dependent Unruh temperature. Note that this non-adiabatic process is essential to produce the Unruh effect.

Earlier theoretical work by Rodriquez-Laguna and collaborators showed [30], in the context of square optical lattices, that such a sudden quench should indeed yield the Unruh effect, provided that the timescale of the switching process is much faster than the timescale at which the electron dynamics operates (governed by the inverse tunnelling

rate). Here I assume the switching on is sufficiently rapid so that, invoking the sudden approximation of quantum mechanics, the correct procedure is to obtain observables by calculating the expectation values of operators in the strained system with respect to states of the unstrained lattice (i.e., the Minkowski vacuum or, at finite real temperature, a Fermi gas of Dirac quasiparticles and holes).

1.4. Superfluid in a Box-Shaped Trap

The area of ultra-cold atoms was developed in the 1990's with the observation of the first Bose-Einstein condensate (BEC) in simultaneous experiments at JILA and MIT [175, 176]. Most of the studies in the first years were devoted to quantum gases of bosonic nature and were aimed at investigating the important consequences of Bose-Einstein condensation, which, before 1995, remained an elusive and inaccessible phenomenon. Since then there has been a flood of work, both experimental and theoretical. Major achievements of these studies have been, among others, the investigation of superfluid features, including the hydrodynamic nature of the collective oscillations, Josephson like effects, realization of quantized vortices, transition to the Mott-insulator phase and the realization of Berezinskii-Kosterlitz-Thouless (BKT) phase transition in two dimensional configurations. For more details please refer to the reviews [177, 178, 179].

These experiments rely on some alkali atoms being fermionic (because they have an odd number of neutrons) and some bosonic (with an even number of neutrons). Thus it has been possible to create atomic Fermi and Bose gases. With the use of evaporative cooling, temperatures have now reached as low as $50n$K [180]. Achieving this range of temperatures allows one to experimentally explore superfluid properties of these cold

atomic gases. In addition to this, recent experiments have used standing waves of light to realize optical lattice traps for cold atoms [181, 178, 182, 183] that helps study solid state properties like high-temperature superconductivity. Besides studying these solid state properties one can also test the Bardeen-Cooper-Schrieffer (BCS) theory [202, 203] for order of million atoms or less, unlike the case of solids where we are forced to work with moles of atoms. Experiments have also pursued exotic forms of superfluidity like the elusive Fulde-Ferrell-Larkin-Ovchinikov (FFLO) phase which was predicted in 1960's [187, 188]. Thus ultra cold atomic gases provide a platform where one can in analogy study other systems. The advantage here is that there is a lot of flexibility in tuning the parameters like particle number, scattering cross-sections, chemical potential and other properties.

However, most of experiments have been performed in harmonic oscillator traps [177], while most theoretical work assumed harmonic or periodic boundary conditions (bulk case). However in recent times, experimentalists have started studying properties of cold atomic gases in 'box'-like traps that have vanishing boundary conditions. The first such experiment in a box trap was done with bosons [184], where a BEC was observed. Then in 2016 a three dimensional cylindrical box-shaped trap was successfully constructed by Zwierlein's group at MIT [185] and next year a group in Germany was able to create the two dimensional version of this [186]. In the 3D box experiment, a cylindrical shaped trap was created by using lasers. Firstly, two parallel sheets of laser beams were used to create the cylinder caps. Secondly, a set of laser beams was arranged in a circle and perpendicular to the caps. This helped create the curved part of the cylinder, as shown in Fig. 1. This was done in such a way that the radius of cylinder was 60μm and length was

120μm. One obvious question that arises is how exact was the box potential like a box. The answer is that the trap was modeled by a power law $V(r) \sim r^{16}$ which is an extremely steep potential, so it more or less mimics an infinite square well.

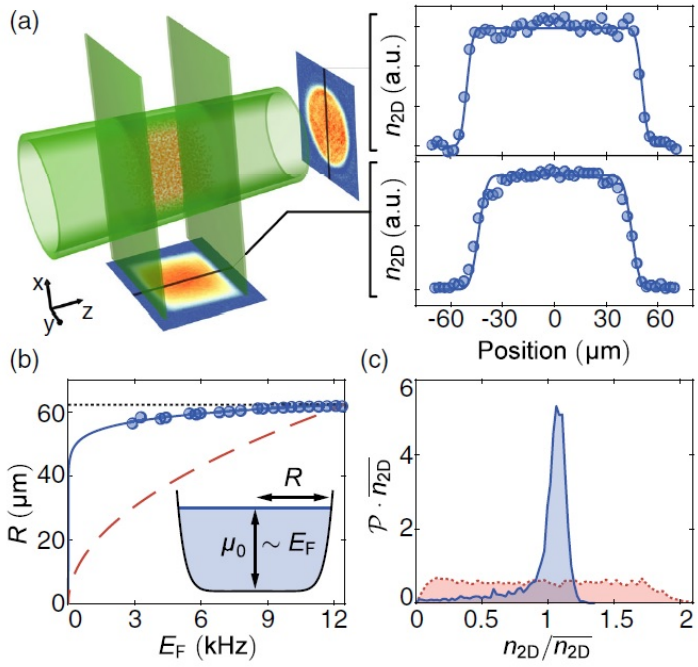

Figure 1.1. Homogeneous Fermi gas in a box shaped trap. (a) Schematic picture of the box trap with planes that cut through the gas to give integrated densities (with respect to position) in the axial and radial directions. (b) Radius of the cloud as a function of the Fermi energy where the dotted black and dashed red lines correspond to a perfect box potential and a harmonic potential respectively. The blue solid fits with a power law potential $V(r) \sim r^{16}$. (c) Measured radial probability density $\mathcal{P}(n_{2D})$ for the integrated density n_{2D}. This figure has been taken from [185].

In this experiment, about 2×10^6 ^{6}Li-atoms were prepared in the two lowest hyperfine states near a Feshbach resonance. These hyperfine levels act as pseudo-spins and there are equal number of atoms in both spin up and down states, i.e., this is spin balanced gas. Then these atoms were put inside the box trap and evaporative cooling was used to create temperatures of order ten nano-kelvins. Thus a density of $n \approx 10^{12}\text{cm}^{-3}$ and Fermi energy of $E_F \approx 13$kHz was achieved. The lifetime of the gas was several tens of

seconds and thus the imaging was done in a very short duration. In the $\hat{z}$-direction there was a weak harmonic potential with a trapping frequency of $\omega_z = 2\pi \cdot 23.9$ Hz. One may ask, how do I know that the confined gas was homogeneous. The answer is to look at the probability distribution $\mathcal{P}(n)$ for the atomic density n. Imaging done along the $\hat{z}$- and $\hat{x}$-directions yielded the radial and axial probability distribution $\mathcal{P}(n_{2D})$ for the integrated density n_{2D} (Fig. 1(c)). The distribution for the homogeneous gas was found to be sharply peaked near the trap average density $\overline{n}_{2D}$, in which $P(n_{2D})$ for an optical gaussian trap is also shown for comparison (spread over a large range of densities).

This box trap set is a promising platform for the observation of the quasiparticle jump in the momentum distribution of a Fermi liquid [190], critical fluctuations in the BEC-BCS crossover and long lived solitons [191]. It is could also be used to test BCS theory and possibly detect other exotic forms of superfluidity like the FFLO state which occurs due to unequal populations of atoms having spins up and down, for example 60 percent atoms in $\uparrow$-state and 40 percent atoms in $\downarrow$-state. Due to their unequal populations their Fermi surfaces will also be of different sizes. Thus, when two fermions will try to pair up they will have momenta opposite in direction and unequal in magnitudes. The difference between the magnitudes of the two momenta gives the Cooper pairs a net momenta called the FFLO pairing wavevector $\boldsymbol{q} = \boldsymbol{k}_{F\uparrow} - \boldsymbol{k}_{F\downarrow}$. As a result, in the bulk, there should be spatial modulation of the gap parameter either of the form $\Delta(\boldsymbol{r}) \sim e^{i\boldsymbol{q}\cdot\boldsymbol{r}}$ [187] or $\Delta(\boldsymbol{r}) \sim \cos(\boldsymbol{q}\cdot\boldsymbol{r})$ [188]. However for the bulk case it has been shown theoretically that in the phase diagram, this FFLO-phase occupies a very narrow range [189] which agrees with no observation of this phase in the experiments. This may change in the box. The reason is that in the bulk any form of the FFLO density wave is translationally invariant which

means that any Goldstone mode of arbitrarily small energy can shift this wave and thus make it unstable. On the other hand, the box is not translationally invariant and thus a form like $\Delta(\boldsymbol{r}) \sim \cos(\boldsymbol{q} \cdot \boldsymbol{r})$ might stabilize for some specific values of $\boldsymbol{q}$ by taking advantage of the vanishing boundary conditions.

CHAPTER 2. INFLATIONARY DYNAMICS AND PARTICLE PRODUCTION IN A TOROIDAL BOSE-EINSTEIN CONDENSATE

In this chapter, I present analytical results to help understand the Eckel et al. experiments [38] and discuss possible observables (other than redshift of phonon wavelengths) that can probe inflationary physics in the context of an analog BEC experiment. In particular, I show that the thinness of the toroid introduces significant quantum pressure corrections in the BEC, that cause damping of sound modes and eventually lead to spontaneous phonon creation. The rest of this chapter is organized as follows: in Sec. 2.1, I investigate the evolution of perturbations (i.e., phonons) in a BEC using the Bogoliubov-de Gennes Hamiltonian. In Sec. 2.2, I show that this approach leads to the Mukhanov-Sasaki equation [40, 41, 42] that governs the evolution of such phonons in the primordial universe. This equation forces the density fluctuations to undergo damping that comes from quantum pressure. In Sec. 2.3, I show that as the ring undergoes an expansion there is a spontaneous generation of phonons which is the analog of particle creation in the early universe. In Sec. 2.4, I study the case of stimulated phonon creation by calculating the average density in a coherent state and showing that an initial traveling density wave bifurcates (due to phonon creation) into two waves, as illustrated in Fig. 2.1. In Sec. 2.5, I calculate the density-density correlation function for this system at zero and finite temperatures, showing that the angle-dependence of density correlations exhibits a signature of phonon production. In Appendix A, I provide details that are omitted from the main text.

2.1. Bogoliubov-de Gennes Hamiltonian

In this section I describe, within the Bogoliubov-de Gennes (BdG) formalism, how a boson gas in a time-dependent trap can exhibit emergent relativistic dynamics that mimic the phenomenon of inflation. I start with the following Hamiltonian that describes a Bose-Einstein condensate (BEC), given in terms of a complex scalar field ($\hat{\Phi}(\boldsymbol{r})$), evolving inside a non-uniform and time dependent toroidal potential $V(\boldsymbol{r},t)$:

$$\begin{aligned}\hat{H} &= \hat{H}_0 + \hat{H}_1, \\ \hat{H}_0 &= \int d^3r\ \hat{\Phi}^\dagger(\boldsymbol{r})\Big[-\frac{\hbar^2}{2M}\nabla^2 + V(\boldsymbol{r},t) - \mu\Big]\hat{\Phi}(\boldsymbol{r}), \\ \hat{H}_1 &= \frac{U}{2}\int d^3r\ \hat{\Phi}^\dagger(\boldsymbol{r})\hat{\Phi}^\dagger(\boldsymbol{r})\hat{\Phi}(\boldsymbol{r})\hat{\Phi}(\boldsymbol{r}),\end{aligned} \tag{2.1}$$

where μ is the chemical potential, $U = \frac{4\pi a_s\hbar^2}{M}$ is the interaction parameter, a_s is the scattering length, $\hbar$ is Planck's constant, and M is the mass of the bosonic atoms. The time-dependent single-particle potential $V(\boldsymbol{r},t)$ describes a time-dependent toroidal potential which, taking a cylindrical coordinate system $\boldsymbol{r} = (\rho,\theta,z)$, I can take to be parabolic in the $\hat{z}$ direction and a higher power law in the radial ($\hat{\rho}$) direction:

$$V(\boldsymbol{r},t) = \frac{1}{2}M\omega_z^2 z^2 + \lambda|\rho - R(t)|^n, \tag{2.2}$$

consistent with the experiments of Eckel et al. [38], who realized a "flat bottomed" trap with the exponent $n \simeq 4$. Here, $R(t)$ is the externally-controlled radius of the toroid that increases with time. The condensate field operator obeys the commutation relation

$$\big[\hat{\Phi}(\boldsymbol{r}), \hat{\Phi}^\dagger(\boldsymbol{r'})\big] = \delta^{(3)}(\boldsymbol{r} - \boldsymbol{r'}). \tag{2.3}$$

Under the BdG approximation, the condensate field operator in the Heisenberg picture $\hat{\Phi}(\boldsymbol{r},t)$ can be written as the sum of a coherent background $\Phi_0(\boldsymbol{r},t)$ and the perturbation

operator $\delta\hat{\phi}(\boldsymbol{r},t)$:

$$\hat{\Phi} = \Phi_0(1+\delta\hat{\phi}). \tag{2.4}$$

Plugging Eq. (2.4) into the Hamiltonian (2.1) and using Heisenberg's equations of motion, I get

$$i\hbar\partial_t\delta\hat{\phi} = -\frac{\hbar^2}{2M}\nabla^2\delta\hat{\phi} - \frac{\hbar^2}{M}\frac{\boldsymbol{\nabla}\Phi_0}{\Phi_0}\cdot\boldsymbol{\nabla}\delta\hat{\phi} + Un_0\left[\delta\hat{\phi}^\dagger + \delta\hat{\phi}\right], \tag{2.5}$$

for the $\delta\hat{\phi}(\boldsymbol{r},t)$ equation of motion [36]. Here, I defined the background density as $n_0(\boldsymbol{r},t) \equiv |\Phi_0(\boldsymbol{r},t)|^2$.

Equation (2.5) describes dynamics of the perturbation operator $\delta\hat{\phi}$ in the presence of a time-dependent background $\Phi_0(\boldsymbol{r},t)$. Below, I find it convenient to transform to the Madelung representation in terms of density $\hat{n}(\boldsymbol{r},t)$ and phase $\hat{\phi}(\boldsymbol{r},t)$ field operators via:

$$\hat{\Phi}(\boldsymbol{r},t) = \sqrt{\hat{n}(\boldsymbol{r},t)}e^{i\hat{\phi}(\boldsymbol{r},t)}. \tag{2.6}$$

To proceed I use Eq. (2.4) on the left hand side of Eq. (2.6) and I introduce linear perturbations for the phase $\hat{\phi} = \phi_0 + \hat{\phi}_1$ and the density $\hat{n} = n_0 + \hat{n}_1$ on the right hand side of Eq. (2.6). Then, keeping first-order contributions, we obtain an expression for the condensate perturbation $\delta\hat{\phi}$ in terms of the perturbations in density $\hat{n}_1(\boldsymbol{r},t)$ and phase $\hat{\phi}_1(\boldsymbol{r},t)$:

$$\delta\hat{\phi}(\boldsymbol{r},t) \;=\; \frac{\hat{n}_1(\boldsymbol{r},t)}{2n_0(\boldsymbol{r},t)} + i\hat{\phi}_1(\boldsymbol{r},t). \tag{2.7}$$

Here $\phi_0(\boldsymbol{r},t)$ denotes the background phase. The phase and density perturbations satisfy the commutation relation $\left[\hat{n}_1(\boldsymbol{r},t), \hat{\phi}_1(\boldsymbol{r'},t)\right] \;=\; i\delta^{(3)}(\boldsymbol{r}-\boldsymbol{r'})$. Substituting the above relation into (2.5) and using Madelung's representation for the background $\Phi_0(\boldsymbol{r},t) \;=\; \sqrt{n_0(\boldsymbol{r},t)}e^{i\phi_0(\boldsymbol{r},t)}$, I get the equations of motion for the phase and density

perturbations [38]:

$$-\frac{\hbar}{U}\partial_t\hat{\phi}_1 = \hat{\mathcal{D}}\hat{n}_1 + \frac{\hbar^2}{MU}\boldsymbol{\nabla}\phi_0\cdot\boldsymbol{\nabla}\hat{\phi}_1, \tag{2.8}$$

$$\partial_t\hat{n}_1 = -\frac{\hbar}{M}\boldsymbol{\nabla}\cdot\Big[\hat{n}_1\boldsymbol{\nabla}\phi_0 + n_0\boldsymbol{\nabla}\hat{\phi}_1\Big], \tag{2.9}$$

where I made use of the continuity equation for n_0: $\partial_t n_0 = -\frac{\hbar}{M}\boldsymbol{\nabla}\cdot\big(n_0\boldsymbol{\nabla}\phi_0\big)$ and I defined the operator

$$\hat{\mathcal{D}} \equiv 1 - \frac{\hbar^2}{2MU}\Big(\frac{\nabla^2}{2n_0} - \frac{\boldsymbol{\nabla}n_0\cdot\boldsymbol{\nabla}}{2n_0^2} - \frac{\nabla^2 n_0}{2n_0^2} + \frac{(\boldsymbol{\nabla}n_0)^2}{2n_0^3}\Big). \tag{2.10}$$

The terms in parentheses in $\hat{\mathcal{D}}$ are due to the quantum pressure, which are often neglected in the hydrodynamic limit where $\hat{\mathcal{D}} \approx 1$. In that situation, Eqs. (2.8) and (2.9) can be readily combined to get a relativistic wave equation for $\hat{\phi}_1$ (see [34, 35, 38]) :

$$0 = \frac{1}{\sqrt{-g}}\partial_\mu(\sqrt{-g}g^{\mu\nu}\partial_\nu\hat{\phi}_1), \tag{2.11}$$

where $\mu = 0$ denotes time and $\mu = 1,2,3$ denote space so $x^\mu = (ct,x,y,z)$ and $\partial_\mu = (\frac{1}{c}\frac{\partial}{\partial t},\boldsymbol{\nabla})$ where $c = \sqrt{Un_0/M}$ is the BEC speed of sound. Here, the metric is

$$g_{\mu\nu} = \begin{bmatrix} -c^3 & 0 & 0 & 0 \\ 0 & c(R+\tilde{\rho})^2 & 0 & 0 \\ 0 & 0 & c & 0 \\ 0 & 0 & 0 & c \end{bmatrix}, \tag{2.12}$$

with determinant $g = -c^6(R+\tilde{\rho})^2$, where $\tilde{\rho} = \rho - R(t)$ is the comoving radial coordinate. Note that the speed of sound c is not a relativistic invariant as the equations for BEC do not reproduce Einstein's equations for the background metric. Instead, Eq. (2.11) tells us that only the equation for a scalar field evolving on an expanding metric is being mimicked. This tells us that the metric in Eq. (2.12) is emergent, i.e., I infer it from the wave

equation for scalar field, and not derive it directly from some analog of Einstein's equations. Thus the analogy between BEC and spacetime does not exist at the background level, but rather at the level of perturbations.

Equation (2.11) shows that a boson gas in a time-dependent toroidal trap indeed simulates an expanding one-dimensional universe with the metric Eq. (2.12). However, below I show that although the quantum pressure terms in $\hat{\mathcal{D}}$ are small, their inclusion qualitatively impacts the dynamics of low-energy modes in the expanding toroidal BEC, leading to damping and spontaneous phonon creation. This quantum pressure provides short distance corrections to the evolution of sound modes in a BEC, which become significant when I reduce the thickness of the ring to make it quasi one-dimensional.

Having obtained equations (2.8) and (2.9), that describe excitations of a superfluid boson gas in a time-dependent trap, in the next section I show how, in the thin-ring limit, these equations reduce to the Mukhanov-Sasaki equation that describes damped sound modes.

2.2. The Mukhanov-Sasaki Equation

Equations (2.8) and (2.9) derived in the preceding section describe phase and density perturbations (i.e., phonons) in a BEC with a generic time-dependent trapping potential $V(\boldsymbol{r}, t)$. In fact, the potential $V(\boldsymbol{r}, t)$ only explicitly appears in the dynamics of the background density (n_0) and phase (ϕ_0) on which phonons propagate (which I study in Appendix A), while the density and phase perturbations $\hat{n}_1$ and $\hat{\phi}_1$ are sensitive to n_0 and ϕ_0 via Eqs. (2.8) and (2.9). Our first task is to make simplifying approximations that apply to the geometry realized in Ref. [38], i.e., a thin expanding toroidal trapping potential.

As I shall see, this leads to the Mukhanov-Sasaki equation for damped sound modes.

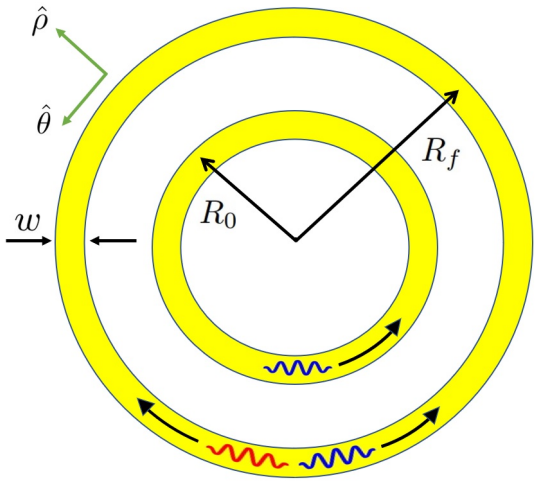

Figure 2.1. Sketch of the initial (with radius R_0) and final (with radius R_f) state of an expanding ring-shaped (toroidal) BEC, as realized in Ref. [38]. As depicted, an initial density wave traveling counterclockwise (*blue*) bifurcates due to phonon creation, into two counter propagating waves (*red and blue*). In the main text, I use polar coordinates (ρ, θ, z) with z directed out of the page. I also indicated the ring diameter w, implying that the ring cross-sectional area $\mathcal{A} \simeq \frac{1}{4}\pi w^2$ for the case of a circular cross section. However, in the main text I shall allow for different radii in the ρ and z direction (denoted by R_ρ and R_z, respectively).

The first simplifying approximation I shall invoke is to neglect the ρ and z dependences of the phase and density perturbations, thereby replacing $\hat{\phi}_1(\boldsymbol{r}, t) \to \hat{\phi}_1(\theta, t)$ and $\hat{n}_1(\boldsymbol{r}, t) \to \mathcal{V}^{-1}\hat{n}_1(\theta, t)$ in Eqs. (2.8) and (2.9), where $\mathcal{V} = R\mathcal{A}$ is a volume scale with $\mathcal{A}$ the cross-sectional area of the toroid (so that $2\pi\mathcal{V}$ is the toroid volume). Note that the angle-dependent density fluctation operator $\hat{n}_1(\theta)$ is dimensionless.

Such an approximation holds in the thin-ring limit, where the toroidal radius $R(t)$ is much larger than the typical length scales R_ρ and R_z (defined in Appendix A) characterizing the ring cross-sectional area (see Fig. 2.1). This implies that an initial angle-dependent perturbation around the ring, such as prepared in the experiments of Ref. [38], will not excite density variations in the ρ and z directions.

The second simplifying approximation I shall invoke is to assume that the background phase ϕ_0 and density n_0 are functions only of ρ and z (i.e., they are independent of θ). This is expected, given the angular symmetry of the toroidal trapping potential. I shall furthermore assume that the condensate and the ring are moving with the same velocity, i.e., the superfluid velocity equals the ring velocity $\boldsymbol{v} = \frac{\hbar}{M}\boldsymbol{\nabla}\phi_0 = \dot{R}\hat{\rho}$ (here $\dot{R} \equiv \frac{dR}{dt}$). The conditions for validity of this assumption are explored in Appendix A. This implies that the gradients in the perturbations are orthogonal to the condensate velocity i.e. $\boldsymbol{v}\cdot\boldsymbol{\nabla}\hat{\phi}_1 = \boldsymbol{v}\cdot\boldsymbol{\nabla}\hat{n}_1 = 0$. By a similar argument, the dot-product term $\boldsymbol{\nabla}n_0\cdot\boldsymbol{\nabla}\hat{n}_1 = 0$ in the quantum pressure also vanishes. On the other hand, the divergence of condensate velocity is not zero: $\boldsymbol{\nabla}\cdot\boldsymbol{v} = \frac{\hbar}{M}\nabla^2\phi_0 \approx \frac{\dot{R}}{R}$.

Within these approximations, the equations of motion (2.8) and (2.9) in the thin ring limit take the form:

$$-\frac{\hbar\mathcal{V}}{U}\partial_t\hat{\phi}_1(\theta,t) = \hat{\mathcal{D}}_\theta\hat{n}_1(\theta,t), \tag{2.13}$$

$$\partial_t\hat{n}_1(\theta,t) = -\frac{\dot{R}}{R}\hat{n}_1(\theta,t) - \frac{\hbar\mathcal{V}n_0}{MR^2}\partial_\theta^2\hat{\phi}_1(\theta,t), \tag{2.14}$$

describing angle-dependent excitations in a thin radially expanding toroidal BEC. Here $\hat{\mathcal{D}}_\theta \equiv 1 - \frac{\hbar^2}{2MU}\left(\frac{\partial_\theta^2}{2n_0R^2} - \frac{\nabla^2 n_0}{2n_0^2} + \frac{(\boldsymbol{\nabla}n_0)^2}{2n_0^3}\right)$ is the projection of $\hat{\mathcal{D}}$ in the θ-space. To solve this system of equations, I introduce mode expansions as :

$$\hat{\phi}_1(\theta,t) = \sqrt{\frac{U}{2\pi\mathcal{V}\hbar}}\sum_{n=-\infty}^{\infty}\left[e^{in\theta}\chi_n(t)\hat{a}_n + e^{-in\theta}\chi_n^*(t)\hat{a}_n^\dagger\right], \tag{2.15}$$

$$\hat{n}_1(\theta,t) = \sqrt{\frac{U\mathcal{V}}{2\pi\hbar}}\sum_{n=-\infty}^{\infty}\left[e^{in\theta}\eta_n(t)\hat{a}_n + e^{-in\theta}\eta_n^*(t)\hat{a}_n^\dagger\right], \tag{2.16}$$

where the ladder operators $\hat{a}_n$ satisfy $\left[\hat{a}_n, \hat{a}_{n'}^\dagger\right] = \delta_{n,n'}$, and the mode functions are assumed to be same whether the modes are traveling clockwise or anticlockwise, i.e. $\chi_{-n} = \chi_n$ and

$\eta_{-n} = \eta_n$. I take $\chi_n(t)$ and $\eta_n(t)$ to satisfy $(\eta_n\chi_n^* - \eta_{-n}^*\chi_{-n}) = i\hbar/U$, which leads to the commutation relation $\left[\hat{n}_1(\theta,t), \hat{\phi}_1(\theta',t)\right] = i\delta(\theta-\theta')$. Substituting these mode expansions in (2.13) and (2.14), I get the following equations of motion for the mode functions:

$$-\frac{\hbar}{U}\dot{\chi}_n(t) = D_n\eta_n(t), \tag{2.17}$$

$$\dot{\eta}_n(t) = -\frac{\dot{R}}{R}\eta_n + \frac{\hbar n_0}{MR^2}n^2\chi_n, \tag{2.18}$$

where $D_n \equiv 1 + \frac{\hbar^2}{4M^2c^2}\left(\frac{n^2}{R^2} + \frac{\nabla^2 n_0}{n_0} - \frac{(\nabla n_0)^2}{n_0^2}\right)$ is the eigenvalue of $\hat{\mathcal{D}}_\theta$.

To arrive at the Mukhanov-Sasaki equation, I eliminate η_n in favor of χ_n:

$$\ddot{\chi}_n + \left(1+\gamma_{\rm QP}\right)\frac{\dot{R}}{R}\dot{\chi}_n + \alpha_{\rm QP}\frac{n^2c^2}{R^2}\chi_n = 0. \tag{2.19}$$

The corrections due to quantum pressure are $\gamma_{\rm QP} = -\frac{R}{\dot{R}}\cdot\frac{\dot{D}_n}{D_n}$ and $\alpha_{\rm QP} = D_n$. In general these are dependent on the density, the radius of the ring and the mode index n. However, I can make an estimate of what values these corrections typically take. We start by approximating the density gradient $\boldsymbol{\nabla} n_0$ by the density divided by the width of the ring w (characterized by the TF radii R_ρ and R_z, see Appendix A). Similarly, I can approximate $\nabla^2 n_0 \simeq -n_0/w^2$. Thus $D_n \approx 1 + \frac{n^2}{2}\left(\frac{\xi}{R}\right)^2 - \left(\frac{\xi}{w}\right)^2$, where $\xi = \frac{\hbar}{\sqrt{2}Mc}$ is the coherence length. In the hydrodynamic limit, where the coherence length is small compared to the dimensions of the ring, $\alpha_{QP} = D_n \approx 1$.

To estimate $\gamma_{\rm QP}$, I need to estimate $\dot{D}_n$. To do this I use experimental parameters from Ref. [38], with M given by the mass of a ^{23}Na atom, the speed of sound $c \approx 2$ mm/s and the width of the ring $w \approx 2$ μm (which is indeed an order of magnitude smaller than the radius $R(t)$ that varies between 10 μm to 50 μm [38]). Thus $\left(\frac{\xi}{w}\right)^2 \approx 10^{-1}$. Also, since the width of the ring is small compared to its radius, $w \ll R(t)$, I find $\dot{D}_n \approx -\frac{1}{2}\left(\frac{\xi}{w}\right)^2\frac{\dot{R}}{R}$.

Here we estimate the ring width via $w = \sqrt{\frac{2\mu}{M\omega_z^2}}$, where ω_z is the trapping frequency in the z direction. We also made use of the local density approximation (LDA) to estimate the chemical potential in a harmonic trap. Following [38], I get $\mu \propto R^{-1/2}$ (see Appendix A). This implies that $\gamma_{\rm QP} \approx \frac{1}{2}\left(\frac{\xi}{w}\right)^2 \approx 10^{-1}$. This shows that short-distance physics of quantum pressure comes into play as we decrease the width of the ring w to make it quasi-1D.

I pause to note that although the quantum-pressure terms in Eq. (2.10) do not have a *direct* cosmological analog, our final Mukhanov-Sasaki equation is in fact relevant for cosmology. Indeed, within inflationary cosmology, the Einstein equations that describe the background evolution of inflationary spacetime yield a Mukhanov-Sasaki equation that is of the form of Eq. (3.5) but with the coefficient of the damping term being the number of spatial dimensions, with a small correction due to the so-called "slow-roll parameters" [43] that is reminscent of the small parameter $\gamma_{\rm QP}$ obtained here. More generally, as I shall show below, Eq. (3.5) leads to a crucial prediction of inflationary theory, which is spontaneous particle creation that leads (in the cosmological context) to the distribution of anisotropies in the CMB.

In fact, the quantum pressure effects in Eq. (3.5) are essential for achieving particle production. To see this, I now examine the implications of making a futher approximation (motivated by our preceding estimates), in which I take $\alpha_{\rm QP} \to 1$ and $\gamma_{\rm QP} \to 0$. Indeed, this approximation brings Eq. (3.5) into a very simple form:

$$\ddot{\chi}_n + \frac{\dot{R}}{R}\dot{\chi}_n + \frac{n^2c^2}{R^2}\chi_n = 0, \tag{2.20}$$

where I assume a constant speed of sound c. Equation (2.20) was discussed in detail in [38]. Here, I solve it by introducing the conformal time $d\eta = \frac{cdt}{R(t)}$ that measures the

size in cosmology. Equation (2.20) then takes the form of a simple harmonic oscillator: $\chi_n''(\eta) + n^2\chi(\eta) = 0$, with plane waves $e^{\pm i|n|\eta}$ as solutions. Switching back to proper time t, I get:

$$\chi_n(t)\Big|_{\gamma=0} \sim \exp\left[\pm i|n| \int_0^t \frac{cdt'}{R(t')}\right]. \tag{2.21}$$

This shows that the amplitude of the modes will be conserved with time in the $\gamma_{\rm QP} \to 0$ limit. Thus the quantum pressure correction $\gamma_{\rm QP}$ plays the role of a damping parameter. As will be seen in Sec. 2.3, nonzero $\gamma_{\rm QP}$ (even if it is small in magnitude) is essential for particle production. This is a well-known fact in cosmology [48], where a conformally invariant scalar field living in a $(1+1)$-dimensional spatially flat FLRW spacetime, has plane wave modes as solutions of the wave equation and thus leads to no particle creation.

Thus, while small, the quantum pressure correction represented by $\gamma_{\rm QP}$ fundamentally modifies the solutions of the Mukhanov-Sasaki equation. In general, the parameters $\gamma_{\rm QP}$ and $\alpha_{\rm QP}$ are dependent on time, but in what follows, I will assume them to be constants ($\gamma_{\rm QP} = \gamma$, $\alpha_{\rm QP} = \alpha$). This approximation gives us an analytic handle on the parameter space, where the basic physical features like the particle creation can be modeled without going in to the fine details of how they evolve with time. I will take γ to be a small number and take $\alpha \to 1$. The reason for the latter approximation is that in this chapter, we are mainly interested in particle creation due to quantum pressure, embodied in the parameter γ. I expect that the slight deviation of α from unity, which effectively yields a time-dependent speed of sound (see [25, 31, 32, 33, 34, 35]), will be a subleading effect here. Within these approximations, (3.5) reduces to the following Mukhanov-Sasaki

equation [40, 41, 42]:

$$\ddot{\chi}_n + \big(1+\gamma\big)\frac{\dot{R}}{R}\dot{\chi}_n + \frac{n^2c^2}{R^2}\chi_n = 0, \tag{2.22}$$

where I have assumed the speed of sound c to be a constant.

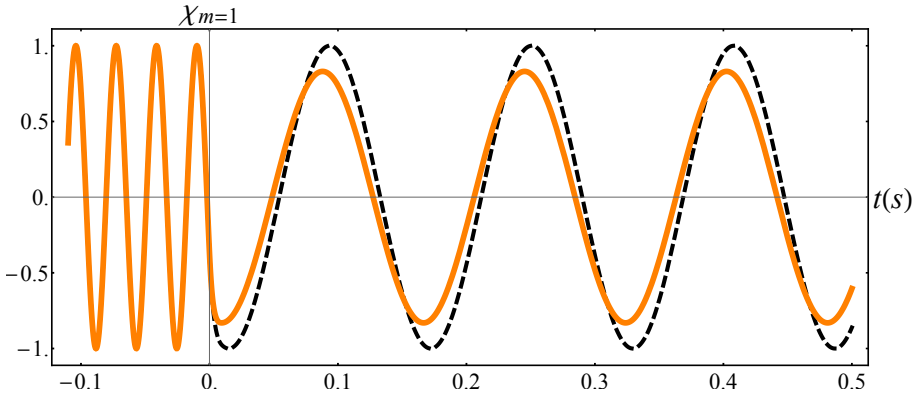

Figure 2.2. Comparison of solutions χ_m of (2.22) for m=1 mode without quantum pressure (γ=0) (*dashed, black*) and with quantum pressure ($\gamma = 0.5$) (*solid, orange*) (for $t < 0$ they coincide). The modes undergo damping and redshift just as they do in the inflationary era. For this plot, I took the speed of sound to be $c = 2$ mm/s, the initial radius to be $R_0 = 10\mu$m, the timescale that governs the expansion of the ring to be $\tau = 6.21$ms and the duration of expansion to be $t_f = 10$ms.

In the following, I also choose a specific form for the time-dependent radius $R(t)$. Our choice is motivated by the fact that, in the inflationary era, the Hubble parameter $H \equiv \frac{\dot{a}}{a} \approx H_0$ is roughly a constant and one could model this phase with a de-Sitter type inflation where the scale factor $a(t) \sim e^{H_0 t}$ [44, 43]. This motivates us to study an exponential expansion $R(t) = R_0 e^{t/\tau}$ of the ring radius, characterized by the timescale τ. Then the general solution to Eq. (2.22) is:

$$\chi_n(t) = e^{-\frac{t}{2\tau}(1+\gamma)}\Big[A_n J_{\frac{1+\gamma}{2}}(z) + B_n J_{-\frac{1+\gamma}{2}}(z)\Big], \tag{2.23}$$

where the time dependent parameter $z = \omega_n \tau$ with the frequency $\omega_n = \frac{|n|c}{R(t)}$ and $J_n(z)$ are Bessel functions of the first kind. The coefficients A_n and B_n are fixed by the initial

conditions.

To illustrate the effect of nonzero γ in the case of exponential inflation in the toroid, in Fig. 2.2 I plot χ_n as a function of t for an $n = 1$ mode for the case of $\gamma = 0$ (dashed curve) and $\gamma = 0.5$ (solid curve). For $t < 0$ (before expansion), both curves show oscillatory motion, and during expansion (for $t > 0$), where they are governed by Eq. (2.23), they both show a redshift [38] i.e. their frequency $\omega_n = \frac{nc}{R(t)}$ decreases as the ring expands. However, while the $\gamma = 0$ curve shows no reduction of amplitude, the $\gamma = 0.5$ curve exhibits damping due to quantum pressure. Both of these phenomena, the redshift and damping, have their respective counterparts in cosmology.

Before concluding this section, note that, as in conventional inflationary theory, the fate of modes after expansion in a toroidal BEC is strongly dependent on the mode index n (which controls the mode wavelength). To see this, note that for exponential expansion $R(t) \propto e^{t/\tau}$, the horizon size is given by $\eta_{\rm H} = \int_0^{t_f} \frac{cdt}{R(t)} = c\tau(1 - e^{-t_f/\tau})$. After the expansion persists long enough i.e. t_f/τ is large, then the horizon size is $\eta_{\rm H} \sim c\tau$. If the parameter $z = \frac{|n|c\tau}{R(t)}$ is small, i.e., $\frac{R}{|n|} \gg c\tau$, then the wavelengths of the modes are much larger than the horizon size and the mode solution (2.23) becomes constant in time:

$$\chi_n(t) \approx \left(\frac{2R_0}{|n|c\tau}\right)^{\frac{1+\gamma}{2}} \frac{B_n}{\Gamma\left(\frac{1-\gamma}{2}\right)}, \tag{2.24}$$

where I have used the result that for small arguments $z \to 0$, the Bessel function goes as $J_n(z) \to \frac{1}{\Gamma(n+1)}\left(\frac{z}{2}\right)^n$. Note that the form of the exponential factor in Eq. (2.23) is essential to get the above result. This *freezing* of super-horizon modes (i.e. those with small mode index) is a very important aspect of the inflationary mechanism as these modes re-enter the horizon at a later time and form large scale structures in the observable universe. In

the next section, I will discuss how phonons are produced due to the mode solution (2.23) and see the importance of the super-horizon modes in the expanding ring.

2.3. Spontaneous Phonon Creation

Now that I have solved the Mukhanov-Sasaki equation for a constant quantum pressure parameter γ, in this section I use its solution (2.23) to understand how a BEC in the vacuum state, when expanded exponentially, will exhibit the dynamical generation of phonons. I start with an initially static BEC in its vacuum state. The mode functions for this initial BEC (which I denote as the "in" state) obey Eq. (2.22), but with $\dot{R} = 0$ (so that they are undamped). These inital mode functions are:

$$\chi_n^{\text{in}}(t) = \frac{1}{\sqrt{2\omega_n^0}} e^{-i\omega_n^0 t}, \tag{2.25}$$

which satisfy $i\partial_t \chi_n^{\text{in}} = \omega_n^0 \chi_n^{\text{in}}$, where ω_n^0 is the frequency at $t = 0$. These positive-frequency 'in'-mode functions satisfy the Wronskian condition $W[\chi_n, \chi_n^*] = \dot{\chi}_n \chi_n^* - \chi_n \dot{\chi}_n^* = -i$, and associated with them is the structure of ladder operators $\hat{a}_n$ that annihilate their associated 'a-vacuum' state: $\hat{a}_n |0_a\rangle = 0$.

Having described the normal modes of the initial BEC, I turn to the impact of a period of exponential growth on the BEC, starting at $t = 0$, and described by the exponential function $R(t) = R_0 e^{t/\tau}$. During this period, the modes evolve according to (2.23), where the coefficients are fixed by matching the mode functions $\chi_n(t)$ and their time derivatives with that of the initial BEC at $t = 0$. This matching results in the condi-

tions:

$$\begin{aligned} A_n &= \frac{J_{\frac{1-\gamma}{2}}(z_0) + iJ_{-\frac{1+\gamma}{2}}(z_0)}{J_{\frac{1+\gamma}{2}}(z_0)J_{\frac{1-\gamma}{2}}(z_0) + J_{-\frac{1+\gamma}{2}}(z_0)J_{\frac{-1+\gamma}{2}}(z_0)}, \\ B_n &= \frac{J_{\frac{-1+\gamma}{2}}(z_0) - iJ_{\frac{1+\gamma}{2}}(z_0)}{J_{\frac{1+\gamma}{2}}(z_0)J_{\frac{1-\gamma}{2}}(z_0) + J_{-\frac{1+\gamma}{2}}(z_0)J_{\frac{-1+\gamma}{2}}(z_0)}, \end{aligned} \tag{2.26}$$

where $z_0 = \frac{|n|c\tau}{R_0}$. Equation (2.23), along with these coefficients, describes the mode functions during the exponential growth regime of the toroidal BEC.

The expansion comes to a halt at some later time $t = t_f$. In this third regime of $t > t_f$, the BEC Hamiltonian is again static, with excitations described by 'out'-mode solutions that are analogous to Eq. (2.25):

$$\chi_n^{\text{out}}(t) = \frac{1}{\sqrt{2\omega_n^f}} e^{-i\omega_n^f(t-t_f)}. \tag{2.27}$$

Due to the quantum evolution during the ring expansion, the final Heisenberg picture results for the operators $\hat{\phi}_1(\theta, t)$ and $\hat{n}_1(\theta, t)$ are still given by Eqs. (2.15) but with the final mode functions a superposition of the 'out'-modes in Eq. (2.27):

$$\chi_n^f(t) = e^{-\frac{t_f}{2\tau}\gamma}\Big[\alpha_n \chi_n^{\text{out}}(t) + \beta_n \chi_n^{\text{out}*}(t)\Big], \tag{2.28}$$

where $\omega_n^f = \frac{|n|c}{R_f}$ is the frequency for $t \geq t_f$. The coefficients in Eq. (2.28) are obtained by again demanding that the mode function and its derivatives are consistent at t_f, with the $t \to t_f^-$ solution given by Eq. (2.23) as described above. By solving these matching conditions I find the coefficients α_n and β_n:

$$\alpha_n = \frac{e^{-\frac{t_f}{2\tau}}}{2}\Big[A_n\Big(J_{\frac{1+\gamma}{2}} - iJ_{\frac{-1+\gamma}{2}}\Big) + B_n\Big(J_{-\frac{1+\gamma}{2}} + iJ_{\frac{1-\gamma}{2}}\Big)\Big], \tag{2.29}$$

$$\beta_n = \frac{e^{-\frac{t_f}{2\tau}}}{2}\Big[A_n\Big(J_{\frac{1+\gamma}{2}} + iJ_{\frac{-1+\gamma}{2}}\Big) + B_n\Big(J_{-\frac{1+\gamma}{2}} - iJ_{\frac{1-\gamma}{2}}\Big)\Big], \tag{2.30}$$

where I have suppressed the arguments of the Bessel functions, which are all evaluated at $z_f = \frac{|n|c\tau}{R_f}$ with R_f the final ring radius. These coefficients, which satisfy $|\alpha_n|^2 - |\beta_n|^2 = 1$, describe the modification of the mode functions χ_n during the expansion process. One can plug in equations (2.29)-(2.30) in Eq. (2.28), and thereby realize that the final mode χ_n^f has the same form as Eq. (2.23), i.e. an exponentially decreasing factor times some linear combination of Bessel functions.

The modified mode function (2.27) in the 'out'-regime, defines a new set of ladder operators $\hat{b}_n$ that annihilate the new 'b-vacuum' state $|0_b\rangle \neq |0_a\rangle$: $\hat{b}_n|0_b\rangle = 0$. The coefficients α_n and β_n provide a Bogoliubov transformation between $\hat{a}_n$ and $\hat{b}_n$ via [45, 46, 47, 48]:

$$\hat{a}_n = \alpha_n^* \hat{b}_n - \beta_n^* \hat{b}_{-n}^\dagger, \tag{2.31}$$

$$\hat{b}_n = \alpha_n \hat{a}_n + \beta_n^* \hat{a}_{-n}^\dagger. \tag{2.32}$$

Thus, assume I start in the 'a-vacuum', characterized by vanishing particle density $\langle 0_a|\hat{n}^a|0_a\rangle = 0$, where $\hat{n}^a = \hat{a}_n^\dagger \hat{a}_n$. During the expansion, the system wavefunction remains $|0_a\rangle$ (since I work in the Heisenberg picture), but the $\hat{a}_n$ evolve into the $\hat{b}_n$ according to Eq. (2.31). A measurement of the particle density will find the final system is bubbling with 'b-particles' [49], as represented by the expectation value $\langle 0_a|\hat{n}^b|0_a\rangle = |\beta_n|^2$. This is known as spontaneous particle creation from the vacuum state, characterized by the power parameter $|\beta_n|^2$ that I plot in Fig. 2.3 with respect to the mode index n, for three values of the quantum pressure parameter $\gamma = 0.2$, $\gamma = 0.35$ and $\gamma = 0.5$.

I now describe the connection of these results to the theory of inflation. It can be inferred from Fig. 2.3 that the power associated with small mode indices such as $n = 1$

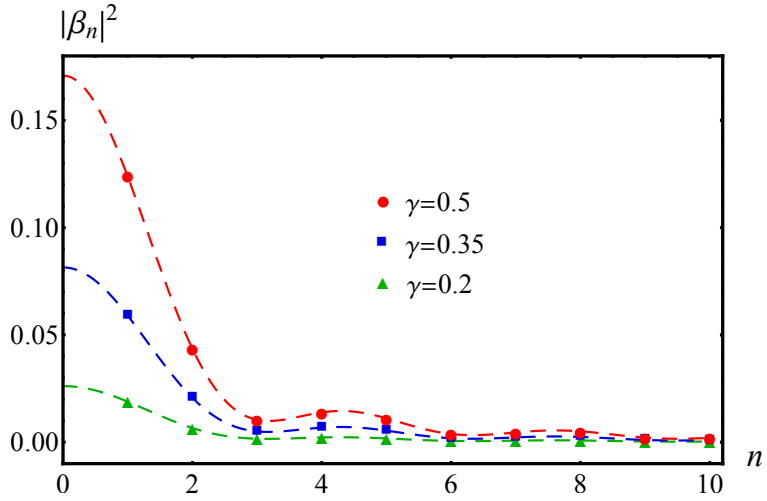

Figure 2.3. The particle production parameter $|\beta_n|^2$ as function of mode index n for various values of the quantum pressure $\gamma = 0.2$ (*green*), $\gamma = 0.35$ (*blue*) and $\gamma = 0.5$ (*red*). The dashed lines show $|\beta_n|^2$ as continuous functions to emphasize their overall dependence on the discrete mode indices. For this plot, I took the speed of sound to be $c = 2$ mm/s, the initial radius to be $R_0 = 10\mu$m, the expansion timescale to be $\tau = 6.21$ms and the duration of expansion to be $t_f = 10$ms.

is much higher than those at larger n. As in inflationary cosmology, this is because during the expansion some modes such as $n = 1$ become super-horizon and freeze (2.24), i.e. their power remains constant. In contrast, modes that are well within the horizon (i.e., at higher n, or smaller wavelength) are strongly damped and thus their power $|\beta_n|^2$ is reduced.

Thus, larger values of the quantum pressure parameter lead to stronger damping of modes (2.22) as well as increased spontaneous phonon production. This suggests that the loss of amplitude is converted into phonon production. In the next section, I will discuss the possibility of observing stimulated creation of phonons from a coherent initial state.

2.4. Stimulated Phonon Creation

Having discussed how phonons can be produced by a BEC that is initially in its vacuum state, I now turn to the possibility of starting with a initial coherent state in the

mode N:

$$|\alpha, N\rangle \;=\; e^{-\frac{1}{2}|\alpha|^2} e^{\alpha \hat{a}_N^\dagger} |0_a\rangle, \tag{2.33}$$

where the complex parameter α is a measure of the average number of particles in the coherent state given by $|\alpha|^2$. Physically, such a state represents a macroscopic current-carrying state of the BEC.

The states $|\alpha, N\rangle$ are eigenfunctions of the annihilation operators:

$$\hat{a}_m |\alpha, N\rangle \;=\; \delta_{m,N} \alpha |\alpha, N\rangle. \tag{2.34}$$

In what follows, I will use these coherent states to calculate the average density in the ring, before and after expansion. The advantage of using coherent states relative to fixed-number Fock states is that in the latter, the average density is zero at all times. This implies that, in an experiment, no significant change will be observed in the average density. For the case of an initial vacuum state, studied in the preceding section, another complication is the presence of other phonon modes, such as thermally excited phonons (since experiments cannot truly reach the zero-temperature vacuum state), that may swamp the signal from spontaneously created phonons. In contrast, in a coherent state, the average densities change with time, making it easier to detect changes due to phonon production.

Since we are in the Heisenberg picture, the system wavefunction is always given by Eq. (2.33), while the density operators change during the rapid expansion of the ring. I start by writing the mode expansion for the initial density operator (before expansion). To do this, I make use of (2.16), and the relation (2.17) between the density η_n and phase χ_n

modes neglecting the quantum pressure corrections (i.e. $D_n \approx 1$ here):

$$\hat{n}_1^i(\theta,t) = \mathcal{N}_0 \sum_{n=-\infty}^{\infty} \left[e^{in\theta}\eta_n^{\rm in}(t)\hat{a}_n + e^{-in\theta}\eta_n^{\rm in*}(t)\hat{a}_n^\dagger \right], \tag{2.35}$$

where $\mathcal{N}_0 = \sqrt{\frac{U\mathcal{V}_0}{2\pi\hbar}}$ is the initial normalization and the 'in'-density modes are $\eta_n^{\rm in}(t) = i\frac{\hbar}{U}\sqrt{\frac{\omega_n^0}{2}}e^{-i\omega_n^0 t}$. Note that we are only neglecting the quantum pressure corrections in the connection between the η_n and χ_n (where they have a small effect) but keeping them in the Mukhanov-Sasaki equation for the mode functions (where including the quantum pressure is qualitatively important, as I have discussed).

Next, I write down the final density operator after expansion, which has a similar form, but with the 'out'-mode density operators discussed above (see Eqs. (2.31) and (2.32)):

$$\hat{n}_1^f(\theta,t) = \mathcal{N}_f e^{-\frac{t_f}{2\tau}\gamma} \sum_{n=-\infty}^{\infty} \left[e^{in\theta}\eta_n^{\rm out}(t)\hat{b}_n + e^{-in\theta}\eta_n^{\rm out*}(t)\hat{b}_n^\dagger \right], \tag{2.36}$$

with the final normalization $\mathcal{N}_f = \sqrt{\frac{U\mathcal{V}_f}{2\pi\hbar}}$ and the 'out'-density modes are defined as $\eta_n^{\rm out}(t) = i\frac{\hbar}{U}\sqrt{\frac{\omega_n^f}{2}}e^{-i\omega_n^f(t-t_f)}$. Now, I define the average density in the coherent state as:

$$\langle \hat{n}_1(\theta,t)\rangle = \langle \alpha, N|\hat{n}_1(\theta,t)|\alpha,N\rangle. \tag{2.37}$$

If I take $\alpha \in \mathcal{R}$, then the initial average density can be written as a wave that travels in the counterclockwise direction ($+\hat{\theta}$):

$$\langle \hat{n}_1^i(\theta,t)\rangle \;=\; -2\sqrt{|N|}\alpha \cdot \sin\left[N\theta - \frac{|N|c}{R_0}t \right], \tag{2.38}$$

where I have set the normalization $\sqrt{\frac{\hbar c\mathcal{V}_0}{4\pi U R_0}}$ to unity for simplicity.

The initial atom density (at $t = 0$) according to Eq. (2.38) is shown in Fig. 2.4 with a dotted line, describing a counterclockwise traveling density wave (in the $+\hat{\theta}$ direction).

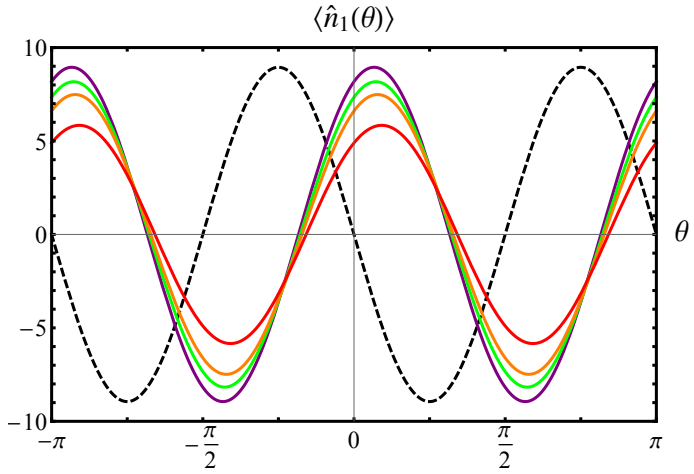

Figure 2.4. Comparison of average density $\langle\hat{n}_1\rangle$ before (*dashed, black*) and just after expansion (*solid*) for four values of the quantum pressure parameter γ. In order of decreasing amplitude, the solid curves correspond to γ=0 (*violet*), γ=0.1 (*green*), $\gamma = 0.2$ (*orange*), and $\gamma = 0.5$ (*red*). Note the $\gamma = 0$ final curve has equal amplitude to the initial density profile (in agreement with our earlier finding shown in Fig. 2.2), with the phase difference $\alpha_n = e^{i(z_f - z_0)}$ between the curves reflecting the fact that the wave travels around the ring during expansion. For this plot I studied a coherent state characterized by $\alpha = \sqrt{10}$ and mode index $N = 2$. I also took the sound speed to be $c = 2$ mm/s, the initial radius to be $R_0 = 10\mu$m, the timescale for expansion to be $\tau = 6.21$ms and the duration of expansion to be $t_f = 10$ms.

However, upon evaluating the density expectation value after expansion, I find that the final average density can be expressed as a sum of two waves (as illustrated schematically above in Fig. 2.1) reflecting phonon creation: A counterclockwise wave traveling wave (direction $+\hat{\theta}$) with amplitude $|\alpha_n|$, representing a reduced initial wave, and a smaller clockwise traveling wave (direction $-\hat{\theta}$) with an amplitude $|\beta_n|$, thus representing the density wave due to newly created phonons. The final time-dependent density is:

$$\langle\hat{n}_1^f(\theta,t)\rangle = -2e^{-\frac{t_f}{2\tau}\gamma}|N|^{\frac{1}{2}}\alpha\left(|\alpha_N|\sin\left[N\theta - \frac{|N|c}{R_f}\Delta t + \varphi_\alpha\right] - |\beta_N|\sin\left[N\theta + \frac{|N|c}{R_f}\Delta t + \varphi_\beta\right]\right), \tag{2.39}$$

where I have again set the normalization $\sqrt{\frac{\hbar c\mathcal{V}_f}{4\pi U R_f}}$ to unity. Here, $\Delta t = (t - t_f)$ is the time

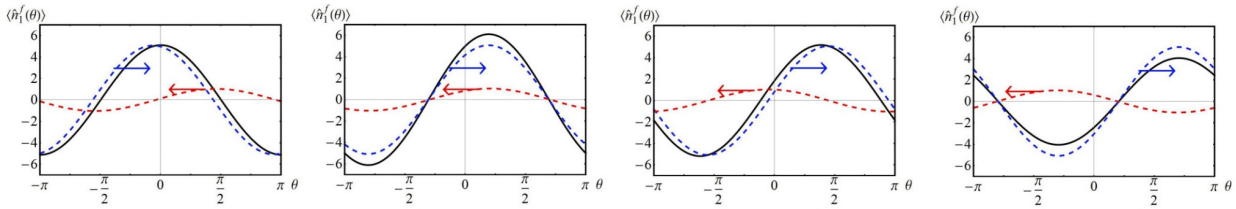

(a) $\Delta t = 1.6\tau$ (b) $\Delta t = 4.8\tau$ (c) $\Delta t = 8.0\tau$ (d) $\Delta t = 11.2\tau$

Figure 2.5. After rapid expansion of the toroidal BEC, an initial traveling wave bifurcates into oppositely-oriented traveling waves, as depicted in Fig. 2.1. The total density of these waves (*solid, black*), given by Eq. (2.39), is a sum of a right-moving wave (*dashed, blue, arrow indicating direction*), representing the ingoing particles and a left-moving wave (*dashed, red, arrow indicating direction*) representing the dynamically created particles. For this plot I studied a coherent state characterized by $\alpha = \sqrt{10}$ and mode index $N = 1$, I set the quantum pressure parameter γ=0.3, the sound speed to be $c = 2$ mm/s, the initial radius to be $R_0 = 10\mu$m, the duration of expansion to be $t_f = 10$ms and took the timescale governing the trap expansion to be $\tau = 6.21$ms.

elapsed after the expansion has ended, and $\varphi_\alpha = \mathrm{Arg}(\alpha_N)$ and $\varphi_\beta = \mathrm{Arg}(\beta_N)$ are, respectively, the phase associated with the incoming and created particles. The final density wave is shown in Fig. 2.4 at $t = t_f$, for various values of quantum pressure. In Fig. 2.5 I show the density vs. angle for increasing values of the elapsed time $\Delta t = (t - t_f)$. The total density is shown as a black solid curve, and the contributions due to the two terms in Eq. (2.39), i.e., the abovementioned counterclockwise and clockwise contributions, are depicted as blue (rightmoving arrow) and red (leftmoving arrow) dashed curves, respectively. Although these two contributions are not separately measurable, they can be inferred from the time dependence of the density vs. angle, showing a concrete experimentally testable signature of particle production in an initial coherent state.

2.5. Density Correlations

As I have discussed, a rapidly expanding toroidal BEC undergoes a modification of its vacuum, leading to particle production with amplitude β_n. In this section, I show how

this is revealed in correlations of the density fluctuations (i.e., noise correlations), an experimental probe that has already been used to study horizons in the context of Hawking radiation [21]. I start by computing density correlations at zero temperature $T = 0$ before generalizing to nonzero temperature.

$T = 0$ limit

I assume our initial system, before expansion, is a vacuum of $\hat{a}_n$ particles $|0\rangle$. The appropriate equal-time fluctuation correlation function is:

$$\mathcal{C}(\theta, \theta') = \langle \hat{n}_1(\theta, t)\hat{n}_1(\theta', t)\rangle - \langle \hat{n}_1(\theta, t)\rangle\langle \hat{n}_1(\theta', t)\rangle, \tag{2.40}$$

where the averages are being taken with respect to the initial vacuum state $|0\rangle$. Then, for the initial static BEC before expansion, I make use of $\langle a_n^\dagger a_{n'}\rangle = 0$ along with (2.35) and (2.38) to calculate the initial noise correlations, obtaining:

$$\mathcal{C}^i(\theta - \theta') = \mathcal{N}_0^2 \sum_{n=-\infty}^{\infty} |\eta_n^{\text{in}}(t)|^2 \mathrm{e}^{in(\theta-\theta')}. \tag{2.41}$$

Since the mode functions in the summand $|\eta_n^{\text{in}}(t)|^2 = \frac{\hbar^2}{2U^2}\omega_n^0 \propto |n|$, this sum is divergent and must be regularized. To implement this regularization, note that this divergence comes from the fact that I have taken a long-wavelength (low energy) approximation. The linear-in-n energy dependence of these modes must become quadratic, as in the conventional Bogoliubov approximation, for sufficiently large $|n| \geq n_c \equiv \frac{2cMR_0}{\hbar}$. I account for this this by replacing the linear summand with the result following from Bogoliubov theory,

which gives:

$$\begin{aligned}\mathcal{C}^i(\theta-\theta') &= \mathcal{N}_0^2\frac{\hbar^2 c}{2U^2R_0}n_c\sum_{n=-\infty}^{\infty}\frac{n^2}{\sqrt{n^2(n^2+n_c^2)}}\mathrm{e}^{in(\theta-\theta')},\\ &= \frac{1}{2\pi}n_0\mathcal{V}_0\sum_{n=-\infty}^{\infty}\frac{n^2}{\sqrt{n^2(n^2+n_c^2)}}\mathrm{e}^{in(\theta-\theta')},\end{aligned} \tag{2.42}$$

where in the second line I inserted our formulas for $\mathcal{N}_0$, n_c, and c (at the initial radius R_0) to simplify the prefactor. This result is precisely what one would obtain for a 1D BEC, at $T = 0$, within standard Bogoliubov theory [50]. The final sum is convergent, although it has a delta-function piece that I can isolate with the Poisson summation formula to arrive at

$$\mathcal{C}^i(\theta-\theta') = n_0\mathcal{V}_0\Big(\delta(\theta-\theta')+\mathcal{S}(\theta-\theta')\Big), \tag{2.43}$$

$$\mathcal{S}(\theta) \equiv \frac{1}{2\pi}\sum_{n=-\infty}^{\infty}\Big[\frac{n^2}{\sqrt{n^2(n^2+n_c^2)}}-1\Big]\mathrm{e}^{in\theta}, \tag{2.44}$$

for the noise correlations before expansion.

The result for the final regularized noise correlations after expansion follow similarly, and can be written in the following manner:

$$\mathcal{C}^f(\theta-\theta') = n_0\mathcal{V}_f e^{-\frac{t_f}{\tau}\gamma}\Big(\delta(\theta-\theta')+\mathcal{S}(\theta-\theta')+\mathcal{C}^{\mathrm{sub}}(\theta-\theta')\Big), \tag{2.45}$$

where I defined the function

$$\mathcal{C}^{\mathrm{sub}}(\theta) \equiv \frac{1}{2\pi}\sum_{n=-\infty}^{\infty}\frac{n^2}{\sqrt{n^2(n^2+n_c^2)}}\times 2\Big[|\beta_n|^2-\mathrm{Re}\Big(\alpha_n\beta_n^* e^{-2i\omega_n^f\Delta t}\Big)\Big]e^{in\theta}, \tag{2.46}$$

which, as can be seen by comparing to Eq. (2.43), is an additional contribution after the rapid expansion of the ring BEC. Here, the superscript "sub" indicates that this is the subtracted noise correlator, i.e., the difference of the final and initial normalized correlators. Note that this contribution depends on $\Delta t = (t - t_f)$, the time elapsed after expansion, so that the summand exhibits oscillatory behavior as a function of Δt. However, I

find that the summand is well approximated by time-averaging over one period ($2\pi/\omega_n$) of these oscillations, which eliminates the interference term $\alpha_n\beta_n^*$ and yields

$$\mathcal{C}^{\rm sub}(\theta) \simeq \frac{1}{\pi}\sum_{n=-\infty}^{\infty} \frac{n^2}{\sqrt{n^2(n^2+n_c^2)}}|\beta_n|^2 e^{in\theta}, \tag{2.47}$$

for the subtracted noise correlations.

The expressions (2.43) and (2.45) for the initial and final noise correlations have a dirac-delta function that is divergent at $\theta = \theta'$. In plotting these functions, I drop this piece, and set the prefactors (i.e., $n_0\mathcal{V}_0/(2\pi)$ and $n_0\mathcal{V}_f \mathrm{e}^{-\frac{t_f}{\tau}\gamma}/(2\pi)$) to unity to simplify comparing the noise before and after expansion. The main part of Fig. 2.6 shows this comparison, with the initial case being a red dashed line and the final case being a solid green line. I see that each case is dominated by a large (though finite) negative contribution at equal angles ($\theta \to 0$). I regard such anti-correlations as reflecting the repulsion of bosonic atoms at short distances [51, 52]. For larger angular separations, the correlations gradually flatten out [53], except for the appearance of a cusp feature at nonzero angle in the final noise correlations. This cusp clearly represents a signature of the phonon creation, proportional to $|\beta_n|^2$, that I have discussed above. In the inset, I plot the subtracted part Eq. (2.47) for three values of the quantum pressure parameter: $\gamma = 0.2$ (solid green), $\gamma = 0.35$ (short-dashed blue) and $\gamma = 0.5$ (long-dashed red). This shows that the magnitude of the cusp increases with increasing quantum pressure, although the cusp location is independent of γ. I do find that the cusp location as a function of angle increases with increasing expansion time t_f, asymptotically approaching $\theta = \pi$ for large t_f.

To better understand the origin of the cusp in Fig. 2.6, and connect it to particle

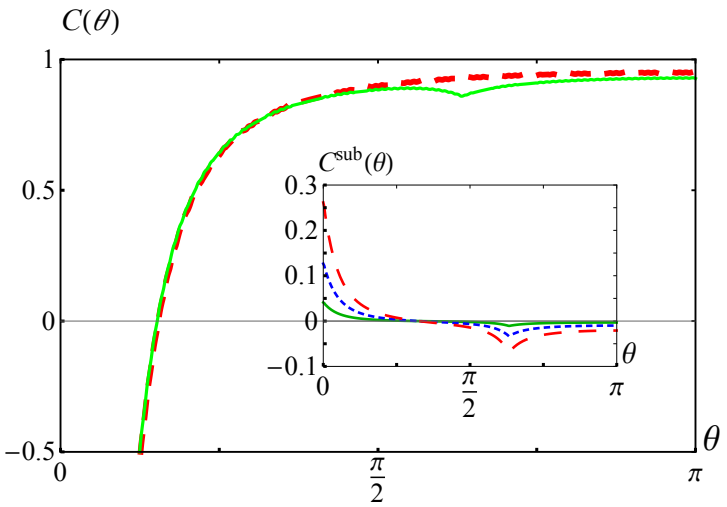

Figure 2.6. Main: Noise correlations $\mathcal{C}(\theta)$ at zero temperature, before (*dashed, red*, given in Eq. (2.43), and after (*solid, green*, given in Eq. (2.45)) expansion, with quantum pressure $\gamma = 0.5$. In each, I focused on $\theta \neq 0$ (dropping the delta-function piece) and dropped overall prefactors. The correlations after expansion show a cusp like feature that I regard as a signature of particle creation. Inset: To emphasize the cusp, I plot the difference between these curves, the subtracted noise correlations $\mathcal{C}^{\rm sub}(\theta - \theta')$ plotted with respect to the angle difference θ. Here I chose three values of quantum pressure parameter $\gamma = 0.2$ (*solid, green*) and $\gamma = 0.35$ (*short-dashed, blue*) and $\gamma = 0.5$ (*long-dashed, red*). For both plots, I took the speed of sound to be $c = 2$ mm/s, the initial radius to be $R_0 = 10\mu$m, the duration of expansion to be t_f=10ms, the timescale governing the trap expansion to be $\tau = 6.21$ms, and $n_c = 10$.

production during expansion of the ring BEC, I differentiate (2.47) to get:

$$\frac{d}{d\theta}\mathcal{C}^{\rm sub}(\theta) = -\frac{2}{\pi}\sum_{n=1}^{\infty}\frac{n^2|\beta_n|^2}{\sqrt{n^2+n_c^2}}\sin(n\theta). \tag{2.48}$$

A good approximation to this sum results if I Taylor expand the creation parameter β_n for small damping $\gamma \ll 1$ and large mode index $n \gg 1$, which gives $n^2|\beta_n|^2 \approx \left(\frac{\gamma}{4}\right)^2\left(\frac{c\tau}{R_0}\right)^{-2}\Big[1 + a^2 - 2a\cos\left(2n\theta_{\rm H}\right)\Big]$, where $a = e^{\frac{t_f}{\tau}}$ is the scale factor and $\theta_{\rm H} = \frac{c\tau}{R_0}\left(1 - a^{-1}\right)$ is the angular horizon size at the end of expansion. Upon plugging this into (2.48), I end up with three

sums that I write as:

$$\begin{aligned}\frac{1}{f(\gamma)}\frac{d}{d\theta}\mathcal{C}^{\rm sub}(\theta) &= a\sum_{n=1}^{\infty}\frac{\sin(n(\theta-2\theta_{\rm H}))}{\sqrt{n^2+n_c^2}} + a\sum_{n=1}^{\infty}\frac{\sin(n(\theta+2\theta_{\rm H}))}{\sqrt{n^2+n_c^2}} \\ &- (1+a^2)\sum_{n=1}^{\infty}\frac{\sin(n\theta)}{\sqrt{n^2+n_c^2}}, \end{aligned} \tag{2.49}$$

where $f(\gamma) = \frac{\gamma^2}{8\pi}\left(\frac{c\tau}{R_0}\right)^{-2}$. I now analyze the angle dependence of this quantity. For $\theta > 0$, the first sum is the dominant one, and approximating it by an integral I get

$$\begin{aligned}&\sum_{n=1}^{\infty}\frac{\sin(n(\theta-2\theta_{\rm H}))}{\sqrt{n^2+n_c^2}} \simeq \int_0^{\infty} dx \frac{\sin\left(n_c(\theta-2\theta_{\rm H})x\right)}{\sqrt{1+x^2}}, \\ &\simeq \frac{\pi}{2}\left[\Theta(\theta-2\theta_{\rm H})I_0\big(n_c(\theta-2\theta_{\rm H})\big) - L_0\big(n_c(\theta-2\theta_{\rm H})\big)\right], \end{aligned} \tag{2.50}$$

where the integration variable $x = n/n_c$, $I_0(x)$ is the modified Bessel function of the first kind, $L_0(x)$ is the modified Struve function and $\Theta(x)$ is the unit step function. The appearance of the latter means that the derivative is discontinuous at $\theta = 2\theta_{\rm H}$, implying that this determines the angular position of the cusp. I therefore conclude that the cusp in the correlation function is determined by the angular horizon size:

$$\theta_{\rm cusp} = 2\theta_{\rm H} = 2\frac{c\tau}{R_0}\left(1 - e^{-\frac{t_f}{\tau}}\right). \tag{2.51}$$

This result shows that the cusp location is independent of the damping parameter γ, as I saw in Fig. 2.6. It also explains why the cusp moves away from the origin, eventually slowing down as it approaches $\theta = \pi$, as the duration of expansion t_f increases. The negative correlation at the cusp signifies creation of phonons that anti-bunch as they are created in pairs that move away from each other with opposite momenta [45, 46, 47, 48]. This is similar to the 'tongue'-like features that were numerically observed in an acoustic black hole [51].

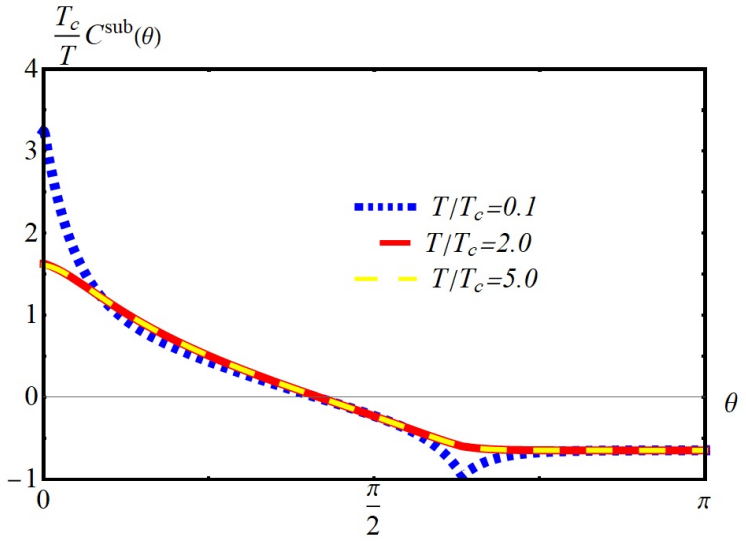

Figure 2.7. Subtracted noise correlations $\frac{T_c}{T}\mathcal{C}^{\rm sub}(\theta)$ plotted with respect to the angle difference θ, at finite temperatures given in Eq. (2.53). In each, I focused on $\theta \neq 0$ (dropping the delta-function piece) and dropped overall prefactors. For low temperature T/T_c=0.1 (*short-dashed, blue*), the correlations after expansion show a cusp like feature as in Fig. 2.6. For high temperatures $T/T_c = 2$ (*solid, red*) and $T/T_c = 5$ (*long-dashed, yellow*), I get similar correlations with a kink at the same location where the cusp appears. The appearance of the kink and the scaling behavior with temperature is a signature of particle creation.

$T \neq 0$ regime

A key question concerns the fate of the cusp feature at finite temperatures. To explore this, I extend the preceding analysis to finite temperatures by assuming the initial unexpanded ring is characterized by a Bose distribution of quasiparticles. I therefore evaluate the averages in Eq. (2.40) using:

$$\langle \hat{a}_n^\dagger \hat{a}_{n'} \rangle = \delta_{n,n'} n_B(E_n), \tag{2.52}$$

where $n_B(x) = (e^{\beta x} - 1)^{-1}$ is the Bose-Einstein distribution with the chemical potential set to zero for massless phonons, $\beta^{-1} = k_B T$ and $E_n = \sqrt{\epsilon_n(\epsilon_n + 2Un_0)}$ is the Bogoliubov dispersion. Following similar steps as in the preceding, I find for the subtracted correlation

function:

$$\mathcal{C}^{\rm sub}(\theta) \simeq \frac{1}{\pi}\sum_{n=-\infty}^{\infty}\frac{n^2}{\sqrt{n^2(n^2+n_c^2)}}\big(1+2n_B(n,T)\big)|\beta_n|^2 e^{in\theta}, \tag{2.53}$$

which is similar to (2.47) except for the appearance of a Bose-Einstein distribution function $n_B(n,T)$ defined as

$$\begin{aligned} n_B(n,T) &= \Big(e^{f(n)\frac{T_c}{T}}-1\Big)^{-1}, \\ f(n) &\equiv \Big|\frac{n}{n_c}\Big|\Big(1+\frac{n^2}{n_c^2}\Big)^{1/2}, \end{aligned} \tag{2.54}$$

where the temperature scale is defined as $T_c \equiv \frac{n_c^2\hbar^2}{2MR^2k_B}$.

In Fig. 2.7, I plot the subtracted noise correlator (2.53), divided by T/T_c, for three different temperatures $T/T_c = 0.1$, $T/T_c = 2$ and $T/T_c = 5$. For these curves, I chose the quantum pressure to be $\gamma = 0.5$, the speed of sound to be $c = 2$ mm/s, the radius to be $R = 10\mu$m, the duration of expansion to be $t_f = 10$ms, the timescale governing the expansion of the trap to be $\tau = 6.21$ms and $n_c = 10$. Using these parameters I get $T_c = 10$ nK for the relevant temperature scale.

These curves show that, while the cusp-like feature is still present at low T, it is smoothed out at higher T. The higher T curves instead exhibit a change of slope (i.e., a kink) at the horizon location. In fact, the two higher temperature curves in Fig. 2.7 overlap. This is due to the fact that they are well approximated by taking the high-temperature limit of the Bose function, replacing $n_B(n,T) \approx T/(fT_c)$ in Eq. (2.53) to obtain for the subtracted correlator:

$$\mathcal{C}^{\rm sub}(\theta) \approx \frac{2T}{\pi T_c}\sum_{n=-\infty}^{\infty}\frac{|\beta_n|^2}{1+(n/n_c)^2}e^{in\theta}. \tag{2.55}$$

The approximate result Eq. (2.55) shows that, with increasing temperature, the angle-

dependent subtracted noise correlations scale linearly with T, but with an angle-dependence that still reflects the horizon location.

From these results, I can outline two experimental procedures to identify stimulated particle creation in an experiment measuring density correlations. Firstly, an experiment that measures correlations at different temperatures (but for the same expansion time) would find an approximate collapse of the curves, when plotted as normalized in Fig 2.7. This probes the predicted linear scaling with temperature. Secondly, experiments at fixed temperature but varying expansion time would detect a change in the location of the angle-dependent kink, representing the moving horizon. These results demonstrate that correlations in the density fluctuations show a clear signature of particle production in a rapidly expanding toroidal BEC, showing another way that cold atom experiments can probe inflationary physics.

To conclude, in this chapter I looked at how a Bose-Einstein condensate confined to a rapidly expanding thin toroidal setup leads to spontaneous creation of phonons, similar to the inflationary universe. For this, I studied the long-wavelength limit of the Bogoliubov-de Gennes equations, yielding a damped harmonic oscillator equation, i.e., the Mukhanov-Sasaki equation. I showed that this damping forces an initial positive-frequency plane wave in the static BEC to end up as a combination of positive and negative frequency modes. As a result, the phonon field operator evolves and sees the initial vacuum as a state filled with phonons. This spontaneous particle creation is maximum for low-energy modes as these modes are the ones that are able to exit the sonic horizon in the BEC. Thus this setup achieves the two key features of the inflationary mechanism: particle creation and horizon exit of long-wavelength modes. I then showed that an initially

excited (coherent) state leads to an amplification in the phonon population, which could be seen as a density modulation. I ended with a discussion of density correlations, where I showed that phonon creation manifests itself as a cusp at zero temperature, and as a kink at finite temperatures.

CHAPTER 3. ENTANGLEMENT IN AN EXPANDING TOROIDAL BOSE-EINSTEIN CONDENSATE

In the previous chapter, I looked at how phonons are spontaneously generated in an expanding toroidal BEC. In this chapter, I will see that these phonons are always created in two-mode squeezed states, i.e., they are entangled in modes n and $-n$. This means that the correlations discussed in the previous chapter (at zero temperature) are purely due to quantum effects, i.e., they are of the EPR (Einstein-Podolsky-Rosen) type [88], that degrade and become classical in nature at finite temperatures, i.e., their features can be reproduced by other classical experiments. These quantum correlations are relevant for the inflationary mechanism, as there too entangled modes are generated in pairs $(\vec{k}, -\vec{k})$, which could possibly have left some imprint in the cosmic microwave background radiation.

The rest of this chapter is organized as follows: in Sec. 3.1, I review how fluctuations (i.e., phonons) evolve in an expanding toroidal BEC using the Mukhanov-Sasaki equation [40, 41, 42] that governs the evolution of fluctuations in the primordial universe. This equation describes how the condensate fluctuations undergo damping due to the presence of quantum pressure, leading to a spontaneous generation of phonons in two-mode squeezed states. In Sec. 3.2, I will use the theory of continuous quantum variables to construct the covariance matrix which has information about all possible system correlations. I will then use this to quantify the amount of entanglement present in this system for an initial vacuum state with no phonons. I will discuss how thermal noise and detector imperfections can lead to loss of entanglement, and how an initial squeezing in a single-

mode of phonons can help recover this lost entanglement. In Sec. 3.3, I propose a protocol, based on the Hanbury-Brown and Twiss [94, 95, 96] like experiment discussed in Ref. [89] that was performed for BECs, to determine the entanglement of an inflationary toroidal BEC. I show that this protocol makes it possible to measure the correlation functions entering the covariance matrix determining the system density matrix, thereby providing a way to quantify the entanglement present in the inflationary toroidal BEC due to analog particle creation.

3.1. Particle creation in toroidal BECs

In this section, I briefly review and expand upon the discussion of the previous chapter (also in Ref. [76]) which analyzed properties of an inflationary toroidal BEC. There it was shown that this sytem can exhibit spontaneous phonon creation that mimics the spontaneous generation of perturbations from the vacuum during the inflationary era of the primordial universe.

In the thin-ring limit [38, 73], the only relevant spatial coordinate is the angle θ around the ring, and fluctuations in the phase $\hat{\phi}_1(\theta)$ and density $\hat{n}_1(\theta)$ are captured by the following Hamiltonian:

$$\hat{H} = \int_0^{2\pi} d\theta \left[\frac{\hbar^2}{2MR^2} n_0 \mathcal{V} \big(\partial_\theta \hat{\phi}_1(\theta)\big)^2 + \frac{1}{2}\frac{U}{\mathcal{V}} \hat{n}_1^2(\theta) \right], \tag{3.1}$$

where $\hbar$ is the reduced Planck's constant, M is the mass of the atoms in the condensate, $R(t)$ is the mean radius of the toroid. Following the experiment of Eckel et al, I assume $R(t)$ to exhibit an experimentally-controllable time dependence. Here, n_0 is the average condensate density, $U = \frac{4\pi a_s \hbar^2}{M}$ is the interaction parameter with a_s being the scattering length, and $\mathcal{V} = R\mathcal{A}$ is a volume scale with $\mathcal{A}$ being the cross-sectional area of the

toroid (such that $2\pi\mathcal{V}$ is the toroid volume). The angle dependent fluctuation field operators $\hat{\phi}_1(\theta,t)$ and $\hat{n}_1(\theta,t)$ are dimensionless and satisfy equal time commutation relations $\big[\hat{n}_1(\theta,t),\hat{\phi}_1(\theta',t)\big] = i\delta(\theta-\theta')$. To study the energy dependence of these angle-dependent mode excitations I assume the following mode expansions for the fluctuation operators [76]:

$$\hat{\phi}_1(\theta,t) = \sqrt{\frac{U}{2\pi\mathcal{V}\hbar}}\sum_{n=-\infty}^{\infty}\big[e^{in\theta}\chi_n^{\rm in}(t)\hat{a}_n + e^{-in\theta}\chi_n^{\rm in*}(t)\hat{a}_n^\dagger\big], \tag{3.2}$$

$$\hat{n}_1(\theta,t) = \sqrt{\frac{U\mathcal{V}}{2\pi\hbar}}\sum_{n=-\infty}^{\infty}\big[e^{in\theta}\eta_n^{\rm in}(t)\hat{a}_n + e^{-in\theta}\eta_n^{\rm in*}(t)\hat{a}_n^\dagger\big], \tag{3.3}$$

where the ladder operators $\hat{a}_n$ satisfy $\big[\hat{a}_n,\hat{a}_{n'}^\dagger\big] = \delta_{n,n'}$, and the mode functions are assumed to be same whether they travel clockwise or anticlockwise, i.e. $\chi_{-n}^{\rm in} = \chi_n^{\rm in}$ and $\eta_{-n}^{\rm in} = \eta_n^{\rm in}$ and they satisfy $(\eta_n^{\rm in}\chi_n^{\rm in*} - \eta_{-n}^{\rm in*}\chi_{-n}^{\rm in}) = i\hbar/U$. The operators $\hat{a}_n$ and $\hat{a}_n^\dagger$ respectively create and annihilate phonons with mode number n. To see this, I note that in the initial static toroidal BEC with radius $R(t=0)\equiv R_0$, there exists a preferred set of 'in'-modes $\chi_n^{\rm in}(t) = (2\omega_n^0)^{-1/2}e^{-i\omega_n^0 t}$, which is a positive frequency mode as $i\partial_t\chi_n^{\rm in} = \omega_n^0\chi_n^{\rm in}$, where $\omega_n^0 = |n|c/R_0$ is the frequency at $t=0$. Associated to these 'in'-modes, is the structure of ladder operators $\hat{a}_n$ that annihilate their associated 'a-vacuum': $\hat{a}_n|0_a\rangle = 0$. The 'in'-density modes η_n can be extracted from the corresponding phase modes χ_n via the Euler equation in [76]: $\hat{n}_1(\theta,t) = -\frac{\hbar\mathcal{V}}{U}\frac{d}{dt}\hat{\phi}_1(\theta,t)$ which upon using the above mode expansion gives $\eta_n = -\frac{\hbar}{U}\frac{d}{dt}\chi_n(t)$. Thus, in this regime, the Hamiltonian diagonalizes and can be written as a sum of harmonic oscillators as follows:

$$\hat{H}^{\rm in} = \sum_{n=-\infty}^{\infty}\frac{1}{2}\hbar\omega_n^0\big[\hat{a}_n\hat{a}_n^\dagger + \hat{a}_n^\dagger\hat{a}_n\big], \tag{3.4}$$

giving us a particle interpretation in the form of phonons excited from the vacuum state

$|0_{\rm a}\rangle$. For the choice where the 'in'-modes are described by plane waves in time, it can be shown that the above Hamiltonian defines a time-translation operator $e^{i\hat{H}^{\rm in}t}$ under whose action the vacuum state $|0_{\rm a}\rangle$ is invariant. Thus the presence of time translation symmetry is intimately connected to the emergence of well-defined quasi-particles.

At $t = 0$, the ring starts expanding according to the form of $R(t)$ that can designed to be an error function [38], an exponential [76] or a power-law in time. As a result, the time translation symmetry gets broken and the modes acquire a non-trivial time-dependence. In this regime, the evolution of phase modes χ_n is governed by the Mukhanov-Sasaki equation, which in the early universe cosmology dictates the evolution of fluctuations in the inflaton field [40, 41, 42]:

$$\ddot{\chi}_n + \big(1+\gamma_{\rm QP}\big)\frac{\dot{R}}{R}\dot{\chi}_n + \alpha_{\rm QP}\frac{n^2c^2}{R^2}\chi_n = 0, \tag{3.5}$$

where $\dot{R} = dR/dt$ is the time derivative of the ring's radius, $\gamma_{\rm QP}$ and $\alpha_{\rm QP}$ are corrections due to quantum pressure that depend on density, radius of the ring and mode index. For the special case when $\gamma_{\rm QP} = \gamma$ is a constant, $\alpha_{\rm QP}$ is unity and the ring expands exponentially $R(t) = R_0 e^{t/\tau}$, τ being the expansion time-scale, the solutions to (3.5) are Bessel functions that undergo damping [76] (see Eq. 2.23 in Chapter 2). The absence of plane wave solutions in this time-dependent regime implies that there are no preferred set of modes and diagonalizing the Hamiltonian as I did in Eq.(3.4) is not possible. Thus, the vacuum state at any instant is not invariant under time translations, and thus there is no notion of 'particles' during this time-dependent regime. In the case of the primordial universe, where there are no static regimes, the procedure to select a preferred set of modes was given by Bunch and Davies [90]. However, in the toroidal BEC case, there is an ini-

tial static regime before $t = 0$ which provides us with initial conditions thereby selecting a preferred vacuum state.

This expansion ends at time $t = t_{\rm f}$, and thus begins the final static regime where again I expect to find a preferred set of positive frequency 'out'-modes $\chi_n^{\rm out}(t) = (2\omega_n^{\rm f})^{-\frac{1}{2}} e^{-i\omega_n^{\rm f}(t-t_{\rm f})}$, that depend on the final frequency $\omega_n^{\rm f} = \frac{|n|c}{R_{\rm f}}$, where $R_f = R_0 e^{t_{\rm f}/\tau}$ is the ring radius at $t = t_{\rm f}$. However, in the Heisenberg picture, the states remain static whereas the operators evolve with time. Thus the expansion makes the fluctuation modes χ_n evolve such that they can be expressed as a superposition of 'out'-modes and their complex conjugates, yielding the following mode expansion for the phase operator:

$$\hat{\phi}_1(\theta,t) = \sqrt{\frac{U}{2\pi\mathcal{V}\hbar}} e^{\frac{\gamma t_f}{2\tau}} \times \sum_{n=-\infty}^{\infty} \Big[e^{in\theta}\Big(\alpha_n \chi_n^{\rm out}(t) + \beta_n \chi_n^{\rm out*}(t)\Big)\hat{a}_n + e^{-in\theta}\Big(\alpha_n^* \chi_n^{\rm out*}(t) + \beta_n^* \chi_n^{\rm out}(t)\Big)\hat{a}_n^\dagger \Big], \tag{3.6}$$

with relative probability amplitudes α_n and β_n, known as the Bogoliubov coefficients that satisfy the normalization condition $|\alpha_n|^2 - |\beta_n|^2 = 1$. Since the quantum field for phase has evolved from the initial mode expansion in Eq. (3.2) to the final in Eq. (3.6), the notion of vacuum state carried by the fluctuations also changes. The above mode expansion can be rearranged to give an expression similar to Eq. (3.2) accompanied by replacing the ladder operators $\hat{a}_n \rightarrow \hat{b}_n$, that annihilate the new 'b-vacuum' state $|0_b\rangle \neq |0_a\rangle$: $\hat{b}_n|0_b\rangle = 0$, yielding the Bogoliubov transformation between these two vacua:

$$\hat{b}_n = \alpha_n \hat{a}_n + \beta_n^* \hat{a}_{-n}^\dagger. \tag{3.7}$$

Thus if I start with a toroidal condensate in a state with no phonons i.e. characterized by the 'a-vacuum' $\langle 0_a|\hat{a}_n^\dagger \hat{a}_n|0_a\rangle = 0$, then after going through an expansion phase, the final

static BEC described by the 'b-vacuum' will be seen as if bubbling with 'a-particles' i.e. $\langle 0_b|\hat{a}_n^\dagger \hat{a}_n|0_b\rangle = |\beta_n|^2$.

In Ref. [76], the particle creation probability $|\beta_n|^2$ was calculated, as a function of the mode index n, for the case of exponential expansion $R(t) = R_0 e^{t_{\rm f}/\tau}$ and for various values of the quantum pressure parameter γ. The probability for particle creation in general decreases with mode index n, being much larger for small mode indices such as $n = 1$. This fact is consistent with the well-known horizon exit phenomena in early-universe cosmology which states that low frequency modes (like $n = 1$), exit the horizon early in the expansion and thus their amplitude freezes, whereas the high frequency modes remain inside the horizon and undergo damping leading to considerable power loss. The reason this spontaneous phonon generation happens is because the quantum pressure parameter γ in (3.5) forces the mode function χ_n to undergo amplitude damping in mode n, which then gets used into creating phonons in mode $-n$, thereby changing the direction of travel inside the toroid. Thus, the two key ingredients responsible for the success of the inflationary paradigm, i.e., particle creation and the horizon exit mechanism, can also manifest in the toroidal BEC setup.

A good approximation to $|\beta_n|^2$ results if I Taylor expand it for small damping $\gamma \ll 1$ and large mode index $n \gg 1$, giving us:

$$|\beta_n|^2 \approx \frac{1}{n^2}\Big(\frac{\gamma}{4}\Big)^2\Big(\frac{c\tau}{R_0}\Big)^{-2}\big[1 + a^2 - 2a\cos\big(2n\theta_{\rm H}\big)\big], \tag{3.8}$$

where the scale factor $a = e^{\frac{t_f}{\tau}}$ is the ratio of final and initial radii R_f/R_0, and $\theta_{\rm H} = \frac{c\tau}{R_0}\big(1 - a^{-1}\big)$ is the angular horizon size at the end of the expansion. The cosine term in Eq. (3.8) leads to oscillations in the particle creation probability versus mode index [76],

with the oscillation scale being $(2\theta_{\rm H})^{-1}$. Using Eq. (3.1), the final static Hamiltonian can be diagonalized in terms of the 'out'-mode basis associated with annihilation operators $\hat{b}_n$:

$$\hat{H}^{\rm out} = \sum_{n=-\infty}^{\infty} \frac{1}{2}\hbar\omega_n^{\rm f}\left[\hat{b}_n\hat{b}_n^\dagger + \hat{b}_n^\dagger\hat{b}_n\right], \tag{3.9}$$

where the presence of time translation symmetry in the final static regime permits a description in terms of particles (phonons). The phenomena of spontaneous particle creation can be understood using an analogy with a quantum mechanical particle occupying the ground state in a one-dimensional box. If the box is now expanded suddenly, then in the sudden approximation of quantum mechanics, the new wave-function for the particle can be written as a linear combination of the eigenstates of the original Hamiltonian. This would not be the case if the box were expanded very slowly, in which case there would be sufficient time for the wave-functions to change their form to conform with the new Hamiltonian.

Using the Bogoliubov transformation Eq. (3.7) along with the annihilation relation $\hat{b}_n|0_b\rangle = 0$, it can be shown that the 'b-vacuum' which characterizes the final static regime can be expressed as a superposition of excited 'a-particle' states as follows [46]:

$$|0_b\rangle = \prod_{n\in\mathcal{Z}} \frac{1}{\sqrt{|\alpha_n|}} e^{\frac{\beta_n}{2\alpha_n}\hat{a}_n^\dagger\hat{a}_{-n}^\dagger}|0_a\rangle. \tag{3.10}$$

This way of expressing a state as an exponential of a quadratic product of creation operators acting on the vacuum is known as a two-mode squeezed state. Thus the 'b-vacuum' is a squeezed state with respect to the 'a-vacuum', and vice-versa. The physical picture here is that the expanding BEC creates pairs of phonons in modes n and $-n$ that travel opposite to each other and are entangled. In the next section, I will use the theory of Gaussian

continuous variables to discuss in what sense these phonon pairs are entangled by first describing the covariance matrix (which has complete information about a system's correlations), how to perform partial transposition on it, and then how to quantify entanglement using Logarithmic Negativity. I will also see how finite temperature of the BEC is detrimental to this mode entanglement and how it can be recovered by preparing the initial BEC with phonons in single mode squeezed states.

3.2. Gaussian States and Entanglement in the Ring

In the previous section, I discussed how a rapidly expanding toroidal BEC spontaneously generates phonons from the vacuum. In Ref. [76], it was shown that the density-density correlations between phonons with respect to the ring angle exhibits a cusp like feature at zero temperature, and a kink like feature at finite temperatures, with their locations scaling with the horizon size, and their amplitude increases with quantum pressure and temperatures. In this section, I will investigate whether these correlations due to dynamical phonon creation are quantum or classical in nature, i.e., whether the phonons are entangled or not. If the system has entanglement in it, then its correlations cannot be reproduced by any classical process, and hence they are called quantum correlations.

The fluctuations inside a BEC can be represented by quantum fields of phase $\hat{\phi}_1(\theta)$ and density $\hat{n}_1(\theta)$, that possess infinite degrees of freedom (as the mode index can be any integer). Therefore, they can be described using continuous variable quantum states. Any quantum state having N degrees of freedom can be described by a vector of $2N$ quadrature operators $\hat{\boldsymbol{r}} = (\hat{x}_1, \hat{p}_1, \hat{x}_2, \hat{p}_2, ...)^{\mathrm{T}}$, made of canonically conjugate Hermitian operators $\hat{x}$ and $\hat{p}$ per degree of freedom. Since I study entanglement between modes n and $-n$ in

the toroid, I need this formalism for the case of $N = 2$. Thus, the hermitian conjugate pairs are $(\hat{X}_n, \hat{P}_n, \hat{X}_{-n}, \hat{P}_{-n})$ that satisfy the canonical commutation relations $[\hat{\boldsymbol{r}}, \hat{\boldsymbol{r}}^{\mathrm{T}}] = i\Omega$, with $\Omega = \Omega_1 \otimes I_n$, where $\Omega_1 = \begin{bmatrix} 0 & 1 \\ -1 & 0 \end{bmatrix}$ is the symplectic form and I_n is the $n \times n$ identity matrix. Gaussian states are defined to be those quantum states where any m-point correlator can be decomposed into two-point correlators. For example, when $m = 4$ and I choose vacuum $|0\rangle$ as our Gaussian state, then the four point correlator of a scalar field $\hat{\phi}(x)$ becomes:

$$\begin{aligned} \langle\hat{\phi}(\theta_1)\hat{\phi}(\theta_2)\hat{\phi}(\theta_3)\hat{\phi}(\theta_4)\rangle &= \langle\hat{\phi}(\theta_1)\hat{\phi}(\theta_2)\rangle\langle\hat{\phi}(\theta_3)\hat{\phi}(\theta_4)\rangle + \langle\hat{\phi}(\theta_1)\hat{\phi}(\theta_3)\rangle\langle\hat{\phi}(\theta_2)\hat{\phi}(\theta_4)\rangle \\ &+ \langle\hat{\phi}(\theta_1)\hat{\phi}(\theta_4)\rangle\langle\hat{\phi}(\theta_2)\hat{\phi}(\theta_3)\rangle, \end{aligned} \tag{3.11}$$

which can be derived using Wick's theorem. Here I assumed that the vacuum average of the individual field operators is zero. Thus any correlation function that involves an even number of phase $\hat{\phi}(\theta)$ and/or density $\hat{n}(\theta)$ operators can be decomposed in terms of the first and second moments, whereas any odd combination of such field operators vanishes identically. Thus Gaussian states are completely characterized by their first moments or the mean vector $\boldsymbol{\mu} = \langle\hat{\boldsymbol{r}}\rangle$, and the anti-symmetrized second moments or the covariance matrix $\boldsymbol{\sigma} = \langle\{(\hat{\boldsymbol{r}} - \boldsymbol{\mu}), (\hat{\boldsymbol{r}} - \boldsymbol{\mu})^{\mathrm{T}}\}\rangle$. I subtract $\boldsymbol{\mu}$ in the definition of $\boldsymbol{\sigma}$ to avoid having redundant information in the first and second moments. One focuses on the symmetric part of the second moments because the anti-symmetric part is determined by the canonical commutation relations, and is state independent.

Alternatively, Gaussian states can also be defined as all the ground and thermal states of Hamiltonians that are quadratic in the quadrature operators [87]: $\hat{H} = \frac{1}{2}\hat{\boldsymbol{r}}^{\mathrm{T}} H \hat{\boldsymbol{r}} + \hat{\boldsymbol{r}}^{\mathrm{T}}\boldsymbol{r}$, where $\boldsymbol{r}$ is a $2N$-dimensional real vector and H is the real, symmetric and positive

definite Hamiltonian matrix. As a result, the density operator for any mixed Gaussian state can be written as:

$$\hat{\rho}_{\mathrm{G}} = \frac{e^{-\beta \hat{H}}}{\mathrm{Tr}\left[e^{-\beta \hat{H}}\right]}, \tag{3.12}$$

where $\beta \in \mathbb{R}^{+}$, and the limit $\beta \to 0$ represents pure Gaussian states. The quadratic nature of the Hamiltonian implies that its unitary action on such states is a linear evolution of the quadrature governed by symplectic transformations [87], thereby preserving the Gaussianity of the quantum states.

To quantify entanglement of Gaussian states, I make use of the positivity of partial transpose (PPT) criterion, which states that if a Gaussian state with a $2N$-dimensional covariance matrix $\boldsymbol{\sigma}$ under partial transposition $\tilde{\boldsymbol{\sigma}} = T\boldsymbol{\sigma}T$, has an eigenvalue with absolute value less than unity, then the system is entangled. The minimum symplectic eigenvalue, if it exists, can then be used to calculate the Logarithmic Negativity $E_{\mathcal{N}}[n]$,

$$E_{\mathcal{N}}[n] = \log_2 ||\tilde{\rho}||, \tag{3.13}$$

where $\tilde{\rho}$ is the partially transposed density matrix and $||\hat{A}||$ represents the sum of the absolute value of the eigenvalues of $\hat{A}$. This corresponds to finding the logarithm of the absolute value of the minimum symplectic eigenvalue of the partially transposed covariance matrix $\tilde{\boldsymbol{\sigma}}$. Note that if all the symplectic eigenvalues are greater than unity, then $E_{\mathcal{N}}[n]$ is defined to be zero. In general for multi-mode Gaussian states, the PPT-criterion is necessary and sufficient for the existence of entanglement between one versus n modes, but for other bi-partitions such as two modes versus n modes, this criterion is sufficient but not necessary. However, $E_{\mathcal{N}}[n]$ is still a consistent entanglement monotone, i.e. a quantity that does not increase under local operations and classical communication (LOCC) [87].

For a bipartite Gaussian state such as the toroidal BEC phonons in modes n and $-n$, the covariance matrix is defined in terms of quadratures $\{\hat{X}_{\pm n}, \hat{P}_{\pm n}\}$ (I take $\boldsymbol{\mu} = 0$ for vacuum, thermal or squeezed state averages of phase and density operators):

$$\boldsymbol{\sigma} = \begin{bmatrix} \langle\{\hat{X}_n, \hat{X}_n\}\rangle & \langle\{\hat{X}_n, \hat{P}_n\}\rangle & \langle\{\hat{X}_n, \hat{X}_{-n}\}\rangle & \langle\{\hat{X}_n, \hat{P}_{-n}\}\rangle \\ \langle\{\hat{P}_n, \hat{X}_n\}\rangle & \langle\{\hat{P}_n, \hat{P}_n\}\rangle & \langle\{\hat{P}_n, \hat{X}_{-n}\}\rangle & \langle\{\hat{P}_n, \hat{P}_{-n}\}\rangle \\ \langle\{\hat{X}_{-n}, \hat{X}_n\}\rangle & \langle\{\hat{X}_{-n}, \hat{P}_n\}\rangle & \langle\{\hat{X}_{-n}, \hat{X}_{-n}\}\rangle & \langle\{\hat{X}_{-n}, \hat{P}_{-n}\}\rangle \\ \langle\{\hat{P}_{-n}, \hat{X}_n\}\rangle & \langle\{\hat{P}_{-n}, \hat{P}_n\}\rangle & \langle\{\hat{P}_{-n}, \hat{X}_{-n}\}\rangle & \langle\{\hat{P}_{-n}, \hat{P}_{-n}\}\rangle \end{bmatrix}. \tag{3.14}$$

Then under partial transposition, i.e. transpose operation $T = \text{diag}(1, 1, 1, -1)$ on one of its modes, I get the partially transposed covariance matrix: $\tilde{\boldsymbol{\sigma}} = T\boldsymbol{\sigma}T$. If this has a an eigenvalue with absolute value less than unity, then according to the PPT-criterion, the system is entangled. Note, that this criterion is a necessary and sufficient for the existence of entanglement in two-mode Gaussian systems, such as between the toroidal BEC phonons in modes n and $-n$.

In the subsequent subsections, I will construct the covariance matrix for states pertaining to the particle creation process (see Eq. (3.10)) for various types of initial inputs (such as vacuum, thermal and single-mode squeezed), describe how to perform partial transposition, and hence calculate the symplectic eigenvalues that will help to quantify entanglement as $E_{\mathcal{N}}[n]$.

Quadratures and time evolution

As I discussed in the previous section, the fluctuations inside the toroidal BEC as described by a real scalar field $\hat{\phi}_1(\theta)$ and its conjugate momenta $\hat{n}_1(\theta)$, is a set of infinite harmonic oscillator for each mode index n. In the initial static regime, I can expand the

the phase field in terms of plane wave modes $\chi_n^{\rm in}(t) = (2\omega_n^0)^{-1/2}e^{-i\omega_n^0 t}$ and ladder operators $\hat{a}_n$, whereas, in the final static phase, the mode expansion in Eq. (3.6) is in terms of $\chi_n^{\rm out}(t) = (2\omega_n^{\rm f})^{-1/2}e^{-i\omega_n^{\rm f} t}$ and $\hat{b}_n$. These modes satisfy the equation $\ddot{\chi}_n + \omega_n^2\chi_n = 0$, and therefore, in analogy with the quantum harmonic oscillator, I can define canonically conjugate Hermitian operators for mode n as $\hat{X}_n = \frac{1}{\sqrt{2}}(\hat{a}_n + \hat{a}_n^\dagger)$ and $\hat{P}_n = -\frac{i}{\sqrt{2}}(\hat{a}_n - \hat{a}_n^\dagger)$. To construct the covariance matrix I define the vector of quadrature operators pertaining to the two modes n and $-n$ as $\hat{\boldsymbol{r}} = (\hat{X}_n, \hat{P}_n, \hat{X}_{-n}, \hat{P}_{-n})^{\rm T}$ and use it in $\boldsymbol{\sigma} = \langle\{(\hat{\boldsymbol{r}} - \boldsymbol{\mu}), (\hat{\boldsymbol{r}} - \boldsymbol{\mu})^{\rm T}\}\rangle$, where I have taken the mean vector $\boldsymbol{\mu} = \langle\hat{\boldsymbol{r}}\rangle = 0$ as I will not be considering coherent states. Using this definition, the covariance matrix for the initial static BEC is:

$$\boldsymbol{\sigma}^{\rm in} = (1 + 2n_{\rm B})\mathbb{I}_4, \tag{3.15}$$

where $n_{\rm B}(x) = (e^x - 1)^{-1}$ is the Bose-Einstein distribution. I can similarly evaluate the final case $\boldsymbol{\sigma}^{\rm out}$ by evaluating all the vacuum averages of the $\hat{b}$-operators. Alternatively, I could define a vector of ladder operators before $\hat{\boldsymbol{A}}^{\rm in} = (\hat{a}_n, \hat{a}_{-n}, \hat{a}_n^\dagger, \hat{a}_{-n}^\dagger)^{\rm T}$, and after expansion $\hat{\boldsymbol{A}}^{\rm out} = (\hat{b}_n, \hat{b}_{-n}, \hat{b}_n^\dagger, \hat{b}_{-n}^\dagger)^{\rm T}$, that satisfy commutation relations: $[\hat{\boldsymbol{A}}, \hat{\boldsymbol{A}}^{\rm T}] = J$, with $J = \begin{bmatrix} 0 & I_2 \\ -I_2 & 0 \end{bmatrix}$ being the symplectic form in this basis. The quadrature operators $\hat{\boldsymbol{r}}$ can be written in terms of ladder operators using the following unitary operation $\hat{U}$:

$$\hat{\boldsymbol{r}} = U\hat{\boldsymbol{A}}, \qquad U \equiv \frac{1}{\sqrt{2}}\begin{bmatrix} 1 & 0 & 1 & 0 \\ -i & 0 & i & 0 \\ 0 & 1 & 0 & 1 \\ 0 & -i & 0 & i \end{bmatrix}, \tag{3.16}$$

To describe the initial state, I build the covariance matrix in the space of annihilation operators as $\boldsymbol{\sigma}_{\rm A}^{\rm in} = \langle\{\hat{\boldsymbol{A}}^{\rm in}, \left(\hat{\boldsymbol{A}}^{\rm in}\right)^{\rm T}\}\rangle$, which is related to the physical covariance matrix via the

unitary evolution $\boldsymbol{\sigma}_{\rm A}^{\rm in} = U^\dagger \boldsymbol{\sigma}^{\rm in} U$. For an initial state with thermal noise (i.e., characterized by a finite temperature T density matrix) I get:

$$\boldsymbol{\sigma}_{\rm A}^{\rm in} = (1 + 2n_{\rm B}(E_n)) \begin{bmatrix} 0 & 1 \\ 1 & 0 \end{bmatrix}, \tag{3.17}$$

where $n_{\rm B}(x) = (e^{\beta x} - 1)^{-1}$ is the Bose-Einstein distribution with $\beta = (k_{\rm B}T)^{-1}$ and $k_{\rm B}$ the Boltzmann constant. Here, the Bogoliubov energy dispersion is $E_n = \sqrt{\epsilon_n(\epsilon_n + 2Mc^2)}$, with c the speed of sound and $\epsilon_n = \frac{\hbar^2 n^2}{2MR^2}$ the single particle energy in the toroid. In the hydrodynamic limit of interest here, in which the mode wavelength is large compared to the coherence length, I can approximate $E_n \simeq \frac{\hbar c}{R}|n|$.

As I have discussed, the impact of the inflationary regime on the toroidal BEC is captured by the Bogoliubov transformation Eq. (3.7), which implies the following relation between the initial (in) and final (out) ladder operators:

$$\hat{\boldsymbol{A}}^{\rm out} = S_{\rm A} \hat{\boldsymbol{A}}^{\rm in}, \qquad S_{\rm A} \equiv \begin{bmatrix} \alpha_n & 0 & 0 & \beta_n \\ 0 & \alpha_n & \beta_n & 0 \\ 0 & \beta_n^* & \alpha_n^* & 0 \\ \beta_n^* & 0 & 0 & \alpha_n^* \end{bmatrix}. \tag{3.18}$$

As a result, the out covariance matrix is easily obtained from the in covariance matrix via $\boldsymbol{\sigma}_{\rm A}^{\rm out} = S_{\rm A} \boldsymbol{\sigma}_{\rm A}^{\rm in} S_{\rm A}^T$. Performing this computation for the case of the initial thermal state in

Eq. (3.17), and transforming back to the physical variables via $\boldsymbol{\sigma}^{\rm out} = U\boldsymbol{\sigma}_{\rm A}^{\rm out}U^\dagger$, I get:

$$\boldsymbol{\sigma}^{\rm out} = (1+2n_{\rm B}) \times \begin{bmatrix} |\alpha_n|^2+|\beta_n|^2 & 0 & \alpha_n\beta_n+\alpha_n^*\beta_n^* & -i(\alpha_n\beta_n-\alpha_n^*\beta_n^*) \\ 0 & |\alpha_n|^2+|\beta_n|^2 & -i(\alpha_n\beta_n-\alpha_n^*\beta_n^*) & -(\alpha_n\beta_n+\alpha_n^*\beta_n^*) \\ \alpha_n\beta_n+\alpha_n^*\beta_n^* & -i(\alpha_n\beta_n-\alpha_n^*\beta_n^*) & |\alpha_n|^2+|\beta_n|^2 & 0 \\ -i(\alpha_n\beta_n-\alpha_n^*\beta_n^*) & -(\alpha_n\beta_n+\alpha_n^*\beta_n^*) & 0 & |\alpha_n|^2+|\beta_n|^2 \end{bmatrix}, \tag{3.19}$$

where I dropped the argument of the Bose function (which is always E_n) for brevity. I note that a vacuum input corresponds to the zero temperature limit of the above covariance matrix that makes the Bose function vanish. Note that the procedure outlined to obtain (3.19), can be summarized by the formula: $\boldsymbol{\sigma}^{\rm out} = \hat{U}\hat{S}_{\rm A}\boldsymbol{\sigma}_{\rm A}^{\rm in}\hat{S}_{\rm A}^{\rm T}\hat{U}^\dagger$. Thus, once the input state $\boldsymbol{\sigma}_{\rm A}^{\rm in}$ has been given, then all is needed are the Bogoliubov transformation matrix (3.18) and the unitary evolution matrix (3.16) to determine the covariance matrix after expansion.

Our next task is to implement the partial transpose of the covariance matrix. To do this, I note that the transpose of ladder operators: $\hat{b}_n^{\rm T} = \hat{b}_n^\dagger$ and $\hat{b}_n^{\dagger{\rm T}} = \hat{b}_n$, results in the following transposition of the quadrature operators: $\hat{X}_n^{\rm T} = \hat{X}_n$ and $\hat{P}_n^{\rm T} = -\hat{P}_n$. Thus, the process of partial transposition on a two-mode Gaussian system is defined as keeping the n undisturbed, and transposing only the mode $-n$. This procedure is equivalent to changing the sign of momenta for the $-n$ mode, i.e. $\hat{P}_{-n} \to -\hat{P}_{-n}$ when evaluating the covariance matrix. Thus the partial transpose of the covariance matrix in Eq. (3.19) can be found as: $\tilde{\sigma}^{\rm out} = \hat{T}\sigma^{\rm out}\hat{T}$, where $\hat{T} = {\rm diag}(1,1,1,-1)$ is the partial transposition operator for two-

mode Gaussian states. The symplectic eigenvalues of $\tilde{\sigma}^{\rm out}$ are the eigenvalues of the matrix $i\Omega\tilde{\boldsymbol{\sigma}}^{\rm out}$, where the absolute minimum is given by $\lambda_T[n] = (1+2n_{\rm B})\big(|\alpha_n| - |\beta_n|\big)^2$, with subscript T denoting the temperature of the initial BEC. The PPT-criterion states that if $\lambda_T[n] \geq 1$, then the system is separable, otherwise it is entangled. Using the normalization condition for Bogoliubov coefficients $|\alpha_n|^2 - |\beta_n|^2 = 1$, the condition for the existence of entanglement, then takes the following form:

$$n_{\rm B} < |\beta_n|\Big[|\beta_n| + \sqrt{1+|\beta_n|^2}\Big]. \tag{3.20}$$

Since the Bose function, for fixed energies, is an increasing function of temperature, this formula implies that increasing temperature will always lead to a destruction of entanglement, implying that thermal phonons present in the system are detrimental to the entanglement between spontaneously generated phonon pairs.

This condition can also be derived using the Cauchy-Schwarz Inequality (Peres-Horodecki criterion), which is a generalization of Bell's inequality to the mode space. This was used by Steinhauer [21] to quantify entanglement in his Hawking radiation experiment, where phonon pairs are spontaneously created due to presence of an analog BEC black hole horizon. Here the relevant quantity Δ is defined as follows:

$$\Delta = \langle \hat{b}_n^\dagger \hat{b}_n\rangle\langle \hat{b}_{-n}^\dagger \hat{b}_{-n}\rangle - |\langle \hat{b}_n \hat{b}_{-n}\rangle|^2, \tag{3.21}$$

where the averages of 'b'-operators $\hat{b}_n$ is taken with respect to the 'a'-vacuum $|0_{\rm a}\rangle$. This criterion states that if $\Delta < 0$, then the system is entangled, otherwise it is separable. To apply this criteria on the toroidal BEC case, I use the Bogoliubov transformation $\hat{b}_n = \alpha_n \hat{a}_n + \beta_n^* \hat{a}_{-n}^\dagger$, and the thermal averages of the 'a'-operators $\langle \hat{a}_n^\dagger \hat{a}_n\rangle = n_{\rm B}(E_n)$ and $\langle \hat{a}_n \hat{a}_n^\dagger\rangle = (1+n_{\rm B}(E_n))$. Then the expression for the Peres-Horodecki parameter in the toroidal BEC

becomes $\Delta = n_{\rm B}^2 - |\beta_n^2| - 2n_{\rm B}|\beta_n|^2$, and therefore, the condition for the existence of entanglement here turns out to be the same as (3.20). However, the parameter Δ is an entanglement witness, i.e., it only tells us whether a system has entanglement or not. In the next subsection, I use the symplectic eigenvalues discussed here to quantify mode entanglement via logarithmic negativity.

Entanglement generation by the BEC expansion

As I have discussed in Eq. (3.10), the BEC expansion spontaneously creates pairs of phonons in modes n and $-n$ (similar to quantum processes like parametric down-conversion), suggesting that modes traveling in opposite directions could be entangled. In this subsection, I quantify these quantum correlations by means of logarithmic negativity for various model parameters, and for vacuum and noisy input states.

For the final static BEC, the discussion following Eq. (3.13) implies finding the logarithm of the minimum symplectic eigenvalue of the partially transposed of covariance matrix in Eq. (3.19), which gives us:

$$E_{\mathcal{N}}[n] = \text{Max}\Big(0, -\log_2\Big[(1+2n_{\rm B})(|\alpha_n| - |\beta_n|)^2\Big]\Big), \tag{3.22}$$

In Fig. 3.1, I plot $E_{\mathcal{N}}[n]$ for the corresponding Bogoliubov coefficients derived in [76] (please see Fig. 2.3), and for the system parameters given in Ref. [38]. The input state for this plot is taken to be the vacuum state, i.e. $T = 0$, resulting in $\boldsymbol{\sigma}^{\rm in} = \mathbb{I}_4$. Since $E_{\mathcal{N}}[n]$ is positive in the plots, therefore entanglement exists for all modes at zero temperature i.e. for a vacuum input in the initial ring. This is due to the fact that particle creation leads to two-mode squeezed phonon states which by definition are entangled.

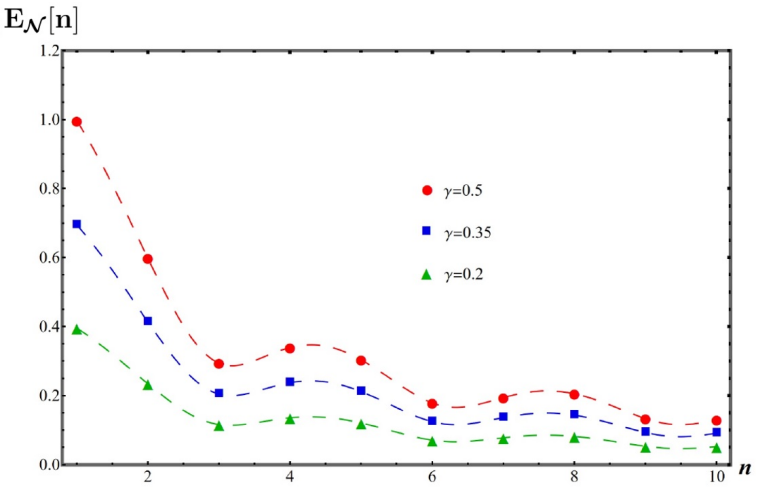

Figure 3.1. Logarithmic Negativity between phonons labeled by n and $-n$, for zero ambient temperature $T=0$, for various values of the quantum pressure $\gamma=0.2$ (*green*), $\gamma = 0.35$ (*blue*) and $\gamma = 0.5$ (*red*). The mode index n is discrete; I have added a continuous dashed line to increase the visibility of the overall dependence of $E_{\mathcal{N}}$ with n. This plot corresponds to an exponentially expanding ring, with radius $R(t) = R_0 e^{t/\tau}$, where I took the initial radius to be $R_0 = 10\mu$m, the duration of expansion to be $t_f = 10$ms, the timescale governing the trap expansion to be $\tau = 6.21$ms, speed of sound to be $c = 2$ mm/s, and $n_c = 10$, as I did for particle creation parameter in Fig. 2.3.

As a next step in our analysis, I study the case of a noisy input, corresponding to $\boldsymbol{\sigma}^{\rm in} = (2n_{\rm B} + 1)\mathbb{I}_4$. The logarithmic negativity as function of the Bogolioubov coefficients and the BEC temperature is given by (3.22). In general, a noisy input in the initial ring i.e. $T_{\rm env} \neq 0$, is detrimental to this mode entanglement as can be clearly seen from Fig. 3.2. Mathematically, this can be understood from the form of the minimum symplectic eigenvalue which is directly proportional to the Bose factor. As the temperature increases, so does the Bose factor and therefore the symplectic value, and at some critical temperature this eigenvalue becomes larger than unity and hence all the entanglement in the system vanishes.

There are some interesting physical features to note from these plots. First, note that entanglement at $T = 0$, is maximum for low energy modes ($n = 1$), and decreases

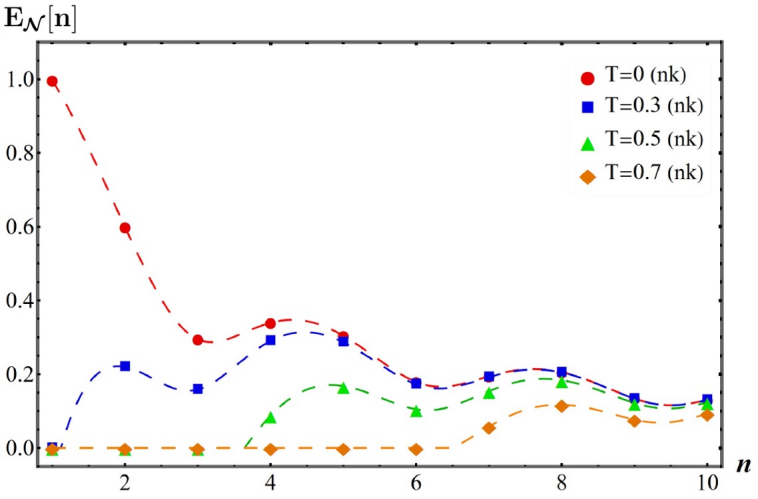

Figure 3.2. Logarithmic negativity $E_{\mathcal{N}}(n)$ versus the mode index n, for various values of the environment temperature, $T = 0$nK (*red*), $T = 0.3$nK (*blue*), $T = 0.5$nK (*green*), and $T = 0.7$nK (*orange*). The figure shows that entanglement in the final state is degraded by ambient thermal noise, and that the entanglement in pairs with small n is more fragile. For this plot I use quantum pressure $\gamma = 0.5$, and used the parameters given in Ref. [76].

with increasing mode index with oscillations at the scale of inverse horizon size, as can be seen from Eq. (3.8). This is due to the fact long wavelength modes, such as $n = 1$, exit the horizon earlier compared to other modes $n \geq 2$ during the expansion phase (see Ref. [76]). Thus their amplitude freezes, thereby conserving their power and producing a relatively larger number of entangled phonon pairs in the final static regime. On the other hand, high frequency modes stay confined well within the horizon and thus go through considerable damping, thus generating much fewer entangled phonons. With increasing temperature, the entanglement in low energy modes disappears at a lower temperature, than the high energy modes. This is due to the fact that spontaneous phonon creation happens with probability $|\beta_n|^2 \sim \frac{1}{n^2}$ (see Eq. (3.8)) and thus dies off slowly, whereas the thermal phonons (similar to blackbody photons) are generated in huge numbers for low energy modes, and die of exponentially with the mode index i.e. $e^{-\beta E_n}$.

To determine the temperature $T_{\rm v}$ at which entanglement in the mode pair $(n, -n)$

vanishes, I set that $E_{\mathcal{N}}[n] = 0$ given by (3.22), and solve for $T_{\rm v}$ as a function of the mode index n, yielding the following expression:

$$T_{\rm v}(n) = \frac{E_n}{k_B}\left[E_{\mathcal{N}}\left\{1 + \frac{1}{|\beta_n|(\beta_n + \sqrt{1+|\beta_n|})}\right\}\right]^{-1}, \tag{3.23}$$

for which I made use of the normalization condition for the Bogoliubov coefficients $|\alpha_n|^2 - |\beta_n|^2 = 1$. The denominator inside the logarithm is the same as the condition for the condition for the existence of entanglement in Eq. (3.20), which was also derived using the Peres-Horodecki parameter Δ in Eq. (3.21). In Fig. 3.3, I plot $T_{\rm v}(n)$, which in general increases with the mode index n confirming that the entanglement at lower modes n is more sensitive to the BEC temperature, as a lower value temperature is needed to remove the entanglement in those modes. The oscillatory nature of the function $T_{\rm v}(n)$ is due to the oscillations in the particle creation parameter $|\beta_n|^2$ due to the presence of a cosine term involving the sonic horizon size $\cos(2n\theta_{\rm H})$, appearing in Eq. (3.8) [76]. In the next subsection, I will discuss how this loss of entanglement due to a thermal bath of phonons could be rescued by the use of single mode squeezed states.

Single mode squeezed states and inputs

In previous subsection, I saw how logarithmic negativity helps us quantify the mode entanglement of phonons in a BEC at zero temperature, and how thermal noise degrades it and makes it vanish at temperature $T_{\rm v}$ given in Eq. (3.23). This could be a problem because according to Fig. 3.2, the entanglement in mode $n = 1$ vanishes at very low temperatures (of the order of nano Kelvins), and it is difficult to create higher angular modes in the ring without exciting the radial or vertical modes (see Ref. [38]).

To mitigate this, in this subsection, I propose using single-mode squeezed states

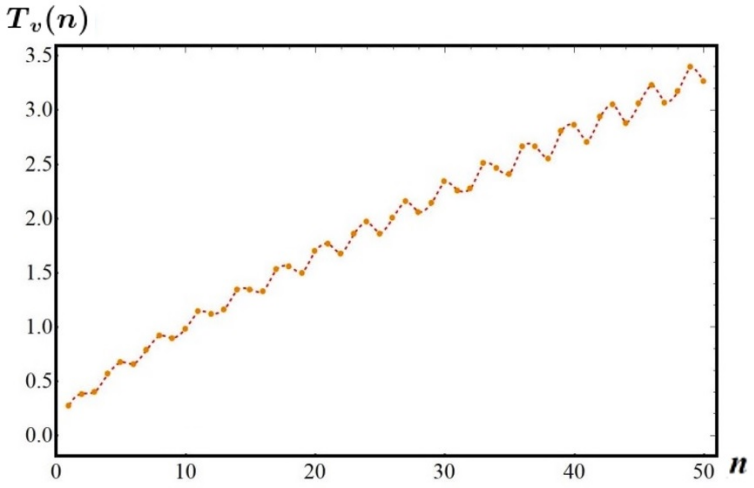

Figure 3.3. The temperature $T_{\rm v}(n)$ (in nK) at which the entanglement in the mode pair $(n, -n)$ completely vanishes. Larger ambient temperature is needed to degrade the entanglement in pairs with large mode index n. The oscillations originate in the oscillatory character of $|\beta_n|^2$. This figure uses the same parameters as in Fig. 3.2.

in mode n, keeping the other mode $-n$ in the vacuum, that acts as a quantum resource. Such states can be generated using the quadratic Hamiltonian [87]: $\hat{H}_n^{\rm sq} = \frac{r}{2}\hat{\boldsymbol{r}}^{\rm T}\sigma_x\hat{\boldsymbol{r}} = r\hat{X}_n\hat{P}_n = \frac{r}{2i}(\hat{a}_n^2 - \hat{a}_n^{\dagger 2})$, where r is the squeezing parameter which in general is complex (physically achieved when a squeezed state goes through a phase shifter that rotates the optical squeezing phase). This squeezing Hamiltonian generates translation in the squeezing parameter r, yielding the state vector: $|r\rangle_n = e^{-ir\hat{H}_n^{\rm sq}} = e^{\frac{r}{2}(\hat{a}_n^{\dagger 2} - \hat{a}_n^2)}$, that corresponds to a mixing of creation and annihilation in the mode n, as follows:

$$\hat{a}_n \to \cosh r\ \hat{a}_n + e^{i\phi}\sinh r\ \hat{a}_n^{\dagger}, \tag{3.24}$$

where ϕ is the squeezing phase or angle. From this, the covariance matrix of a two mode

system that is squeezed in one of the subsystems takes the following form:

$$\boldsymbol{\sigma}_r^{\text{in}} = (1+2n_{\text{B}}) \begin{bmatrix} e^{2r} & 0 & 0 & 0 \\ 0 & e^{-2r} & 0 & 0 \\ 0 & 0 & 1 & 0 \\ 0 & 0 & 0 & 1 \end{bmatrix}, \tag{3.25}$$

where I have taken $r \in \mathbb{R}$. This is the covariance matrix for the initial static BEC prepared in a thermally seeded single-mode squeezed state. Evolving this state, I obtain the entanglement between modes n and $-n$ to be:

$$\begin{aligned} \lambda_{\text{T},r}[n] &= (1+2n_{\text{B}})\Big[\big(|\alpha_n|^2+|\beta_n|^2\big)^2 + 4|\alpha_n|^2|\beta_n|^2\cosh(2r) \\ &- 4|\alpha_n||\beta_n|\cosh r\sqrt{|\alpha_n|^4+|\beta_n|^4+2|\alpha_n|^2|\beta_n|^2\cosh(2r)}\Big]^{\frac{1}{2}}, \end{aligned} \tag{3.26}$$

which is invariant under the phase transformations $r \to re^{i\theta}$, and therefore, real and complex squeezing give the same result for entanglement as (3.26).

In Fig. 3.4, I have plotted the mode entanglement $E_{\mathcal{N}}[n] = -\log_2\big(\lambda_{\text{T},r}[n]\big)$ for various choices of single-mode squeezing parameter r, and fixed values of quantum pressure $\gamma = 0.5$ and thermal noise $T = 0.5$nK. For small values of the squeezing parameter r, the entanglement in the low energy modes like $n = 1$ still dies off, which can be recovered by tuning $r \geq 1.5$, whereas the larger modes always see some enhancement. Thus, initial squeezing amplifies the entanglement generated by the expansion and potentially facilitates in the recovery of the quantum correlations that otherwise would have been lost due to the background thermal noise, as I saw in Fig. 3.2. To explore the dependence of entanglement on the parameter space of the input state, I constructed the color plots in Fig. 3.5

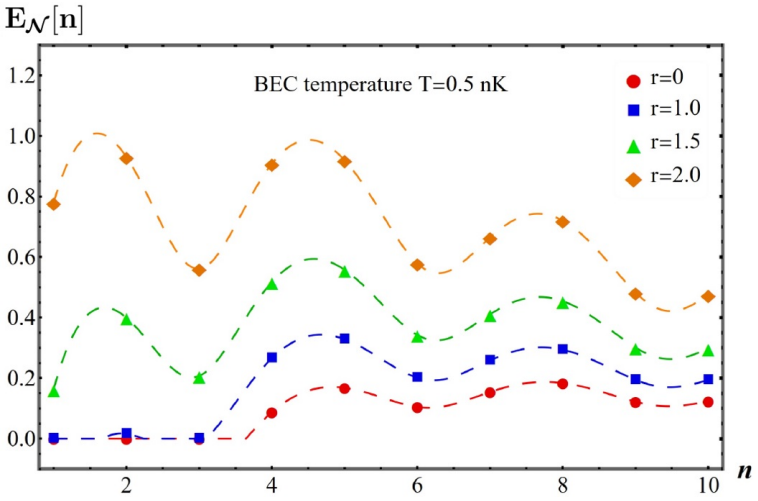

Figure 3.4. Logarithmic negativity $E_{\mathcal{N}}[n]$ for pairs $(n, -n)$, versus the squeezing intensity r and ambient temperature T=0.5nK. Various values of initial squeezing r are shown. This plot corresponds to quantum pressure $\gamma = 0.5$, and the rest of the parameters are the same as in previous plots.

for two different values of the mode index $n = 1$ and $n = 5$, where on the horizontal axis I vary T, on the vertical r, and the color represents the value of $E_{\mathcal{N}}[n]$. The color plots in Fig. 3.5 confirm that the optimal direction in the parameter space for increasing entanglement is moving towards low temperature values T and high initial squeezing r. This is a generic feature regardless of the mode index n. The white regions represent the separability domain, i.e. $E_{\mathcal{N}}[n] = 0$, and there are no quantum correlations in the resulting mode pair due to the dominance of the background temperature over the initial squeezing.

Note that the temperatures needed to observe mode entanglement (see Figs. 3.2, 3.4 and 3.5), appear to be below nano-Kelvins. However, I would like to point out that these results depend on the choice of the temperature scale T_c associate with the BEC interactions, that can be tuned to larger values near a Feshbach resonance. An alternative to this could be to use the techniques in Refs. [91, 92, 93], that have achieved pico-Kelvin temperatures. Thus it should be possible to reduce thermal noise in the toroid such that

entanglement could be detected, and also reduce the thermal losses due to Landau and Beliaev damping [38].

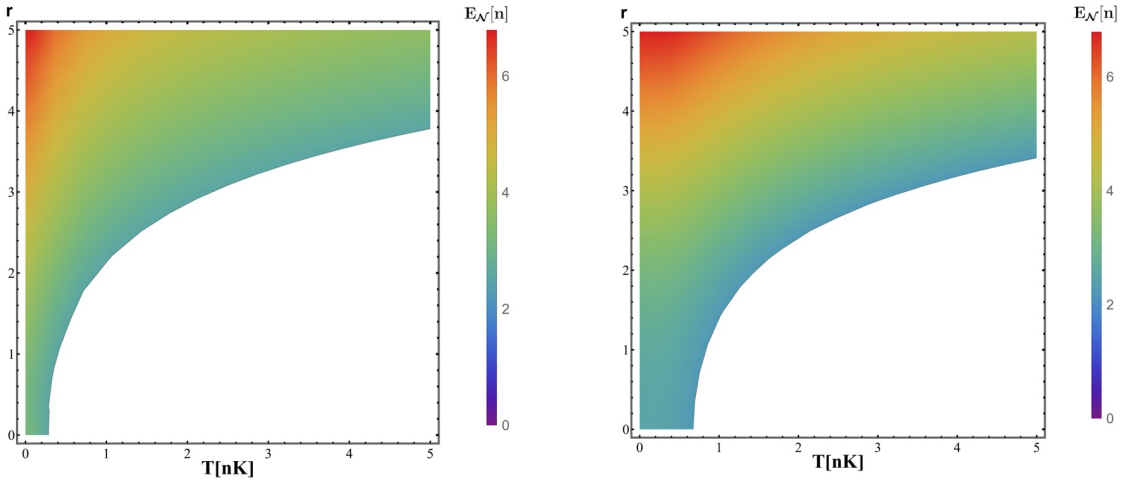

(a) $n = 1$ (b) $n = 5$

Figure 3.5. Color plots of logarithmic negativity $E_{\mathcal{N}}[n]$ as a function of environmental thermal noise T (horizontal axis) and single-mode squeezing parameter r (vertical axis), for two mode numbers: (a) $n = 1$ and (b) $n = 5$. The white region corresponds to no entanglement, i.e., the phonons are classically correlated. A darker shade represents an increase of mode entanglement. For low temperatures and high values of the squeezing parameter, the entanglement is maximum.

Losses and efficiency

The discussion until now assumes an ideal situation where the BEC phonons can be prepared in states (with low temperatures and high squeezing parameters), the process of expansion is an ideal quantum channel, and the probes used to detect fluctuations in the final static BEC are performed with no losses. In reality, finite environment temperatures can give rise to damping due to thermally excited phonons, and the supersonic expansion can give rise to the formation of vortices and solitons [38]. Such processes create an environment where the entangled phonons could undergo decoherence.

I model the losses due to the entire evolution of the toroid by a quantum attenu-

ator channel with efficiency parameter η (see Ref. [87]). I start with a thermally seeded single-mode squeezed state as I discussed in Eq. (3.25), which after unitary evolution gives us $\boldsymbol{\sigma}^{\rm out}$, and then perform an imperfect detection, i.e., $\boldsymbol{\sigma}^{\rm out} \to \eta\boldsymbol{\sigma}^{\rm out}+(1-\eta)\mathbb{I}_4$. In the limit of highly efficient detector $\eta \to 1$, the final covariance matrix possesses entanglement given by Eq. (3.26), whereas in the limit of an inefficient detector (or significant losses) $\eta \to 0$, yields the identity matrix representing a perfectly mixed state with no entanglement. Following the procedure of the previous subsections, I obtain the symplectic eigenvalues as follows:

$$
\begin{aligned}
& \lambda_{{\rm T},r,\eta}[n] = \frac{1}{4\sqrt{2}}\sqrt{X-\sqrt{Y}}, \\
X &= 16\Big[2(1-\eta)^2 + 2(1+2n_{\rm B})^2\eta^2(|\alpha_n|^4+|\beta_n|^4) \\
&+ 4(1+2n_{\rm B})\eta(1-\eta)\cosh^2 r(|\alpha_n|^2+|\beta_n|^2) \\
&+ 4(1+2n_{\rm B})^2\eta^2(1+2\cosh(2r))|\alpha_n|^2|\beta_n|^2\Big], \\
Y &= 256(1+2n_{\rm B})^2\eta^2\Big[16\sinh^4 r(1-\eta)^2(|\alpha_n|^4+|\beta_n|^4) \\
&+ 128(1+2n_{\rm B})^2\eta^2\cosh^2 r\cosh(2r)|\alpha_n|^4|\beta_n|^4 \\
&+ 64(1+2n_{\rm B})^2\eta^2\cosh^2 r(|\alpha_n|^4+|\beta_n|^4)|\alpha_n|^2|\beta_n|^2 \\
&+ 4(1-\eta)^2\big(3+12\cosh(2r)+\cosh(4r)\big)|\alpha_n|^2|\beta_n|^2 \\
&+ 128(1+2n_{\rm B})\eta(1-\eta)\cosh^4 r(|\alpha_n|^2+|\beta_n|^2)|\alpha_n|^2|\beta_n|^2\Big], \qquad (3.27)
\end{aligned}
$$

I took the squeezing parameter r to be real. The logarithmic negativity is then given by $E_{\mathcal{N}}[n] = {\rm Max}\big(0, -\log_2\lambda_{{\rm T},r,\eta}[n]\big)$, which is independent of the squeezing angle ϕ (see Eq. (3.24)). I plot this in Fig. 3.6 which shows that even for highly efficient detectors $\eta = 0.95$, the entanglement loss is significant, especially for low-energy modes. On the other

hand, for large losses, $\eta = 0.70$ the low-energy modes ($n \leq 3$) are completely devoid of any quantum correlations. This shows how important it is to carefully design detectors of high efficiency.

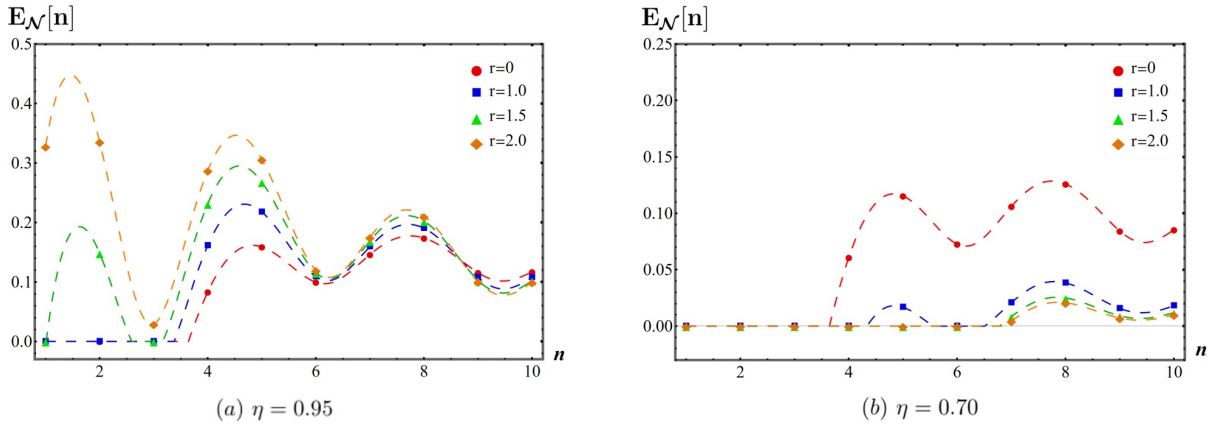

(a) $\eta = 0.95$ (b) $\eta = 0.70$

Figure 3.6. Logarithmic negativity $E_{\mathcal{N}}[n]$ for various values of squeezing intensity r and ambient temperature $T = 0.5$nK, for (a) efficient $\eta = 0.95$, and (b) lossy detectors $\eta = 0.70$ detectors. This plot corresponds to quantum pressure $\gamma = 0.5$, and the rest of the parameters are the same as in previous plots.

In this section, I discussed how entanglement emerges in the exponentially expanding toroidal BEC, for various possible input states such as the vacuum state which gives us the ideal amount of entanglement due the spontaneous creation entangled phonon pairs, thermal noise that degrades this entanglement and squeezed states that could amplifying it. I also looked at losses due to imperfections in the initial state preparation, in the expansion or the detection processes, that could cause decoherence. In the next section, I will present a protocol to experimentally determine the covariance matrix for the final static BEC prepared in any initial state, and thereby deduce the amount of entanglement present in this system.

3.3. Protocol to Measure Entanglement

In Sec. 3.2, I discussed how the covariance matrix is a way to completely specify the quantum state of a system (i.e. its density operator as discussed in Eq. (3.12)), and thus provides us with the information needed to extract observables. I also saw how the quantum states and evolution of the spontaneously generated phonons in an expanding toroidal BEC can be modeled using covariance matrices for two-mode Gaussian states, and how the PPT-criterion helps quantify entanglement between phonons in modes n and $-n$. In this section, our aim is to discuss a protocol that can experimentally measure this entanglement. To that end, I need to build the covariance matrix in the mode space n, where I need two types of vacuum averages of 'b-operators': $\langle\{\hat{b}_n, \hat{b}_n^\dagger\}\rangle$ and $\langle\{\hat{b}_n, \hat{b}_{-n}\}\rangle$ In general, a direct measurement of these mode averages in the BEC is not accessible. On the other hand, it is possible to measure real space correlations between fluctuations separated by angle α. There are three elementary spatial correlations i.e. density-density $C_{nn}(\alpha)$, phase-phase $C_{\phi\phi}(\alpha)$, and the mixed correlation between density and phase $C_{n\phi}(\alpha)$ defined as follows:

$$C_{nn}(\alpha) = \langle\{\hat{n}_1(\alpha), \hat{n}_1(0)\}\rangle, \tag{3.28}$$

$$C_{\phi\phi}(\alpha) = \langle\{\hat{\phi}_1(\alpha), \hat{\phi}_1(0)\}\rangle, \tag{3.29}$$

$$C_{n\phi}(\alpha) = \langle\{\hat{n}_1(\alpha), \hat{\phi}_1(0)\}\rangle. \tag{3.30}$$

In this section, I will discuss a protocol that measures these three independent spatial correlations, thereby yielding all the elements of the covariance matrix, and thus making it possible to experimentally quantify the amount of entanglement in this system.

To measure these spatial correlations, I propose a toroidal version of the technique

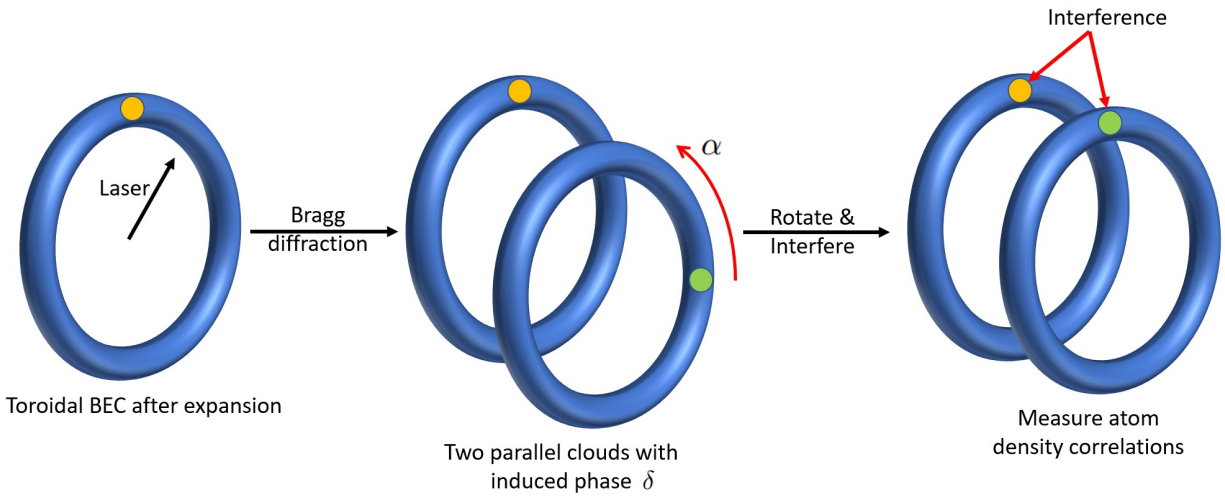

Figure 3.7. A schematic figure showing the protocol to measure mode entanglement in the BEC. The first stage (first panel) is where the expanded BEC is Bragg diffracted using a laser, which then splits into two parallel clouds with an induced phase difference of δ. Then, in the second stage (second panel), one of the rings is rotated by an angle α which brings the two points (shown in green and orange colors) in front of each other. In the third stage (third panel), the two clouds are made to interfere with each other and the atom density correlations are obtained. This setup measures all types of correlations between phase and density fluctuations, and thus the covariance matrix can be built.

due to Hellweg et al. [89], and shown in Fig. 3.7. Suppose the initial static BEC is prepared in either a thermal or a thermally seeded one-mode squeezed state, which upon going through an expansion phase is filled with squeezed phonons. Once the expansion ends, lasers are applied to split the toroidal cloud into two parallel rings. This interaction with lasers leads to Bragg diffraction of the BEC inducing an experimentally controllable phase difference δ between the two separated annular clouds, after which the two clouds that are then allowed to evolve freely for some time. To measure the correlations between any two points on the toroid separated by angle α, one of rings is rotated by this angle with respect to the other. For such controllable angular displacements α and controllable induced

phase difference δ, the final condensate field operator is:

$$\hat{\Phi}(\theta) = \frac{1}{2}\Big[\sqrt{n_0 + \hat{n}_1(\theta - \alpha/2)}e^{i\left(\phi_0 + \hat{\phi}_1(\theta-\alpha/2)\right)} + e^{i\delta}\sqrt{n_0 + \hat{n}_1(\theta + \alpha/2)}e^{i\left(\phi_0 + \hat{\phi}_1(\theta+\alpha/2)\right)}\Big], \tag{3.31}$$

where I have made use of the Madelung representation $\hat{\Phi}(\theta) = \sqrt{\hat{n}}e^{i\hat{\phi}}$ to write the condensate field operator in terms of density $\hat{n}$ and phase operators $\hat{\phi}$, and introduced angle-dependent perturbations in them $\hat{n} = n_0 + \hat{n}_1(\theta)$ and $\hat{\phi} = \phi_0 + \hat{\phi}_1(\theta)$ as described in Eq. (3.1).

The two clouds are then made to interfere with each other and the condensate density correlations are measured for two points opposite to each other present on the two rings i.e. $\langle \hat{N}(\theta)\hat{N}(\theta)\rangle$, where $\hat{N}(\theta) = \hat{\Phi}^\dagger(\theta)\hat{\Phi}(\theta)$ is the condensate density. For simplicity, I will set $\theta = 0$, and work with the anti-symmetrized correlations $\langle\{\hat{N}(0), \hat{N}(0)\}\rangle_{\alpha,\delta}$ labelled by chosen values of rotation angle α and induced Bragg phase δ. Since the condensate density can be written in terms of phase $\hat{\phi}_1(\theta)$ and density $\hat{n}_1(\theta)$ of fluctuations, the condensate correlation can be written in terms of the three types of correlators between fluctuations as follows:

$$\langle\{\hat{N}(0), \hat{N}(0)\}\rangle_{\alpha,\delta} = \frac{1}{2}n_0^2(1+\cos\delta)^2 + \frac{1}{16}\Big[\tilde{C}_{nn}(\alpha)(1+\cos\delta)^2 + 4n_0^2\tilde{C}_{\phi\phi}(\alpha)\sin^2\delta\Big]. \tag{3.32}$$

Fixing the relative rotation angle α and choosing two different induced phases, say δ_1 and δ_2, the above linear equation can be solved yielding the modified correlation functions (marked by a tilde $\tilde{C}$) that can be related to the elementary correlation functions between density and phase i.e. C_{nn}, $C_{\phi\phi}$ and $C_{n\phi}$ as follows:

$$\tilde{C}_{nn}(\alpha) = -2\Big(C_{nn}(\alpha) - C_{nn}(0)\Big), \tag{3.33}$$

$$\tilde{C}_{\phi\phi}(\alpha) = -2\Big(C_{\phi\phi}(\alpha) - C_{\phi\phi}(0)\Big), \tag{3.34}$$

that gives the difference between the elementary correlations measured with some rotation angle α and with no relative ring rotation.

In order to extract the elementary correlations, the above steps need to be repeated for several relative rotation angles $\alpha \in (0, 2\pi)$ (in discrete steps owing to angular resolution). Then, an angular average can be performed on the above modified correlations by numerically integrating over all possible angles α, giving:

$$\begin{aligned}
\frac{1}{4\pi}\int_0^{2\pi} d\alpha\ \tilde{C}_{nn}(\alpha) &= \frac{1}{4\pi}\int_0^{2\pi} d\alpha\ -2\Big(C_{nn}(\alpha) - C_{nn}(0)\Big) \\
&= -\frac{1}{2\pi}\int_0^{2\pi} d\alpha\ C_{nn}(\alpha) + \frac{1}{2\pi}\int_0^{2\pi} d\alpha\ C_{nn}(0) \\
&= C_{nn}(0), \qquad (3.35)
\end{aligned}$$

where in the first line I made use of (3.33), and in going from second to third line, I made use of the identity: $\int_0^{2\pi} d\alpha\ e^{in\alpha} = \delta_{n,0}$. Since we are dealing with perturbations here, therefore $n \neq 0$, and thus the angular integral of $C_{nn}(\alpha)$ is zero. Thus, using this angular averaging procedure, the elementary correlations between density-density and phase-phase can be extracted as follows:

$$C_{nn}(\alpha) = -\frac{1}{2}\tilde{C}_{nn}(\alpha) + \frac{1}{4\pi}\int_0^{2\pi} d\alpha\ \tilde{C}_{nn}(\alpha), \qquad (3.36)$$

$$C_{\phi\phi}(\alpha) = -\frac{1}{2}\tilde{C}_{\phi\phi}(\alpha) + \frac{1}{4\pi}\int_0^{2\pi} d\alpha\ \tilde{C}_{\phi\phi}(\alpha). \qquad (3.37)$$

Density correlations C_{nn} can also be measured using in-situ imaging. In this technique, light is shined on the condensate. If a region of the BEC contains more atoms, then light will undergo larger attenuation through this. This way, the data for the density is coded in the form of pixels. By measuring the correlations between these pixels, one measures C_{nn}, which can then be compared to the result in Eq. (3.36) coming from the angular in-

terference set-up.

It should be noted that this angular rotation-interference method does not directly determine the mixed correlations $C_{n\phi}$. However, this mixed correlator is related to the time derivative of the phase-phase correlation:

$$C_{n\phi}(\alpha) \equiv \langle \{\hat{n}_1(\alpha,t), \hat{\phi}_1(0,t)\} \rangle = -\frac{\hbar \mathcal{V}_f}{U} \frac{d}{dt} C_{\phi\phi}(\alpha,t), \tag{3.38}$$

where I have made use of the Euler equation in [76]: $\hat{n}_1(\theta,t) = -\frac{\hbar \mathcal{V}}{U} \frac{d}{dt} \hat{\phi}_1(\theta,t)$ that relates density fluctuation to the time derivative of the phase operator. Thus, in order to determine $C_{n\phi}$, I need to repeat the above steps of rotation and interference of toroidal BEC clouds and measure $C_{\phi\phi}$ for different times after expansion $t > t_f$. This requires preparing an assembly of identical condensates, where the first BEC will be expanded, Bragg diffracted, rotated and interfered giving the atom density correlations (3.32) from which I extract phase-phase correlation using Eq. (3.36) at $t = t_f$. The second BEC will be subjected a similar process but measuring its phase correlation at $t = t_f + \Delta t$, and so on for the entire assembly of BECs. This procedure will yield the time evolution data for the phase-phase correlations $C_{\phi\phi}(\alpha,t)$, and using Eq. (3.38) will result in the required mixed correlation function. Note that the time interval Δt, should be much smaller compared to any other time scales in the system, such as the frequency associated with the smallest mode $\omega^{\rm f}_{n=1} = c/R_{\rm f}$, or the time scale associated with the damping of density fluctuations as was seen in [38]. The spatial correlations (3.36), (3.37), and (3.38) can now be used to characterized the state of the system.

To convert these spatial correlation functions to the mode space, I express the mode annihilation operator $\hat{b}_n$ in terms of the fluctuation field operators $\hat{n}_1(\theta)$ and

$\hat{\phi}_1(\theta)$ using the scalar product of two Klein-Gordon wave-functions ϕ and χ defined as $(\phi,\chi) \equiv i\int dx\ \big[\phi^*(x,t)\big\{\partial_t\chi(x,t)\big\} - \big\{\partial_t\phi^*(x,t)\big\}\chi(x,t)\big]$ (see [97]):

$$\hat{b}_n = -i\sqrt{\frac{U}{\hbar\mathcal{V}_f}}e^{\frac{\gamma t_f}{2\tau}}\int_0^{2\pi}\frac{d\theta}{\sqrt{2\pi}}e^{-in\theta}\Big[\chi_n^*\hat{n}_1(\theta,t) - \mathcal{V}_f\eta_n^*\hat{\phi}_1(\theta,t)\Big], \tag{3.39}$$

which in turn can be used to express the fundamental mode correlations $\langle\{\hat{b}_n,\hat{b}_{-n}\}\rangle$ and $\langle\{\hat{b}_n^\dagger,\hat{b}_{-n}^\dagger\}\rangle$ in terms of real space correlators as follows:

$$\begin{aligned}
\langle\{\hat{b}_n,\hat{b}_{-n}\}\rangle &= -\frac{U}{\hbar\mathcal{V}_f}e^{\frac{\gamma t_f}{\tau}}\int_0^{2\pi}d\alpha\ e^{-in\alpha}\Big[(\chi_n^*)^2C_{nn}(\alpha) + \mathcal{V}_f^2(\eta_n^*)^2C_{\phi\phi}(\alpha) - \mathcal{V}_f\chi_n^*\eta_n^*C_{n\phi}(\alpha)\Big],\\
\langle\{\hat{b}_n,\hat{b}_n^\dagger\}\rangle &= \frac{U}{\hbar\mathcal{V}_f}e^{\frac{\gamma t_f}{\tau}}\int_0^{2\pi}d\alpha\ e^{-in\alpha}\Big[|\chi_n|^2C_{nn}(\alpha) + \mathcal{V}_f^2|\eta_n|^2C_{\phi\phi}(\alpha)\Big],
\end{aligned} \tag{3.40}$$

where for the second vacuum average I made use of the property $\chi_n^*\eta_n + \eta_n^*\chi_n = \frac{i\hbar}{2U} - \frac{i\hbar}{2U} = 0$. Plugging the data for spatial correlations (3.36), (3.37), and (3.38) into the above Fourier transforms, gives us the vacuum averages after expansion in the mode space. These experimentally determined vacuum averages can also be compared with the theoretical results $\langle\{\hat{b}_n,\hat{b}_{-n}\}\rangle = 2\alpha_n\beta_n^*\big(1+2n_B(E_n)\big)$ and $\langle\{\hat{b}_n,\hat{b}_n^\dagger\}\rangle = \big(1+n_B(E_n)\big)\big(|\alpha_n|^2+|\beta_n|^2\big)$. Then, the covariance matrix can be constructed for the expanded ring in the mode space, and the procedure outlined in Sec. 3.2 can be followed to calculate the Logarithmic Negativity $E_{\mathcal{N}}[n]$, thus determining the amount of entanglement in the toroidal BEC.

In this chapter, I revisited the setup discussed in Chapter 1, where a rapidly expanding Bose-Einstein condensate (BEC) trapped inside a thin toroidal laser trap (effectively a one-dimensional ring), spontaneously generates phonons in two-mode squeezed states which manifests itself as a cusp (at zero temperature) or kink (finite temperature) like features in the density-density correlations. Naturally, a question arises as to whether these correlations are quantum (entangled) or classical in nature. For this purpose, I then

briefly reviewed the theory of Gaussian quantum continuous variables for bosons, wherein the state of the fluctuations (phonons) can be completely specified by the mean vector and the covariance matrix for a system of two modes n and $-n$. To discuss entanglement, I reviewed the PPT criterion that helps define logarithmic negativity as an entanglement quantifier. Using this, I found that in an initial static BEC prepared in vacuum state, the entanglement is maximum for lowest energy modes $n = 1$, and decreases with increasing n in an oscillatory manner that is due to the presence of sonic horizon in the system. This entanglement degrades due to thermal noise or detector inefficiencies, which could be recovered using single-mode squeezed states of phonons. I ended this chapter with the discussion of a protocol of Bragg splitting the BEC into two condensates, rotating one of them and then making them interfere. I showed that this procedure gives all types of real space correlations and hence mode entanglement can be determined experimentally in the toroidal BEC setup.

For future work, one could look into the work by Glenz and Parker in Ref. [98], that suggests slope discontinuities in the radius of expanding toroid $R(t)$ can yield unphysical results. This is the scale factor that I have used for our work, and it yields $|\beta_n|^2$ that has oscillations with respect to mode index and dies of as n^{-2} for large n. I could repeat our calculations for a smooth (C^2 function) radius such that $R(t)$, dR/dt and d^2R/dt^2 are all continuous. One such suggestion [98] is to have the initial and final BECs

to be asymptotically smooth with an exponentially expanding phase static in between:

$$\frac{R(t)}{R_0} = \begin{cases} \left[a_{1i}^4 + (a_{2i}^4 - a_{1i}^4) n_{\rm F}(t/s_i)\right]^p, & \text{for } t < t_i \\ e^{Ht}, & \text{for } t_i \leq t \leq t_f \\ \left[a_{1f}^4 + (a_{2f}^4 - a_{1f}^4) n_{\rm F}(t/s_f)\right]^p, & \text{for } t > t_f \end{cases}$$

Here $n_F(x) = (e^x + 1)^{-1}$ is the Fermi-Dirac function, and the constants a_{1i}, a_{2i}, s_i, H, a_{1f}, a_{2f} and s_f will have to be chosen such that $R(t)$ is everywhere C^2-smooth. Then, the task will be to evaluate particle creation probability $|\beta_n|^2$, and study the limit in which the initial and final regimes join the intermediate exponential phase in a non-smooth manner, i.e. tune s, and see if it agrees with our results or not.

CHAPTER 4. UNRUH EFFECT AND TAKAGI'S STATISTICS INVERSION IN STRAINED GRAPHENE

In this chapter, I theoretically study the dynamics of low-energy and long-wavelength fermions in a mechanically strained graphene sheet. Due to these strains, a horizon appears diving the sheet into two-disconnected pieces forbidding the fermions to crossover. In addition to spontaneous creation of electron-hole pairs, I will show that observables confined to one side show emergent thermality. In relativity, accelerated observers fall into two causally disconnected families (Rindler wedges), thereby, also leading to similar thermal effects, also known as the Unruh effect. Here, I aim to explore this effect and its consequences in the context of graphene. The rest of this chapter is organized as follows. In Sec. 4.1, I describe how the Rindler Hamiltonian can be realized for low-energy and long wavelength fermions in mechanically strained graphene. Since the basic effect relies only on engineering a spatially-varying tunneling matrix element, I expect it should be similarly possible to engineer the Rindler Hamiltonian in cold-atom systems. In Sec. 4.2, I revisit the Hamiltonian for fermions in flat spacetime (or flat graphene sheet) and identify the normal modes of this system that correspond to particle and hole excitations. In Sec. 4.3, I derive the Dirac equation due to the Rindler Hamiltonian, obtaining a similar mode expansion for the strained case. In Sec. 4.4, I use the mode expansions in flat and strained (Rindler) honeycomb lattices to derive how a sudden strain can induce spontaneous electron-hole creation with an emergent Fermi-Dirac distribution, which is the analog Unruh effect. In Sec. 4.5 I analyze the Green's functions after such a sudden strain, showing how signatures of the analog Unruh effect may be measured in observables

such as photoemission spectroscopy and scanning tunneling microscopy and how the form of the emergent thermality is connected to the violation of Huygens' principle. In Sec. 4.6, I study the frequency-dependent optical conductivity of this system, which I find to increase approximately linearly with increasing frequency, in contrast to flat graphene, where it is known to be nearly constant (i.e., frequency-independent) [139, 140, 141, 142]. In Sec. 4.7, I discuss the effects of this sudden switching-on of the Rindler Hamiltonian on the total internal energy of fermions at finite environment temperature. In Sec. 6.3 I provide brief concluding remarks and in Appendix B, I give details that are omitted from the main text on the Dirac equation in curved spacetime.

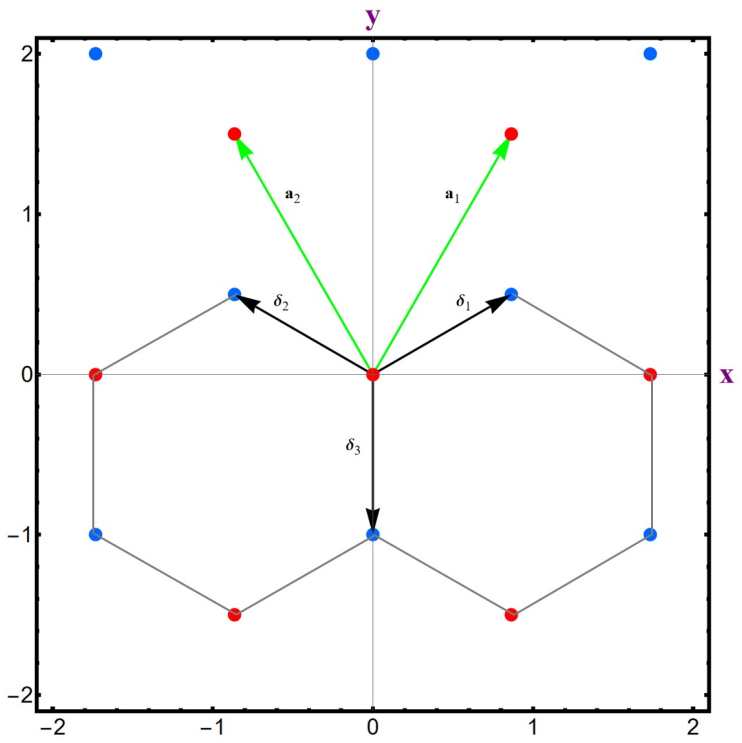

Figure 4.1. The honeycomb lattice of graphene where the carbon atoms in red color for the Bravais lattice with primitive lattice vectors $\boldsymbol{a}_1 = a(\sqrt{3}/2, 3/2)$ and $\boldsymbol{a}_2 = a(-\sqrt{3}/2, 3/2)$, connected to the nearest neighbor carbon atoms shown in blue by $\boldsymbol{\delta}_i$, $i = 1, 2, 3$, as defined in Eq. (4.2).

4.1. Creating the Rindler Hamiltonian

In this section, I will show how the Rindler Hamiltonian can be realized via graphene with a spatially-varying strain that yields a Hamiltonian with a spatially-varying Fermi velocity. This is in contrast to the low-energy theory of conventional graphene that exhibits a spatially-uniform Fermi velocity.

To see how such a spatially-varying Fermi velocity can be engineered, I start with the tight binding Hamiltonian for graphene which involves (π orbital) electrons hopping from carbon atoms in the A sub-lattice to their nearest neighboring B carbon atoms (as shown in Fig. 4.1), and vice versa:

$$\hat{H} = -\sum_{\boldsymbol{R}_j,n} t_{\boldsymbol{R}_j,n}\Big[\hat{a}^\dagger_{\boldsymbol{R}_j}\hat{b}_{\boldsymbol{R}_j+\boldsymbol{\delta}_n} + \hat{b}^\dagger_{\boldsymbol{R}_j+\boldsymbol{\delta}_n}\hat{a}_{\boldsymbol{R}_j}\Big], \tag{4.1}$$

where $\boldsymbol{R}_j$ labels the Bravais lattice points formed by the A-atoms, and index n denotes the three nearest neighboring B atoms. Here, the $\hat{a}$ and $\hat{b}$ operators annihilate fermions on the A and B sublattices, respectively, with hopping amplitude $t_{\boldsymbol{R}_j,n}$ (that I have taken to be real). The nearest neighbor vectors $\boldsymbol{\delta}_n$ joining the A and B atoms are as follows:

$$\boldsymbol{\delta}_1 = a\bigg(\frac{\sqrt{3}}{2},\frac{1}{2}\bigg),\ \boldsymbol{\delta}_2 = a\bigg(\frac{-\sqrt{3}}{2},\frac{1}{2}\bigg),\ \boldsymbol{\delta}_3 = a\big(0,-1\big), \tag{4.2}$$

with a the nearest-neighbor carbon distance. When a graphene sheet undergoes a mechanical strain, with $u_{ij} \equiv \frac{1}{2}(\partial_i u_j + \partial_j u_i)$ being the strain tensor, the distance between two carbon atoms changes and thus the hopping amplitude gets adjusted accordingly. For perturbative strains, I can then Taylor expand the hopping amplitude as follows [143]:

$$t_{\boldsymbol{R}_j,n} = t_0\Big[1 - \beta\Delta u_n^{(1)} - \beta\Delta u_n^{(2)}\Big], \tag{4.3}$$

with

$$\Delta u_n^{(1)} = \frac{\delta_n^i \delta_n^j}{a^2} u_{ij}, \tag{4.4}$$

$$\Delta u_n^{(2)} = \frac{\delta_n^i \delta_n^j \delta_n^k}{2a^2} \partial_i u_{jk}, \tag{4.5}$$

where $\Delta u_n^{(1)}$ is the first order change due to strains alone, and $\Delta u_n^{(2)}$ denotes the first order change due to strains and their derivatives (which is a low energy approximation). Here, a is the lattice spacing, and $\beta = |\frac{\partial \log t}{\partial \log a}|$ is the Grüneisen parameter. Note I also assume that the electrons cannot hop to the next nearest neighbors, i.e. $t' = 0$.

With the aim of realizing the Rindler Hamiltonian, henceforth I choose the following components for the strain tensor:

$$\begin{aligned} u_{xx} &= u_{yy} = -\frac{|x|}{\beta\lambda}, \qquad u_{xy} = 0, \\ t_1(x) &= 1 + \frac{|x|}{\lambda} + \frac{\sqrt{3}}{4}\frac{a}{\lambda}\mathrm{sgn}(x), \\ t_2(x) &= 1 + \frac{|x|}{\lambda} - \frac{\sqrt{3}}{4}\frac{a}{\lambda}\mathrm{sgn}(x), \\ t_3(x) &= 1 + \frac{|x|}{\lambda}, \end{aligned} \tag{4.6}$$

where λ is the strain scale that measures the distance over which an appreciable inhomogeneity develops in the honeycomb lattice. With this choice of strain tensor, the distance between atoms decreases with increasing distance from $x = 0$. At low energies, the electron dynamics is governed by two nodes in the reciprocal space $\mathbf{K} = \left(\frac{4\pi}{3a\sqrt{3}}, 0\right) = -\mathbf{K}'$. I can thus write down the a and b operators localized near these nodes as [144]:

$$\hat{a}_{\boldsymbol{R}_j} = e^{i\boldsymbol{K}\cdot\boldsymbol{R}_j}\hat{A}(\boldsymbol{R}_j) + e^{i\boldsymbol{K}'\cdot\boldsymbol{R}_j}\hat{A}'(\boldsymbol{R}_j), \tag{4.7}$$

$$\hat{b}_{\boldsymbol{R}_j+\boldsymbol{\delta}_n} = e^{i\boldsymbol{K}\cdot(\boldsymbol{R}_j+\boldsymbol{\delta}_n)}\hat{B}(\boldsymbol{R}_j+\boldsymbol{\delta}_n) + e^{i\boldsymbol{K}'\cdot(\boldsymbol{R}_j+\boldsymbol{\delta}_n)}\hat{B}'(\boldsymbol{R}_j+\boldsymbol{\delta}_n), \tag{4.8}$$

where the prime $'$ denotes operators associated to the $\mathbf{K}'$ node. For low energies, it suffices to Taylor expand the $\hat{b}_{\boldsymbol{R}+\boldsymbol{\delta}_n}$ operators to linear order in gradients of these operators [144]:

$$\hat{B}(\boldsymbol{R}_j+\boldsymbol{\delta}_n) \;\approx\; \hat{B}(\boldsymbol{R}_j)+\boldsymbol{\delta}_n\cdot\boldsymbol{\nabla}\hat{B}(\boldsymbol{R}_j). \tag{4.9}$$

Plugging into the tight-binding Hamiltonian (4.1), the expressions for operators near the nodes (4.7), and the Taylor expansions for the hopping amplitude (4.3) and for the operators on B carbon atoms (4.9), gives us the following:

$$\begin{aligned}\hat{H} &= -t_0\sum_{\boldsymbol{R}_j,n}\Big[1-\beta\Delta u_n^{(1)}-\beta\Delta u_n^{(2)}\Big]\\ &\times \Bigg\{\Big[\hat{A}^\dagger(\boldsymbol{R}_j)\Big\{\hat{B}(\boldsymbol{R}_j)+\boldsymbol{\delta}_n\cdot\boldsymbol{\nabla}\hat{B}(\boldsymbol{R}_j)\Big\}e^{i\boldsymbol{K}\cdot\boldsymbol{\delta}_n}+\text{h.c.}\Big]\\ &+ \Big[\hat{A}'^\dagger(\boldsymbol{R}_j)\Big\{\hat{B}'(\boldsymbol{R}_j)+\boldsymbol{\delta}_n\cdot\boldsymbol{\nabla}\hat{B}'(\boldsymbol{R}_j)\Big\}e^{i\boldsymbol{K}'\cdot\boldsymbol{\delta}_n}+\text{h.c.}\Big]\Bigg\},\end{aligned} \tag{4.10}$$

where second term in each line is the hermitian conjugate of the first, denoted by h.c.. Here I have ignored cross-terms between the two nodes like $\sim\sum_{\boldsymbol{R}_j}\hat{A}^\dagger(\boldsymbol{R}_j)\hat{B}'(\boldsymbol{R}_j)e^{i(\boldsymbol{K}-\boldsymbol{K}')\cdot\boldsymbol{R}_j}$, that destructively interfere and thus vanish. I now simplify this expression by using the Rindler strain pattern (4.6) and keeping terms that are linear order in gradients, terms that are linear order in strains and terms that are both linear in gradients as well as strains. I also introduce two-component field operators at the $\mathbf{K}$ and $\mathbf{K}'$ nodes:

$$\hat{\psi}_{\mathbf{K}}(\boldsymbol{R}_j)=\begin{pmatrix}\hat{B}(\boldsymbol{R}_j)\\ \hat{A}(\boldsymbol{R}_j)\end{pmatrix}, \tag{4.11}$$

$$\hat{\psi}_{\mathbf{K}'}(\boldsymbol{R}_j)=\begin{pmatrix}\hat{A}'(\boldsymbol{R}_j)\\ \hat{B}'(\boldsymbol{R}_j)\end{pmatrix}. \tag{4.12}$$

Upon approximating the sums over Bravais lattice points $\boldsymbol{R}_j$ to spatial integrals over $\boldsymbol{r}$, relabeling the $\mathbf{K}$ and $\mathbf{K}'$ points to be the right (R) and left (L) nodes, I finally arrive at

the effective Hamiltonian:

$$\hat{H} = \sum_{i=R,L} \int d^2 r \hat{\psi}_i^\dagger(\boldsymbol{r}) \hat{h}_i \hat{\psi}_i(\boldsymbol{r}), \tag{4.13}$$

$$\hat{h}_R \equiv \sqrt{v(x)}\boldsymbol{\sigma} \cdot (\boldsymbol{\sigma} \cdot \hat{\boldsymbol{p}}) \sqrt{v(x)} = -\hat{h}_L, \tag{4.14}$$

where $\boldsymbol{\sigma} = \big(\sigma_x, \sigma_y\big)$ is the vector of Pauli matrices, $\hat{\boldsymbol{p}} = -i\hbar\boldsymbol{\nabla}$ is the momentum operator, with $\boldsymbol{\nabla} = \big(\partial_x, \partial_y\big)$ being the gradient. Here, $v(x) = v_0\big(1 + \frac{|x|}{\lambda}\big)$ represents a spatially-varying Fermi velocity with $v_0 = \frac{3t_0 a}{2\hbar}$ being the Fermi velocity of the unstrained Honeycomb lattice. If I had instead chosen a plus sign for the strain tensor components in (4.6), then I would get a spatially decreasing Fermi velocity $v_0\big(1 - \frac{|x|}{\lambda}\big)$.

In the next step, I establish two different limiting cases of the Hamiltonian Eq. (4.13): The unstrained case, $\lambda \to \infty$, that yields the well known 2D Dirac Hamiltonian, and the case of strong strains, $\lambda \to 0$, in which the system Hamiltonian describes Dirac particles moving in a Rindler metric [101]. In the strong-strain limit, I can neglect the unit contribution in $v(x)$, leaving $v(x) = v_0|x|/\lambda$. In fact, as I now argue, this approximation also holds in the long-wavelength limit. Our argument relies on translation symmetry in the y-direction, which implies eigenfunctions of $\hat{h}_R$ are plane waves in the y direction, $\propto \mathrm{e}^{ik_y y}$ with wavevector k_y. Re-scaling the coordinates via $x \to x/|k_y|$ and $y \to y/|k_y|$ changes the spatially dependent Fermi velocity to $v(x) \to v_0\big(1 + \frac{|x|}{|k_y|\lambda}\big)$ and the momentum operator becomes $\hat{\boldsymbol{p}} \to |k_y| \cdot \hat{\boldsymbol{p}}$. In the long-wavelength limit ($|k_y|\lambda \ll 1$), the contribution of unity inside $v(x)$ becomes negligible and $|k_y|$ cancels out, giving us the 2D Rindler Hamiltonian which is just (4.13) with the Fermi velocity $v(x) = v_0|x|/\lambda$.

Having discussed how the Rindler Hamiltonian can be realized in strained honeycomb lattices, in the coming sections, I apply these ideas to see how a sudden switch on of

the system strain, suddenly changing the Hamiltonian from the 2D Dirac Hamiltonian to the 2D Rindler Hamiltonian can strongly modify low-energy and long-wavelength properties leading to the analog Unruh effect. To begin with, in the next section, I start with a review of fermions in flat unstrained honeycomb lattices, i.e., the case of graphene.

4.2. Mode expansion: Flat honeycomb lattice

In this section, I review the Dirac equation for flat (unstrained) graphene and derive the resulting normal mode expansion that describes electron and hole excitations. As I have already discussed, the low-energy Hamiltonian for fermions hopping on a uniform (unstrained) honeycomb lattice follows from taking the $\lambda \to \infty$ limit of Eq. (4.13), resulting in $\hat{H} = \hat{H}_{\rm R} + \hat{H}_{\rm L}$ with

$$\hat{H}_{\rm R} = v_0 \int d^2r \; \hat{\psi}^\dagger_{\rm R}(\boldsymbol{r}) \boldsymbol{\sigma} \cdot \hat{\boldsymbol{p}} \hat{\psi}_{\rm R}(\boldsymbol{r}), \tag{4.15}$$

where to get $\hat{H}_{\rm L}$ I simply replace $R \to L$ and take $v_0 \to -v_0$. The field operators $\hat{\psi}_i$ ($i = L, R$) satisfy the anticommutation relation

$$\{\hat{\psi}_i, \hat{\psi}^\dagger_j\} = \delta_{ij} \delta(\boldsymbol{r} - \boldsymbol{r}'), \tag{4.16}$$

In the following I focus on the right node, with results from the left node easily following. The Heisenberg equation of motion for the field operators $\hat{\psi}_{\rm R}(\boldsymbol{r}, t)$ is:

$$i\hbar \partial_t \hat{\psi}_{\rm R}(\boldsymbol{r}, t) = [\hat{\psi}_{\rm R}(\boldsymbol{r}, t), \hat{H}] = v_0 \boldsymbol{\sigma} \cdot \hat{\boldsymbol{p}} \; \hat{\psi}_{\rm R}(\boldsymbol{r}, t), \tag{4.17}$$

the massless Dirac equation (Weyl equation) that describes how fermions (with zero rest mass) propagate in a flat spacetime with an emergent $(2+1)$-dimensional Minkowski line element labeled by the inertial coordinates (T, X, Y):

$$ds^2_{\rm Mink} = -v_0^2 dT^2 + dX^2 + dY^2, \tag{4.18}$$

where the speed of light is now replaced by the Fermi velocity $c \to v_0$. In Appendix B, I describe how a metric expressed in inertial coordinates like (4.18) (see Eq. (B.2)) leads to a Dirac equation in inertial coordinates (4.17) (see Eq. (B.13)). This metric describes the dynamical trajectories of inertial observers in a flat spacetime. Suppose two inertial frames S and S' moving with relative speed v, then the coordinates of an observer in frame S' i.e. (T', X', Y'), are related to the ones in S via Lorentz transformations:

$$\begin{aligned} v_0 T' &= v_0 T \cosh\theta - x \sinh\theta, \\ X' &= x \cosh\theta - v_0 T \sinh\theta, \\ Y' &= Y, \end{aligned} \tag{4.19}$$

where $\cosh\theta = \gamma = \frac{1}{\sqrt{1-\beta^2}}$ is the Lorentz factor with $\beta = \frac{v}{v_0}$, and $\sinh\theta = \gamma\beta$. The ratio of these factors relate the velocity with rapidity $\theta \in (-\infty, \infty)$: $\tanh\theta = \beta \in (-1, 1)$. In either frame, the trajectory of an inertial observer is of the form $-v_0^2 T^2 + X^2 + Y^2 =$ constant.

Thus, as one might expect, fermions hopping in an unstrained honeycomb lattice obey an analog Dirac equation with the Fermi velocity v_0 playing the role of the speed of light. Our next task is to expand the fermion field operators into normal modes corresponding to positive energy "particle" and negative energy "hole" excitations in graphene's Dirac band structure. Since the system is homogeneous in space and time (or alternatively the emergent metric components (4.18) are constants), the Dirac equation solutions that describe the evolution of fermions are plane waves of the form $e^{\pm i(\boldsymbol{k}\cdot\boldsymbol{x} - \omega_k t)}$ and thus the field operators on the right node can be expressed in terms of the following

mode expansion [145]:

$$\hat{\psi}_{\rm R}(\boldsymbol{r}) = \int \frac{d^2k}{2\pi} \Big(e^{i(\boldsymbol{k}\cdot\boldsymbol{r} - v_0 kt)} u_{\boldsymbol{k}} \hat{a}_{\boldsymbol{k}} + e^{-i(\boldsymbol{k}\cdot\boldsymbol{r} - v_0 kt)} v_{-\boldsymbol{k}} \hat{b}^{\dagger}_{\boldsymbol{k}} \Big), \tag{4.20}$$

where the wave-vector $\boldsymbol{k} = (k_x, k_y)$ is related to the linear momenta in spatial directions via $\boldsymbol{p} = \hbar\boldsymbol{k}$ and, thanks to translation symmetry, is related to the energy $\epsilon_k = \hbar\omega_k$ (ω_k is the mode frequency), via the dispersion relations $\epsilon_k = \hbar v_0 |\boldsymbol{k}|$ or $\omega_k = v_0 k$ where $k \equiv |\boldsymbol{k}| = \sqrt{k_x^2 + k_y^2}$ is the wavevector magnitude.

This mode expansion for the right node $\mathbf{K}_{\rm R}$ (right-handed Weyl fermions) should have positive helicity, which is defined as the projection of the Pauli spin operator onto the direction of the momentum vector $h = \boldsymbol{\sigma} \cdot \hat{\boldsymbol{k}}$. Thus the flat spinors used in the mode expansion (4.20) are defined as follows:

$$u_{\boldsymbol{k}} = \frac{1}{\sqrt{2}} \begin{bmatrix} 1 \\ \frac{k_x + i k_y}{k} \end{bmatrix}, \qquad v_{\boldsymbol{k}} = \frac{1}{\sqrt{2}} \begin{bmatrix} -\left(\frac{k_x - i k_y}{k}\right) \\ 1 \end{bmatrix}. \tag{4.21}$$

In the above definitions, $u_{\boldsymbol{k}}$ has positive helicity $h = +1$, whereas $v_{\boldsymbol{k}}$ has negative helicity $h = -1$. The particle $\hat{a}$ and hole $\hat{b}$ operators satisfy anti-commutation relations and annihilate the flat honeycomb (Minkowski) vacuum state $|0_{\mathcal{M}}\rangle$:

$$\begin{aligned} \{\hat{a}_{\boldsymbol{k}}, \hat{a}^{\dagger}_{\boldsymbol{k}'}\} &= \delta(\boldsymbol{k} - \boldsymbol{k}'), \qquad \{\hat{b}_{\boldsymbol{k}}, \hat{b}^{\dagger}_{\boldsymbol{k}'}\} = \delta(\boldsymbol{k} - \boldsymbol{k}'), \\ \hat{a}_{\boldsymbol{k}} |0_{\mathcal{M}}\rangle &= 0, \qquad\qquad \hat{b}_{\boldsymbol{k}} |0_{\mathcal{M}}\rangle = 0. \end{aligned} \tag{4.22}$$

To obtain the mode expansion for the left node $\boldsymbol{K}_{\rm L}$ (left-handed Weyl fermions), the particle and hole spinors $u_{\boldsymbol{k}}$ and $v_{-\boldsymbol{k}}$ in Eq. (4.20) need to be switched with $v_{\boldsymbol{k}}$ and $u_{-\boldsymbol{k}}$, respectively, which means they both have negative helicities.

As is well known, the particle and hole fermionic excitations in graphene obey a linear dispersion relation, with $\omega_k \propto |\boldsymbol{k}|$. In Fig. 4.2(a), I depict this linear energy dis-

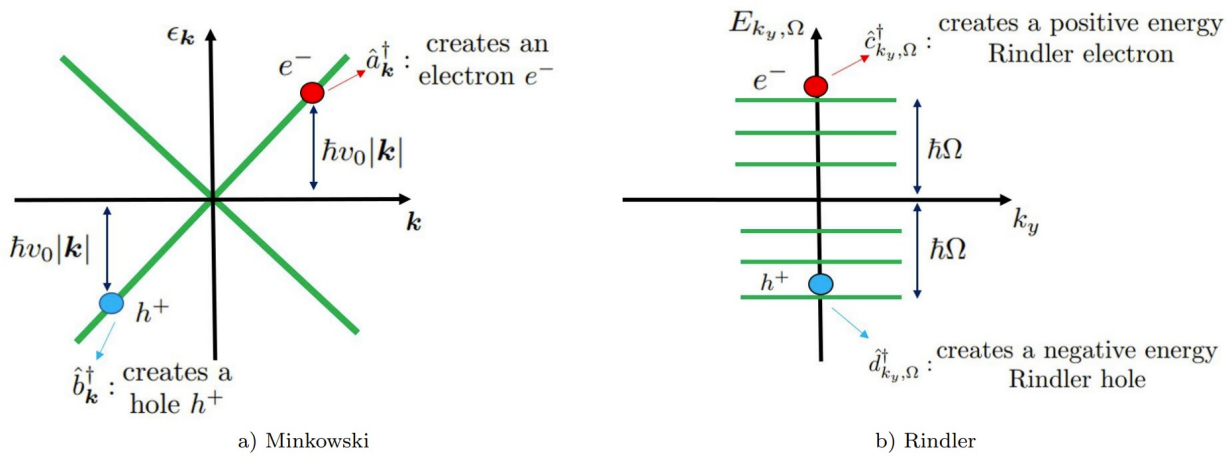

Figure 4.2. A schematic figure to depict the (a) Minkowski and (b) Rindler mode expansions. In flat graphene, the existence of translation symmetry yields a Dirac-like linear energy dispersion $\epsilon_{\boldsymbol{k}} = \hbar v_0|\boldsymbol{k}|$ (shown in green in panel a). The electron and hole excitation energies are both positive ($\epsilon_{\boldsymbol{k}} > 0$) with the operators $\hat{a}_{\boldsymbol{k}}|0_{\mathcal{M}}\rangle = 0 = \hat{b}_{\boldsymbol{k}}|0_{\mathcal{M}}\rangle$ annihilating the Minkwoski vacuum. In strained graphene, the Rindler energy $E_{k_y,\Omega} = \hbar\Omega > 0$ (shown in green in panel b) and transverse momenta $\hbar k_y$ are decoupled, with their associated electron and hole operators annihilating the Rindler vacuum state $\hat{c}_{k_y,\Omega}|0_{\mathcal{R}}\rangle = 0 = \hat{d}_{k_y,\Omega}|0_{\mathcal{R}}\rangle$.

persion, with the system ground state being a fully occupied valence band at negative energies and a fully unoccupied conduction band at positive energies. This figure also depicts the positive energy particle (or electron) and hole excitations that are captured by the mode expansion (4.20).

4.3. Mode expansion: Rindler system

In this section, I study the case of fermions hopping in a honeycomb lattice in the presence of a strain field that leads to the Rindler low-energy Hamiltonian, obtained by approximating $v(x) \simeq \frac{v_0}{\lambda}|x|$. As in the flat case, the system Hamiltonian comprises terms from the left and right nodes, $\hat{H} = \hat{H}_{\rm R} + \hat{H}_{\rm L}$, with the right-node Hamiltonian:

$$\hat{H}_{\rm R} = \frac{v_0}{\lambda}\int d^2r\ \hat{\psi}^\dagger_{\rm R}(\boldsymbol{r})\sqrt{|x|}\boldsymbol{\sigma}\cdot\hat{\boldsymbol{p}}\sqrt{|x|}\hat{\psi}_{\rm R}(\boldsymbol{r}), \tag{4.23}$$

which I call the Rindler Hamiltonian by analogy with the well-known Rindler metric, that describes how the flat Minkowski spacetime is seen by an accelerating observer [101]. Following the discussion in the homogeneous case, I find the equation of motion

$$i\hbar\partial_t\hat{\psi}_{\rm R}(\boldsymbol{r}) = \frac{v_0}{\lambda}\sqrt{|x|}\boldsymbol{\sigma}\cdot\hat{\boldsymbol{p}}\sqrt{|x|}\ \hat{\psi}_{\rm R}(\boldsymbol{r}), \tag{4.24}$$

the Dirac equation for massless fermions in Rindler spacetime with Rindler coordinates (t, x, y) [147, 146, 148] described by the line element

$$ds^2 \;=\; -\Big(\frac{x}{\lambda}\Big)^2 v_0^2 dt^2 + dx^2 + dy^2. \tag{4.25}$$

In Appendix B, I describe how the Rindler metric (see Eq. (B.3)) leads to a Dirac equation for accelerating electrons (see Eq. (B.14)). To understand the role of this metric in the context of honeycomb systems, I first need to understand its role in relativistic physics. Imagine a Rindler observer in the frame $S_{\rm R}$, moving with some acceleration $\boldsymbol{a} = a\hat{x}$ $(a > 0)$ with respect to an inertial frame S. The observer starts their journey far away at $x = \infty$ at time $t = -\infty$ with velocity close to the speed of light c moving towards the origin $x = 0$. Initially they decelerate, eventually stopping at a certain distance from the origin $x_{\rm min} = \frac{c^2}{a}$, and then return to $x = +\infty$ at $t = +\infty$. Since at any one instant of time, the Rindler observer is moving at a certain velocity v, I expect a hyperbolic-like trajectory similar to the Minkowski case: $-v_0^2T^2 + X^2 + Y^2 =$ constant, and the transformation between inertial coordinates (T, X) and Rindler (t, x) coordinates to be similar to (4.19). This is reminiscent of non-relativistic physics, where the trajectory of an accelerated observer is parabolic: $x = x_0 + u_0t + \frac{1}{2}at^2$. However, relativistic accelerations need to be hyperbolic as motion also affects the rate at which the observer's clock ticks. Thus the

relation between the inertial and Rindler coordinates are as follows [147, 146, 148]:

$$\begin{aligned} cT &= x_{\min} \sinh \frac{ct}{x_{\min}}, \\ X &= x_{\min} \cosh \frac{ct}{x_{\min}}, \end{aligned} \tag{4.26}$$

which gives us the trajectory of a Rindler observer viewed from an inertial frame S: $X^2 - c^2T^2 = x_{\min}^2$. The above coordinates (T, X) label the worldline of an accelerated observer from the perspective of an inertial frame. If the acceleration is changed to a different but constant value, then I get a family of Rindler observers, each with a different closest distance of approach $x_{\min}$. This family is parameterized using a new coordinate $x_{\min} \to x$, giving us the Rindler metric in Eq. (4.25). If I set the spatial coordinates to zero, i.e. $dx = dy = 0$ then t behaves like the proper time as seen on the watch of a Rindler observer. Similar arguments hold for an observer accelerating in the opposite direction with $a < 0$. Note that (4.25) becomes degenerate at $x = 0$, i.e. the time-time component of the metric tensor vanishes ($g_{tt} = 0$) and hence has no inverse. This is known as the *Rindler horizon*. Because of this horizon, oppositely accelerating observers can never communicate with each other. Note that the connection between the coordinates (T, X) and (t, x) is just a switch of variables, therefore the metric (4.25), is basically flat spacetime written in disguise, and thus the Riemann curvature of this spacetime is zero. Also note that the coordinates (t, x, y) cover only two portions of the flat Minkowski spacetime: the right Rindler wedge $x > 0$ for positive accelerations and the left Rindler wedge $x < 0$ for negative accelerations.

In the context of strained graphene, the emergent metric in Eq. (4.25) tells us that similar Rindler physics is expected provided I replace the speed of light with the Fermi ve-

locity $c \to v_0$, and the distance of closest approach with the strain scale $x_{\min} \to \lambda$. Once I do this, then I can interpret the electron dynamics inside graphene as Rindler fermions where the analog acceleration is given by $a = \frac{v_0^2}{\lambda}$, where a choice of strain λ corresponds to choosing a unique Rindler observer with this acceleration. Such analog accelerations are expected here because under the semiclassical model of electron dynamics, the strained graphene has an environment with broken translation symmetry that forces the Fermi velocity to be spatially dependent $v(x) = v_0(1 + \frac{|x|}{\lambda})$. Moreover, the strain pattern in Eq. (4.6) tells us that carbon atoms become closer with distance from the origin, thus enhancing electron hopping. This hopping from one carbon atom to another will be most difficult at the origin itself, especially for low-energy and long-wavelength modes which cannot tunnel from one side to the other. Therefore, $x = 0$ being a barrier for such modes acts as an analog of the Rindler horizon, breaking the strained graphene into two disconnected pieces: the right side mimics the right Rindler wedge, and the left side mimics the left Rindler wedge.

Our next task is to identify the normal mode expansion for the field operator $\hat{\psi}_{\mathrm{R}}(\boldsymbol{r})$ in the Rindler Dirac equation (4.24) [149, 150, 151, 152, 153, 154, 116, 108]. In doing this, I define the frequency scale $\Omega > 0$ and look for positive energy ($E = \hbar\Omega > 0$) solutions (corresponding to Rindler particles) and negative energy ($E = -\hbar\Omega < 0$) solutions (corresponding to Rindler holes). Starting with the $E > 0$ case, the solutions take the form $\psi_\Omega^+(x, k_y)e^{i(k_y y - \Omega t)}$, where $p_y = \hbar k_y$ is the momentum in the y-direction. If I define the

components of the spinor part via

$$\psi^{+}_{\Omega}(x,k_y) = \begin{pmatrix} f(x) \\ \\ g(x) \end{pmatrix}, \tag{4.27}$$

then the functions $f(x)$ and $g(x)$ satisfy (henceforth I set $\hbar \to 1$):

$$\left(|x|\frac{d}{dx} + k_y|x| + \frac{\mathrm{sgn}(x)}{2}\right)g(x) = i\Omega f(x), \tag{4.28a}$$

$$\left(|x|\frac{d}{dx} - k_y|x| + \frac{\mathrm{sgn}(x)}{2}\right)f(x) = i\Omega g(x). \tag{4.28b}$$

The dimensionless form of these equations came because I measured energy (or frequency, Ω) relative to the scale

$$\omega_c = v_0/\lambda, \tag{4.29}$$

characterizing the strain magnitude.

Starting with the case of $x > 0$ and $k_y > 0$, and focusing on solutions that are normalizable at $|x| \to \infty$, I find:

$$f(x) = K_{\frac{1}{2}-i\Omega}\big(k_y x\big) - K_{\frac{1}{2}+i\Omega}\big(k_y x\big), \tag{4.30a}$$

$$g(x) = K_{\frac{1}{2}-i\Omega}\big(k_y x\big) + K_{\frac{1}{2}+i\Omega}\big(k_y x\big), \tag{4.30b}$$

where $K_\nu(x)$ is the modified Bessel function of the second kind, that diverges at the origin $x = 0$ and for large negative arguments $x \to -\infty$. This divergence can be attributed to the form of the analog Rindler metric (4.25), whose time-time component vanishes at $x = 0$, and contributes a non-smooth modulus function $|x|$ in the Weyl equations which leads to different solutions in the left and right spatial regions of the strained honeycomb lattice. As I have already discussed, this demarcation of the system at $x = 0$ is known as the Rindler horizon. In analogy with relativity, the left spatial portion acts as the left

Rindler wedge, and similarly for the right portion. There, an observer in right wedge will never be able to communicate with their counterpart in the left wedge. In the next section, I will see that this is an essential reason why a natural temperature emerges in this system.

The solutions for f and g above have Bessel functions with positive arguments. Therefore they are finite and vanish asymptotically for $k_y x \to \infty$. For the case $x > 0$ and $k_y < 0$, the equations (4.28a) and (4.28b) get interchanged, resulting in an exchange of the spinor components $f(x) \leftrightarrow g(x)$. The case of $x < 0$ and $k_y > 0$ effectively switches $\Omega \to -\Omega$ and $k_y \to -k_y$ relative to the $x > 0$ and $k_y > 0$ case, while the case of $x < 0$ and $k_y < 0$ effectively switches $\Omega \to -\Omega$ relative to the $x > 0$ and $k_y > 0$ case. Taken together, these considerations imply the positive energy spinor

$$\psi^+_\Omega(x, k_y) = \begin{cases} \begin{pmatrix} K_{\frac{1}{2}-i\Omega} - \mathrm{sgn}(k_y) K_{\frac{1}{2}+i\Omega} \\ K_{\frac{1}{2}-i\Omega} + \mathrm{sgn}(k_y) K_{\frac{1}{2}+i\Omega} \end{pmatrix} & \text{if } x > 0 \\ \begin{pmatrix} K_{\frac{1}{2}+i\Omega} + \mathrm{sgn}(k_y) K_{\frac{1}{2}-i\Omega} \\ K_{\frac{1}{2}+i\Omega} - \mathrm{sgn}(k_y) K_{\frac{1}{2}-i\Omega} \end{pmatrix} & \text{if } x < 0 \end{cases}$$

where $K_{\frac{1}{2}\pm i\Omega}$ is shorthand for $K_{\frac{1}{2}\pm i\Omega}(|k_y x|)$. I emphasize here that the above two solutions come from solving the Rindler-Dirac equation separately for $x > 0$ and $x < 0$, pertaining to the two sides of the honeycomb lattice. Thus I define orthonormality separately in the $x > 0$ and $x < 0$ regimes.

Turning to the $E < 0$ case, I take the solutions to have the form $\psi^-_\Omega(x, k_y) e^{-i(k_y y - \Omega t)}$, which effectively changes the sign of k_y and Ω relative to the positive energy case. This

leads to the negative energy spinors:

$$\psi^{-}_{\Omega}(x,k_y) = \begin{cases} \begin{pmatrix} K_{\frac{1}{2}+i\Omega} + \mathrm{sgn}(k_y) K_{\frac{1}{2}-i\Omega} \\ K_{\frac{1}{2}+i\Omega} - \mathrm{sgn}(k_y) K_{\frac{1}{2}-i\Omega} \end{pmatrix} & \text{if } x > 0 \\ \begin{pmatrix} K_{\frac{1}{2}-i\Omega} - \mathrm{sgn}(k_y) K_{\frac{1}{2}+i\Omega} \\ K_{\frac{1}{2}-i\Omega} + \mathrm{sgn}(k_y) K_{\frac{1}{2}+i\Omega} \end{pmatrix} & \text{if } x < 0 \end{cases}$$

The normal mode expansion then takes the form: [149, 150, 151, 152, 153, 154, 116, 108]

$$\hat{\psi}_{\mathrm{R}}(\boldsymbol{r},t) = \int_{-\infty}^{\infty} \frac{dk_y}{\sqrt{2\pi}} \int_0^{\infty} d\Omega \; N_{k_y,\Omega} \Big[\psi^{+}_{\Omega}(x,k_y) e^{i(k_y y - \Omega t)} \hat{c}_{k_y,\Omega} + \psi^{-}_{\Omega}(x,k_y) e^{-i(k_y y - \Omega t)} \hat{d}^{\dagger}_{k_y,\Omega} \Big], \quad (4.31)$$

where the operators $\hat{c}_{k_y,\Omega}$ annihilate positive energy Rindler particles and the operator $\hat{d}^{\dagger}_{k_y,\Omega}$ creates a negative energy Rindler hole, as illustrated in Fig. 4.2(b). These particle and hole operators satisfy fermionic anticommutation relations:

$$\{\hat{c}_{k_y,\Omega}, \hat{c}^{\dagger}_{k'_y,\Omega'}\} = \delta(k_y - k'_y)\delta(\Omega - \Omega'), \quad (4.32)$$

$$\{\hat{d}_{k_y,\Omega}, \hat{d}^{\dagger}_{k'_y,\Omega'}\} = \delta(k_y - k'_y)\delta(\Omega - \Omega'). \quad (4.33)$$

I emphasize that, in our convention, the energy scale $\hbar\Omega > 0$, so that both particle and hole excitations have positive energy (although the latter emerge from below the Fermi level). Thus the Rindler vacuum $|0_{\mathcal{R}}\rangle$ is annihilated by both the electron and hole operators:

$$\hat{c}_{k_y,\Omega}|0_{\mathcal{R}}\rangle = 0, \quad (4.34)$$

$$\hat{d}_{k_y,\Omega}|0_{\mathcal{R}}\rangle = 0. \quad (4.35)$$

For the left handed electrons, I need to solve the corresponding set of Weyl equations, which is the same as the equation for right-handed electrons, except for a minus sign associated with the time derivative. This amounts to saying that the fermions on $\mathbf{K}_{\mathrm{L}}$ node will be described by the same mode expansion as (4.31), except that the spinors will all change signs for the frequency i.e. $\psi^{\pm}_{\Omega}(x,k_y) \to \psi^{\pm}_{-\Omega}(x,k_y)$. Finally, to determine the normalization factor $N_{k_y,\Omega} = \sqrt{\frac{|k_y|}{2\pi^2}\cosh\pi\Omega}$ I make use of the inner product for Weyl spinors [108, 45]:

$$\left(\psi^{\sigma'}_{\Omega'}(x,k_y), \psi^{\sigma}_{\Omega}(x,k_y)\right) \equiv \int_0^\infty dx\ \psi^{\sigma'\dagger}_{\Omega'}(x,k_y)\psi^{\sigma}_{\Omega}(x,k_y) = \delta^{\sigma\sigma'}\delta(\Omega-\Omega'), \tag{4.36}$$

where $\sigma = \pm$ denotes the positive or negative energy spinors, and the following identity for Bessel functions [154, 155]:

$$\int_0^\infty dx \left[K_{\frac{1}{2}+i\Omega}(x)K_{\frac{1}{2}-i\Omega'}(x) + K_{\frac{1}{2}-i\Omega}(x)K_{\frac{1}{2}+i\Omega'}(x)\right] = \pi^2\,\mathrm{sech}(\pi\Omega)\delta(\Omega-\Omega'). \tag{4.37}$$

Now that I have derived the mode expansion (4.31) in terms of Bessel functions that are singular at the horizon for the field operators in a strained graphene system (or in an ultracold honeycomb optical lattice that has a linear-in-position Fermi velocity), in the next section, I will describe how this leads to spontaneous creation of electron-hole pairs, which is equivalent to saying that a sudden change in the Fermi velocity $v_0 \to v_0\frac{|x|}{\lambda}$ leads to a spontaneous jump of electrons from the valence to conduction band.

4.4. Spontaneous Electron-Hole Pair Creation

In the last two sections, I discussed the Dirac Hamiltonian (4.15) and its solutions (4.20) for a flat honeycomb system with homogeneous Fermi velocity $v(x) = v_0$, and the Rindler Hamiltonian (4.23) and its solutions (4.31) for an inhomogeneous honeycomb lat-

tice with a spatially-varying Fermi velocity $v(x) = v_0 \frac{|x|}{\lambda}$. The latter solutions are made out of spinors of Bessel functions that diverge at the horizon $x = 0$, with separate solutions at $x > 0$ and $x < 0$. In this section, I will describe how this set-up leads to spontaneous creation of electron-hole pairs, with the spectrum of these excitations described by an emergent Fermi-Dirac distribution that is a function of Rindler mode frequency Ω and the characteristic frequency ω_c, defined in Eq. (4.29), that is proportional to the Unruh temperature.

Since the Rindler $|0_{\mathcal{R}}\rangle$ and the Minkowski vacua $|0_{\mathcal{M}}\rangle$ are associated with strained and flat honeycomb lattices respectively, they are expected to be very different from each other, i.e. the notion of particles that one ascribes to with respect to the Minkowski vacuum cannot be same as the Rindler case, since in the former case there exists translation symmetry, whereas in the latter, the mechanical strain strongly modifies the properties of system eigenstates.

I consider the situation where I start with the flat honeycomb Hamiltonian (4.15) described by the mode expansion (4.20) for the field operators, and then suddenly switch on the linear-in-position Fermi velocity with a characteristic strain length λ, thereby invoking the Rindler Hamiltonian (4.23) and the corresponding mode expansion (4.31). In the Heisenberg picture then, I expect that the mode expansion for the fermionic field operators $\hat{\psi}_{\mathrm{R}}$ on the right node evolve from Eq. (4.20) to Eq. (4.31), whereas the state of the system will remain the Minkowski vacuum state $|0_{\mathcal{M}}\rangle$. This is just the sudden approximation of quantum mechanics, where if a potential suddenly changes its shape, then the original ground state can be expressed as a linear combination of the eigenstates of the new Hamiltonian, and thus the observables can be found by taking expectation values of oper-

ators in the modified system with respect to the ground state of the original Hamiltonian. Thus, in the present case, to find observables I need to know how the Rindler operators $\hat{c}$ and $\hat{d}$ act on the Minkowski vacuum state $|0_{\mathcal{M}}\rangle$. For this, I need to find an expression of these Rindler operators in terms of the Minkowski annihilation operators $\hat{a}$ and $\hat{b}$.

To connect these operators, I can simply equate the two mode expansions (4.20) and (4.31) as they describe the same quantum field operator $\hat{\psi}_{\rm R}$. Then I take its inner product with positive energy solutions $\left(\psi^{+}_{\Omega}(x,k_y),\hat{\psi}_{\rm R}(x)\right)$ for electron, and negative energy solutions $\left(\psi^{-}_{\Omega}(x,k_y),\hat{\psi}_{\rm R}(x)\right)$ for hole Rindler operators, as defined in (4.36) [108, 45], yielding:

$$\begin{aligned}
\hat{c}^{>}_{k_y,\Omega} &= \int d^2k' \left[\alpha^{+,>}_{\boldsymbol{k}',k_y,\Omega}\hat{a}_{\boldsymbol{k}'} + \beta^{+,>}_{\boldsymbol{k}',k_y,\Omega}\hat{b}^{\dagger}_{\boldsymbol{k}'}\right],\\
\hat{d}^{>\dagger}_{k_y,\Omega} &= \int d^2k' \left[\beta^{-,>}_{\boldsymbol{k}',k_y,\Omega}\hat{a}_{\boldsymbol{k}'} + \alpha^{-,>}_{\boldsymbol{k}',k_y,\Omega}\hat{b}^{\dagger}_{\boldsymbol{k}'}\right],
\end{aligned} \tag{4.38}$$

the Bogoliubov transformations that express the Rindler ladder operators for $x > 0$ (denoted by superscript $>$) as a linear combination of the Minkwoski ladder operators. Similar relations hold for $x < 0$ region with the superscript $<$ at the appropriate places. Following Takagi [108], the coefficients of this linear relationship $\alpha^{\pm}_{\boldsymbol{k},k'_y,\Omega'}$ and $\beta^{\pm}_{\boldsymbol{k},k'_y,\Omega'}$, known as Bogoliubov coefficients, are found to be:

$$\begin{aligned}
\alpha^{+,>}_{\boldsymbol{k}',k_y,\Omega} &= \sqrt{n_{\rm F}(-2\pi\Omega)}\;\delta(k_y-k'_y)\;\mathcal{P}(\boldsymbol{k}',\Omega),\\
\beta^{+,>}_{\boldsymbol{k}',k_y,\Omega} &= -i\sqrt{n_{\rm F}(2\pi\Omega)}\;\delta(k_y+k'_y)\;\mathcal{P}(\boldsymbol{k}',\Omega),\\
\alpha^{-,>}_{\boldsymbol{k}',k_y,\Omega} &= \alpha^{+,<}_{\boldsymbol{k}',k_y,\Omega} = \left(\alpha^{+,>}_{\boldsymbol{k}',k_y,\Omega}\right)^{*} = \left(\alpha^{-,<}_{\boldsymbol{k}',k_y,\Omega}\right)^{*},\\
\beta^{-,>}_{\boldsymbol{k}',k_y,\Omega} &= \beta^{+,<}_{\boldsymbol{k}',k_y,\Omega} = \left(\beta^{+,>}_{\boldsymbol{k}',k_y,\Omega}\right)^{*} = \left(\beta^{-,<}_{\boldsymbol{k}',k_y,\Omega}\right)^{*},
\end{aligned} \tag{4.39}$$

where the first Bogoliubov coefficient $\alpha^{+,>}$ for the right side of graphene is found by tak-

ing the inner product of the positive energy Rindler spinor for $x > 0$ with the positive energy Minkowski modes, whereas the second coefficient $\beta^{+,>}$ is found using the negative energy Minkowski modes. Similarly, the other two coefficients $\alpha^{-,>}$ and $\beta^{-,>}$ can be found by using negative energy Rindler spinors. In the last two lines, I list how the rest of the coefficients are related to the first two via complex conjugation. These coefficients are written in terms of the Fermi-Dirac function $n_{\rm F}(x) = (e^x + 1)^{-1}$ and the projection operator:

$$\mathcal{P}(\boldsymbol{k}, \Omega) = \frac{1+i}{\sqrt{2}} \frac{1}{\sqrt{2\pi k}} \left(\frac{k + k_x}{k - k_x} \right)^{\frac{i\Omega}{2}} \left(\sqrt{\frac{k + k_x}{2k}} + i \sqrt{\frac{k - k_x}{2k}} \right). \tag{4.40}$$

The anticommutation relations for the Rindler operators $\hat{c}_{k_y,\Omega}$ and $\hat{d}_{k_y,\Omega}$, along with those of the Minkowski operators $\hat{a}_{\boldsymbol{k}}$ and $\hat{b}_{\boldsymbol{k}}$ and the transformations Eq. (4.38) imply the following normalization condition for the Bogoliubov coefficients:

$$\int d^2\tilde{k} \left(\alpha^{\sigma,r}_{\tilde{\boldsymbol{k}},k_y,\Omega} \alpha^{\sigma',r'*}_{\tilde{\boldsymbol{k}},k'_y,\Omega'} + \beta^{\sigma,r}_{\tilde{\boldsymbol{k}},k_y,\Omega} \beta^{\sigma',r'*}_{\tilde{\boldsymbol{k}},k'_y,\Omega'} \right) = \delta^{\sigma\sigma'} \delta^{rr'} \delta(k_y - k'_y) \delta(\Omega - \Omega'), \tag{4.41}$$

where the superscript $\sigma = \pm$ labels the positive and negative energy solutions, and $r =>, <$ labels the right ($x > 0$) or left ($x < 0$) region of graphene. To find these Bogoliubov coefficients, I made use of the Fourier transform of the modified Bessel functions of the second kind [154, 155]:

$$\begin{aligned} \int_0^\infty dx\ K_\nu(ax) e^{ibx} &= \frac{\pi}{4\sqrt{a^2 + b^2}} \\ \times \quad & \left[\frac{(\sqrt{r^2+1} + r)^\nu + (\sqrt{r^2+1} - r)^\nu}{\cos(\pi\nu/2)} + i\ \frac{(\sqrt{r^2+1} + r)^\nu - (\sqrt{r^2+1} - r)^\nu}{\sin(\pi\nu/2)} \right], \end{aligned} \tag{4.42}$$

where $r = b/a$. The conditions required for the validity of the sine transform are Re $a > 0$, $b > 0$, $|\text{Re } \nu| < 2$ and $\nu \neq 0$. Whereas the conditions for the cosine transform are

Re $a > 0$, $b > 0$, $|\text{Re } \nu| < 1$. For our case, $a = k_y > 0$ and $\nu = \frac{1}{2} \pm i\Omega$ satisfy the conditions. However, $b = k_x$ could be positive or negative. For $k_x > 0$ case, the above Fourier transform can be used whereas for $k_x < 0$, one needs to take the complex conjugate of the above transform.

Note that the transformation in (4.38) and the corresponding Bogoliubov coefficients in (4.39), can be re-written in a much cleaner way [108]:

$$\hat{c}^{>}_{k_y,\Omega} = \sqrt{n_{\rm F}(-2\pi\Omega)}\,\hat{A}_{k_y,\Omega} - i\sqrt{n_{\rm F}(2\pi\Omega)}\,\hat{B}^{\dagger}_{-k_y,\Omega}, \tag{4.43a}$$

$$\hat{d}^{>\dagger}_{k_y,\Omega} = i\sqrt{n_{\rm F}(2\pi\Omega)}\,\hat{A}^{*}_{-k_y,\Omega} + \sqrt{n_{\rm F}(-2\pi\Omega)}\,\hat{B}^{*\dagger}_{k_y,\Omega}, \tag{4.43b}$$

where instead of using momentum integrations as in (4.38), the Rindler operators are expressed in terms of modified Minkowski $\hat{A}$ and $\hat{B}$, that are defined as a complex linear combination of the original Minkowski operators $\hat{a}$ and $\hat{b}$ as follows [108]:

$$\begin{aligned} \hat{A}_{k_y,\Omega} &= \int_{-\infty}^{\infty} dk_x\ \mathcal{P}(\boldsymbol{k},\Omega)\ \hat{a}_{\boldsymbol{k}}, \\ \hat{B}^{\dagger}_{k_y,\Omega} &= \int_{-\infty}^{\infty} dk_x\ \mathcal{P}(\boldsymbol{k},\Omega)\ \hat{b}^{\dagger}_{\boldsymbol{k}}, \end{aligned} \tag{4.44}$$

that (like the operators $\{\hat{a},\hat{b}\}$) also annihilate the Minkowski vacuum:

$$\hat{A}_{k_y,\Omega}|0_{\mathcal{M}}\rangle = \hat{B}_{k_y,\Omega}|0_{\mathcal{M}}\rangle = 0, \tag{4.45}$$

which follows from Eq. (4.22). In addition, they satisfy the anti-commutation relations:

$$\begin{aligned} \left\{\hat{A}_{k_y,\Omega}, \hat{A}^{\dagger}_{k'_y,\Omega'}\right\} &= \left\{\hat{B}_{k_y,\Omega}, \hat{B}^{\dagger}_{k'_y,\Omega'}\right\} \\ &= \delta(k_y - k'_y)\delta(\Omega - \Omega'). \end{aligned} \tag{4.46}$$

As a result of these properties, the expectation value of modified operators in the

Minkowski vacuum state $|0_{\mathcal{M}}\rangle$ become:

$$\begin{aligned}\langle 0_{\mathcal{M}}|\hat{A}_{k_y,\Omega}\hat{A}^{\dagger}_{k'_y,\Omega'}|0_{\mathcal{M}}\rangle &= \langle 0_{\mathcal{M}}|\hat{B}_{k_y,\Omega}\hat{B}^{\dagger}_{k'_y,\Omega'}|0_{\mathcal{M}}\rangle = \delta(k_y-k'_y)\delta(\Omega-\Omega'),\\ \langle 0_{\mathcal{M}}|\hat{A}^{\dagger}_{k_y,\Omega}\hat{A}_{k'_y,\Omega'}|0_{\mathcal{M}}\rangle &= \langle 0_{\mathcal{M}}|\hat{B}^{\dagger}_{k_y,\Omega}\hat{B}_{k'_y,\Omega'}|0_{\mathcal{M}}\rangle = 0,\end{aligned} \tag{4.47}$$

where in order to derive the Dirac delta function in energies $\delta(\Omega-\Omega')$, in the above vacuum averages, the following identity was used [108]:

$$\int_{-\infty}^{\infty}\frac{dk_x}{2\pi k}\left(\frac{k+k_x}{k-k_x}\right)^{i(\Omega-\Omega')/2} = \int_{-\infty}^{\infty}\frac{dy}{2\pi}e^{i(\Omega-\Omega')y} = \delta(\Omega-\Omega'), \tag{4.48}$$

where in the first equality I made the substitution $y=\frac{1}{2}\log\left(\frac{k+k_x}{k-k_x}\right)$.

The advantage of (4.43) emerges when I evaluate the expectation value of Rindler operators in the Minkwoski vacuum, where I only need vacuum averages of modified Minkwoski operators, simplifying our calculations. Interestingly, when I compute expectation values of the Rindler operators with respect to the Minkoski vacuum I find that such averages involve an emergent Fermi distribution:

$$\langle 0_{\mathcal{M}}|\hat{c}^{>\dagger}_{k_y,\Omega}\hat{c}^{>}_{k'_y,\Omega'}|0_{\mathcal{M}}\rangle = \langle 0_{\mathcal{M}}|\hat{d}^{>\dagger}_{k_y,\Omega}\hat{d}^{>}_{k'_y,\Omega'}|0_{\mathcal{M}}\rangle = n_{\rm F}(2\pi\Omega)\delta(k_y-k'_y)\delta(\Omega-\Omega'), \tag{4.49}$$

that arise solely due to strains in the material, rather than due to any real heat bath. This implies that although the occupancy of Rindler electrons and holes in the Rindler vacuum is zero, in the Minkowski vacuum state it is proportional to the Fermi function. Thus surprisingly, spontaneous particle creation here has a spectrum that turns out to be *thermal* in nature. This is known as the Fulling-Davies-Unruh effect which, in the conventional setting, says that an accelerating observer views the Minkowski spacetime as a thermal bath of particles at the Unruh temperature $T_{\rm U}=\frac{\hbar a}{2\pi k_{\rm B}c}$. Within the present analog

setup, in which the accelerating observer is replaced by a sudden switch on of a spatially-inhomogeneous strain, the analog Unruh temperature is given by $T_{\rm U} = \frac{\hbar\omega_c}{2\pi k_{\rm B}} = \frac{\hbar v_0}{2\pi k_{\rm B}\lambda}$.

To see how this thermality arises in a concrete way, I re-write the (4.43) for electrons in the right side of graphene ($x > 0$) and holes on the left side ($x < 0$):

$$\hat{c}^{>}_{k_y,\Omega} = \sqrt{n_{\rm F}(-2\pi\Omega)}\hat{A}_{k_y,\Omega} - i\sqrt{n_{\rm F}(2\pi\Omega)}\hat{B}^{\dagger}_{-k_y,\Omega}, \tag{4.50a}$$

$$\hat{d}^{<\dagger}_{-k_y,\Omega} = -i\sqrt{n_{\rm F}(2\pi\Omega)}\hat{A}_{k_y,\Omega} + \sqrt{n_{\rm F}(-2\pi\Omega)}\hat{B}^{\dagger}_{-k_y,\Omega}, \tag{4.50b}$$

where I made use of the symmetry properties of Bogoliubov coefficients in (4.39) and I chose to evaluate the hole operator for $x < 0$ region and with inverted momentum $-k_y$ with respect to the electrons. These can be inverted to write the modified operators in terms of Rindler operators:

$$\hat{A}_{k_y,\Omega} = \sqrt{n_{\rm F}(-2\pi\Omega)}\hat{c}^{>}_{k_y,\Omega} + i\sqrt{n_{\rm F}(2\pi\Omega)}\hat{d}^{<\dagger}_{-k_y,\Omega}, \tag{4.51a}$$

$$\hat{B}^{\dagger}_{-k_y,\Omega} = i\sqrt{n_{\rm F}(2\pi\Omega)}\hat{c}^{>}_{k_y,\Omega} + \sqrt{n_{\rm F}(-2\pi\Omega)}\hat{d}^{<\dagger}_{-k_y,\Omega}. \tag{4.51b}$$

Equation (4.49) suggests that what I see as the vacuum of a flat graphene sheet, may appear as a state filled with Rindler strained particles. Thus I can express the Minkowski vacuum in terms of Rindler excited states in the following way [156, 157]:

$$|0_{\mathcal{M}}\rangle = \prod_{k_y,\Omega} |0_{k_y,\Omega}\rangle_{\mathcal{M}}, \tag{4.52}$$

$$|0_{k_y,\Omega}\rangle_{\mathcal{M}} = \sum_{m,n=0}^{1} A_{mn}|m^{>}_{k_y,\Omega}\rangle_{\mathcal{R}}\ |n^{<}_{-k_y,\Omega}\rangle_{\mathcal{R}}, \tag{4.53}$$

which expresses the Minkowski vacuum state in terms of a Rindler state with m electrons on the right and n holes on the left side. Note that the sum has only two entries because of the Pauli principle for fermions which according to (4.45), means that the electron annihilation operator (also true for holes) acting on the state with no electrons as well as

the corresponding electron creation operator acting on a state with one electron will yield zero, i.e. $\hat{c}|0_{\mathcal{R}}\rangle = \hat{c}^{\dagger}|1_{\mathrm{R}}\rangle = 0$. Dropping the quantum labels k_y and Ω, and the subscript $\mathcal{R}$, and applying the modified Minkowski electron annihilation operator $\hat{A}_{k_y,\Omega}$ to the above Minkwoski state in Eq. (4.52), I get ([156, 157]):

$$\begin{aligned} 0 &= \hat{A}|0_{k_y,\Omega}\rangle_{\mathcal{M}} \\ &= \big[n_{\mathrm{F}}^{\frac{1}{2}}(2\pi\Omega)A_{11} + in_{\mathrm{F}}^{\frac{1}{2}}(-2\pi\Omega)A_{00}\big]|0^{>}\rangle|1^{<}\rangle \\ &+ n_{\mathrm{F}}^{\frac{1}{2}}(-2\pi\Omega)A_{10}|0^{>}\rangle|0^{<}\rangle + in_{\mathrm{F}}^{\frac{1}{2}}(2\pi\Omega)A_{10}\big]|1^{>}\rangle|1^{<}\rangle. \end{aligned} \tag{4.54}$$

If the right hand side vanishes for arbitrary Rindler Fock states, then this yields the summation coefficients as $A_{10} = A_{01} = 0$, and $A_{11} = -iA_{00}e^{-\pi\Omega}$. Also normalizing the ansatz in (4.52) yields $|A_{00}|^2 + |A_{11}|^2 = 1$. Combining these ideas, I get $A_{00} = n_{\mathrm{F}}^{\frac{1}{2}}(2\pi\Omega)$ and $A_{11} = -in_{\mathrm{F}}^{\frac{1}{2}}(-2\pi\Omega)$, and therefore the flat graphene vacuum state can be expressed as a two-mode squeezed state of Rindler-strained fermions:

$$|0_{\mathcal{M}}\rangle = \prod_{k_y,\Omega} n_{\mathrm{F}}^{\frac{1}{2}}(-2\pi\Omega)\Big[|0^{>}_{k_y,\Omega}\rangle_{\mathcal{R}}\ |0^{<}_{-k_y,\Omega}\rangle_{\mathcal{R}} - ie^{-\pi\Omega}|1^{>}_{k_y,\Omega}\rangle_{\mathcal{R}}\ |1^{<}_{-k_y,\Omega}\rangle_{\mathcal{R}}\Big], \tag{4.55}$$

similar to the Bardeen-Cooper-Schrieffer (BCS) state [158, 159] for electrons that form a Cooper pair [160] inside a superconductor or superfluid. From this, a density matrix can be constructed $\hat{\rho} = |0_{\mathcal{M}}\rangle\langle 0_{\mathcal{M}}|$ representing the pure state of the flat graphene sheet, and when traced over the left side ($x < 0$) Rindler particle states, I get a reduced density matrix in terms of the Rindler Hamiltonian expressed in terms of modes pertaining to the right side only ($x > 0$):

$$\hat{\rho}^{>} = \frac{e^{-2\pi\hat{H}^{>}}}{\mathrm{Tr}\ e^{-2\pi\hat{H}^{>}}}, \tag{4.56}$$

where the normal ordered Hamiltonian constrained to the right side should be understood

in terms of a sum in modes $\hat{H}^{>} = \sum_{k_y,\Omega} \Omega\{\hat{c}^{>\dagger}_{k_y,\Omega}\hat{c}^{>}_{k_y,\Omega} + \hat{d}^{>\dagger}_{k_y,\Omega}\hat{d}^{>}_{k_y,\Omega}\}$. This density matrix is clearly of the Gibbs' thermal ensemble form.

In the case of the conventional Unruh effect with an accelerating observer, the Rindler horizon that bars any communication between the two wedges presents a natural trace of the density matrix. In the present setting of a strained honeycomb lattice, the low-energy and long-wavelength modes see the point $x = 0$ as an analog horizon and thus leakage of such modes between the two sides is either zero or minuscule. Hence, even though the global state of the honeycomb system might be a pure state, when I make measurements on one side of the sheet, the degrees of freedom on the other side are not available to us and hence get *naturally* traced out from the density matrix giving us a reduced mixed thermal state as in Eq. (4.56) [100, 108, 161, 116]. This is known as the thermalization theorem which says that the presence of horizons in a spacetime is sufficient for thermality to emerge. It is intimately connected to the Kubo-Martin-Schwinger (KMS) condition [105, 106] and the principle of detailed balance which I shall discuss in the next section. Thus any strain pattern that realizes an analog spacetime with a natural horizon such as black holes, de-Sitter or Rindler, can lead to the appearance of such thermal effects.

So far I have discussed how a Rindler Hamiltonian (4.23) forms from assuming a linear-in-position Fermi velocity $v(x) = v_0\frac{|x|}{\lambda}$, how this leads to the Bogoliubov transformations (4.43) between the strained (Rindler) and flat (modified Minkowski) honeycomb operators, giving rise to the vacuum averages in (4.49) that behave as thermal averages over an ensemble represented by the density matrix (4.56). These results collectively are termed as the Unruh effect which emerges due to the presence of a natural demarcation in

the material. Before we discuss the implications of this spontaneous electron-hole formation on observables like the electronic conductivity and internal energy, in the next section I will present the Green's functions pertaining to the strained graphene system to discuss in what sense is the Unruh effect a genuine thermal phenomena. I will also discuss how the dimensionality of graphene leads to the violation of Huygens' principle and the inversion of statistics which could possibly be seen in photo-emission experiments.

4.5. Green's Functions

In this section, I describe properties of single-particle Green's functions that will help us explain how thermal behavior emerges, how the Huygens' principle is violated and how this leads to the phenomena of apparent statistics inversion in the excitation spectrum of fermions. Towards the end of this section, I discuss how these properties can be detected in experiments like photoemission spectroscopy (PES) and scanning tunneling microscopy (STM).

Following Ooguri [109], I introduce two fundamental single particle Green's functions defined with respect to the flat graphene vacuum state $|0_{\mathcal{M}}\rangle$:

$$G_+(\boldsymbol{r},t;\boldsymbol{r}',t') = \langle 0_{\mathcal{M}}|\hat{\psi}_{\mathrm{R}}(x,y,t)\hat{\psi}^{\dagger}_{\mathrm{R}}(x',y',t')|0_{\mathcal{M}}\rangle, \tag{4.57a}$$

$$G_-(\boldsymbol{r},t;\boldsymbol{r}',t') = \langle 0_{\mathcal{M}}|\hat{\psi}^{\dagger}_{\mathrm{R}}(x,y,t)\hat{\psi}_{\mathrm{R}}(x',y',t')|0_{\mathcal{M}}\rangle. \tag{4.57b}$$

Here G_+ creates a particle at location $\boldsymbol{r}' = (x', y')$ and time t', and then annihilates it at another location $\boldsymbol{r} = (x, y)$ and time t, whereas G_- does the opposite. In the condensed-matter context, these are called the $>$ and $<$ Green's functions, respectively [162] (up to factors of i), and their physical interpretation will become clear when I discuss their Fourier transforms below.

Interestingly, despite the intrinsically nonequilibrium nature of this setup, i.e., a sudden switch-on of the system strain that changes the system Hamiltonian from the Dirac to the Rindler Hamiltonian, these Green's functions have simple forms, at least in the local real-space limit. To see this, we set the positions equal i.e. $x' = x$ and $y' = y$. Making use of mode expansion (4.31) for the right node fields and the vacuum averages (4.49) for Rindler ladder operators with respect to Minkowski vacuum, and taking the spinor trace, I find:

$$\text{Tr } G_+(x, y, \Delta t) = \frac{1}{2\pi x^2} \int_0^\infty d\Omega \; \Omega \coth \pi\Omega \Big[e^{i\Omega\Delta t} n_{\text{F}}(2\pi\Omega) + e^{-i\Omega\Delta t} n_{\text{F}}(-2\pi\Omega) \Big], \tag{4.58}$$

$$\text{Tr } G_-(x, y, \Delta t) = \frac{1}{2\pi x^2} \int_0^\infty d\Omega \; \Omega \coth \pi\Omega \Big[e^{i\Omega\Delta t} n_{\text{F}}(-2\pi\Omega) + e^{-i\Omega\Delta t} n_{\text{F}}(2\pi\Omega) \Big], \tag{4.59}$$

where $\Delta t = (t - t')$. If I define a typical timescale associated with the Unruh temperature, $\hbar/(k_{\text{B}} T_{\text{U}})$ (equal to 2π in our units) then it can be shown that the above Green's functions are periodic in imaginary shifts by this timescale:

$$\text{Tr } G_+(x, y, \Delta t - 2\pi i) = \text{Tr } G_-(x, y, \Delta t). \tag{4.60}$$

This is known as the Kubo-Martin-Schwinger (KMS) condition [105, 106] which in the conventional equilibrium case at temperature T, guarantees that the thermal average of any two operators $\hat{A}$ and $\hat{B}$ for a system kept in contact with a heat bath at temperature $\beta = (k_{\text{B}} T)^{-1}$ is also periodic in imaginary time, i.e. $\langle \hat{A}(t)\hat{B}(t') \rangle = \langle \hat{B}(t')\hat{A}(t + i\beta) \rangle$. For example, if I take the operators $\hat{A}$ and $\hat{B}$ as the graphene right-node field operators, then I get the following KMS condition for the Green's functions in (4.57a) and (4.57b):

$$G_+(\boldsymbol{r}, \boldsymbol{r}', \Delta t - 2\pi i) = G_-(\boldsymbol{r}, \boldsymbol{r}', \Delta t). \tag{4.61}$$

Note that here I have assumed that the Green's functions depend solely on the time dif-

ference Δt because the system exhibits time translation invariance when it is in thermal equilibrium. In an isolated strained graphene sheet, this condition implies that the vacuum (pure state) average of field operators behaves as a legitimate thermal (mixed state) average with respect to the reduced density operator (4.56) (that can be thought of as an evolution operator [162, 163]), as if it is kept in contact with a real heat bath set at the Unruh temperature, i.e. $T = T_{\rm U}$.

To further understand the meaning of the KMS condition, I take the Fourier transforms of the above Green's functions (4.58) and (4.59) defined as

$$F_{\pm}(x,\omega) = \int_{-\infty}^{\infty} d(\Delta t)\; e^{-i\omega\Delta t}{\rm Tr}\; G_{\pm}(x,y,\Delta t), \tag{4.62}$$

from which I obtain:

$$F_{+}(x,\omega) \;=\; \frac{\omega}{x^2} n_{\rm B}(2\pi\omega), \tag{4.63}$$

$$F_{-}(x,\omega) \;=\; -\frac{\omega}{x^2} n_{\rm B}(-2\pi\omega). \tag{4.64}$$

As discussed by Coleman [162], $F_{+}(x,\omega)$ is the photo-emission spectra that gives the total excitation of electrons when graphene is illuminated by light. Similarly, $F_{-}(x,\omega)$ measures the de-excitation spectra. The ratio of these two power spectra turns out to be:

$$\frac{F_{+}(x,\omega)}{F_{-}(x,\omega)} = e^{-2\pi\omega}, \tag{4.65}$$

which says that the rate of excitation versus de-excitation is of the Boltzmann form with the strain frequency $1/2\pi$ playing the role of temperature. This is the principle of detailed balance which originates from Boltzmann's principle of microscopic reversibility [164, 165], but was first applied to quantum systems by Einstein in [201] that predicted the phenomena of stimulated emission. He studied the set up where an atom with two energy levels

$E_1 < E_2$ is in thermal contact with a bath of photons such that when equilibrium sets in the ratio of number of particles in the excited state $|E_2\rangle$ versus $|E_1\rangle$ is $e^{-\beta(E_2-E_1)}$. Then by demanding that the excitation probability should match de-excitation (spontaneous and stimulated) at equilibrium, the number distribution of photons will be given by a Planck distribution $\rho(\omega) = (\exp(\beta\omega) - 1)^{-1}$, where $\omega = (E_2 - E_1)$ is the energy of the photon wave-packet that is absorbed by the two-level atoms. Such two-level systems are termed Unruh-DeWitt detectors in the relativistic context [104, 161]. Thus the Fourier transform of the KMS condition, i.e., the principle of detailed balance, tells us that accelerated fermionic fields have a Fermi-Dirac spectrum and when they are in contact with a two-level or more atom or detector, then the latter comes into global thermal equilibrium with the field with the Unruh temperature defined everywhere on the real or analog spacetime.

The discussion above can be summarized by stating the thermalization theorem. For a comprehensive account of its various versions, see [108]. It states that if the spacetime (or the analog system) has a causal horizon (like the Minkowski spacetime in Rindler coordinates), then any quantum field on that spacetime will spontaneously emit particles in a thermal distribution characterized by a Bose or Fermi function which is captured by the reduced density matrix (4.56) in Gibbs' ensemble form. Once this density operator is achieved, then the KMS condition (4.60), or more generally Eq. (4.61), guarantees that the field will also thermalize any other system (like an atom or a detector) in its contact, that has energy levels, thus establishing a global thermal equilibrium with temperature $T = 1/2\pi$.

To discuss Huygens' principle and how its violation leads to statistics inversion, I

now consider two other fundamental Green's functions pertaining to the commutator and the anti-commutator of fermionic fields, that are similar to the Green's functions defined in (4.58) and (4.59). The former is related to the Keldysh Green's function [167] and the latter is related to the retarded Green's function that takes causality into account:

$$G_C(\boldsymbol{r},t;\boldsymbol{r}',t') = \langle 0_{\mathcal{M}}|\Big[\hat{\psi}_{\rm R}(x,y,t),\hat{\psi}^{\dagger}_{\rm R}(x',y',t')\Big]|0_{\mathcal{M}}\rangle, \tag{4.66a}$$

$$G_A(\boldsymbol{r},t;\boldsymbol{r}',t') = \langle 0_{\mathcal{M}}|\Big\{\hat{\psi}^{\dagger}_{\rm R}(x,y,t),\hat{\psi}_{\rm R}(x',y',t')\Big\}|0_{\mathcal{M}}\rangle. \tag{4.66b}$$

After setting $x=x'$ and $y=y'$, computing these Green's functions, and taking the trace, I get:

$$\text{Tr } G_C(x,y,\Delta t) = -\frac{i}{\pi x^2}\int_0^{\infty} d\Omega\ \Omega\sin(\Omega\Delta t), \tag{4.67}$$

$$\text{Tr } G_A(x,y,\Delta t) = \frac{1}{\pi x^2}\int_0^{\infty} d\Omega\ \Omega\coth(\pi\Omega)\cos(\Omega\Delta t). \tag{4.68}$$

Conventionally, the Huygens' principle states that, if I have a source in even spacetime dimensions, then its wave-fronts can be constructed by drawing circles (appropriate to the dimensions) with the source at the center [108]. This means that the retarded Green's function that describes the propagation of waves to any point (x,y,t) with the source at (x',y',t') has support only on the light cone, i.e. it vanishes when (x',y',t') and (x,y,t) are either timelike or spacelike separated. This implies that the retarded Green's function in even spacetime dimensions is proportional to a Dirac delta function and its derivatives. However, strained graphene mimics an odd-dimensional spacetime where I find that the anticommutator in Eq. (4.68) is not a Dirac delta function. This is the manifestation of the well-known violation of Huygens' principle [108],[168]. It says that in odd spacetime dimensions, our intuition for wave propagation breaks down, i.e. a sharp source of wave

does not lead to a single spherical wavefront, and instead the observer notices a continuously decreasing tail.

Curiously, although the anticommutator Green's function violates Huygens' principle, from Eq. (4.67) I see that the commutator Green's function G_C amounts to $\frac{2i}{x^2}\delta'(\Delta t)$, i.e. it has support on the light cone. As a result, it is expected that the Fourier transform of the G_C will be a polynomial in ω, whereas for G_A it will lead to the following:

$$F_C(x,\omega) = -\frac{\omega}{x^2}, \tag{4.69}$$

$$F_A(x,\omega) = \frac{\omega}{x^2}\coth \pi\omega. \tag{4.70}$$

To see the connection of this violation of Huygens' principle with statistics inversion, I need the fluctuation-dissipation theorem. They can be derived in general by writing (4.68) and (4.67) in terms of (4.57a) and (4.57b), i.e. $G_A = G_+ + G_-$ and $G_C = G_+ - G_-$, Fourier transforming them, and finally applying the KMS condition or the principle of detailed balance i.e. $F_- = e^{2\pi\omega}F_+$, yields two different but equivalent versions of the theorem:

$$F_+(x,\omega) = n_{\rm F}(2\pi\omega)\times F_{\rm A}(x,\omega), \tag{4.71}$$

$$= n_{\rm B}(2\pi\omega)\times -F_{\rm C}(x,\omega). \tag{4.72}$$

The excitation or power spectrum $F_+(x,\omega)$ is related to the rate at which an accelerated detector senses Rindler particles, and shows inversion of statistics depending on the dimension of the spacetime [108, 110, 109, 111, 113, 112, 114, 115]. Following Ooguri [109], there are two interpretations for this. The first makes use of (4.71), which says that the excitation spectrum is basically the Fermi-Dirac function coming from the real statistics of the fermions, multiplied with the spectral density of states coming from the Fourier transform of anti-commutator which I know violates Huygens' principle and thus is not simply

a polynomial in ω. This, coupled with the particular form of the mode functions in (4.31) gives us a hyperbolic cotangent which coincidentally inverts the Fermi to a Bose function. The other interpretation comes from (4.72), where one can argue that since we are in odd spacetime dimensions in graphene, therefore I would expect the Fourier transform of the commutator to be polynomial in ω (see (4.69)). Thus the excitation spectrum should be expected to be a Bose-Einstein distribution multiplied by a factor which is polynomial in ω, thereby removing the need to invoke any inversion.

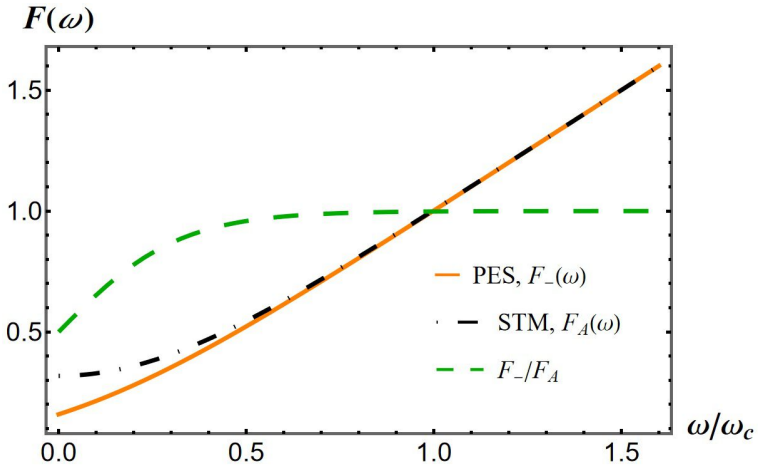

Figure 4.3. The orange solid curve is a plot of the power spectrum $F_{-}(\omega)$, that can be measured in photo-emission spectroscopy (PES) experiments. The black dot-dashed curve is a plot of $F_A(\omega)$ that can be measured in scanning-tunneling microscopy (STM) experiments that measure the density of states. Their ratio (in green), yields the expected Fermi-Dirac spectrum in accordance with the Unruh effect predictions.

To see how these power spectra could manifest themselves in experiments, I focus at the first version (4.71) of the Fluctuation-Dissipation theorem, but instead for F_{-}, i.e. $F_{-}(\omega) = n_{\rm F}(-2\pi\omega)F_{\rm A}(\omega)$. To do this, the experimenter will first obtain the photo-emission data from the Photo Emission Spectroscopy or the PES experiment [30]. For low-energies and long wavelengths, this will give us a plot of fermion occupancy in

graphene's lowest energy band which in this limit, should mimic the Planck distribution $F_- = -\frac{\omega}{x^2} n_{\rm B}(-2\pi\omega)$. As can be seen from Fig. 4.3, $F_-(\omega)$ increases with energy, which is due to the fact that the PES-experiment measures the occupancy of valence band electrons by extracting them by shining light. If the intensity of light is increased, then more electrons residing in the lower valence energy levels will be detected. The experimenter can then obtain the data regarding the local density of states by performing the Scanning Tunneling Microscopy or the STM experiment [124, 126] which, in the low-energy and long-wavelength limit (where our calculations are valid), will be given by the statistics inversion factor $F_A = \frac{\omega}{x^2} \coth \pi\omega$, which implies that Huygens' principle is being violated in strained graphene. Now if I take the ratio of the PES and STM data, I will find:

$$\frac{\text{PES data}}{\text{STM data}} = \frac{F_-(x,\omega)}{F_A(x,\omega)} = n_{\rm F}(-2\pi\omega), \tag{4.73}$$

I will obtain the Fermi-Dirac distribution as expected from the Unruh effect of fermions, as can be seen in Fig. 4.3.

Equipped with the Bogoliubov transformations (4.43) between the strained (Rindler) and flat (modified Minkowski) honeycomb operators, that lead to the vacuum averages in (4.49) and the statistics inversion in Eqs. (4.71)-(4.72), we are now ready to discuss in the next two sections, the implications of this spontaneous electron-hole formation on observables like the electronic conductivity and total internal energy.

4.6. Electronic Conductivity

In this section, I consider another observable that is sensitive to the Unruh effect in strained graphene, the frequency-dependent conductivity. For this calculation, I shall require the Bogoliubov transformations (4.43), derived in Sec. 4.4, that establish the re-

lationship between the Rindler operators $\{\hat{c}, \hat{d}\}$ in a strained honeycomb system with the modified Minkowski operators $\{\hat{A}, \hat{B}\}$ in a flat (unstrained) honeycomb system. This led us to the expectation value (4.49) of the Rindler operators with respect to the Minkowski vacuum. To use these results, I will need the Kubo formula that relates the frequency-dependent conductivity to an associated current-current correlation function. For generality, we'll briefly recall the Kubo formula derivation for both the setups considered here, i.e., the case of electronic graphene (in which the fermions are charged electrons) and the case of neutral cold atoms in an optical lattice.

For the electronic graphene case, I can start with the Rindler Hamiltonian (4.23) minimally coupled to an electromagnetic vector potential $\boldsymbol{A}(\boldsymbol{r}, t)$, i.e. I can make the replacement $-i\hbar\boldsymbol{\nabla} \to -i\hbar\boldsymbol{\nabla} - e\boldsymbol{A}$ in the derivative operators giving us the following new Hamiltonian [190]:

$$\begin{aligned} \hat{H}(t) &= \hat{H}_{\rm R} + \hat{H}^1(t), \\ \hat{H}^1(t) &= -\int d^2r\ \hat{\boldsymbol{j}}(\boldsymbol{r}, t) \cdot \boldsymbol{A}(\boldsymbol{r}, t), \end{aligned} \tag{4.74}$$

where $\hat{H}_{\rm R}$ is the Rindler Hamiltonian (4.23). Here, the conserved current operator in the strained (Rindler) system is:

$$\hat{\boldsymbol{j}}(\boldsymbol{r}, t) \equiv ev_0 \frac{|x|}{\lambda} \hat{\psi}^\dagger_{\rm R}(\boldsymbol{r}, t) \boldsymbol{\sigma} \hat{\psi}_{\rm R}(\boldsymbol{r}, t). \tag{4.75}$$

Within linear response theory, I can treat the vector potential term as a perturbation, and to linear order the response of the average current is given by:

$$\begin{aligned} \langle \hat{j}_\mu(\boldsymbol{r}, t) \rangle &= -\frac{i}{\hbar} \int_{-\infty}^{t} dt'\ \big\langle \big[\hat{j}_\mu(\boldsymbol{r}, t), \hat{H}^1(t') \big] \big\rangle, \\ &= \frac{i}{\hbar} \int_{-\infty}^{t} dt' \int d^2r'\ \big\langle \big[\hat{j}_\mu(\boldsymbol{r}, t), \hat{j}_\nu(\boldsymbol{r}', t') \big] \big\rangle A_\nu(\boldsymbol{r}', t'). \end{aligned} \tag{4.76}$$

The time-dependent vector potential can be written as $A_\nu(\boldsymbol{r}', t') = \frac{1}{i\omega^+} E_\nu(\boldsymbol{k}, \omega) e^{-i(\boldsymbol{k}\cdot\boldsymbol{r}' + \omega^+ t')}$, where $\omega^+ = \omega + i\delta$, with $\delta = 0^+$. Here, $E_\nu(\boldsymbol{k}, \omega)$ is the electric field at wavevector $\boldsymbol{k}$ and frequency ω. Upon plugging this into Eq. (4.76), multiplying both sides by $e^{-i\boldsymbol{q}\cdot\boldsymbol{r}}$ and integrating over $\boldsymbol{r}$ in the limit of $\boldsymbol{q} \to 0$ (corresponding to spatial averaging), I obtain:

$$\langle \hat{j}_\mu(\boldsymbol{q} \to 0, t) \rangle \;=\; \frac{1}{\hbar\omega^+} \int_{-\infty}^{\infty} dt' \Theta(t - t') e^{-i\omega^+ t'} \big\langle \big[\hat{j}_\mu(0, t), \hat{j}_\nu(0, t') \big] \big\rangle E_\nu(0, \omega). \tag{4.77}$$

Noting that the time-dependent electric field $E_\nu(0, t) = E_\nu(0, \omega) e^{-i\omega^+ t}$, redefining the variable of integration to $T = (t - t')$ and taking the ratio of current and electric field, I find the average conductivity tensor $\sigma_{\mu\nu} = \frac{\langle \hat{j}_\mu(0,t) \rangle}{E_\nu(0,t)}$:

$$\sigma_{\mu\nu} = \frac{1}{\hbar\omega^+} \int_{-\infty}^{\infty} dT \; \Theta(T) e^{i\omega^+ T} \big\langle \big[\hat{j}_\mu(0, T), \hat{j}_\nu(0, 0) \big] \big\rangle. \tag{4.78}$$

The preceding derivation depends on the use of the vector potential as an external stimulus. But, for a system that is not made of charged particles such as neutral ultracold atomic gases, I must use a different approach. In this case, a change in the local chemical potential creates a pressure difference and hence affects the density of fermions. Instead of Eq. (4.74), the perturbing Hamiltonian involves a coupling of the atom density $\hat{n}(\boldsymbol{r}, t) = \hat{\psi}^\dagger(\boldsymbol{r}, t)\hat{\psi}(\boldsymbol{r}, t)$ to a spatially and temporally varying chemical potential:

$$\hat{H}^1(t) = -\int d^2 r \; \mu(\boldsymbol{r}, t) \hat{n}(\boldsymbol{r}, t). \tag{4.79}$$

Plugging this into Eq. (4.76) with $\mu(\boldsymbol{r}, t) = \mu(\boldsymbol{r}) e^{-i\omega t}$, integrating by parts in the t' integral and also integrating by parts in space using the equation of continuity $0 = \frac{\partial}{\partial t}\hat{n}(\boldsymbol{r}, t) + \boldsymbol{\nabla} \cdot \hat{\boldsymbol{j}}(\boldsymbol{r}, t)$, I finally arrive at the Kubo formula for neutral atoms, with the average atom current related to the chemical potential gradient as $\boldsymbol{j} \;=\; -\sigma \boldsymbol{\nabla} \mu$ where σ is given by (4.78).

Thus, in either case I require the current-current correlation function, with the averages being performed with respect to the Minkowski vacuum. I start with the computation of σ_{xx}. Instead of directly using Eq. (4.78) that involves the spatially Fourier-transformed current correlator, I start with the real-space current-current correlation function, perform spatial averages (on $\boldsymbol{r}$ and $\boldsymbol{r}'$), and finally Fourier transform to frequency space. The average current correlation function at the right node has the following form :

$$\bar{C}^{xx}(t-t') \;=\; \int d^2r \int d^2r' \langle 0_{\mathcal{M}}|\hat{j}^x(\boldsymbol{r},t)\hat{j}^x(\boldsymbol{r}',t')|0_{\mathcal{M}}\rangle, \tag{4.80}$$

where we are evaluating the correlations only between fields on the right node. In what follows, I will set $e \to 1$, $\hbar \to 1$ and $\omega_c \to 1$.

I performed spatial integrals on (4.80) along the coordinates $\boldsymbol{r}$ and $\boldsymbol{r}'$ because the conductivity Eq. (4.78) requires the current-current correlation in the reciprocal space in the limit $\boldsymbol{q} \to 0$. Integration along y and y' will yield Dirac delta functions in wavevectors $\delta(k_y - k_y')$, after which integration of spinor products is performed over x and x' directions using the following identity:

$$\int_0^\infty dx\; x\Big[K_{\frac{1}{2}+i\Omega}(x)K_{\frac{1}{2}-i\Omega'}(x) - K_{\frac{1}{2}-i\Omega}(x)K_{\frac{1}{2}+i\Omega'}(x)\Big] = \frac{i\pi^2(\Omega^2-\Omega'^2)}{2[\sinh(\pi\Omega)+\sinh(\pi\Omega')]}. \tag{4.81}$$

Thus the average current-current correlator as a function of time for the right handed fermions looks as follows:

$$\begin{aligned}\bar{C}^{xx}(\Delta t) = \frac{1}{2}\int_{-\infty}^{\infty} d\Omega \int_{-\infty}^{\infty} d\Omega'\;\; &\cosh\pi\Omega\cosh\pi\Omega' \\ &n_{\mathrm{F}}(2\pi\Omega)n_{\mathrm{F}}(-2\pi\Omega')e^{i(\Omega-\Omega')\Delta t}\;\frac{(\Omega^2-\Omega'^2)^2}{[\sinh(\pi\Omega)+\sinh(\pi\Omega')]^2},\end{aligned} \tag{4.82}$$

where $\Delta t = (t-t')$. I now subtract from this the current correlator with time coordinates

interchanged, $t \leftrightarrow t'$ i.e. $\bar{C}^{xx}(t'-t) = \bar{C}^{xx}(-\Delta t)$, to obtain the vacuum average of the commutator of current-current correlation. Plugging this into the expression for conductivity tensor (4.78), where I perform the Fourier transform of a retarded function in time using the Plemelj formula $\lim_{\delta\to 0^+} \frac{1}{x+i\delta} = \mathcal{P}\frac{1}{x} - i\pi\delta(x)$, and extracting the imaginary part, I finally obtain the xx-component of the dissipative average conductivity as follows:

$$\bar{\sigma}''_{xx}(\omega) = \frac{\pi\omega}{2}\int_{-\infty}^{\infty} d\Omega \ \cosh\pi\Omega\cosh\pi(\Omega+\omega) \tag{4.83}$$
$$\times\frac{(2\Omega+\omega)^2}{(\sinh\pi\Omega+\sinh\pi(\Omega+\omega))^2}\big[n_{\rm F}(2\pi\Omega) - n_{\rm F}(2\pi(\Omega+\omega))\big],$$

where the double prime $''$ denotes the imaginary part of conductivity that leads to dissipation of electronic current. In this formula, I have dropped dimensionful prefactors (such as $e^2/\hbar$, the typical units of conductivity), and I have dropped an extensive factor

$$\mathcal{A} = \int_0^\infty \frac{dk_y}{2\pi}\frac{1}{k_y^2}\int_{-\infty}^{\infty} dy = L_y\int_0^\infty \frac{dk_y}{2\pi}\frac{1}{k_y^2}, \tag{4.84}$$

with L_y the size of the system in the y direction. Properly handling the remaining integral would require analyzing our problem in a finite system along x, a task I leave for future work.

I have plotted Eq. (4.83) in Fig. 4.4 which shows that the conductivity grows approximately linearly with the probing frequency and vanishes in the DC-limit ($\omega \to 0$). As I discussed in Sec. 4.1, the Rindler Hamiltonian with Fermi velocity $v(x) \simeq v_0|x|/\lambda$, can be achieved for modes with low energies and long wavelengths. Hence, the results for conductivity (and for internal energy) for strained honeycomb lattices are valid if I choose to probe long-wavelength modes $k_y\lambda \ll 1$. This is valid because in order to evaluate these observables, spatial averages need to be performed equivalent to setting $\boldsymbol{q} \to 0$ in $\sigma(\omega, \boldsymbol{q}\to 0)$ as I discussed in Eq. (4.77).

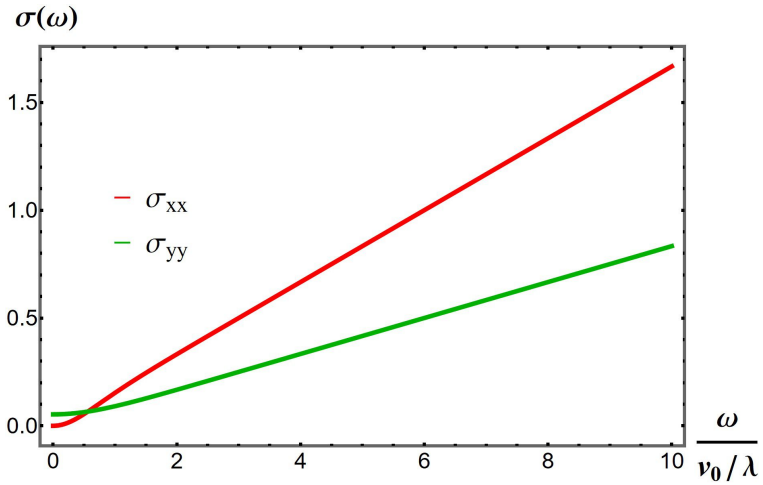

Figure 4.4. A plot showing how the average dissipative conductivity (in units of $e^2/\hbar$) grows approximately linearly as a function of AC-frequency (in units of strain frequency $\omega_c = v_0/\lambda$). The longitudinal components $\sigma''_{xx}(\omega)$ (in red) and $\sigma''_{yy}(\omega)$ (in green) both vanish in the DC-limit $\omega \to 0$.

To understand the result in Eq. (4.83), I revisit the electronic conductivity of flat graphene (per node and per spin) in the collisionless limit and at a finite environment temperature $\beta = (k_{\rm B}T)^{-1}$ [170]:

$$\bar{\sigma}''_{xx}(\omega) = \frac{1}{16}\Big[n_{\rm F}\Big(-\frac{\beta\omega}{2}\Big) - n_{\rm F}\Big(\frac{\beta\omega}{2}\Big)\Big] \tag{4.85}$$

$$= \frac{1}{16}\Big[1 - 2n_{\rm F}\Big(\frac{\beta\omega}{2}\Big)\Big], \tag{4.86}$$

where the left hand side is measured in units of $e^2/\hbar$. The right hand side vanishes in the DC-limit $\omega \to 0$. This happens because in this limit, only the energy levels close to the Dirac point participate in electronic transitions due to switching on the vector potential in (4.74). However, here the electron occupancy in conduction band, given by $n_{\rm F}(\beta\omega) \sim 0.5$, is equal to the electron occupancy in the valence band, given by $n_{\rm F}(-\beta\omega) \sim 0.5$. Thus the rate of excitation and de-excitation are equal and hence the electrons near the Dirac point (DC-limit) do not participate in conductivity. On the other hand, as the probing frequency is increased, the electron occupancy in the valence band starts exceeding the

conduction band, thus giving us a net rate of excitation of electrons that give non-zero conductivity. In the opposite limit of $\omega \gg (\hbar\beta)^{-1}$, the high energy modes are unaffected by the thermal scale and hence, the electron occupancy here is approximately unity, i.e. the de-excitation is minuscule and conductivity reaches it maximum value of $e^2/16\hbar$. The density of states in a two-dimensional material such as graphene, is expected to be linear in energy. However this gets cancelled out due to the $1/\omega$ in the expression for conductivity (4.78), and therefore only the Fermi functions are needed to physically understand the behavior of conductivity.

Since the strained graphene system is effectively at an Unruh temperature T_U, by analogy with the preceding argument I might also expect to find that $\sigma(\omega) \to 0$ for $\omega \to 0$, as I indeed find in Fig. 4.4. To derive the approximate linear behavior, I use the fact that the factor multiplying the Fermi functions in square brackets in Eq. (4.83) is sharply peaked at $\Omega = -\omega/2$. Then, we are allowed to make this replacement in the square brackets, yielding $\left[n_{\rm F}(-\pi\omega) - n_{\rm F}(\pi\omega)\right]$ that can be pulled outside the integral. Upon evaluating the remaining Ω integration over the peak region finally gives

$$\bar{\sigma}''_{xx}(\omega) \simeq \frac{\sqrt{3}}{2\pi^{3/2}}\omega \tanh\frac{\pi\omega}{2}, \tag{4.87}$$

which agrees with our numerical result in Fig. 4.4.

I can also interpret these results by focusing on the second version similar to (4.86) and noting that the conductivity is reduced due to the presence of emergent Fermi functions. This happens due to stimulated particle reduction [58, 171, 172, 173, 174]. The process of straining the honeycomb lattice leads to creation of fermions in the conduction band with a Fermi distribution $n_{\rm F}(2\pi\Omega)$ characterized by Unruh temperature (here $1/2\pi$),

yielding a thermally excited state. To study the linear electronic response of this system, a vector potential stimulus is provided because of which more electrons from the valence band jump to the conduction band. Pauli's exclusion principle does not allow the strained electrons to co-exist with the electronically excited ones, hence leading to an overall reduction in the response. Since particle creation is maximum at zero energy where the two bands meet (as the Unruh-Fermi function is maximum at low energies), it is easiest for strains to create electrons at this zero-energy level, and hence the stimulated reduction is maximum for zero probing frequency i.e. the DC-limit $\omega \to 0$. In contrast higher energies overpower the strains making the Fermi functions small, and hence maximum conductivity is achieved.

Next I turn to the conductivity σ_{yy} for directions perpendicular to the strain fields, which, following the same procedure, leads to the similar result:

$$\bar{\sigma}''_{yy}(\omega) = \frac{\pi\omega}{2}\int_{-\infty}^{\infty} d\Omega \ \cosh\pi\Omega\cosh\pi(\Omega+\omega) \times \frac{(2\Omega+\omega)^2}{(\sinh\pi\Omega - \sinh\pi(\Omega+\omega))^2}\big[n_{\rm F}(2\pi\Omega) - n_{\rm F}(2\pi(\Omega+\omega))\big], \tag{4.88}$$

the only difference being a minus sign in the denominator of one factor in the integrand. In this case the factor multiplying the Fermi functions in square brackets is not a narrow peak at $-\omega/2$; nonetheless the qualitative behavior is similar as seen in Fig. 4.4 which shows that just like the xx-component, the yy-component of conductivity also grows approximately linearly with the probing frequency and vanishes in the DC-limit ($\omega \to 0$). One key difference is that $\bar{\sigma}''_{yy}(\omega)$ is smaller in magnitude. The reason is that in $\hat{x}$-direction the atoms have been forced to come closer to each other using strains of type (4.6) thereby increasing the Fermi velocity, and thus hopping becomes easier. Whereas in

the $\hat{y}$-direction, the strains do not depend on coordinate y, and thus the atoms are further apart in this direction as compared to $\hat{x}$, hence the hopping and the conductivity here are lower.

The transverse or off-diagonal components of conductivity tensor are anti-symmetric i.e. $\sigma_{xy}(\omega) = -\sigma_{yx}(\omega)$, which can be readily inferred from the commutator in Eq. (4.78). This means that knowledge of one, determines the other. Performing similar calculations as the longitudinal case, yields a vanishing transverse conductivity:

$$\sigma''_{xy}(\omega) = -\sigma''_{yx}(\omega) = 0. \tag{4.89}$$

This can be expected because if $\sigma^{xy} \neq 0$, then an electric field in the x-direction E_x would be able to create a current in the y-direction. However due to translation symmetry, there is no reason why $+\hat{y}$ would be favored over $-\hat{y}$, and thus the current is expected to be zero by symmetry. This symmetry gets broken when there is a real magnetic field in the system.

In this section I showed how the Rindler Hamiltonian (4.23) leads to a linear in probing frequency behavior of longitudinal components of the electronic conductivity (4.83), (4.88), and that the transverse (4.89) components simply vanish. These results for average dissipative conductivity are summarized in Fig. 4.4, where both the longitudinal components scale linearly for frequencies. In the next section, I will take a look at the consequence of Rindler Hamiltonian on the internal energy of such honeycomb systems.

4.7. Internal Energy

As I saw in the previous section, that spontaneous particle creation due to us assuming a linear-in-position Fermi velocity had a profound effect on the behavior of elec-

tronic conductivity which scaled linearly in the probing frequency, as opposed to the flat honeycomb case where it has a constant value for all frequencies. In this section, I will be looking at how this Rindler-Unruh particle creation affects the response of honeycomb systems when brought in contact with a thermal heat bath, i.e. I will find the total electronic energy in the system U, which can be calculated using the expectation value of the Rindler Hamiltonian (4.23) with respect to a Minkowski thermal density matrix labeled by the temperature parameter $\beta = (k_{\rm B}T)^{-1}$ as a subscript:

$$\begin{aligned} U_{\rm M} &= \langle \hat{H}_{\rm R} \rangle_{\beta}, \\ &= i\hbar \left\langle \int d^2x \; \hat{\psi}^{\dagger}_{\rm R}(x) \cdot \partial_t \hat{\psi}_{\rm R}(x) \right\rangle_{\beta,\mathcal{M}}, \end{aligned} \tag{4.90}$$

where to get the second line I made use of the Dirac equation (4.24) to simplify further calculations. Equivalently, this can also be calculated using the energy-momentum tensor operator as discussed in Ref. [108]. However, the above Minkowski thermal average is divergent and thus requires normal ordering. This involves subtracting off the Rindler thermal average (i.e. the limit of zero strains $\lambda \to \infty$) of the Rindler Hamiltonian from the Minkowski average as follows:

$$U = \langle \hat{H}_{\rm R} \rangle_{\beta,\mathcal{M}} - \langle \hat{H}_{\rm R} \rangle_{\beta,\mathcal{R}}. \tag{4.91}$$

This renormalization is needed because the Hamiltonian is quadratic in the fields $\hat{\psi}^2(x)$ [45, 48, 99, 100, 46, 47], and thus the expectation value has a genuine divergence since even smearing the field operators will not cure this divergence, unlike the case of two-point functions which are bi-distributions and their divergences at short distances can be cured by smearing.

To evaluate these expectation values, the physical picture that I will be needing is that the honeycomb lattice is initially in a thermal state (due to contact with a heat bath or the surroundings), and then strains are put on it. As a result, the initial state of the flat honeycomb lattice is described by the eigenstates of the standard Dirac Hamiltonian (4.15), whose excitations are described by Minkowski operators $\{\hat{a}_{\boldsymbol{k}}, \hat{b}_{\boldsymbol{k}}\}$ in Eq. (4.20) labeled by momentum vector $\boldsymbol{k}$. Since this system is also kept in contact with a heat bath at temperature $\beta = (k_{\rm B}T)^{-1}$, the thermal averages of Minkowski operators will be given by the Fermi distributions:

$$\langle \hat{a}^{\dagger}_{\boldsymbol{k}} \hat{a}_{\boldsymbol{k}} \rangle_{\beta,\mathcal{M}} = \langle \hat{b}^{\dagger}_{\boldsymbol{k}} \hat{b}_{\boldsymbol{k}} \rangle_{\beta,\mathcal{M}} = n_{\rm F}(\beta\epsilon_k) \equiv \frac{1}{e^{\beta\epsilon_k}+1}, \tag{4.92}$$

as a function of the Minkowski energy dispersion relation $\epsilon_k = \hbar\omega_k = \hbar v_0 |\boldsymbol{k}|$. When the strains are turned on, then the system is described the Rindler Hamiltonian (4.23), whose excitations are governed by the Rindler operators $\{\hat{c}_{k_y,\Omega}, \hat{d}_{k_y,\Omega}\}$, labeled by the independent pair of momenta $\hbar k_y$ and energy $\hbar\Omega$. I have seen in Sec. 4.3, that the Bogoliubov transformations (4.43) help express these Rindler operators in terms of modified Minkowski operators $\{\hat{A}^{\pm}_{k_y,\Omega}, \hat{B}^{\pm}_{k_y,\Omega}\}$, which are in turn complex linear combinations of the standard ones $\{\hat{a}_{\boldsymbol{k}}, \hat{b}_{\boldsymbol{k}}\}$ as given in Eq. (4.44). Thus making use of this transformation between operators, and the thermal averages in Eq. (4.92), I obtain the thermal averages of the Rindler operators in the Minkowski vacuum as follows:

$$\begin{aligned}
& \left\langle \hat{c}^{\dagger}_{k_y,\Omega} \hat{c}_{k'_y,\Omega'} \right\rangle_{\beta,\mathcal{M}} = \left\langle \hat{d}^{\dagger}_{k_y,\Omega} \hat{d}_{k'_y,\Omega'} \right\rangle_{\beta,\mathcal{M}} \\
= \;& \delta(k_y - k'_y) \Bigg[\delta(\Omega - \Omega') \sqrt{n_{\rm F}(2\pi\Omega)} \sqrt{n_{\rm F}(2\pi\Omega')} \\
+ \;& \left\{ \sqrt{n_{\rm F}(-2\pi\Omega)} \sqrt{n_{\rm F}(-2\pi\Omega')} - \sqrt{n_{\rm F}(2\pi\Omega)} \sqrt{n_{\rm F}(2\pi\Omega')} \right\} Z_{k_y}(\Delta) \Bigg],
\end{aligned} \tag{4.93}$$

where $\Delta \equiv \Omega - \Omega'$ and I define the function $Z_{k_y}(\Delta)$:

$$Z_{k_y}(\Delta) = \int_{-\infty}^{\infty} \frac{dk_x}{2\pi k} \left(\frac{k + k_x}{k - k_x} \right)^{-i\Delta/2} n_{\mathrm{F}}(\beta \epsilon_k), \tag{4.94}$$

which I emphasize is real (i.e., $Z^*_{k_y}(\Delta) = Z_{k_y}(\Delta)$). Note the difference between the two types of Fermi distributions being used here. The first $n_{\mathrm{F}}(\beta\epsilon_k)$, is due to a heat bath labeled by the environment temperature parameter β and is a function of the Minkowski energy ϵ_k. The second one $n_{\mathrm{F}}(2\pi\Omega)$ is an emergent thermal distribution governed by the strain frequency $\omega_c = v_0/\lambda$.

The thermal averages in (4.93) have a temperature-independent part proportional to a delta function in energy $\delta(\Omega - \Omega')$ and a temperature-dependent part having the function $Z_{k_y}(\Omega - \Omega')$. To get an intuition for this formula, I discretize the wavevector and frequency delta functions to Kronecker delta functions, effectively smearing the Rindler operators [108]. Then taking $k'_y = k_y$ and $\Omega' = \Omega$, the electron (or hole) thermal averages take the following form:

$$\begin{aligned} & N_{k_y,\Omega} \equiv \left\langle \hat{c}^\dagger_{k_y,\Omega} \hat{c}_{k_y,\Omega} \right\rangle_{\beta,\mathcal{M}} - Z_{k_y}(0) \\ = \;& n_{\mathrm{F}}(2\pi\Omega) \left[1 - \frac{1}{\pi} \int_{-\infty}^{\infty} \frac{d\hat{k}_x}{\sqrt{\hat{k}_x^2 + \hat{k}_y^2}} n_{\mathrm{F}}\left(\sqrt{\hat{k}_x^2 + \hat{k}_y^2} \right) \right], \end{aligned} \tag{4.95}$$

where Ω is the dimensionless frequency used elsewhere (in which the Unruh temperature is $1/(2\pi)$) and the wavevectors $\hat{\boldsymbol{k}} = \frac{\hbar v_0 \boldsymbol{k}}{k_B T}$ are normalized using the real system temperature T. I have also renormalized the number average by subtracting off the Rindler vacuum contribution which can be found by setting $T_{\mathrm{U}} = 0$ ($\lambda \to \infty$) in (4.93), or equivalently subtracting off $Z_{k_y}(0)$ from the expectation value in the first line. This is the same procedure as was discussed in (4.91) without which the integrals inside the expectation values diverge.

In Fig. 4.5, I plot the renormalized occupancy as a function of frequency for various values of the normalized wavevector $\hat{k}_y$. This figure shows that nonzero environment temperature leads to a stimulated reduction of fermions [58, 171, 172, 173, 174], i.e., a smaller Unruh effect. However, this reduction is dependent on the momentum k_y, with the $\hat{k}_y \to \infty$ curve (dashed line) identical to the zero-temperature Unruh effect, and an increasing stimulated reduction with decreasing $\hat{k}_y$. This happens because I start with an initial thermal state of fermions and Pauli's exclusion principle does not allow new fermions to co-exist with them that are spontaneously created via strains, hence leading to reduction. The higher the initial temperature, the lower the value of $\hat{k}_y$ and therefore the further away the spectrum is from the Fermi-Dirac. In other words, if I keep the environment temperature fixed, then in the limit of small wavelength I recover the Unruh effect and for larger wavelengths the average fermion number strays away from the perfect Fermi-Dirac distribution.

Next, I turn to the direct calculation of the internal energy U using Eq. (4.91). For this task I shall use Eq. (4.93) without making the abovementioned discretization that was used for Fig. 4.5. I find that the internal energy has two contributions $U = U^0 + U^\beta$. For the zero temperature part U^0, the energy and momentum integrals inside the thermal averages can be simplified by using the Dirac delta functions $\delta(\Omega - \Omega')$ and $\delta(k_y - k_y')$ that pin $\Omega' = \Omega$ and $k_y = k_y'$. Then integration can be performed over momenta k_y using the following identity:

$$\int_0^\infty dk_y \; k_y \; K_{\frac{1}{2}+i\Omega}(k_y x) K_{\frac{1}{2}-i\Omega}(k_y x) \;\; = \;\; \frac{\pi^2}{4x^2} \frac{\Omega}{\sinh \pi\Omega}, \tag{4.96}$$

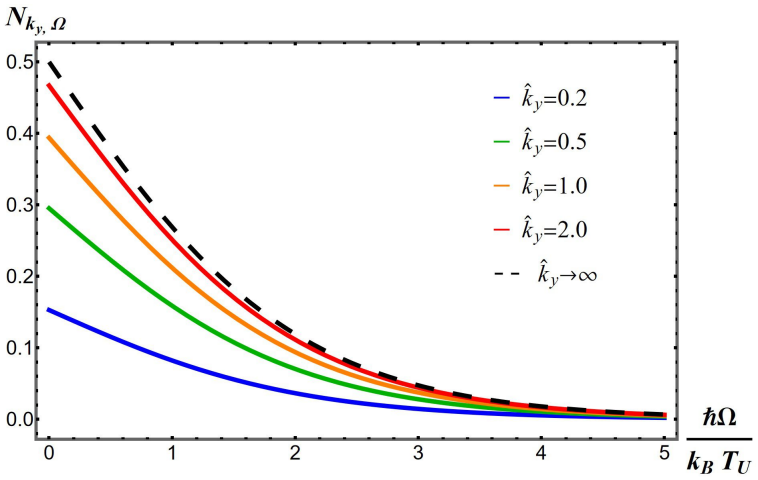

Figure 4.5. A figure showing the average number of fermions (plotted with respect to mode energy normalized with Unruh temperature, see Eq.(4.95)) in a graphene sheet which is initially in a thermal state and is then strained leading to stimulated particle reduction, for various values of momenta $\hat{k}_y$ normalized with real temperature. The dashed black curve represents the Unruh effect with a perfect Fermi-Dirac distribution which could be achieved in the limit of $\hat{k}_y\to\infty$, i.e. large k_y or zero environment temperature. As the temperature rises, the Fermi-Dirac distribution gets reduced due to Pauli's principle.

which leads to:

$$\begin{aligned} U^0 &= \frac{L_y}{\pi}\int\frac{dx}{x^2}\int_0^\infty d\Omega\ \hbar\Omega\ \Omega\coth\pi\Omega\ n_{\rm F}(2\pi\Omega), \\ &= \frac{L_y}{\pi}\int_a^\infty\frac{dx}{x^2}\int_0^\infty d\Omega\ \hbar\Omega\ \Omega\ n_{\rm B}(2\pi\Omega), \end{aligned} \tag{4.97}$$

where in going from first to second line I used the identity $\coth x\cdot n_{\rm F}(2x) = n_{\rm B}(2x)$, and I cutoff the x spatial integral at the lattice scale a. I also note that the energy labels Ω that are not associated with an $\hbar$, need to be understood as being normalized with ω_c. This result is for the right side of the honeycomb lattice per node and per spin state. This temperature independent contribution U^0 is made up of three elements: the mode energy $\hbar\Omega$, the density of states $\Omega\coth\pi\Omega$ and the occupancy of energy levels given by a Fermi-Dirac distribution $n_{\rm F}(2\pi\Omega)$. In the last line, however, I see that the product of the last two factors in the first line effectively yields a linear-in-energy density of states multiplied

by the Bose-Einstein distribution. This is Takagi's apparent *statistics inversion* [108] that I discussed in equations (4.71) and (4.72). Thus, although Eq. (4.97) pertains to fermions, the final result looks like Planck's black body result for photons.

The temperature-dependent part of the total internal energy, U^β, depends on the temperature-dependent terms of the thermal averages in Eq. (4.93). For this contribution, the momentum integrals inside the thermal averages can be simplified by using the Dirac delta function $\delta(k_y - k'_y)$, pinning $k'_y = k_y$. Then, integrating over x using Eq. (4.37) gives us a Dirac delta function $\delta(\Omega - \Omega')$. This along with the finite temperature renormalization discussed in Eq. (4.91) gives the temperature dependent part of internal energy:

$$U^\beta = -\frac{L_y}{\pi}\int_0^\infty d\Omega\ \hbar\Omega\ n_{\rm F}(2\pi\Omega)\int_{-\infty}^\infty dk_y\ Z_{k_y}(0), \tag{4.98}$$

The momentum integral can be simplified by switching to polar coordinates, i.e. $(k_x, k_y) \to (k, \theta)$, and using the identity $\int_0^\infty dx\ n_{\rm F}(x) = \log 2$, thus yielding:

$$\int_{-\infty}^\infty dk_y\ Z_{k_y}(0) = \frac{k_{\rm B}T\log 2}{\hbar v_0}. \tag{4.99}$$

Compiling the results for the temperature independent and dependent cases I find that the renormalized total internal energy $U = U^0 + U^\beta$ for a strained graphene sheet kept in an environment with finite temperature is:

$$\begin{aligned} U &= \frac{L_y}{\pi a}\int_0^\infty d\Omega\ \Omega\coth\pi\Omega\ \hbar\Omega\ n_{\rm F}(2\pi\Omega) \\ &- \frac{L_y}{\pi\lambda}\frac{\log 2}{\beta\epsilon_c}\int_0^\infty d\Omega\ \hbar\Omega\ n_{\rm F}(2\pi\Omega), \end{aligned} \tag{4.100}$$

where $\epsilon_c = \hbar\omega_c$. This result depends linearly on temperature and manifestly shows that because I started with an initial thermal state of fermions in flat graphene, then the pro-

cess of straining leads to stimulated particle reduction due to Pauli's exclusion principle [58, 171, 172, 173, 174].

In this chapter, I studied what happens when a graphene sheet with no strains, is suddenly brought into a state with the Rindler strain pattern, where the strains are minimum at the origin and increase as I go away. I showed that this leads to spontaneous creation of electron-hole pairs, similar to the toroidal BEC case where phonons were spontaneously generated due to the time dependence of the trap. The Rindler pattern is such that it effectively divides the entire graphene sheet into two disconnected pieces, i.e. the long-wavelength modes are not able to traverse from one side to the other. As a result, the pure state of the initial flat graphene sheet, when now viewed from the lens of strained operators confined to one region, see it as a thermal bath of electrons and holes, with an emergent temperature that is proportional to the strains. This is analogous to the situation in relativity, where the Minkowski vacuum is seen as a thermal bath by an accelerating observer, i.e., the Unruh effect.

However, in two dimensions, the power spectra of a fermionic field is given by a Bose-Einstein distribution. This is known as Takagi's statistics inversion which happens because Huygens' principle is violated in even space dimensions, i.e. a single light pulse does not spread out as a single circular wavefront, rather it has wake following it. I argues that this could possibly be seen in the photo-emission experiments. I then discussed this emergent Unruh effect manifests itself in the electronic conductivity as two features: firstly, the conductivity vanishes is the DC-limit ($\omega \to 0$). Secondly, apart from a density of states linear in ω, the conductivity is given by a hyperbolic tangent, which is similar to the electronic conductivity of flat graphene sheet kept at finite environment temperatures.

I ended this chapter with a discussion of the total internal energy at zero and finite environment temperatures. At zero temperature, I get a result similar to Planck's blackbody radiation formula for photons, indicating that statistics inversion is at play here. At finite temperatures, I find a stimulated particle reduction due to the fact that unlike phonons in a BEC, here we are dealing with fermions that obey Pauli's exclusion principle. Thus, when a flat graphene sheet is at finite temperature, then the conduction band with thermal electrons, and after straining, the emergent electrons enter into a competition with the already present thermal electrons, thus annihilating each other.

CHAPTER 5. ULTRACOLD FERMIONS IN A BOX SHAPED TRAP

In this chapter, I will discuss how the properties of an ultracold atom superfluid are affected when it is confined to an atomic trap that has the geometry of box or a thin slab. Although the experiments have constructed cylindrical [185] and circular traps [186], I will study a cubical box shaped trap. In particular, I will be looking into how the presence of fixed boundary conditions and pseudo-potential interactions affect the superfluid transition temperature and the local pairing amplitude change compared to the bulk. For this purpose, I will discuss the Bogoliubov-de Gennes (BdG) Hamiltonian which describes trapped fermions that interact via short ranged attraction. Due to the presence of the trapping potential, I expect and inhomogeneous pairing amplitude $\Delta(\boldsymbol{R})$. As I will see, this spatial in-homogeneity makes it difficult to regularize divergences that occur in the theoretical description of this system. This is because the typical way to regularize the theory (by connecting the coupling constant in the Hamiltonian to the scattering length) implicitly assumes spatially homogeneous pairing (that is, an infinite and uniform system). A key question that I will answer here is the interplay between regularization and the inhomogeneous pairing. Since it is well known that short range interactions lead to singularities in the self-consistent gap equation, therefore, I will regularize this by relating the coupling constant to the scattering length.

To understand how ultra cold fermions behave in the presence of a trap $V(\boldsymbol{r}, t)$, I

will start with the following Hamiltonian $H = H_0 + H_1$, (see [192]):

$$H_0 = \sum_{\sigma=\uparrow,\downarrow} \int d^3r \ \Psi^\dagger_\sigma(\boldsymbol{r}) \Big[\frac{\hat{p}^2}{2m} - \mu + V(\boldsymbol{r},t) \Big] \Psi_\sigma(\boldsymbol{r}), \tag{5.1}$$

$$\begin{aligned} H_1 &= \int d^3R d^3r d^3r' \ \langle \boldsymbol{r'}|\hat{U}|\boldsymbol{r}\rangle \\ &\times \ \Psi^\dagger_\uparrow\Big(\boldsymbol{R} + \frac{1}{2}\boldsymbol{r'}\Big)\Psi^\dagger_\downarrow\Big(\boldsymbol{R} - \frac{1}{2}\boldsymbol{r'}\Big)\Psi_\downarrow\Big(\boldsymbol{R} - \frac{1}{2}\boldsymbol{r}\Big)\Psi_\uparrow\Big(\boldsymbol{R} + \frac{1}{2}\boldsymbol{r}\Big), \end{aligned} \tag{5.2}$$

where $\boldsymbol{R}$ is the center of mass coordinate and $\boldsymbol{r}, \boldsymbol{r'}$ are radial coordinates, $\hat{p} = -i\hbar\nabla$ is the momentum operator, m is the mass of atoms in the Fermi gas, μ is the chemical potential, λ is the interaction parameter, $\sigma = \uparrow, \downarrow$ is the spin label, $\Psi^\dagger_\sigma$ and Ψ_σ are field operators which create/destroy a fermion of spin σ and, H_0 and H_1 are the kinetic and interaction parts respectively. The kinetic part H_0 has $V(\boldsymbol{r},t)$ which describes a general time and position dependent trap. There are two specific cases of $V(\boldsymbol{r})$ for us to consider: the bulk case, and the case of a gas confined to a box trap. In the bulk case I have superfluid everywhere in space with $V(\boldsymbol{r},t) = 0$ and periodic boundary conditions are imposed on the single-particle wavefunctions (thus they are plane waves) and for the box case $V(\boldsymbol{r},t) = 0$ for $0 < (x,y,z) < L$ and $V(\boldsymbol{r},t) = \infty$ everywhere else. The interaction Hamiltonian H_1 has a term which looks like the matrix element of the interaction potential between two fermions $\langle \boldsymbol{r'}|\hat{U}|\boldsymbol{r}\rangle$. This could be modelled either by a Delta potential $\langle \boldsymbol{r'}|\hat{U}|\boldsymbol{r}\rangle = \lambda\delta(\boldsymbol{r'} - \boldsymbol{r})$ which basically means that the interaction is largest when two fermions are nearby, which is also how Van der Waals force works. One could also use the Fermi-Huang pseudo-potential $\hat{U}(\boldsymbol{r'}, \boldsymbol{r}) = \lambda\delta(\boldsymbol{r'})\partial_{r'}(r'\delta(\boldsymbol{r'} - \boldsymbol{r}))$ which is discussed in Appendix. D. The picture the interaction Hamiltonian H_1 portrays is as follows: Two fermions are created out of vacuum at positions $\boldsymbol{R} + \frac{1}{2}\boldsymbol{r'}$ and $\boldsymbol{R} - \frac{1}{2}\boldsymbol{r'}$ by the field operators $\Psi^\dagger_\uparrow$ and $\Psi^\dagger_\downarrow$ respectively giving them spins up and down. These field operators satisfy the

anti-commutation relation:

$$\{\Psi_\sigma(\boldsymbol{r}), \Psi^\dagger_{\sigma'}(\boldsymbol{r'})\} = \delta^{(3)}_{\sigma\sigma'}\delta(\boldsymbol{r} - \boldsymbol{r'}) \tag{5.3}$$

These fermions then propagate radially from $\boldsymbol{r'} \to \boldsymbol{r}$ with the centre of mass coordinates fixed at $\boldsymbol{R}$, and during this time they interact via the potential $\langle \boldsymbol{r'}|\hat{U}|\boldsymbol{r}\rangle$. Finally they reach $\boldsymbol{R} + \frac{1}{2}\boldsymbol{r}$ and $\boldsymbol{R} - \frac{1}{2}\boldsymbol{r}$ where they are annihilated by the field operators $\Psi_\uparrow$ and $\Psi_\downarrow$ respectively.

The rest of this chapter is organized as follows: In Sec. 5.1, I will discuss elements of the BCS theory that describes properties of a bulk superfluid. In Sec. 5.2 I start with a one-dimensional confined superfluid described by point interactions and how the transition temperature and gap parameter gets corrections from the confinement size. I then introduce the pseudo-potential in Sec. 5.3, which when incorporated in the Bogoliubov-de Gennes approach leads to an integral gap equation. In Sec. 5.5 and Sec. 5.6 I approximately solve the real space gap equation using Taylor expansion of the gap parameter, in a thin slab and a cubical box.

5.1. The BCS Theory

In this section, I will briefly review the BCS theory and how it leads to the gap equation that explains the bulk properties of superconductors and superfluids. Superconductivity was discovered by Kamerlingh Onnes in 1911 [196] when he saw that the resistance of solid mercury abruptly vanished at 4.2 K. In addition to a vanishing resistivity superconductors exhibit other phenomena such as the Meissner effect in which superconductors expel magnetic fields ([197]). Superfluidity on the other hand, was discovered by Kapitza [198], Allen and Misener in 1938 [199]. This also exhibits strange properties like

zero viscosity and the fountain effect (where the superfluid creeps up the walls of the container and starts flowing out). There is a related phenomenon known as Bose-Einstein condensation which was proposed by S. N. Bose [200] and Albert Einstein in 1925 [201] and observed in 1995 [175, 176]. A Bose-Einstein condensate (BEC) is a state of matter in which a macroscopic number of atoms occupy a single particle wavefunction, below a certain critical temperature. These bosonic atoms occupy(condense) to the lowest energy level and act as a single giant atom. In a superfluid, a similar coherence of constituents exists but the key difference between them is that the BEC is made up of bosons whereas a superfluid is made up of fermions which are interacting with each other and thus form Copper pairs. In cold atom experiments when interacting Fermi gases are made, besides exhibiting a superfluid phase they also have a BEC phase (see Fig. 2) which is very weakly interacting. The microscopic theory for superfluidity was found by Bardeen, Cooper and Schrieffer(BCS Theory) in 1957 [202, 203]. According to this, electrons in a superconductor interact via phonons in such a way that they effectively attract each other and thus form 'Cooper pairs' which 'act' like bosons in a condensate described by a single wavefunction. This attractive interaction builds up a gap near the Fermi surface and thus any collision of these electrons with the ions or disorder is not strong enough to excite them i.e. the electrons become invisible to the lattice and thus the resistivity drops to zero. Similar ideas apply to superfluids and the more modern ultracold atomic Fermi gases. The attractive interaction does not need to be due phonons and thus Van der Waal's interaction does the job in the case ultracold fermions.

To understand BCS theory, I will start with the Hamiltonian given in (5.1)-(5.2) which describes a Fermi gas kept in a spatial trap $V(\boldsymbol{r})$ and chemical potential μ, with a

the interactions being modeled by a Dirac delta potential $\langle \boldsymbol{r'}|\hat{U}|\boldsymbol{r}\rangle = \lambda\delta(\boldsymbol{r'}-\boldsymbol{r})$ which basically means that the interaction is largest when two fermions approach each other. Using mean-field theory (see Appendix C), I arrive at the gap equation for general temperature T:

$$\frac{1}{\lambda} = -\sum_{\boldsymbol{k}} \frac{\tanh\frac{E_k}{2T}}{2E_k}, \tag{5.4}$$

where $E_k = \sqrt{(\epsilon_k-\mu)^2+\Delta^2}$ is the quasi-particle (Cooper pairs) energy dispersion relation, ϵ_k is the single-particle energy, and Δ is the gap parameter which quantifies the amount of pairing in the system. The solution to this equation determines pairing Δ as a function of interaction parameter λ. The sum $\sum_{\boldsymbol{k}}$ in (5.4) is a sum over all momentum vectors $\boldsymbol{k}$, and is thus divergent in three dimensions. This divergence in the many-body problem comes from the singular nature of the δ-function interactions, and a similar divergence occurs in the two-body scattering problem associated with the Hamiltonian. The two-body scattering problem relates the bare coupling parameter λ to the scattering length a_s:

$$\frac{1}{\lambda} = \frac{m}{4\pi a_s} - \sum_{\boldsymbol{k}} \frac{1}{2\epsilon_{\boldsymbol{k}}}, \tag{5.5}$$

The divergence of the sum in (5.4) is of the same form as the divergent sum in (5.4). I can regularize both equations by eliminating λ to get:

$$\frac{m}{4\pi a_s} = -\sum_{\boldsymbol{k}} \Big(\frac{\tanh\frac{E_k}{2T}}{2E_k} - \frac{1}{2\epsilon_k}\Big). \tag{5.6}$$

The regularization of this gap equation relies on translation invariance of the bulk, i.e. it depends on the assumption that our system is spatially uniform. Therefore, the above regularization does not work in the box trap where I expect spatially varying pairing strength.

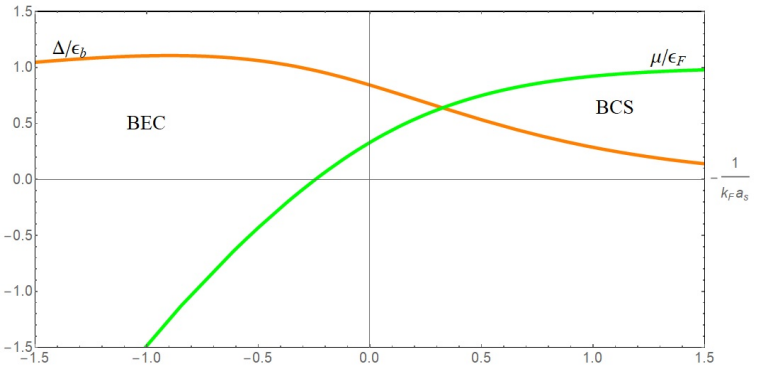

Figure 5.1. The BEC-BCS Crossover [204, 205]. Plot of $\frac{\Delta}{\epsilon_F}$(orange) v/s $\frac{-1}{k_F a_s}$ and $\frac{\mu}{\epsilon_F}$(green) v/s $\frac{-1}{k_F a_s}$ for the bulk case of an ultracold Fermi gas. The left side of the plot $\frac{-1}{k_F a_s} < -0.5$ is the BEC regime, right side $\frac{-1}{k_F a_s} > +0.5$ is the BCS regime and the middle part is the Unitary regime where the scattering length diverges $a_s \to \infty$.

This equation relates the pairing amplitude Δ to the two-body scattering length a_s which can be measured in experiments. Note that in the limit $\tanh \frac{E_k}{2T} \to 1$ I recover a regularized zero temperature gap equation:

$$\frac{m}{4\pi a_s} = -\sum_{\boldsymbol{k}} \left(\frac{1}{2E_k} - \frac{1}{2\epsilon_k} \right). \tag{5.7}$$

The solution of this equation for gap parameter Δ is plotted in Fig. 5.1. Near the transition temperature $\Delta \ll |\mu|$ which implies $E_k \approx |\xi_k|$ and thus the gap equation (5.6) becomes:

$$\frac{m}{4\pi a_s} = -\sum_{\boldsymbol{k}} \left(\frac{\tanh \frac{\xi_k}{2T}}{2\xi_k} - \frac{1}{2\epsilon_k} \right). \tag{5.8}$$

This equation is also known as the transition temperature T_c-equation since it determines the temperature of the second order phase transition to the superconducting phase. If the number of particles in a system is fixed (like in cold atom experiments), then there is another equation called the number equation that comes by setting the derivative of the free energy (see Eq. (C.12)) with respect to the chemical potential to be equal to the number

of particles in the system i.e. $N = -\frac{\partial \Phi}{\partial \mu}$:

$$n = \sum_{\boldsymbol{k}} \Big(1 - \frac{\xi_k}{E_k}\Big), \tag{5.9}$$

where the sum on the right hand side is convergent. For $T = 0$ I can combine equations (5.7) and (5.9) to get relationships between: (a) $\frac{\Delta}{\epsilon_F}$ versus $\frac{-1}{k_F a_s}$ and (b) $\frac{\mu}{\epsilon_F}$ versus $\frac{-1}{k_F a_s}$, where $\epsilon_F = \hbar^2 k_F^2/2m$ is the Fermi energy (chemical potential at zero temperature), with $k_F = (3\pi^2 n)^{1/3}$ being the Fermi wave-vector. This was done in [204] and I have plotted these relationships in Fig. 5.1. Note that solving the gap equation (5.7) gives a level pairing amplitude or gap Δ that is independent of mode index k, i.e. I have uniform pairing in momentum space. This implies furthermore homogeneous and isotropic pairing in real space. Fig. 5.1 shows that the gap parameter (Δ in orange) or the pairing is very large for the BEC (Bose-Einstein condensate) regime on the left but decreasing as I go to the BCS or SF (superfluid) regime on the right. The chemical potential (μ in green) is negative for BEC and increases as I move to the BCS regime.

5.2. One-Dimensional Box Trap

Now that I have reviewed BCS theory in the bulk case, in this section, I turn to the case of a superfluid confined to a one-dimensional box trap. In the bulk case I saw that the pairing is homogeneous and isotropic but I expect this to change in the box trap because it has fixed boundaries and sharp edges which make it intrinsically inhomogeneous and non-isotropic. Thus our goal is to find the local pairing amplitude $\Delta(\boldsymbol{r})$ and the local fermion density $n(\boldsymbol{r})$. Inside the box and away from boundary, I expect the superfluid to behave as if it was in the bulk, whereas, near the boundary the probability of finding Cooper pairs should vanish due to vanishing boundary conditions. Thus I expect $\Delta(\boldsymbol{r})$ to

satisfy Dirichlet boundary conditions, and to have a contribution from the bulk and corrections of order $\frac{1}{L}$ due to finite size L of the box. Different theoretical works have been performed on this topic and they have found different phenomenology, thus providing us with the motivation to study the problem of confined Fermi gases. In the area of electronic condensed matter [206, 207], it was shown that when one analyses BCS theory with vanishing boundary conditions (in a slab of finite thickness L), then the gap parameter decreases with increase in slab thickness ($\sim \frac{1}{L}$ behaviour) along with level oscillations in the gap with peaks at resonance values when the energy level due to slab thickness crosses the Fermi surface. More recently it was shown in Ref. [208] that similar oscillations can be seen in the value of the critical temperature with slab thickness and in Ref. [209] it was shown that the local gap and density have spatial dependences. Non-interacting fermions have been dealt with in [210] where they show that inside a box the density is spatially varying. Having briefly reviewed the literature on confined Fermi gases and superconductors I now turn to our approach to this problem.

In the rest of this section, I will study fermions confined to a one-dimensional box interacting via a Dirac delta function. Unlike the three-dimensional case, the one-dimensional gap equation is not divergent, and thus no regularization is required here. I start with the one dimensional version of the Hamiltonian in (5.1)-(5.2), where I set the trap potential $V(x) = 0$ inside the box i.e. $0 \leq x \leq L$ and interaction potential to be a delta function $\hat{U}(x' - x) = \lambda\delta(x' - x)$:

$$H_0 = \sum_\sigma \int dx\ \Psi^\dagger_\sigma(x)\Big[\frac{\hat{p}^2}{2m} - \mu + V(x)\Big]\Psi_\sigma(x), \tag{5.10}$$

$$H_1 = \lambda \int dx\ \Psi^\dagger_\uparrow(x)\Psi^\dagger_\downarrow(x)\Psi_\downarrow(x)\Psi_\uparrow(x), \tag{5.11}$$

where H_0 is the kinetic part, H_1 is the interaction part, $\hat{p} = -i\frac{d}{dx}$ and $\Psi^\dagger_\sigma(x)$ and $\Psi_\sigma(x)$ are field operators which create/annihilate fermions. These field operators satisfy the anti-commutation relation: $\{\Psi_\sigma(x), \Psi^\dagger_{\sigma'}(x')\} = \delta_{\sigma\sigma'}\delta(x - x')$. They can be decomposed in the basis of box states as:

$$\Psi_\sigma(x) = \sum_n \psi_n(x) c_{n\sigma}, \tag{5.12}$$

$$\Psi^\dagger_\sigma(x) = \sum_n \psi_n(x) c^\dagger_{n\sigma}, \tag{5.13}$$

where $\psi_n(x) = \sqrt{\frac{2}{L}} \sin\left(\frac{n\pi x}{L}\right)$ are single particle box wavefunctions, and $c^\dagger_{n\sigma}$ and $c_{n\sigma}$ are creation/annihilation operators for fermions in the energy level n that satisfy anti-commutation relations $\{c_{n\sigma}, c^\dagger_{n'\sigma'}\} = \delta_{\sigma\sigma'}\delta_{nn'}$. Plugging (5.12)-(5.13) into (5.10)-(5.11) I get the Hamiltonian in n-space

$$H = \sum_{n\sigma} \xi_n c^\dagger_{n\sigma} c_{n\sigma} + \lambda \sum_{n_1,n_2,n_3,n_4} \hat{\lambda}_{n_1 n_2 n_3 n_4} c^\dagger_{n_1\uparrow} c^\dagger_{n_2\downarrow} c_{n_3\downarrow} c_{n_4\uparrow}, \tag{5.14}$$

where $\xi_n = \epsilon_n - \mu$ and $\hat{\lambda}_{n_1 n_2 n_3 n_4} = \int dx\ \psi_{n_1}(x)\psi_{n_2}(x)\psi_{n_3}(x)\psi_{n_4}(x)$ is the interaction function which takes into account that the box has fixed boundaries.

Now I need to invoke two further approximations. Firstly I note that in the bulk case, pairing of fermions is strongest when they are in $(+\boldsymbol{k}, -\boldsymbol{k})$ states. Similarly here I will assume that the pairing is at its peak when $n_1 = n_2 \equiv m$ and $n_3 = n_4 \equiv n$. This amounts to a BCS-type pairing approximation. Thus our interaction function reduces to $\hat{\lambda}_{n_1 n_2 n_3 n_4} \to \hat{\lambda}_{m,n}$:

$$\hat{\lambda}_{m,n} = \frac{1}{L}\Big(1 + \frac{1}{2}\delta_{m,n}\Big), \tag{5.15}$$

where the Kronecker delta $\delta_{m,n}$ is zero for $m \neq n$, and unity for $m = n$. The Hamiltonian

then reduces to:

$$H = \sum_{n\sigma} \xi_n c^\dagger_{n\sigma} c_{n\sigma} + \lambda \sum_{m,n} \hat{\lambda}_{m,n} c^\dagger_{m\uparrow} c^\dagger_{m\downarrow} c_{n\downarrow} c_{n\uparrow}. \tag{5.16}$$

Upon going through the same steps as described in equations (C.5)-(C.8), I arrive at the gap equation at zero temperature, that is similar to (C.8):

$$\Delta_m = -\lambda \sum_n \hat{\lambda}_{m,n} \frac{\Delta_n}{2E_n}, \tag{5.17}$$

where $E_n = \sqrt{(\epsilon_n - \mu)^2 + \Delta^2}$ is the Cooper pair energy in the box and $\epsilon_n = \frac{n^2\pi^2\hbar^2}{2mL^2}$ are the single particle box energies. Secondly, I can take the large system limit keeping corrections of the order of $\frac{1}{L}$. Under this assumption the summations become integrals $\sum_n \to \int \frac{Ldk}{2\pi}$:

$$\hat{\lambda}_{k,p} \approx 1 + \frac{\pi}{2L}\delta(k-p). \tag{5.18}$$

and the gap equation becomes:

$$\Delta(k) = -\lambda \int_{-\infty}^{\infty} \frac{dp}{2\pi} \Big[1 + \frac{\pi}{2L}\delta(k-p)\Big] \frac{\Delta(p)}{2\tilde{E}(p)}, \tag{5.19}$$

where $\tilde{E}(k) = \sqrt{\xi^2(k) + \Delta^2(k)}$ is energy dispersion relation for the quasi-particles in the box. To solve (5.19) I will assume the ansatz $\Delta(k) = \Delta_0 + \frac{1}{L}\Delta_1(k)$ because we are looking for the leading connection to the bulk result in the large L limit. Thus I get:

$$\Delta_0 + \frac{1}{L}\Delta_1(k) \;=\; -\lambda \int_{-\infty}^{\infty} \frac{dp}{2\pi} \frac{\Delta(p)}{2\tilde{E}(p)} - \frac{\lambda}{8L} \frac{\Delta(k)}{\tilde{E}(k)}. \tag{5.20}$$

Now I compare $\mathcal{O}(1)$ and $\mathcal{O}(\frac{1}{L})$ on both sides of (5.20) which gives us the regular gap equation for bulk and corrections due to boundary:

$$\Delta_0 \;=\; -\lambda \int_{-\infty}^{\infty} \frac{dp}{2\pi} \frac{\Delta(p)}{2\tilde{E}(p)}, \tag{5.21}$$

$$\Delta_1(k) \;=\; -\frac{\lambda}{8L} \frac{\Delta_0}{E(k)}, \tag{5.22}$$

where $E(k) = \sqrt{\xi^2(k) + \Delta_0^2}$ is energy dispersion relation for the quasi-particles in bulk. Thus the level pairing amplitude in k-space looks like:

$$\Delta(k) \approx \Delta_0 - \frac{\lambda}{4L}\frac{\Delta_0}{2E(k)}. \tag{5.23}$$

Let us examine this result. Since a large box is the same as bulk, thus $L \to \infty$ gives $\Delta(k) \to \Delta_0$ (as expected). For high energies the pairing between fermions should not be affected the box size, thus $k \to \infty$ gives $\Delta(k) \to \Delta_0$. Equation (5.23) is invariant with respect to box symmetry $k \to -k$, is a maximum for $\epsilon_k = \mu$ and is in general less than the bulk gap (which means the boundary lowers pairing ability).

I just discussed $T = 0$ results. Let us now look at near transition temperature $T = T_c$ regime where the gap parameter is vanishingly small $|\mu| \gg \Delta(k)$ and thus I can set $\tilde{E}(k) \approx |\xi(k)|$. In this limit the gap equation in the continuum limit is:

$$\begin{aligned}
\Delta(k) &= -\lambda \int_{-\infty}^{\infty} \frac{dp}{2\pi}\Big[1 + \frac{\pi}{2L}\delta(k-p)\Big]\Delta(p)\frac{\tanh\left[\frac{\xi(p)}{2T}\right]}{2\xi(p)}, \\
&= -\lambda \int_{-\infty}^{\infty} \frac{dp}{2\pi}\frac{\tanh\left[\frac{\xi(p)}{2T}\right]}{2\xi(p)}\Delta(p) - \frac{\lambda}{4L}\frac{\tanh\left[\frac{\xi(k)}{2T}\right]}{2\xi(k)}\Delta(p), \\
&= C - \frac{\lambda}{4L}\frac{\tanh\left[\frac{\xi(k)}{2T}\right]}{2\xi(k)}\Delta(k),
\end{aligned} \tag{5.24}$$

that gives us the solution $\Delta(k) = C\Big(1 + \frac{\lambda}{4L}\frac{\tanh\left[\frac{\xi(k)}{2T}\right]}{2\xi(k)}\Big)^{-1}$, similar to (5.23), which means that the pairing amplitude is energy dependent and has finite size corrections. Now plugging this into the definition of C i.e. $C = -\lambda\int_{-\infty}^{+\infty}\frac{dp}{2\pi}\frac{\tanh\left[\frac{\xi(p)}{2T}\right]}{2\xi(p)}\Delta(p)$ I get the T_c-equation:

$$\begin{aligned}
1 &= -\lambda \int_{-\infty}^{+\infty} \frac{dp}{2\pi}\frac{\tanh\left[\frac{\xi(p)}{2T}\right]}{2\xi(p)}\frac{1}{1 + \frac{\lambda}{4L}\frac{\tanh\left[\frac{\xi(k)}{2T}\right]}{2\xi(k)}}, \\
&\approx -\lambda\left[\int_{-\infty}^{+\infty} \frac{dp}{2\pi}\frac{\tanh\left[\frac{\xi(p)}{2T}\right]}{2\xi(p)}\right]\frac{1}{1 + \frac{\lambda}{4L}\frac{1}{4T_c}}, \\
&= -\frac{\lambda}{1 + \frac{\lambda}{4L}\frac{1}{4T_c}} \times N_{1D}\left(\ln\frac{\mu}{T_c} + \gamma\right),
\end{aligned} \tag{5.25}$$

where $N_{1D} = \frac{\sqrt{m}}{2\pi\hbar\sqrt{2\mu}}$ is the density of states in one dimension, and I used the identity:

$$\int_0^{\mu} dx \frac{1}{x} \tanh \frac{x}{2T} = \log \frac{\mu}{T} + \gamma - \log \frac{\pi}{2}. \tag{5.26}$$

Now I will use the ansatz that the transition temperature should have a bulk value with a correction due to the finite size of the box $T_c = T_{c0} + \frac{1}{L} T_{c1}$. I used the following series expansions: $\left(1 + \frac{\lambda}{16LT_c}\right)^{-1} \approx \left(1 - \frac{\lambda}{16LT_{c0}}\right)$ and $\ln\left(\frac{\mu}{T_c}\right) \approx \ln\left(\frac{\mu}{T_{c0}}\right) - \frac{T_{c1}}{T_{c0}L}$. Again comparing the $\mathcal{O}(1)$ and $\mathcal{O}(\frac{1}{L})$ terms I get $T_{c1} = \frac{1}{16N_{1D}}$ and thus the transition temperature is:

$$T_c = T_{c0} + \frac{1}{16N_{1D}L}. \tag{5.27}$$

In summary, in this section I looked at the case of fermions confined to a one-dimensional box, with point interactions represented by a Dirac delta function that depends on their relative coordinates. In the large system limit, I saw that the interaction function has a size-correction of the form $\frac{1}{L}$. This helped us derive similar size corrections to the pairing amplitude and the transition temperature. However, extending this approach (perturbation in $\frac{1}{L}$) to higher dimensions does not work, and leads us to consider pseudo-potential interactions. In the next section, I will look at how a pseudopotential interaction modifies the gap equation providing us with an alternative method of describing interacting fermions in a box trap.

5.3. Three-Dimensional Box Traps

In the previous section, I discussed a procedure to solve the gap equation for a one-dimensional superfluid with interactions given by Dirac delta function. I assumed that the gap has a bulk part and a correction due to the finite size of the box. However, extend-

ing this method to higher dimensions does not work as the gap equation becomes divergent, and the form of this divergence is different from the one in the two-body problem, hence I regularization is not possible. Another assumption that I made was that the pairing is uniform. However, for box-shaped traps I expect the gap to have a spatially-varying profile, and thus the procedure of the previous will not work here either. This leads us to model the interactions using the pseudopotential. In this section I will discuss the derivation of Bogoliubov de Gennes(BdG) equations by describing interacting fermions with two-body scattering length a_s using the pseudopotential, and apply it to the near transition temperature regime. I will then show that this method recovers the bulk case in the large volume limit.

Pseudopotential and the BdG Approach

I start with the BdG Hamiltonian for interacting fermions in a laser trapping potential $V(\boldsymbol{r})$, as discussed in Eqs. (5.1)-(5.2), that describes two fermions created at $\boldsymbol{R} \pm \frac{1}{2}\boldsymbol{r'}$ and destroyed at $\boldsymbol{R} \pm \frac{1}{2}\boldsymbol{r}$ and in the meantime they interact via a potential $\hat{U}$. For a Fermi gas this interaction can be described using the pseudo-potential $\langle \boldsymbol{r'}|\hat{U}|\boldsymbol{r}\rangle = \lambda\delta(\boldsymbol{r'})\partial_{r'}\Big[r'\delta(\boldsymbol{r} - \boldsymbol{r'})\Big]$, which is an operator acting on functions. Unlike Eq. (5.11), here $\lambda = \frac{4\pi\hbar^2 a_s}{m}$, i.e. the scattering length is already included in the definition of the pseudopotential. Thus I now no longer require the two-body problem to regularize the gap equation. Also note that the pseudopotential scheme regularizes the model without the need for translation invariance. It does this by enforcing the correct behavior for two-body scattering in the limit of zero inter-particle distance, i.e., $r \to 0$. Please see Appendix. D where I discuss the motivation behind the pseudopotential.

Following the analysis of Bruun et al [192], I wish to study the evolution of $\langle\Psi_\uparrow(\boldsymbol{r}_1,t)\Psi_\downarrow(\boldsymbol{r}_2,t)\rangle$ with time, for which I will need Heisenberg's equation of motion for the field operators $\frac{\partial\Psi_\sigma}{\partial t}=\frac{i}{\hbar}\big[\Psi_\sigma,H\big]$ and the following commutators:

$$\begin{aligned}\Big[H_0,\Psi_\sigma(\boldsymbol{r},t)\Big] &= -\Big[-\frac{\nabla^2}{2m}-\mu+V(\boldsymbol{r})\Big]\Psi_\sigma(\boldsymbol{r},t), &(5.28)\\ \Big[H_1,\Psi_{\uparrow\downarrow}(\boldsymbol{r},t)\Big] &= \mp\lambda\int d^3y\int d^3r'\langle\boldsymbol{r}-\boldsymbol{r'}|\hat{U}|\boldsymbol{y}\rangle\\ &\times\ \Psi_\downarrow\Big(\frac{1}{2}(\boldsymbol{r}+\boldsymbol{r'}-\boldsymbol{y},t)\Big)\Psi_\uparrow\Big(\frac{1}{2}(\boldsymbol{r}+\boldsymbol{r'}+\boldsymbol{y},t)\Big)\Psi^\dagger_{\downarrow,\uparrow}(\boldsymbol{r'},t). &(5.29)\end{aligned}$$

Next, I invoke the mean field approximation by taking the average of two field operators in Eq. (5.29) and calling it the local pairing amplitude $\Delta(\boldsymbol{R})$ [192]:

$$\begin{aligned}\Delta(\boldsymbol{r},\boldsymbol{r'}) &= \lambda\int d^3y\langle\boldsymbol{r}-\boldsymbol{r'}|\hat{U}|\boldsymbol{y}\rangle\Big\langle\Psi_\downarrow\Big(\frac{1}{2}(\boldsymbol{r}+\boldsymbol{r'}-\boldsymbol{y},t)\Big)\Psi_\uparrow\Big(\frac{1}{2}(\boldsymbol{r}+\boldsymbol{r'}+\boldsymbol{y},t)\Big)\Big\rangle,\\ &= \delta(\boldsymbol{r}-\boldsymbol{r'})\times\lambda\int d^3y\partial_y\Big[y\delta(\boldsymbol{y})\Big\langle\Psi_\downarrow(\boldsymbol{R}-\frac{1}{2}\boldsymbol{y},t)\Psi_\uparrow(\boldsymbol{R}+\frac{1}{2}\boldsymbol{y},t)\Big\rangle\Big],\\ &= \delta(\boldsymbol{r}-\boldsymbol{r'})\times\Delta(\boldsymbol{R}), &(5.30)\end{aligned}$$

where $\boldsymbol{y}$ is a radial separation coordinate, and the short-distance $\boldsymbol{y}\ \to\ 0$ divergence in the pairing strength is regularized by the pseudopotential as: $\Delta(\boldsymbol{R})\ =\ \lambda\int d^3y\partial_y\Big[y\delta(\boldsymbol{y})\Big\langle\Psi_\downarrow(\boldsymbol{R}-\frac{1}{2}\boldsymbol{y},t)\Psi_\uparrow(\boldsymbol{R}+\frac{1}{2}\boldsymbol{y},t)\Big\rangle\Big]$, thereby eliminating the need to invoke the two-body problem for regularization. With this new definition of local pairing in terms of pseudopotential, I can then write down the Heisenberg equations of motion as follows:

$$\begin{aligned}i\hbar\partial_t\Psi_\uparrow(\boldsymbol{r},t) &= \hat{h}(\boldsymbol{r})\Psi_\uparrow(\boldsymbol{r},t)+\Delta(\boldsymbol{r})\Psi^\dagger_\downarrow(\boldsymbol{r},t), &(5.31)\\ i\hbar\partial_t\Psi_\downarrow(\boldsymbol{r},t) &= \hat{h}(\boldsymbol{r})\Psi_\downarrow(\boldsymbol{r},t)-\Delta(\boldsymbol{r})\Psi^\dagger_\uparrow(\boldsymbol{r},t), &(5.32)\end{aligned}$$

where the operator $\hat{h}\ =\ -\frac{\nabla^2}{2m}\ -\ \mu\ +\ V(\boldsymbol{r})$. Our next ask is to derive the self consistency condition for the local pairing amplitude. Using (5.31)-(5.32), the evolution of

$\langle \Psi_\uparrow(\boldsymbol{r}_1,t)\Psi_\downarrow(\boldsymbol{r}_2,t)\rangle$ in the steady state is:

$$
\begin{aligned}
& 0 = i\hbar\partial_t\langle \Psi_\uparrow(\boldsymbol{r}_1,t)\Psi_\downarrow(\boldsymbol{r}_2,t)\rangle, \\
= & \Big[-\frac{\hbar^2}{2m}(\nabla^2_{r_1}+\nabla^2_{r_2}) - 2\mu + V(\boldsymbol{r_1}) + V(\boldsymbol{r_2})\Big]\langle \Psi_\uparrow(\boldsymbol{r}_1,t)\Psi_\downarrow(\boldsymbol{r}_2,t)\rangle \\
+ & \Delta(\boldsymbol{r}_1)\langle \Psi^\dagger_\downarrow(\boldsymbol{r}_1,t)\Psi_\downarrow(\boldsymbol{r}_2,t)\rangle + \Delta(\boldsymbol{r}_2)\langle \Psi^\dagger_\uparrow(\boldsymbol{r}_1,t)\Psi_\uparrow(\boldsymbol{r}_2,t)\rangle - \Delta(\boldsymbol{r}_2)\delta(\boldsymbol{r}_1-\boldsymbol{r}_2), \\
= & \Big[-\frac{\hbar^2}{m}(\nabla^2_y + \frac{1}{4}\nabla^2_R) - 2\mu + V(\boldsymbol{R}-\frac{1}{2}\boldsymbol{y}) + V(\boldsymbol{R}+\frac{1}{2}\boldsymbol{y})\Big]\langle \Psi_\uparrow(\boldsymbol{R}+\boldsymbol{\frac{1}{2}}\boldsymbol{y},t)\Psi_\downarrow(\boldsymbol{R}-\boldsymbol{\frac{1}{2}}\boldsymbol{y},t)\rangle \\
+ & \Delta(\boldsymbol{R}+\frac{1}{2}\boldsymbol{y})\langle \Psi^\dagger_\downarrow(\boldsymbol{R}+\frac{1}{2}\boldsymbol{y},t)\Psi_\downarrow(\boldsymbol{R}-\frac{1}{2}\boldsymbol{y},t)\rangle + \Delta(\boldsymbol{R}-\frac{1}{2}\boldsymbol{y})\langle \Psi^\dagger_\uparrow(\boldsymbol{R}-\frac{1}{2}\boldsymbol{y},t)\Psi_\uparrow(\boldsymbol{R}+\frac{1}{2}\boldsymbol{y},t)\rangle \\
- & \Delta(\boldsymbol{R})\delta(\boldsymbol{y}), \qquad (5.33)
\end{aligned}
$$

where in the second line I have $(\boldsymbol{r}_1,\boldsymbol{r}_2) = \Big(\boldsymbol{R}+\frac{1}{2}\boldsymbol{y}, \boldsymbol{R}-\frac{1}{2}\boldsymbol{y}\Big)$. Now the Dirac delta in the last term of (5.33) is a singular function and needs to be cancelled out by the action of ∇^2_y on the average $\langle \Psi_\uparrow\Psi_\downarrow\rangle$ in the limit when two fermions are close i.e. $\boldsymbol{y} \to 0$. This constrains the form of the average $\langle \Psi_\uparrow\Psi_\downarrow\rangle$ to be:

$$
\Big\langle \Psi_\uparrow(\boldsymbol{R}+\boldsymbol{\frac{1}{2}}\boldsymbol{y},t)\Psi_\downarrow(\boldsymbol{R}-\boldsymbol{\frac{1}{2}}\boldsymbol{y},t)\Big\rangle = \frac{m}{4\pi\hbar^2 y}\Delta(\boldsymbol{R}) + F_{reg}(\boldsymbol{R}) + \mathcal{O}(\boldsymbol{y}). \qquad (5.34)
$$

This implies that the local pairing amplitude is:

$$
\begin{aligned}
\Delta(\boldsymbol{R}) &= \lambda\int d^3y\partial_y\Big[y\delta^{(3)}(\boldsymbol{y})\Big\langle \Psi_\downarrow\big(\boldsymbol{R}-\frac{1}{2}\boldsymbol{y},t\big)\Psi_\uparrow\big(\boldsymbol{R}+\frac{1}{2}\boldsymbol{y},t\big)\Big\rangle\Big], \\
&= -\lambda F_{reg}(\boldsymbol{R}). \qquad (5.35)
\end{aligned}
$$

Thus our goal will be to first calculate the expectation value $\langle \Psi_\uparrow\Psi_\downarrow\rangle$ using the BdG equations and then split the expression to get a singular part $\sim \frac{1}{y}$ (which will be removed by the pseudo-potential) and a regularized part which I will give us a finite result.

The Bogoliubov-de Gennes (BdG) approach is just another representation of the BCS theory where instead of working with the field operators $\Psi_\sigma(\boldsymbol{r})$ and their expansions

in terms of box wavefunctions $\psi_{\boldsymbol{n}}(\boldsymbol{r})$, and single particle creation $c^{\dagger}_{\boldsymbol{n}\sigma}$ and annhilation operators $c_{\boldsymbol{n}\sigma}$, I define:

$$\Psi_{\uparrow}(\boldsymbol{r}) = \sum_{\boldsymbol{n}} \Big(u_{\boldsymbol{n}}(\boldsymbol{r}) e^{-iE_{\boldsymbol{n}}t} \gamma_{\boldsymbol{n}\uparrow} - v^{*}_{\boldsymbol{n}}(\boldsymbol{r}) e^{iE_{\boldsymbol{n}}t} \gamma^{\dagger}_{\boldsymbol{n}\downarrow} \Big), \tag{5.36}$$

$$\Psi_{\downarrow}(\boldsymbol{r}) = \sum_{\boldsymbol{n}} \Big(u_{\boldsymbol{n}}(\boldsymbol{r}) e^{-iE_{\boldsymbol{n}}t} \gamma_{\boldsymbol{n}\downarrow} + v^{*}_{\boldsymbol{n}}(\boldsymbol{r}) e^{iE_{\boldsymbol{n}}t} \gamma^{\dagger}_{\boldsymbol{n}\uparrow} \Big), \tag{5.37}$$

where the functions $u_{\boldsymbol{n}}, v_{\boldsymbol{n}}$ are solutions of the BdG equations:

$$\begin{bmatrix} \hat{h}(\boldsymbol{r}) & \Delta(\boldsymbol{r}) \\ \Delta^{*}(\boldsymbol{r}) & -\hat{h}(\boldsymbol{r}) \end{bmatrix} \begin{bmatrix} u_{\boldsymbol{n}}(\boldsymbol{r}) \\ v_{\boldsymbol{n}}(\boldsymbol{r}) \end{bmatrix} = E_{\boldsymbol{n}} \begin{bmatrix} u_{\boldsymbol{n}}(\boldsymbol{r}) \\ v_{\boldsymbol{n}}(\boldsymbol{r}) \end{bmatrix}, \tag{5.38}$$

which can deduced by putting the expansions (5.36)-(5.37) into the equations of motion (5.31)-(5.32). Using (5.36)-(5.37) I get for the expectation $\langle \Psi_{\downarrow}\Psi_{\uparrow} \rangle$:

$$\begin{aligned} \Big\langle \Psi_{\uparrow}(\boldsymbol{R}+\frac{\mathbf{1}}{\mathbf{2}}\boldsymbol{y},t)\Psi_{\downarrow}(\boldsymbol{R}-\frac{\mathbf{1}}{\mathbf{2}}\boldsymbol{y},t) \Big\rangle &= \sum_{\boldsymbol{n}} \Big[u_{\boldsymbol{n}}\big(\boldsymbol{R}+\frac{1}{2}\boldsymbol{y}\big) v^{*}_{\boldsymbol{n}}\big(\boldsymbol{R}-\frac{1}{2}\boldsymbol{y}\big)(1-n_F(E_{\boldsymbol{n}})) \\ &- v^{*}_{\boldsymbol{n}}\big(\boldsymbol{R}+\frac{1}{2}\boldsymbol{y}\big) u_{\boldsymbol{n}}\big(\boldsymbol{R}-\frac{1}{2}\boldsymbol{y}\big) n_F(E_{\boldsymbol{n}}) \Big], \end{aligned} \tag{5.39}$$

where I have used the results $\langle \gamma_{\boldsymbol{n}_1\uparrow}\gamma^{\dagger}_{\boldsymbol{n}_2\uparrow} \rangle = \delta_{\boldsymbol{n}_1,\boldsymbol{n}_2}(1-n_F(E_{\boldsymbol{n}_1}))$ and $\langle \gamma^{\dagger}_{\boldsymbol{n}_1\downarrow}\gamma_{\boldsymbol{n}_2\downarrow} \rangle = \delta_{\boldsymbol{n}_1,\boldsymbol{n}_2} n_F(E_{\boldsymbol{n}_1})$. I will come back to this result later. Let us first look at the BdG Hamiltonian in (5.38)

$$H_{BdG} = \begin{bmatrix} \hat{h}(\boldsymbol{r}) & \Delta(\boldsymbol{r}) \\ \Delta^{*}(\boldsymbol{r}) & -\hat{h}(\boldsymbol{r}) \end{bmatrix}, \tag{5.40}$$

and its associated Green's function $\mathcal{G}(\boldsymbol{r},\boldsymbol{r'};i\omega)$:

$$\mathcal{G}(\boldsymbol{r},\boldsymbol{r'};i\omega) = \sum_{\boldsymbol{n}} \left[\frac{\langle \boldsymbol{r}|\boldsymbol{n}^{+}\rangle\langle \boldsymbol{n}^{+}|\boldsymbol{r}\rangle}{i\omega - E_{\boldsymbol{n}^{+}}} + \frac{\langle \boldsymbol{r}|\boldsymbol{n}^{-}\rangle\langle \boldsymbol{n}^{-}|\boldsymbol{r}\rangle}{i\omega - E^{-}_{\boldsymbol{n}}} \right], \tag{5.41}$$

where $\langle \boldsymbol{n}^{+}|\boldsymbol{r}\rangle = [u_{\boldsymbol{n}}\ v_{\boldsymbol{n}}]$ and $\langle \boldsymbol{n}^{-}|\boldsymbol{r}\rangle = [-v^{*}_{\boldsymbol{n}}\ u^{*}_{\boldsymbol{n}}]$ are eigenfunctions of (5.40) with eigenvalues $E_{\boldsymbol{n}^{+}} = E_{\boldsymbol{n}}$ and $E_{\boldsymbol{n}^{-}} = -E_{\boldsymbol{n}}$ respectively. Plugging these eigenfunctions in (5.41) and

focussing on the Matsubara sum of 12-component of the Green's function I get:

$$\begin{aligned} T\sum_{\omega}\mathcal{G}_{12}(\boldsymbol{r},\boldsymbol{r'}) &= \sum_{\boldsymbol{n}}\Big[u_{\boldsymbol{n}}(\boldsymbol{r})v^{*}_{\boldsymbol{n}}(\boldsymbol{r'})n_F(E_{\boldsymbol{n}}) - v^{*}_{\boldsymbol{n}}(\boldsymbol{r})u_{\boldsymbol{n}}(\boldsymbol{r'})(1-n_F(E_{\boldsymbol{n}}))\Big], \\ &= \langle\Psi_{\uparrow}(\boldsymbol{r})\Psi_{\downarrow}(\boldsymbol{r'})\rangle, \end{aligned} \tag{5.42}$$

where in the last line I used (5.39). This is precisely what is needed in Eq.(5.35). I will now discuss the near transition temperature regime.

Near Transition Temperature $T \to T_c$

The preceding results show how to obtain the local paining amplitude in a trapped Fermi superfluid. In this section, I focus on the regime of $T \to T_c$ in which the BdG-equations simplify. As I saw in the previous subsection, if I want to evaluate the local pairing amplitude I need to first find the Matsubara sum of 12-component of BdG Green's function and then plug into (5.35). For this I need to solve the BdG equation:

$$\begin{bmatrix} i\omega - \hat{h}(\boldsymbol{r}) & \Delta(\boldsymbol{r}) \\ \Delta^{*}(\boldsymbol{r}) & i\omega + \hat{h}(\boldsymbol{r}) \end{bmatrix} \mathcal{G}(\boldsymbol{r},\boldsymbol{r'};i\omega) = \begin{bmatrix} \delta(\boldsymbol{r}-\boldsymbol{r'}) & 0 \\ 0 & \delta(\boldsymbol{r}-\boldsymbol{r'}) \end{bmatrix}, \tag{5.43}$$

To solve this I need the functions $u_{\boldsymbol{n}}$ and $v_{\boldsymbol{n}}$ which I can get by solving (5.38). In general this is very difficult as this is a pair of coupled second-order differential equations. Instead, I will use a Ginzburg-Landau approach to Taylor expand in the pairing amplitude $\Delta(\boldsymbol{r})$. This is valid near the transition temperature T_c, where I expect that the pairing amplitude is vanishingly small. In that case I can use this $\Delta(\boldsymbol{r})$ as a perturbation around the BdG Hamiltonian when there is no pairing. Thus instead of solving for the full Green's function $\mathcal{G}(\boldsymbol{r},\boldsymbol{r'};i\omega)$ in (5.43), I can solve for $\mathcal{G}_0(\boldsymbol{r},\boldsymbol{r'};i\omega)$ in

$$\hat{H}_0\mathcal{G}_0(\boldsymbol{r},\boldsymbol{r'};i\omega) = \begin{bmatrix} i\omega - \hat{h}(\boldsymbol{r}) & 0 \\ 0 & i\omega + \hat{h}(\boldsymbol{r}) \end{bmatrix} \mathcal{G}_0(\boldsymbol{r},\boldsymbol{r'};i\omega) = \begin{bmatrix} \delta(\boldsymbol{r}-\boldsymbol{r'}) & 0 \\ 0 & \delta(\boldsymbol{r}-\boldsymbol{r'}) \end{bmatrix}, \tag{5.44}$$

while treating $\hat{H}_\Delta$ as a perturbation on $\hat{H}_0$ defined as:

$$\hat{H}_\Delta = \begin{bmatrix} 0 & \Delta(\boldsymbol{r}) \\ \Delta(\boldsymbol{r}) & 0 \end{bmatrix}. \tag{5.45}$$

Then I can use the Dyson series to evaluate the full Green's function via:

$$\mathcal{G}(\boldsymbol{r},\boldsymbol{r'};i\omega) = \mathcal{G}_0(\boldsymbol{r},\boldsymbol{r'};i\omega) + \int d^3r_1 \mathcal{G}_0(\boldsymbol{r},\boldsymbol{r}_1;i\omega)\hat{H}_\Delta(\boldsymbol{r}_1)\mathcal{G}_0(\boldsymbol{r}_1,\boldsymbol{r}_2;i\omega) + ... \tag{5.46}$$

To evaluate this I will need the 0^{th} order Green's function:

$$\mathcal{G}_0(\boldsymbol{r},\boldsymbol{r'};i\omega) = \begin{bmatrix} G_0(\boldsymbol{r},\boldsymbol{r'};i\omega) & 0 \\ 0 & -G_0(\boldsymbol{r},\boldsymbol{r'};-i\omega) \end{bmatrix}, \tag{5.47}$$

where $G_0(\boldsymbol{r},\boldsymbol{r'};i\omega) = \sum_{\boldsymbol{n}} \frac{\psi_{\boldsymbol{n}}(\boldsymbol{r})\psi_{\boldsymbol{n}}(\boldsymbol{r'})}{i\omega-\xi_{\boldsymbol{n}}}$ is the box Green's function. Now I need the (1,2)-component of $\mathcal{G}(\boldsymbol{r},\boldsymbol{r'};i\omega)$ for which I use Dyson series (5.46) to first order:

$$\mathcal{G}(\boldsymbol{r},\boldsymbol{r'};i\omega)\Big|_{(1,2)} = -\int d^3r_1 G_0(\boldsymbol{r},\boldsymbol{r}_1;i\omega)\Delta(\boldsymbol{r})G_0(\boldsymbol{r}_1,\boldsymbol{r'};-i\omega). \tag{5.48}$$

Summing over all the Matsubara frequencies and then using (5.35) and (5.42) I get an expression for the local pairing amplitude:

$$\begin{aligned} \Delta(\boldsymbol{R}) &= \lambda \int d^3y \delta^{(3)}(\boldsymbol{y})\partial_y \Big[y \int d^3r' \sum_{\boldsymbol{n_1},\boldsymbol{n_2}} \frac{n_F(\xi_{\boldsymbol{n_1}}) - n_F(-\xi_{\boldsymbol{n_2}})}{\xi_{\boldsymbol{n}_1} + \xi_{\boldsymbol{n}_2}} \\ &\times \psi_{\boldsymbol{n}_1}\Big(\boldsymbol{R} - \frac{1}{2}\boldsymbol{y}\Big)\psi_{\boldsymbol{n}_1}(\boldsymbol{r'})\psi_{\boldsymbol{n}_2}(\boldsymbol{r'})\psi_{\boldsymbol{n}_2}\Big(\boldsymbol{R} + \frac{1}{2}\boldsymbol{y}\Big)\Delta(\boldsymbol{r'})\Big] \end{aligned} \tag{5.49}$$

An alternative way of writing (5.49) is to write it in the form of an eigenvalue equation $\Delta(\boldsymbol{R}) = \int d^3r' \mathcal{K}(\boldsymbol{R},\boldsymbol{r'})\Delta(\boldsymbol{r'})$ where the kernel is defined as follows:

$$\begin{aligned} \mathcal{K}(\boldsymbol{R},\boldsymbol{r'}) &= \lambda \int d^3y \delta^{(3)}(\boldsymbol{y})\partial_y \Big[y \sum_{\boldsymbol{n_1},\boldsymbol{n_2}} \frac{n_F(\xi_{\boldsymbol{n_1}}) - n_F(-\xi_{\boldsymbol{n_2}})}{\xi_{\boldsymbol{n}_1} + \xi_{\boldsymbol{n}_2}} \\ &\times \psi_{\boldsymbol{n}_1}\Big(\boldsymbol{R} - \frac{1}{2}\boldsymbol{y}\Big)\psi_{\boldsymbol{n}_1}(\boldsymbol{r'})\psi_{\boldsymbol{n}_2}(\boldsymbol{r'})\psi_{\boldsymbol{n}_2}\Big(\boldsymbol{R} + \frac{1}{2}\boldsymbol{y}\Big)\Big]. \end{aligned} \tag{5.50}$$

In the comings sections, I will use (5.49) to determine the superfluid transition temperature and the local pairing amplitude in a box trap in the vicinity of T_c. In the next subsection, I will see how to recover the bulk transition temperature equation.

Recovering the Bulk Limit

In this section, I will use the real space kernel in Eq. (5.50) to get the well known result for bulk T_c-equation. In the bulk case, the wavefuctions are plane waves which enter Green's functions $G_0(\boldsymbol{r_1}, \boldsymbol{r_2}) = \sum_{\boldsymbol{k}} \frac{e^{i\boldsymbol{k}\cdot(\boldsymbol{r_1}-\boldsymbol{r_2})}}{i\omega-\xi_{\boldsymbol{k}}}$. Thus a similar procedure as above can be followed to get an expression for the bulk kernel $\mathcal{K}^b(\boldsymbol{R}, \boldsymbol{R'})$:

$$\mathcal{K}^b(\boldsymbol{R}, \boldsymbol{R'}) = \lambda \int d^3y \delta(\boldsymbol{y}) \partial_y \Big[y \sum_{\boldsymbol{k_1},\boldsymbol{k_2}} \frac{n_F(\xi_{\boldsymbol{k_1}}) - n_F(-\xi_{\boldsymbol{k_2}})}{\xi_{\boldsymbol{k}_1} + \xi_{\boldsymbol{k}_2}} e^{i\boldsymbol{k_1}\cdot\left(\boldsymbol{R}-\frac{1}{2}\boldsymbol{y}-\boldsymbol{R'}\right)} e^{i\boldsymbol{k_2}\cdot\left(\boldsymbol{R'}-\frac{1}{2}\boldsymbol{y}-\boldsymbol{R}\right)} \Big]. \quad (5.51)$$

Now as I discussed in the paragraph following (5.35), I will split this kernel into two parts by adding and subtracting $\mathcal{K}_0^b$ i.e. $\mathcal{K}^b = \mathcal{K}_0^b + (\mathcal{K}^b - \mathcal{K}_0^b) = \mathcal{K}_0^b + \mathcal{K}_1^b$ where $\mathcal{K}_0^b$ is the $T \to 0$ and $\mu \to 0$ limit of $\mathcal{K}^b$ and it is the singular part $\sim \frac{1}{y}$ which will be removed by the pseudo-potential

$$\begin{aligned} \mathcal{K}_0^b(\boldsymbol{R}, \boldsymbol{R'}) &= \lambda \int d^3y \delta(\boldsymbol{y}) \partial_y \Big[y \sum_{\boldsymbol{k_1},\boldsymbol{k_2}} \frac{1}{\epsilon_{\boldsymbol{k}_1} + \epsilon_{\boldsymbol{k}_2}} e^{i\boldsymbol{k_1}\cdot\left(\boldsymbol{R}-\frac{1}{2}\boldsymbol{y}-\boldsymbol{R'}\right)} e^{i\boldsymbol{k_2}\cdot\left(\boldsymbol{R'}-\frac{1}{2}\boldsymbol{y}-\boldsymbol{R}\right)} \Big], \\ &= -\lambda \frac{m}{2\pi^3} \int d^3y \delta(\boldsymbol{y}) \partial_y \Big[y \frac{4}{(y^2 + 4|\boldsymbol{R}-\boldsymbol{R'}|^2)} \Big]. \end{aligned} \quad (5.52)$$

where in the second line I have taken the continuum limit and thus converted sums to integrals. On the other hand $\mathcal{K}_1^b$ is the regularized part where I can safely set $\boldsymbol{y} \to 0$

$$\mathcal{K}_1^b(\boldsymbol{R}, \boldsymbol{R'}) = \lambda \sum_{\boldsymbol{k_1},\boldsymbol{k_2}} \left(\frac{n_F(\xi_{\boldsymbol{k_1}}) - n_F(-\xi_{\boldsymbol{k_2}})}{\xi_{\boldsymbol{k}_1} + \xi_{\boldsymbol{k}_2}} + \frac{1}{\epsilon_{\boldsymbol{k_1}} + \epsilon_{\boldsymbol{k_2}}} \right) e^{i(\boldsymbol{k_1}-\boldsymbol{k_2})\cdot(\boldsymbol{R}-\boldsymbol{R'})}. \quad (5.53)$$

I cannot evaluate (5.52)-(5.53) yet because they need to act on another an eigenfunction. Thus I will first find the eigenfunctions. It turns out that the plane waves or any linear

combination of them $e^{i\boldsymbol{p}\cdot\boldsymbol{R'}}$ is an eigenfunction of both (5.52)-(5.53). However in the bulk limit I know that the local pairing amplitude is uniform i.e. $\Delta(\boldsymbol{r}) = \Delta_0 = \sum_{\boldsymbol{p}} \Delta_{\boldsymbol{p}} e^{i\boldsymbol{p}\cdot\boldsymbol{r}}$ which can be satisfied iff $\Delta_{\boldsymbol{p}} = 0$ for all $\boldsymbol{p} \neq 0$. Thus our eigenvalue equation becomes:

$$\begin{aligned}
\int d^3R' \mathcal{K}^b(\boldsymbol{R}, \boldsymbol{R'}) e^{i\boldsymbol{p}\cdot\boldsymbol{R'}} &= \int d^3R' \mathcal{K}_0^b(\boldsymbol{R}, \boldsymbol{R'}) e^{i\boldsymbol{p}\cdot\boldsymbol{R'}} + \int d^3R' \mathcal{K}_1^b(\boldsymbol{R}, \boldsymbol{R'}) e^{i\boldsymbol{p}\cdot\boldsymbol{R'}}, \\
&= \frac{m\lambda}{8\pi} p e^{i\boldsymbol{p}\cdot\boldsymbol{R}} \\
&+ e^{i\boldsymbol{p}\cdot\boldsymbol{R}} \lambda \sum_{\boldsymbol{k}} \left(\frac{n_F(\xi_{\boldsymbol{k}+\frac{1}{2}\boldsymbol{p}}) - n_F(-\xi_{\boldsymbol{k}-\frac{1}{2}\boldsymbol{p}})}{\xi_{\boldsymbol{k}+\frac{1}{2}\boldsymbol{p}} + \xi_{\boldsymbol{k}-\frac{1}{2}\boldsymbol{p}}} + \frac{1}{\epsilon_{\boldsymbol{k}+\frac{1}{2}\boldsymbol{p}} + \epsilon_{\boldsymbol{k}-\frac{1}{2}\boldsymbol{p}}} \right), \\
-\frac{1}{\lambda} &= \sum_{\boldsymbol{k}} \left(\frac{\tanh \frac{\xi_{\boldsymbol{k}}}{2T}}{2\xi_{\boldsymbol{k}}} - \frac{1}{2\epsilon_{\boldsymbol{k}}} \right),
\end{aligned} \tag{5.54}$$

where in the last line I have put $\boldsymbol{p} = 0$. Thus, I get the standard T_c-equation for the bulk limit. This tells us that the pseudopotential approach is valid.

5.4. Regularizing the Box Kernel

In order to solve the superfluid gap equation in Eq. (5.49), in this section, I will discuss how to divide the real-space kernel $\mathcal{K}(\boldsymbol{R}, \boldsymbol{R'})$ into two parts: a regular part, and a term which is divergent in the limit of $\boldsymbol{R} = \boldsymbol{R'}$ such that, the latter can be regularized using the pseudopotential. This procedure is similar to the one I discussed to recover the bulk limit in the previous section. I start by re-writing the real space kernel as follows:

$$\begin{aligned}
\mathcal{K}(\boldsymbol{R}, \boldsymbol{r'}) &= \lambda \int d^3y \delta(\boldsymbol{y}) \partial_y \Big[y \sum_{\boldsymbol{n_1}, \boldsymbol{n_2}} \frac{n_F(\xi_{\boldsymbol{n_1}}) - n_F(-\xi_{\boldsymbol{n_2}})}{\xi_{\boldsymbol{n}_1} + \xi_{\boldsymbol{n}_2}} \\
&\times \psi_{\boldsymbol{n}_1}\Big(\boldsymbol{R} - \frac{1}{2}\boldsymbol{y}\Big) \psi_{\boldsymbol{n}_1}(\boldsymbol{r'}) \psi_{\boldsymbol{n}_2}(\boldsymbol{r'}) \psi_{\boldsymbol{n}_2}\Big(\boldsymbol{R} + \frac{1}{2}\boldsymbol{y}\Big) \Big],
\end{aligned} \tag{5.55}$$

where $\psi_{\boldsymbol{n}}(\boldsymbol{r}) = \left(\frac{2}{L}\right)^{\frac{3}{2}} \sin\left(\frac{n_x \pi x}{L}\right) \sin\left(\frac{n_y \pi y}{L}\right) \sin\left(\frac{n_z \pi z}{L}\right)$ are the box wavefunctions that vanish at the box edges. Our objective is to first break (5.55) into singular $\mathcal{K}_0$ and non-singular parts $\mathcal{K}_1$ where the singular part will be dealt with by the pseudo-potential. Then

I will need to simplify the sums in kernels and finally find their eigenfunctions. To split this kernel into two parts I use the idea that at very high energies $\epsilon_{\boldsymbol{n}} \gg \mu$ and $\epsilon_{\boldsymbol{n}} \gg T$ and thus I get $\xi_{\boldsymbol{n}} \approx \epsilon_{\boldsymbol{n}}$ and $\frac{\xi_{\boldsymbol{n}}}{2T} \to \infty$. This means that effectively we are taking the limit $(\mu, T) \to 0$. In this limit the Fermi functions become step functions i.e. $n_F(\xi_{\boldsymbol{n_1}}) = \Theta(-\epsilon_{\boldsymbol{n_1}}) = 0$ and $n_F(-\xi_{\boldsymbol{n_2}}) = \Theta(\epsilon_{\boldsymbol{n_2}}) = 1$ and kernel (5.55) becomes $\mathcal{K}_0$:

$$\mathcal{K}_0(\boldsymbol{R}, \boldsymbol{r'}) = \lambda \int d^3y \delta(\boldsymbol{y}) \partial_y \Big[y \sum_{\boldsymbol{n_1}, \boldsymbol{n_2}} \frac{1}{\epsilon_{\boldsymbol{n}_1} + \epsilon_{\boldsymbol{n}_2}} \psi_{\boldsymbol{n}_1}\Big(\boldsymbol{R} - \frac{1}{2}\boldsymbol{y}\Big) \psi_{\boldsymbol{n}_1}(\boldsymbol{r'}) \psi_{\boldsymbol{n}_2}(\boldsymbol{r'}) \psi_{\boldsymbol{n}_2}\Big(\boldsymbol{R} + \frac{1}{2}\boldsymbol{y}\Big) \Big]. \tag{5.56}$$

Adding and subtracting this from (5.55) i.e. writing $\mathcal{K} = \mathcal{K}_0 + (\mathcal{K} - \mathcal{K}_0) = \mathcal{K}_0 + \mathcal{K}_1$, I get the regularized part $\mathcal{K}_1$ as:

$$\begin{aligned} \mathcal{K}_1(\boldsymbol{R}, \boldsymbol{r'}) &= \lambda \int d^3y \delta(\boldsymbol{y}) \partial_y \Big[y \sum_{\boldsymbol{n_1}, \boldsymbol{n_2}} \left[\frac{n_F(\xi_{\boldsymbol{n_1}}) - n_F(-\xi_{\boldsymbol{n_2}})}{\xi_{\boldsymbol{n}_1} + \xi_{\boldsymbol{n}_2}} - \frac{1}{\epsilon_{\boldsymbol{n}_1} + \epsilon_{\boldsymbol{n}_2}} \right] \\ &\times \psi_{\boldsymbol{n}_1}\Big(\boldsymbol{R} - \frac{1}{2}\boldsymbol{y}\Big) \psi_{\boldsymbol{n}_1}(\boldsymbol{r'}) \psi_{\boldsymbol{n}_2}(\boldsymbol{r'}) \psi_{\boldsymbol{n}_2}\Big(\boldsymbol{R} + \frac{1}{2}\boldsymbol{y}\Big) \Big]. \end{aligned} \tag{5.57}$$

Te next step is to evaluate the sum in (5.56) and (5.57) and then find their eigenfunctions. The idea is to evaluate both these sums using the following identity:

$$\int \frac{d^3k_1}{(2\pi)^3} \int \frac{d^3k_1}{(2\pi)^3} \frac{e^{i\boldsymbol{k}_1 \cdot \boldsymbol{r}_1} e^{i\boldsymbol{k}_2 \cdot \boldsymbol{r}_2}}{\epsilon_{\boldsymbol{k}_1} + \epsilon_{\boldsymbol{k}_2}} = \frac{m}{2\pi^3} \frac{1}{(r_1^2 + r_2^2)^2}. \tag{5.58}$$

This can be done in principle because the wavefunctions $\psi(\boldsymbol{r})$ can be written in terms of exponentials using the identity $\sin(x) = \frac{e^{ix} - e^{-ix}}{2i}$. However when I look at say (5.56), I see that there are four wavefunctions and using the identity just described, this will lead to 8^4 exponentials, which is difficult to deal with. Thus I will simplify our problem by studying the thin film case first and later generalize it to the cubical geometry. I will confine the thin film in the $\hat{x}$ direction i.e. behaves like an infinite square well of size L and keep it infinite in the remaining two directions, which means it behaves like bulk. This greatly

simplifies our problem as now I have to deal with only 4 exponential terms. Thus using (5.58) I get:

$$\mathcal{K}_0(\boldsymbol{R},\boldsymbol{R'}) = \mathcal{K}_0^b(\boldsymbol{R},\boldsymbol{R'}) + \frac{m}{8\pi^3}\left[\frac{1}{4R_+^4} + \frac{2}{(R_+^2+R_-^2)^2}\right] \tag{5.59}$$

were $\boldsymbol{R}_+ \equiv (X+X', Y-Y', Z-Z')$ and $\boldsymbol{R}_- \equiv (X-X', Y-Y', Z-Z') = \boldsymbol{R}-\boldsymbol{R'}$. Our plan is to next evaluate (5.57) and then find their eigenfunctions. I will also try using the Poisson summation to evaluate (5.56) and (5.57), which converts a sum into a series:

$$\begin{aligned}\sum_{n=-\infty}^{\infty} f(n) &= \sum_{q=-\infty}^{\infty} F(q) \\ F(q) &= \int_{-\infty}^{\infty} dx\ e^{2\pi i q x} f(x)\end{aligned} \tag{5.60}$$

Alternatively, I can use the image charge representation (that can be derived using the Poisson sum formula) for the box Green's function which appear in sums in the kernels:

$$\begin{aligned}G(\boldsymbol{r}_1,\boldsymbol{r}_2) = -\frac{1}{4\pi}\sum_{\boldsymbol{n}}\Bigg[&\frac{1}{\sqrt{(x_1-x_2+2n_xL)^2+(y_1-y_2+2n_xL)^2+(z_1-z_2+2n_xL)^2}} \\ -\ &\frac{1}{\sqrt{(x_1+x_2+2n_xL)^2+(y_1-y_2+2n_xL)^2+(z_1-z_2+2n_xL)^2}} \\ -\ &\frac{1}{\sqrt{(x_1-x_2+2n_xL)^2+(y_1+y_2+2n_xL)^2+(z_1-z_2+2n_xL)^2}} \\ +\ &\frac{1}{\sqrt{(x_1+x_2+2n_xL)^2+(y_1+y_2+2n_xL)^2+(z_1-z_2+2n_xL)^2}} - (z_2\to -z_2)\Bigg],\end{aligned} \tag{5.61}$$

where $\boldsymbol{r}_1 = (x_1,y_1,z_1) = (X+\frac{x}{2}, Y+\frac{x}{2}, Z+\frac{x}{2})$ and $\boldsymbol{r}_2 = (x_2,y_2,z_2) = (X-\frac{x}{2}, Y-\frac{x}{2}, Z-\frac{x}{2})$. Here terms with higher values of $\boldsymbol{n}$ will be sub-dominant and since we are looking for $\frac{1}{L}$-corrections I can limit ourselves to working with only $\boldsymbol{n}=0$ terms:

$$\begin{aligned}G(\boldsymbol{r}_1,\boldsymbol{r}_2) = -\frac{1}{4\pi}\Bigg[&-\frac{1}{r} + \frac{1}{\sqrt{4X^2+y^2+z^2}} + \frac{1}{\sqrt{x^2+4Y^2+z^2}} + \frac{1}{\sqrt{x^2+y^2+4Z^2}} \\ -\ &\frac{1}{\sqrt{4X^2+4Y^2+z^2}} - \frac{1}{\sqrt{x^2+4Y^2+4Z^2}} - \frac{1}{\sqrt{4X^2+y^2+4Z^2}} \\ +\ &\frac{1}{\sqrt{4X^2+4Y^2+4Z^2}}\Bigg],\end{aligned} \tag{5.62}$$

where the first term is the one responsible for all the singular behavior and rest of the terms represent the boundary of the box.

Since we are interested in eliminating the singularities in the kernel $\mathcal{K}_0$ I need to see exactly how they come about. One thing is for sure that the singularities appear as two fermions approach each other i.e. when the relative coordinate goes to zero $\boldsymbol{y} \to 0$. Thus I study this kernel in two cases. Case 1 is when the fermions get created and annihilated at different center of mass locations i.e. $\boldsymbol{R} \neq \boldsymbol{R'}$. In this situation, I can safely set $\boldsymbol{y} \to 0$ in (5.56) and get:

$$\begin{aligned} \mathcal{K}_0(\boldsymbol{R}, \boldsymbol{R'}) &= -\lambda \sum_{\boldsymbol{n_1}, \boldsymbol{n_2}} \frac{1}{\epsilon_{\boldsymbol{n}_1} + \epsilon_{\boldsymbol{n}_2}} \sin(n_{1x}\pi X) \sin(n_{1x}\pi X') \sin(n_{2x}\pi X') \sin(n_{2x}\pi X') \\ &\times \quad e^{-2i\pi(n_{1y}-n_{2y})(Y-Y')} \times e^{-2i\pi(n_{1z}-n_{2z})(Z-Z')}. \end{aligned} \tag{5.63}$$

where I have set the box length $L = 1$. This expression is non-singular and can be evaluated using (5.58). On the other hand, case 2 is when the fermions get created and annihilated at the same centre of mass location i.e. $\boldsymbol{R} = \boldsymbol{R'}$. In this situation I will have to analyse the following in the limit $\boldsymbol{y} \to 0$:

$$\begin{aligned} \mathcal{K}_0(\boldsymbol{R}, \boldsymbol{R'}) = \lambda \int d^3y \delta(\boldsymbol{y}) \partial_y \Big[y \sum_{\boldsymbol{n_1}, \boldsymbol{n_2}} \frac{1}{\epsilon_{\boldsymbol{n}_1} + \epsilon_{\boldsymbol{n}_2}} e^{i\pi(n_{1y}+n_{2y})y} \times e^{i\pi(n_{1z}+n_{2z})z} \Big] \\ \times \quad \sin(n_{1x}\pi(X - \frac{x}{2})) \sin(n_{1x}\pi X) \sin(n_{2x}\pi X) \sin(n_{2x}\pi(X + \frac{x}{2})). \end{aligned} \tag{5.64}$$

In Sec. 5.6, I will analytically evaluate these kernels for two cases: a thin slab and a cubical box. In the next section, I will discuss how to use Taylor expansion in the $\Delta(\boldsymbol{R})$ parameter to solve the real-space gap equation.

5.5. Taylor Expansion Method: Transition Temperature

In this section, I will use the method of Taylor expansion to simplify the gap equation, and approximately obtain the transition temperature inside a box-shaped trap. As I saw in equations (5.49) and (5.34)-(5.35) of the previous sections, the linearized gap equation takes the form of an integral eigenvalue equation:

$$\begin{aligned}\Delta(\boldsymbol{R}) &= \int d^3R'\mathcal{K}(\boldsymbol{R},\boldsymbol{R}')\Delta(\boldsymbol{R}') \\ &= \Delta(\boldsymbol{R})\int d^3R'\mathcal{K}(\boldsymbol{R},\boldsymbol{R}') + \int d^3R'\mathcal{K}(\boldsymbol{R},\boldsymbol{R}')\big[\Delta(\boldsymbol{R}')-\Delta(\boldsymbol{R})\big], \qquad (5.65)\end{aligned}$$

where in the second line I added and subtracted $\Delta(\boldsymbol{R})$. Since singularities appear in $\mathcal{K}(\boldsymbol{R},\boldsymbol{R}')$ for $\boldsymbol{R} = \boldsymbol{R}'$, I expect that the vanishing of the term in square brackets will regularize this. Using Eq. (5.62), I can write the first $\boldsymbol{R}'$-integral as follows:

$$\int d^3R'\mathcal{K}(\boldsymbol{R},\boldsymbol{R}') = -g\sum_{\boldsymbol{n}}\left(\frac{\tanh(\frac{\xi_n}{2T})}{2\xi_n}-\frac{1}{2\epsilon_n}\right)\psi^2_{\boldsymbol{n}}(\boldsymbol{R}) + g\frac{m}{\hbar^2}F(0,\boldsymbol{R}), \qquad (5.66)$$

where I define the function $F(\boldsymbol{r},\boldsymbol{R})$ as the non-singular part of the two-particle Green's function in Eq. (5.62),

$$\sum_{\boldsymbol{n}}\frac{1}{2\epsilon_{\boldsymbol{n}}}\psi_{\boldsymbol{n}}\Big(\boldsymbol{R}-\frac{\boldsymbol{r}}{2}\Big)\psi_{\boldsymbol{n}}\Big(\boldsymbol{R}+\frac{\boldsymbol{r}}{2}\Big) = -\frac{m}{\hbar^2}G(\boldsymbol{r},\boldsymbol{R}) = -\frac{m}{\hbar^2}\left[F(\boldsymbol{r},\boldsymbol{R})-\frac{1}{4\pi r}\right]. \qquad (5.67)$$

Once the singular part is removed by the pseudo-potential in the kernel $\mathcal{K}(\boldsymbol{R},\boldsymbol{R}')$, I can then safely set $\boldsymbol{r}\to 0$. Note that since $\mathcal{K}(\boldsymbol{R},\boldsymbol{R}')$ diverges for $\boldsymbol{R} = \boldsymbol{R}'$, therefore I expect that the second integral has a dominant contribution in this limit. Thus I can Taylor expand the gap parameter to linear order, i.e. $\Delta(\boldsymbol{R}')\simeq\Delta(\boldsymbol{R})+(\boldsymbol{R}-\boldsymbol{R})\cdot\boldsymbol{\nabla}\Delta(\boldsymbol{R})$, giving us the following approximate expression for the second integral:

$$\begin{aligned}\int d^3R'\mathcal{K}(\boldsymbol{R},\boldsymbol{R}')\big[\Delta(\boldsymbol{R}')-\Delta(\boldsymbol{R})\big] &= g\boldsymbol{\nabla}\Delta(\boldsymbol{R})\cdot\int d^3R'\sum_{\boldsymbol{n_1},\boldsymbol{n_2}}\frac{n_F(\xi_{n_1})-n_F(-\xi_{n_2})}{\xi_{n_1}+\xi_{n_2}} \\ &\times\ \psi_{\boldsymbol{n_1}}(\boldsymbol{R})\psi_{\boldsymbol{n_1}}(\boldsymbol{R}')\psi_{\boldsymbol{n_2}}(\boldsymbol{R}')\psi_{\boldsymbol{n_2}}(\boldsymbol{R})(\boldsymbol{R}'-\boldsymbol{R}). \qquad (5.68)\end{aligned}$$

Plugging these results into the integral gap equation (5.65), I get the following (approximate but equivalent) differential equation for the gap parameter:

$$1 + gB(\boldsymbol{R}) = g\boldsymbol{A}(\boldsymbol{R}) \cdot \boldsymbol{\nabla} \log \Delta(\boldsymbol{R}), \tag{5.69}$$

where the functions $B(\boldsymbol{R})$ and $\boldsymbol{A}(\boldsymbol{R})$ are defined as follows:

$$B(\boldsymbol{R}) \equiv \sum_{\boldsymbol{n}} \left(\frac{\tanh(\frac{\xi_n}{2T})}{2\xi_n} - \frac{1}{2\epsilon_n} \right) \psi^2_{\boldsymbol{n}}(\boldsymbol{R}) - \frac{m}{\hbar^2} F(0, \boldsymbol{R}), \tag{5.70}$$

$$\boldsymbol{A}(\boldsymbol{R}) \equiv \int d^3R' \sum_{\boldsymbol{n}_1, \boldsymbol{n}_2} \frac{n_F(\xi_{n_1}) - n_F(-\xi_{n_2})}{\xi_{n_1} + \xi_{n_2}}$$

$$\times \psi_{\boldsymbol{n_1}}(\boldsymbol{R}) \psi_{\boldsymbol{n_1}}(\boldsymbol{R'}) \psi_{\boldsymbol{n_2}}(\boldsymbol{R'}) \psi_{\boldsymbol{n_2}}(\boldsymbol{R}) (\boldsymbol{R'} - \boldsymbol{R}). \tag{5.71}$$

Now I will prove that the vector $\boldsymbol{A}$ vanishes at the center of the box i.e. $\boldsymbol{A}(\boldsymbol{R_c}) = 0$ where $R_c = (\frac{1}{2}, \frac{1}{2}, \frac{1}{2})$. I will do this for the X-component and argue that similar procedure holds for the other two components,

$$A_X(\boldsymbol{R}_c) = \int d^3R' \sum_{\boldsymbol{n}_1, \boldsymbol{n}_2} F(n_1, n_2) \psi_{\boldsymbol{n_1}}(\boldsymbol{R}_c) \psi_{\boldsymbol{n_1}}(\boldsymbol{R'}) \psi_{\boldsymbol{n_2}}(\boldsymbol{R'}) \psi_{\boldsymbol{n_2}}(\boldsymbol{R}_c) \Big(X' - \frac{1}{2} \Big), \tag{5.72}$$

where I define $F(n_1, n_2) \equiv \frac{n_F(\xi_{n_1}) - n_F(-\xi_{n_2})}{\xi_{n_1} + \xi_{n_2}}$, and $n_i = |\boldsymbol{n_i}|$ for $i = 1, 2$. Now evaluating $\psi_{\boldsymbol{n}}(\boldsymbol{R}_c)$ gives us ± 1 if $\boldsymbol{n}$ is odd and zero otherwise. Thus (5.72) becomes :

$$\begin{aligned}
A_X(\boldsymbol{R}_c) &= \int d^3R' \sum_{\boldsymbol{n_1},\boldsymbol{n_2}} F(2n_1+1, 2n_2+1)\psi_{\boldsymbol{2n_1}+1}(\boldsymbol{R'})\psi_{\boldsymbol{n_2}+1}(\boldsymbol{R'})\Big(X' - \frac{1}{2}\Big) \cdot (-1)^{\sum n_i}, \\
&= \sum_{\boldsymbol{n_1},\boldsymbol{n_2}} (-1)^{\sum n_i} F(2n_1+1, 2n_2+1)\delta_{n_{1y}n_{2y}}\delta_{n_{1z}n_{2z}} \\
&\times \int_0^1 dX' \Big(X' - \frac{1}{2}\Big) \sin[(2n_{1x}+1)\pi X'] \sin[(2n_{2x}+1)\pi X'], \\
&= \sum_{\boldsymbol{n_1},\boldsymbol{n_2}} (-1)^{\sum n_i} F(2n_1+1, 2n_2+1)\delta_{n_{1y}n_{2y}}\delta_{n_{1z}n_{2z}} \\
&\times \int_{-1/2}^{+1/2} dX' X' \sin[(2n_{1x}+1)\pi(X' + \frac{1}{2})] \sin[(2n_{2x}+1)\pi(X' + \frac{1}{2})], \\
&= \sum_{\boldsymbol{n_1},\boldsymbol{n_2}} (-1)^{\sum n_i} F(2n_1+1, 2n_2+1)\delta_{n_{1y}n_{2y}}\delta_{n_{1z}n_{2z}} \\
&\times \int_{-1/2}^{+1/2} dX' X' \cos[(2n_{1x}+1)\pi X'] \cos[(2n_{2x}+1)\pi X'], \\
&= 0, \qquad (5.73)
\end{aligned}$$

where in the first line I define $(-1)^{\sum n_i} \equiv (-1)^{n_{1x}+n_{1y}+n_{1z}+n_{2x}+n_{2y}+n_{2z}}$, in the second line I have used the orthogonality of wave-functions in y and z directions to give us Kronecker deltas, in the third line I have shifted $X' \to X' - 1/2$ and in the last two lines I have used the fact that the integral of an even and an odd function is zero.

Using this result in the gap equation (5.69) at the center of the box results in the transition temperature or the T_c-equation:

$$\begin{aligned}
-\frac{1}{g} &= \sum_{\boldsymbol{n}} \left(\frac{\tanh(\frac{\xi_n}{2T})}{2\xi_n} - \frac{1}{2\epsilon_n} \right) \psi^2_{\boldsymbol{n}}(\boldsymbol{R}_c) - \frac{m}{\hbar^2} F(0, \boldsymbol{R}), \\
&= \left(\frac{2}{L}\right)^3 \sum_{\boldsymbol{n} \in \text{ODD}} \left[\frac{\tanh(\frac{\xi_n}{2T})}{2\xi_n} - \frac{1}{2\epsilon_n} \right] - \frac{m}{\hbar^2} F(0, \boldsymbol{R}_c), \qquad (5.74)
\end{aligned}$$

where in the summation $\boldsymbol{n} \in$ ODD means that each of n_x, n_y, n_z in $\boldsymbol{n}$ can only be positive

odd integers. Now replacing the coupling constant with the scattering length and converting the sum to an integral I get:

$$\begin{aligned} -\frac{1}{4\pi a_s} &= \int \frac{d^3k}{(2\pi)^3}\left[\frac{\tanh(\frac{\xi_k}{2T})}{2\xi_k} - \frac{1}{2\epsilon_k}\right] - \frac{m}{\hbar^2}F(0,\boldsymbol{R}_c), \\ &= \frac{\sqrt{2m\mu}}{2\pi^2\hbar}\left[\ln\left(\frac{8\mu e^{-2}}{\pi k_B T_c}\right) + \gamma\right] + \frac{\delta}{L}, \end{aligned} \tag{5.75}$$

where the second line is valid only for $\mu > 0$ and $\mu \gg T$, and δ is a constant. To evaluate this constant δ, I look at the expression for $F(0,\boldsymbol{R}_c)$ defined in equations (5.67) and (5.61)-(5.62), in terms of positions (X,Y,Z) and the box length L. Re-scaling $(X/L, Y/L, Z/L) \to (X,Y,Z)$, I get $F(0,\boldsymbol{R}_c)$ in terms of dimensionless function $f[X,Y,Z]$:

$$\begin{aligned} F(0,\boldsymbol{R}) &= \frac{1}{4\pi}\Big[\frac{1}{\sqrt{(2X+2L)^2+(2Y+2L)^2+(2Z+2L)^2}} + ...\Big], \\ &= \frac{1}{L}\cdot\frac{1}{4\pi}\Big[\frac{1}{\sqrt{(2X+2)^2+(2Y+2)^2+(2Z+2)^2}} + ...\Big], \\ &= \frac{1}{L}\cdot f[X,Y,Z], \end{aligned} \tag{5.76}$$

which at the box center becomes $F(0,\boldsymbol{R}_c) = \frac{1}{L}f\left[\frac{1}{2},\frac{1}{2},\frac{1}{2}\right] = \frac{0.139062}{L}$, giving us $\delta = 0.139062$. In the next subsections, I will study the transition temperature equations (5.74)-(5.75) for the bulk and box cases.

Bulk Case

For the bulk superfluid, I start with the transition temperature equation in (5.8) and re-write it as follows:

$$-\frac{1}{k_F a_s} = \frac{2}{\pi}\int_0^\infty dx\; x^2\left[\frac{\tanh\left(\frac{x^2-\hat{\mu}}{2\hat{T}}\right)}{x^2-\hat{\mu}} - \frac{1}{x^2}\right], \tag{5.77}$$

where I have introduced a new variable $x = \frac{k}{k_F}$, and accordingly defined $\hat{\mu} = \frac{\mu}{\epsilon_F}$ and $\hat{T} = \frac{k_B T}{\epsilon_F}$, where k_F and $\epsilon_F = \frac{\hbar^2 k_F^2}{2m}$ are the Fermi wavevector and energy respectively. This

equation has three unknowns: the chemical potential $\hat{\mu}$, the temperature $\hat{T}$, and the coupling $-\frac{1}{k_F a_s}$. In order to extract T_c versus the coupling, I need the number equation that relates chemical potential to the temperature:

$$\frac{k_F^3}{3\pi^2} = \frac{N}{V} = 2\int d^3k\; n_F(\xi_k) = \frac{k_F^3}{2\pi^2}\int_0^\infty dx \frac{x^2}{e^{\frac{x^2-\hat{\mu}}{\hat{T}}}+1}, \tag{5.78}$$

where I have made use of Fermi wavevector and energy to write this equation in a dimensionless form. The final integral can be simplified using the definition of polylogarithms: $-\mathbf{Li}_{j+1}(-e^x) \equiv \frac{1}{\Gamma(j+1)}\int_0^\infty dt \frac{t^j}{e^{t-x}+1}$:

$$-1 = \frac{3\sqrt{\pi}}{4}\hat{T}^{3/2}\mathbf{Li}_{3/2}(-e^{\frac{\hat{\mu}}{\hat{T}}}). \tag{5.79}$$

Solving this equation gives us the chemical potential in terms of the temperature which I have shown in Fig. 5.2. Then plugging in the data for $(\hat{\mu}, \hat{T})$ into Eq. (5.77) yields the transition temperature versus the coupling (see Fig. 5.3).

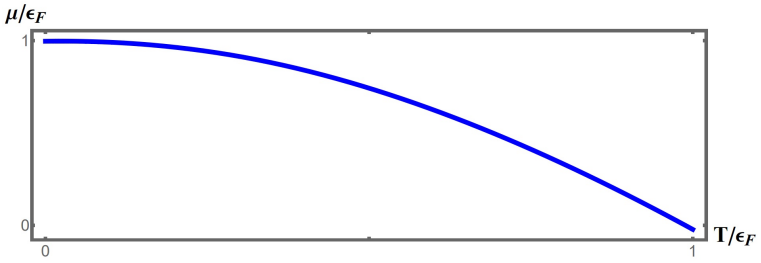

Figure 5.2. Plot of $\hat{\mu} = \frac{\mu}{\epsilon_F}$ versus $\hat{T} = \frac{k_B T}{\epsilon_F}$ for the bulk case.

Box Case : Including Size Corrections

Having discussed the bulk case, I now turn to the transition temperature equation for the case of a superfluid confined inside a box of size L (see Eqs. (5.74)-(5.75)):

$$-\frac{1}{k_F a_s} = \frac{2}{\pi}\int_0^\infty dx\; x^2\left[\frac{\tanh\left(\frac{x^2-\hat{\mu}}{2\hat{T}}\right)}{x^2-\hat{\mu}} - \frac{1}{x^2}\right] - \frac{4\pi\delta}{k_F L}, \tag{5.80}$$

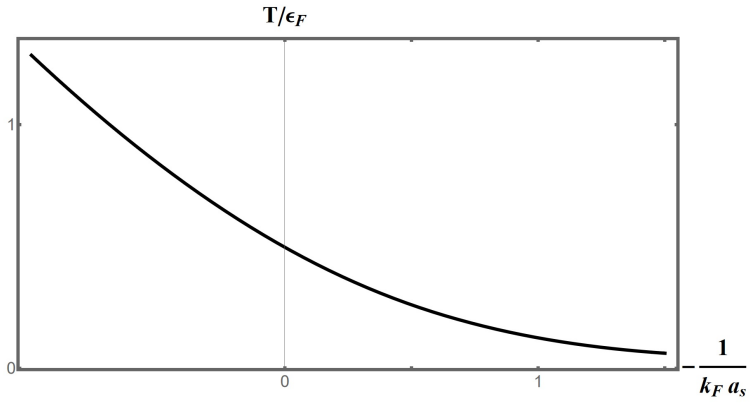

Figure 5.3. Plot of $\hat{T} = \frac{k_B T}{\epsilon_F}$ versus the coupling $-\frac{1}{k_F a_s}$ for the bulk case.

Comparing this with Eq. (5.77), I see that the last term introduces another variable in addition to $\hat{\mu}$, $\hat{T}_c$ and coupling: the number of particles as $k_F L = (3\pi^2 N)^{1/3}$. I first fix the number of particles, with three possible cases: $N = 2 \times 10^6$, $N = 2 \times 10^4$ and $N = 2 \times 10^3$. Then using the number equation (5.79) I eliminate $\hat{\mu}$. This gives us the transition temperature $\hat{T}_c$ in the box as a function of coupling, which I plot in Fig. 5.4 which shows small deviations from the bulk case. To show the BCS-limit, I zoom in at $-\frac{1}{k_F a_s} = +1.0$, giving us Fig. 5.5 where the deviations in T_c are clearly visible. To quantify this, I calculate the percentage change in the transition temperature:

$$\% = \frac{T_{c,Bulk} - T_{c,Box}}{T_{c,Bulk}} \times 100. \tag{5.81}$$

I have summarized our percentage change results in Table. 5.1. Our results show that the lesser the number of atoms I trap inside the box, the lower is the transition temperature.

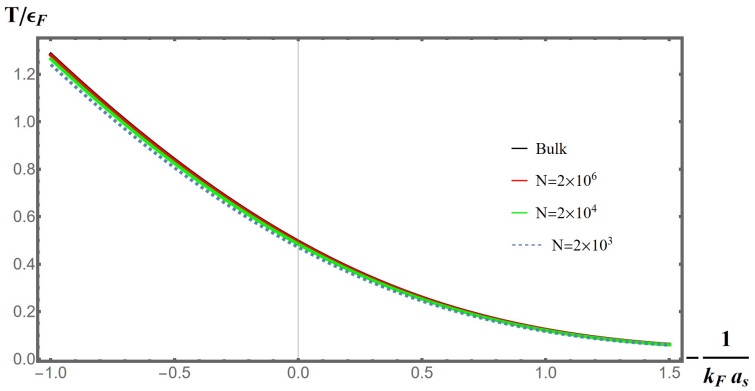

Figure 5.4. Plot of $\hat{T} = \frac{k_B T}{\epsilon_F}$ versus the coupling $-\frac{1}{k_F a_s}$ with corrections due to finite size of the box. Here the black line is the bulk case, and the red, green and dashed lines are $N = 2 \times 10^6, 2 \times 10^4, 2 \times 10^3$-atoms respectively.

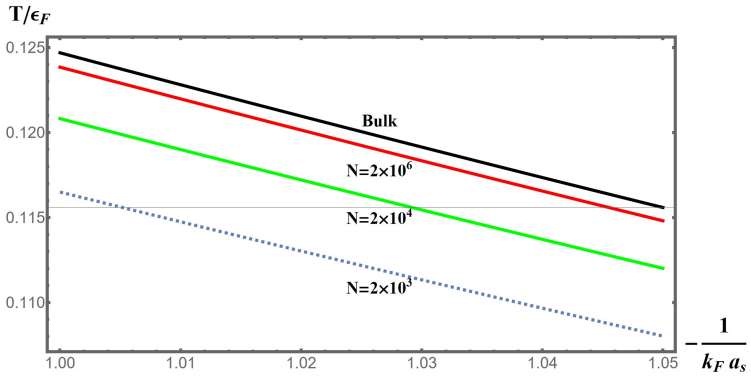

Figure 5.5. Plot of $\hat{T} = \frac{k_B T}{\epsilon_F}$ versus the coupling $-\frac{1}{k_F a_s}$ near the BCS limit, with corrections due to finite size of the box. Here the black line represents the bulk case, and the red, green, dashed lines represent the box cases with N=$2 \times 10^6, 2 \times 10^4, 2 \times 10^3$-atoms respectively.

Table 5.1. Comparison of percentage corrections in the transition temperature due to finite size of the box. Here I took the coupling to be in the BCS-regime, i.e., $-\frac{1}{k_F a_s} = +1.0$, where the bulk transition temperature is $\hat{T}_{c0} = 0.1247$.

Cases	N	$k_F L$	$\hat{T}_c$	SIZE Corrections
High	2×10^6	389.80	0.1215	0.4%
Medium	2×10^4	83.97	0.1102	3.2%
Low	2×10^3	38.98	0.0939	6.4%

5.6. Taylor Expansion Method: Local Pairing Amplitude

In the previous section, I solved the gap equation (5.69) that I got by Taylor expanding the local pairing amplitude, at the center of box which gave us the transition temperature as a function of coupling and number of atoms. In this section, I will be solving the gap equation to obtain $\Delta(\boldsymbol{R})$ as a function of position $\boldsymbol{R}$ inside a box with slab and cubical geometries.

Slab Geometry

Here I consider a rectangular slab which has a height that is much smaller than its length and breadth. Thus I approximately say that it is finite in $\hat{z}$ and infinite in $\hat{x}$ and $\hat{y}$. Thus the wavefunction will entail sine function in $\hat{z}$ (due to confinement) and plane waves in the other two directions i.e.

$$\begin{aligned}\Psi_{\boldsymbol{n}}(\boldsymbol{r}) &= \frac{\sqrt{2}}{L^{3/2}}\sin\Big(\frac{n_z\pi z}{L}\Big)e^{\frac{2\pi i}{L}(n_x x+n_y y)},\\ &= \frac{\sqrt{2}}{L^{3/2}}\sin(k_z z)e^{i(k_x x+k_y y)},\end{aligned} \tag{5.82}$$

where the fixed boundary conditions give us $k_z = \frac{n_z\pi}{L}$ and periodic boundary conditions give us $k_x = \frac{2n_x\pi}{L}$ and $k_y = \frac{2n_y\pi}{L}$. I start with the gap equation:

$$\Delta(\boldsymbol{R}) = \int d^3R'\mathcal{K}(\boldsymbol{R},\boldsymbol{R'})\Delta(\boldsymbol{R'}), \tag{5.83}$$

where the kernel $\mathcal{K}(\boldsymbol{R},\boldsymbol{R'})$ is defined as follows :

$$\begin{aligned}\mathcal{K}(\boldsymbol{R},\boldsymbol{R'}) &= g\int d^3y\delta^{(3)}(\boldsymbol{y})\partial_y\Bigg[y\sum_{\boldsymbol{n_1},\boldsymbol{n_2}}\frac{n_F(\xi_{n_1})-n_F(\xi_{n_2})}{\xi_{n_1}+\xi_{n_2}}\\ &\times \Psi_{\boldsymbol{n_1}}\Big(\boldsymbol{R}-\frac{\boldsymbol{y}}{\boldsymbol{2}}\Big)\Psi_{\boldsymbol{n_1}}(\boldsymbol{R'})\Psi_{\boldsymbol{n_2}}(\boldsymbol{R'})\Psi_{\boldsymbol{n_2}}\Big(\boldsymbol{R}+\frac{\boldsymbol{y}}{\boldsymbol{2}}\Big)\Bigg],\end{aligned} \tag{5.84}$$

where $n_F(\xi_n) = \frac{1}{1+\exp(\frac{\xi_n}{k_B T})}$ is the Fermi function, $\xi_n = \epsilon_n - \mu$ with ϵ_n being the single particle energy, μ is the chemical potential and T is the temperature. Firstly, the dimensions of the integral of this kernel are $\left[\int d^3R' \mathcal{K}(\boldsymbol{R}, \boldsymbol{R'})\right] = \left[\frac{a_s}{L}\right]$, which is dimensionless. So I will evaluate all the expressions for $L = 1$ and towards the end I will re-introduce L by making the switch $\frac{gm}{\hbar^2} \to \frac{gm}{\hbar^2 L}$. Secondly, the sum inside the kernel is divergent, and therefore, I will split the kernel into two parts, a convergent piece $\mathcal{K}_1$

$$\begin{aligned}\mathcal{K}_1(\boldsymbol{R}, \boldsymbol{R'}) &= g \int d^3y \delta^{(3)}(\boldsymbol{y}) \partial_y \Bigg[y \sum_{\boldsymbol{n_1}, \boldsymbol{n_2}} \left(\frac{n_F(\xi_{n_1}) - n_F(\xi_{n_2})}{\xi_{n_1} + \xi_{n_2}} + \frac{1}{\epsilon_{n_1} + \epsilon_{n_2}} \right) \\ &\times \Psi_{\boldsymbol{n_1}}\Big(\boldsymbol{R} - \frac{\boldsymbol{y}}{\boldsymbol{2}}\Big) \Psi_{\boldsymbol{n_1}}(\boldsymbol{R'}) \Psi_{\boldsymbol{n_2}}(\boldsymbol{R'}) \Psi_{\boldsymbol{n_2}}\Big(\boldsymbol{R} + \frac{\boldsymbol{y}}{\boldsymbol{2}}\Big) \Bigg], \end{aligned} \tag{5.85}$$

and a divergent piece $\mathcal{K}_0$ (found by setting $\mu = 0, T = 0$ in $\mathcal{K}$) which will be regularized by the pseudopotential. :

$$\begin{aligned}\mathcal{K}_0(\boldsymbol{R}, \boldsymbol{R'}) &= g \int d^3y \delta^{(3)}(\boldsymbol{y}) \partial_y \Bigg[y \sum_{\boldsymbol{n_1}, \boldsymbol{n_2}} \frac{1}{\epsilon_{n_1} + \epsilon_{n_2}} \\ &\times \Psi_{\boldsymbol{n_1}}\Big(\boldsymbol{R} - \frac{\boldsymbol{y}}{\boldsymbol{2}}\Big) \Psi_{\boldsymbol{n_1}}(\boldsymbol{R'}) \Psi_{\boldsymbol{n_2}}(\boldsymbol{R'}) \Psi_{\boldsymbol{n_2}}\Big(\boldsymbol{R} + \frac{\boldsymbol{y}}{\boldsymbol{2}}\Big) \Bigg]. \end{aligned} \tag{5.86}$$

I can simplify $\mathcal{K}_0$ further by integrating over X' and Y' that pins $n_{1x} = n_{2x} \equiv n_x$ and $n_{1y} = n_{2y} \equiv n_y$, and thus (5.86) becomes:

$$\begin{aligned}&\int_0^1 dX' \int_0^1 dY' \sum_{\boldsymbol{n_1}, \boldsymbol{n_2}} \frac{1}{\epsilon_{n_1} + \epsilon_{n_2}} \Psi_{\boldsymbol{n_1}}\Big(\boldsymbol{R} - \frac{\boldsymbol{y}}{\boldsymbol{2}}\Big) \Psi_{\boldsymbol{n_1}}(\boldsymbol{R'}) \Psi_{\boldsymbol{n_2}}(\boldsymbol{R'}) \Psi_{\boldsymbol{n_2}}\Big(\boldsymbol{R} + \frac{\boldsymbol{y}}{\boldsymbol{2}}\Big), \\ = \; & -\frac{8gm}{\hbar^2} \sum_{\substack{k_x, ky \\ k_{1z}, k_{2z}}} \frac{e^{-i(k_x x + k_y y)}}{(2k_x^2 + 2k_y^2 + k_{1z}^2 + k_{2z}^2)} \\ \times \; & \sin\left[k_{1z}\Big(Z - \frac{z}{2}\Big)\right] \sin[k_{1z} Z'] \sin[k_{2z} Z'] \sin\left[k_{2z}\Big(Z + \frac{z}{2}\Big)\right]. \end{aligned} \tag{5.87}$$

Now I will convert the sums to integrals that can be evaluated analytically, and the denominator of the last term can be written as the integral of an exponential as follows:

$$\begin{aligned}
\int_0^\infty dx\ e^{-\lambda x} &= \frac{1}{\lambda}, \\
\int_{-\infty}^{\infty}\frac{dk_x}{2\pi}\int_{-\infty}^{\infty}\frac{dk_y}{2\pi}\ e^{-i(k_x x+k_y y)}e^{-2\lambda(k_x^2+k_y^2)} &= \frac{1}{8\pi\lambda}e^{-\frac{(x^2+y^2)}{8\lambda}}, \\
\int_0^\infty \frac{dk_z}{\pi}\ \sin[k_z R]\sin[k_z R']e^{-\lambda k_z^2} &= \frac{1}{4\sqrt{\pi\lambda}}\Big[e^{-\frac{R-R'}{4\lambda}} - e^{-\frac{R+R'}{4\lambda}}\Big]. \qquad (5.88)
\end{aligned}$$

Plugging all these identities, I get that the divergent part of the slab kernel $\mathcal{K}_0(Z,Z')$ takes the form:

$$\mathcal{K}_0(Z,Z') = -\frac{gm}{8\pi^2}\int d^3r\,\delta^{(3)}(\boldsymbol{r})\partial_r\left(r\cdot\left[\frac{1}{\frac{r^2}{4}+(Z-Z')^2}+\frac{1}{(Z+Z')^2}-\frac{2}{Z^2+Z'^2}\right]\right). \quad (5.89)$$

At this point, it will be good for us to revisit the gap equation. Along the $\hat{x}$ and $\hat{y}$ directions I expext the gap to be constant just like the bulk case. It is only in the $\hat{z}$ direction that I expect the gap to have spatial variation, thus $\Delta(\boldsymbol{R}) = \Delta(Z)$. Thus the gap equation (5.83) becomes :

$$\begin{aligned}
\Delta(Z) &= \int dZ'\mathcal{K}(Z,Z')\Delta(Z'), \\
&= \int dZ'\Big[\mathcal{K}_0(Z,Z')+\mathcal{K}_1(Z,Z')]\Delta(Z'). \qquad (5.90)
\end{aligned}$$

Now I will Taylor expand the local gap parameter to linear order as I did in the previous section:

$$\Delta(Z') = \Delta(Z) + (Z'-Z)\cdot\frac{d}{dz}\Delta(Z) + \mathcal{O}(Z'-Z)^2, \qquad (5.91)$$

which when plugged into the gap equation yields:

$$\begin{aligned}
\Delta(Z) &= \Delta(Z)\int_0^1 dZ'\Big[\mathcal{K}_0(Z,Z')+\mathcal{K}_1(Z,Z')\Big], \\
&+ \Delta'(Z)\int_0^1 dZ'\Big[\mathcal{K}_0(Z,Z')+\mathcal{K}_1(Z,Z')\Big]\cdot(Z'-Z). \qquad (5.92)
\end{aligned}$$

Thus I need to analytically evaluate four integrals. Let us first look at the integrals involving $\mathcal{K}_0$. The first of these is :

$$I_1 = \int_0^1 dZ' \mathcal{K}_0(Z, Z') = -\frac{gm}{8\pi^2} \int d^3r \delta^{(3)}(\boldsymbol{r}) \partial_r \bigg(r \cdot I \bigg), \tag{5.93}$$

where the integral I is :

$$I = \int_0^1 dZ' \bigg[\frac{1}{\frac{r^2}{4} + (Z - Z')^2} + \frac{1}{(Z + Z')^2} - \frac{2}{Z^2 + Z'^2} \bigg]. \tag{5.94}$$

This has a singular piece with r^2 and a non-singular piece. Let us deal with the singular piece first. I cannot simply integrate this from $Z' = 0$ to $Z' = 1$ as it is singular for $Z = Z'$ and $r \to 0$. So instead, I will break the integral into two parts, one from $Z' = 0$ to $Z' = Z - r$ and the other from $Z' = Z + r$ to $Z' = 1$, along with setting $r = 0$ in the integrands. This way I can incorporate the r behavior and also never let $Z' = Z$:

$$\begin{aligned} I^S &= \int_0^1 dZ' \frac{1}{\frac{r^2}{4} + (Z - Z')^2}, \\ &= \int_0^{Z-r} dZ' \frac{1}{(Z - Z')^2} + \int_{Z+r}^1 dZ' \frac{1}{(Z - Z')^2}, \\ &= \frac{2}{r} + \frac{1}{Z(Z-1)}, \end{aligned} \tag{5.95}$$

where the superscript 'S' denotes singular part. Now for the non-singular part I need to remember that (5.89) is valid only for $Z + Z' < 1$. For $Z + Z' > 1$ I need to replace $Z \to (1 - Z)$ and $Z' \to (1 - Z')$. Thus I will replace $\int_0^1 dZ' \mathcal{K}_0(Z, Z') \to \int_0^{1-Z} dZ' \mathcal{K}_0(Z, Z') + \int_{1-Z}^1 dZ' \mathcal{K}_0(1 - Z, 1 - Z')$ that gives us :

$$\begin{aligned} I^{NS} &= \int_0^{1-Z} dZ' \bigg[\frac{1}{(Z + Z')^2} - \frac{2}{Z^2 + Z'^2} \bigg] \\ &+ \int_{1-Z}^1 dZ' \bigg[\frac{1}{(2 - Z - Z')^2} - \frac{2}{(1 - Z)^2 + (1 - Z')^2} \bigg], \\ &= -2 + \frac{1}{Z(1-Z)} - \frac{2}{Z} \tan^{-1} \Big(\frac{1 - Z}{Z} \Big) - \frac{2}{(Z-1)} \tan^{-1} \Big(\frac{Z}{Z - 1} \Big), \end{aligned} \tag{5.96}$$

where the superscript 'NS' denotes the non-singular part. Thus our first integral is:

$$\begin{aligned} I_1 &= \int_0^1 dZ' \mathcal{K}_0(Z, Z'), \\ &= \frac{gm}{\hbar^2} \cdot \frac{1}{4\pi^2} \left[1 + \frac{1}{Z} \tan^{-1}\left(\frac{1-Z}{Z}\right) + \frac{1}{(Z-1)} \tan^{-1}\left(\frac{Z}{Z-1}\right) \right]. \end{aligned} \tag{5.97}$$

Similarly, applying the above discussed ideas to the second integral I get :

$$\begin{aligned} I_2 &= \int_0^1 dZ' \mathcal{K}_0(Z, Z') \cdot (Z' - Z), \\ &= \frac{gm}{\hbar^2} \cdot -\frac{1}{4\pi^2} \left[2Z - 1 + \tan^{-1}\left(\frac{1-Z}{Z}\right) + \tan^{-1}\left(\frac{Z}{Z-1}\right) \right]. \end{aligned} \tag{5.98}$$

The remaining temperature dependent integrals are as follows:

$$I_3 = \int dZ' \mathcal{K}_1(Z, Z') = \frac{gm}{\hbar^2} \cdot -\frac{4}{\pi^2} \sum_{\boldsymbol{n}} \left[\frac{\tanh\left(a(n^2 - n_\mu^2)\right)}{n^2 - n_\mu^2} - \frac{1}{n^2} \right] \sin^2(n_z \pi Z), \tag{5.99}$$

$$\begin{aligned} I_4 &= \int dZ' \mathcal{K}_1(Z, Z') \cdot (Z' - Z) \\ &= \frac{gm}{\hbar^2} \cdot \frac{8}{\pi^2} \sum_{\substack{n_x, n_y \\ n_{1z}, n_{2z}}} I_{n_{1z}, n_{2z}}(Z) \sin(n_{1z}\pi Z) \sin(n_{2z}\pi Z) \\ &\times \left[\frac{n_F\Big(2a(n_x^2 + n_y^2 + n_{1z}^2 - n_\mu^2)\Big) - n_F\Big(2a(n_\mu^2 - n_x^2 - n_y^2 - n_{2z}^2)\Big)}{2n_x^2 + 2n_y^2 + n_{1z}^2 + n_{2z}^2 - 2n_\mu^2} \right. \\ &- \left. \frac{1}{2n_x^2 + 2n_y^2 + n_{1z}^2 + n_{2z}^2} \right], \end{aligned} \tag{5.100}$$

where I have introduced new parameters such as the temperature normalized with minimum energy in the box ($\epsilon_1 = \frac{\hbar^2}{2mL^2}$), normalized inverse temperature $a \equiv \frac{\hbar^2}{4mk_BTL^2} = \frac{\epsilon_1}{k_BT_c} = \frac{\hat{\epsilon}_1}{\hat{T}_c}$, the normalized chemical potential $n_\mu^2 \equiv \frac{2m\mu L^2}{\hbar^2} = \frac{\hat{\mu}}{\hat{\epsilon}_1}$, and the various energies normalized using Fermi energy $\hat{\epsilon}_1 \equiv \frac{\epsilon_1}{\epsilon_F} = \frac{\hbar^2/2mL^2}{\epsilon_F}$, $\hat{T}_c = \frac{k_BT_c}{\epsilon_F}$, $\hat{\mu} = \frac{\mu}{\epsilon_F}$. The integral function I is defined as :

$$I_{n_{1z}, n_{2z}}(Z) = \begin{cases} \frac{2\Big((-1)^{n_{1z}+n_{2z}} - 1\Big) n_{1z} n_{2z}}{\pi^2 (n_{1z}^2 - n_{1z}^2)^2} & \text{for } n_{1z} \neq n_{2z} \\ \\ \frac{1}{4}(1 - 2Z) & \text{for } n_{1z} = n_{2z}. \end{cases}$$

Now I can use the integrals (5.97)-(5.100) in Eq. (5.92) and re-instate the box length L, which yields a gap equation (similar to Eq. (5.69)) in the slab as follows:

$$\frac{L\hbar^2}{gm} + B(Z) = A(Z) \cdot \frac{d}{dz} \log \Delta(Z), \tag{5.101}$$

where the expressions for the functions $B(Z)$ and $A(Z)$ are as follows:

$$\begin{aligned} B(Z) &= \frac{4}{\pi^2} \sum_{n_z} \int_{-\infty}^{\infty} dn_x \int_{-\infty}^{\infty} dn_y \left[\frac{\tanh\left(a(n^2 - n_\mu^2)\right)}{n^2 - n_\mu^2} - \frac{1}{n^2} \right] \sin^2(n_z \pi Z) \\ - \; & \frac{1}{4\pi^2} \left[1 + \frac{1}{Z} \tan^{-1}\left(\frac{1-Z}{Z}\right) + \frac{1}{(Z-1)} \tan^{-1}\left(\frac{Z}{Z-1}\right) \right], \end{aligned} \tag{5.102}$$

$$\begin{aligned} A(Z) &= \frac{8}{\pi^2} \sum_{n_{1z}, n_{2z}} \int_{-\infty}^{\infty} dn_x \int_{-\infty}^{\infty} dn_y \; I_{n_{1z}, n_{2z}}(Z) \sin(n_{1z}\pi Z) \sin(n_{2z}\pi Z) \\ \times \; & \left[\frac{n_F\Big(2a(n_x^2 + n_y^2 + n_{1z}^2 - n_\mu^2)\Big) - n_F\Big(2a(n_\mu^2 - n_x^2 - n_y^2 - n_{2z}^2)\Big)}{2n_x^2 + 2n_y^2 + n_{1z}^2 + n_{2z}^2 - 2n_\mu^2} \right. \\ - \; & \left. \frac{1}{2n_x^2 + 2n_y^2 + n_{1z}^2 + n_{2z}^2} \right] - \frac{1}{4\pi^2} \left[2Z - 1 + \tan^{-1}\left(\frac{1-Z}{Z}\right) + \tan^{-1}\left(\frac{Z}{Z-1}\right) \right]. \end{aligned} \tag{5.103}$$

Note that I have summed over the indices in the $\hat{z}$-direction and integrated over the $\hat{x}, \hat{y}$-directions. This means I first took periodic boundary conditions in the two infinite directions of the slab and then took thermodynamic limit, whereas in the direction of the confinement ($\hat{z}$), I kept the levels to be discrete.

To solve the gap equation (5.101), I will subtract from it the T_c equation, i.e. the Eq. (5.101) with $Z = 0.5$:

$$\frac{L\hbar^2}{gm} + B(Z = 0.5) = A(Z) \cdot \frac{d}{dz} \log \Delta(Z) = 0. \tag{5.104}$$

This procedure eliminates the coupling term $L\hbar^2/gm$ and yielding the following differential equation:

$$B(Z) - B(0.5) = A(Z) \cdot \frac{d}{dz} \log \Delta(Z), \tag{5.105}$$

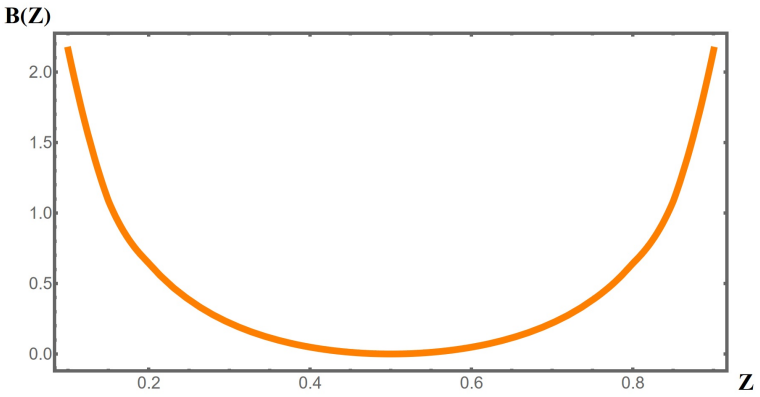

Figure 5.6. Plot of $B(Z)$ (see Eq. (5.102) in the text) versus position inside a slab. It is symmetric about the box-center. For this plot I took $n_\mu = 5.1$ and $a = 0.02$.

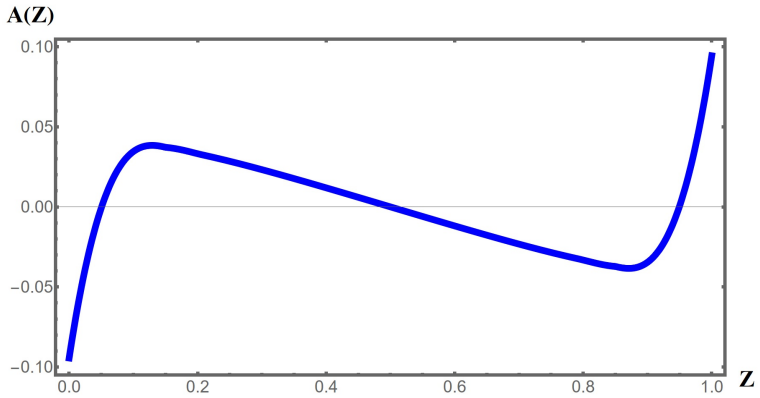

Figure 5.7. Plot $A(Z)$ (see Eq. (5.103) in the text versus position inside a slab. It vanishes and is anti-symmetric about the box-center. For this plot I took $n_\mu = 5.1$ and $a = 0.02$.

whose solution is as follows:

$$\Delta(Z) = e^{\int_0^Z dZ \left[\frac{B(Z)-B(0.5)}{A(Z)}\right]}. \tag{5.106}$$

In Fig.(5.8) I have plotted the local pairing amplitude inside the box shaped trap.

Cubical Box

In the previous subsection, I discussed the Taylor expansion method of solving the superfluid gap equation in a slab geometry. In this subsection, I will follow a similar approach to extract the local gap parameter inside a box with cubical geometry. I choose to study the pairing amplitude along the path $\mathcal{P}$: $\boldsymbol{R} = \left(X, \frac{1}{2}, \frac{1}{2}\right)$, which is a line joining one

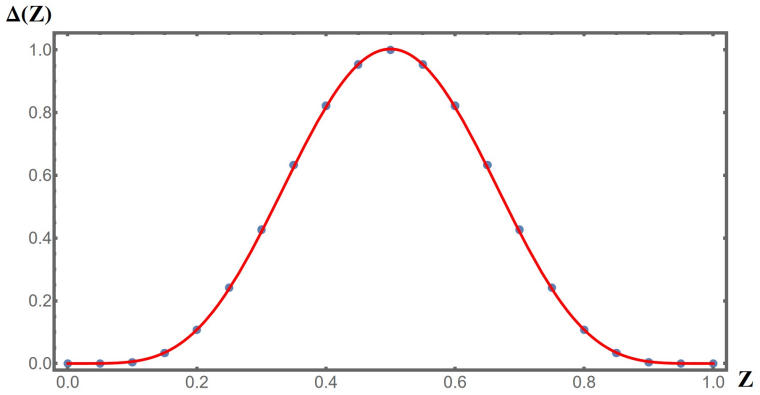

Figure 5.8. Plot of local pairing amplitude $\Delta(Z)$ versus position Z inside a slab. The blue dots represent the solutions to the gap equation at various positions. For this plot I took $n_\mu = 5.1$ and $a = 0.02$. The red curve is a variational guess $\Delta(Z) = 1027 \cdot [Z(1-Z)]^5$ that fits the blue dots.

face center of the box to another. In principle, pairing could also be studied along other paths such as the diagonal. Here the wavefunction is made of sine functions in all three directions:

$$\begin{aligned} \Psi_{\boldsymbol{n}}(\boldsymbol{r}) &= \left(\frac{2}{L}\right)^{3/2} \sin\left(\frac{n_x \pi x}{L}\right) \sin\left(\frac{n_y \pi y}{L}\right) \sin\left(\frac{n_z \pi z}{L}\right), \\ &= \left(\frac{2}{L}\right)^{3/2} \sin(k_x \pi x) \sin(k_y \pi y) \sin(k_z \pi z), \end{aligned} \tag{5.107}$$

where the fixed boundary conditions give us $\boldsymbol{k} = (k_x, k_y, k_z) = (\frac{n_x \pi}{L}, \frac{n_y \pi}{L}, \frac{n_z \pi}{L})$.

To solve the gap equation (5.83), I split the kernel $\mathcal{K}$ into divergent $\mathcal{K}_0$ and convergent $\mathcal{K}_1$ parts, as I did in Eqs. (5.85)-(5.86). Since I have chosen the path $\mathcal{P}$ which only varies in $\hat{x}$, therefore I expect that the pairing along $\mathcal{P}$ will only be a function of X, i.e., $\Delta(X)$. As a result, the Y' and Z' integrals in (5.83) can be performed. Let us first do this for $\mathcal{K}_0(\boldsymbol{R}, \boldsymbol{R'})$ in Eq. (5.86):

$$\int_0^1 dY' \int_0^1 dZ' \mathcal{K}_0(\boldsymbol{R}, \boldsymbol{R'}) = g \int d^3y \delta^3(\boldsymbol{y}) \partial_y \big[y \cdot S\big], \tag{5.108}$$

where the sum S is :

$$\begin{aligned} S &= \sum_{\substack{k_{1x},k_{2x}\\ k_y,k_z}} \sin\Big[k_{1x}\Big(X-\frac{x}{2}\Big)\Big]\sin\Big[k_{1x}X'\Big]\sin\Big[k_{2x}X'\Big]\sin\Big[k_{2x}\Big(X+\frac{x}{2}\Big)\Big] \\ &\times \sin\Big[k_{1y}\Big(Y-\frac{y}{2}\Big)\Big]\sin\Big[k_{2y}\Big(Y+\frac{y}{2}\Big)\Big] \\ &\times \sin\Big[k_{1z}\Big(Z-\frac{z}{2}\Big)\Big]\sin\Big[k_{2z}\Big(Z+\frac{z}{2}\Big)\Big]/\big(k_{1x}^2+k_{2x}^2+2k_y^2+2k_z^2\big). \end{aligned} \tag{5.109}$$

Converting all the momentum sums to integrals and making use of the identity (5.88), I end up with an approximate expression for $\mathcal{K}_0$ as :

$$\begin{aligned} \mathcal{K}_0(X,X') &= \frac{gm}{L\hbar^2}\cdot\frac{-1}{8\pi^2}\times\Bigg[\int d^3r\delta^{(3)}(\boldsymbol{r})\partial_r\Bigg(\frac{r}{(X-X')^2+\frac{r^2}{4}}\Bigg) \\ &+ \frac{1}{(X+X')^2}-\frac{2}{X^2+X'^2}+\frac{1}{(X-X')^2+\frac{1}{2}}+\frac{1}{(X+X')^2+\frac{1}{2}} \\ &- \frac{2}{X^2+X'^2+\frac{1}{2}}-\frac{1}{(X-X')^2+\frac{1}{4}}-\frac{1}{(X+X')^2+\frac{1}{2}}+\frac{1}{X^2+X'^2+\frac{1}{4}}\Bigg]. \end{aligned} \tag{5.110}$$

It is instructive at this point to compare this expression for the box-$\mathcal{K}_0$ with the slab case. The first line is the same as (5.89) and the rest of the terms appear because of confinement in the other two directions.

Following the steps for the slab case, I now Taylor expand the local gap parameter to linear order: $\Delta(X')\simeq\Delta(X)+(X'-X)\cdot\frac{d}{dx}\Delta(X)$ and plug it into the gap equation, yielding:

$$\begin{aligned} \Delta(X) &= \Delta(X)\int_0^1 dX'\Big[\mathcal{K}_0(X,X')+\mathcal{K}_1(X,X')\Big], \\ &+ \Delta'(X)\int_0^1 dX'\Big[\mathcal{K}_0(X,X')+\mathcal{K}_1(X,X')\Big]\cdot(X'-X), \end{aligned} \tag{5.111}$$

which is similar to Eq. (5.92). Thus I need to evaluate four integrals. I start with the spa-

tial integral of $\mathcal{K}_0$:

$$\frac{L\hbar^2}{gm}I_1 = \int_0^1 dX'\mathcal{K}_0(X,X') = \frac{1}{4\pi^2}\Bigg[1 + \frac{1}{X}\tan^{-1}\left(\frac{1-X}{X}\right)$$
$$+\frac{1}{(X-1)}\tan^{-1}\left(\frac{X}{X-1}\right) + 2\tan^{-1}(2) - \sqrt{2}\tan^{-1}(\sqrt{2})$$
$$+\frac{1}{\sqrt{X^2+\frac{1}{2}}}\tan^{-1}\frac{1-X}{\sqrt{X^2+\frac{1}{2}}} - \frac{1}{\sqrt{X^2+\frac{1}{4}}}\tan^{-1}\frac{1-X}{\sqrt{X^2+\frac{1}{4}}}$$
$$+\frac{1}{\sqrt{(X-1)^2+\frac{1}{2}}}\tan^{-1}\frac{X}{\sqrt{(X-1)^2+\frac{1}{2}}} - \frac{1}{\sqrt{(X-1)^2+\frac{1}{4}}}\tan^{-1}\frac{X}{\sqrt{(X-1)^2+\frac{1}{4}}}\Bigg], \tag{5.112}$$

where the first three terms match with the slab case (5.97) and the rest are due to confinement in two other directions. Similarly, the spatial integral of $\mathcal{K}_0$ multiplied with $(Z'-Z)$ gives us the following result:

$$\frac{L\hbar^2}{gm}I_2 = \int_0^1 dX'\mathcal{K}_0(X,X')\cdot(X'-X) = -\frac{1}{4\pi^2}\Bigg[2X - 1 + \tan^{-1}\left(\frac{1-X}{X}\right)$$
$$+\tan^{-1}\left(\frac{X}{X-1}\right) + 2X\tan^{-1}(2) - 2X\tan^{-1}(2X)$$
$$+4(X-1)\tan^{-1}(2) + 4(X-1)\tan^{-1}(2(X-1)) + 2X\sqrt{2}\tan^{-1}(\sqrt{2}X)$$
$$-2X\sqrt{2}\tan^{-1}(\sqrt{2}) - 2\sqrt{2}(X-1)\tan^{-1}(\sqrt{2}) - 2\sqrt{2}(X-1)\tan^{-1}(\sqrt{2}(X-1))$$
$$-\frac{2(X-1)\tan^{-1}\left(\frac{X}{\sqrt{(X-1)^2+\frac{1}{4}}}\right)}{\sqrt{(X-1)^2+\frac{1}{4}}} + \frac{2X\tan^{-1}\left(\frac{1-X}{\sqrt{X^2+\frac{1}{2}}}\right)}{\sqrt{X^2+\frac{1}{2}}} - \frac{2X\tan^{-1}\left(\frac{1-X}{\sqrt{X^2+\frac{1}{4}}}\right)}{\sqrt{X^2+\frac{1}{4}}}$$
$$+\frac{2(X-1)\tan^{-1}\left(\frac{X}{\sqrt{(X-1)^2+\frac{1}{2}}}\right)}{\sqrt{(X-1)^2+\frac{1}{2}}}\Bigg], \tag{5.113}$$

where the first four terms are the same as (5.98) as I saw in the slab case. The temperature dependent part of the kernel has the following two spatial integrals associated with

it:

$$\frac{L\hbar^2}{gm} I_3 = \int d^3R' \mathcal{K}_1(\boldsymbol{R}, \boldsymbol{R'})$$

$$= -\frac{8}{\pi^2} \sum_{\substack{n_x \\ n_y, n_z \in \text{ODD}}} \left[\frac{\tanh\Big(a(n^2 - n_\mu^2)\Big)}{n^2 - n_\mu^2} - \frac{1}{n^2} \right] \sin^2(n_x \pi X), \tag{5.114}$$

$$\frac{L\hbar^2}{gm} I_4 = \int d^3R' \mathcal{K}_1(\boldsymbol{R}, \boldsymbol{R'}) \cdot (Z' - Z)$$

$$= \frac{32}{\pi^2} \sum_{\substack{n_{1x}, n_{2x} \\ n_y, n_z \in \text{ODD}}} \left[\frac{n_F\Big(2a(n_{1x}^2 + n_y^2 + n_z^2 - n_\mu^2)\Big) - n_F\Big(2a(n_\mu^2 - n_{2x}^2 - n_y^2 - n_z^2)\Big)}{n_{1x}^2 + n_{2x}^2 + 2n_y^2 + 2n_z^2 - 2n_\mu^2} \right.$$

$$\left. - \frac{1}{n_{1x}^2 + n_{2x}^2 + 2n_y^2 + 2n_z^2} \right] I_{n_{1x}, n_{2x}}(X) \sin(n_{1x}\pi X) \sin(n_{2x}\pi X), \tag{5.115}$$

that are also similar to the slab case (5.99) and (5.100) respectively. Note that the summation indices of I_3 and I_4 change as compared to slab case as n_y, n_z can only be odd positive integers. Here $a \equiv \frac{\hbar^2}{4mk_BTL^2} = \frac{\hat{\epsilon}_1}{\hat{T}_c}$, $n_\mu^2 \equiv \frac{2m\mu L^2}{\hbar^2} = \frac{\hat{\mu}}{\hat{\epsilon}_1}$, $\hat{\epsilon}_1 \equiv \frac{\epsilon_1}{\epsilon_F} = \frac{\hbar^2/2mL^2}{\epsilon_F}$, $\hat{T}_c = \frac{k_BT_c}{\epsilon_F}$, $\hat{\mu} = \frac{\mu}{\epsilon_F}$ and the integral function I is defined as :

$$I_{n_{1x}, n_{2x}}(X) = \begin{cases} \frac{2\Big((-1)^{n_{1x}+n_{2x}} - 1\Big) n_{1x} n_{2x}}{\pi^2 (n_{1x}^2 - n_{2x}^2)^2} & \text{for } n_{1x} \neq n_{2x} \\ \\ \frac{1}{4}(1 - 2X) & \text{for } n_{1x} = n_{2x}. \end{cases}$$

Collecting the spatial integrals in equations (5.112)-(5.115) into the Taylor expanded gap equation (5.111), I arrive at the following differential equation:

$$\frac{L\hbar^2}{gm} + B(X) = A(X) \cdot \frac{d}{dx} \log \Delta(X), \tag{5.116}$$

where the functions $B(X)$ for the box case is:

$$B(X) = \frac{2}{\pi^2} \sum_{n_x} \int_1^\infty dn_y \int_1^\infty dn_z \left[\frac{\tanh\Big(a(n^2 - n_\mu^2)\Big)}{n^2 - n_\mu^2} - \frac{1}{n^2} \right] \sin^2(n_z \pi Z)$$

$$- \frac{1}{4\pi^2} \left[1 + \frac{1}{Z} \tan^{-1}\left(\frac{1 - Z}{Z}\right) + \frac{1}{(Z-1)} \tan^{-1}\left(\frac{Z}{Z-1}\right) \right], \tag{5.117}$$

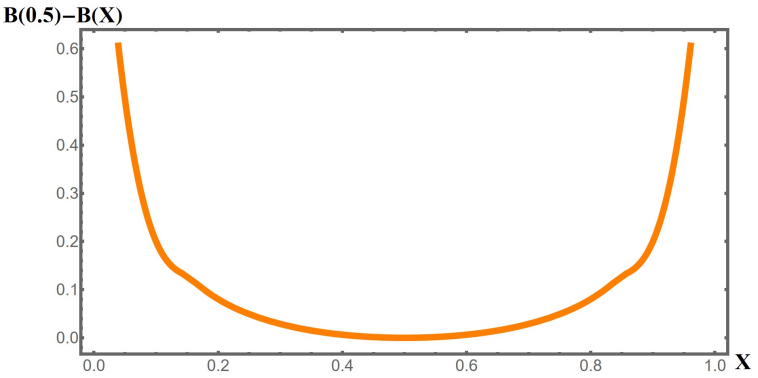

Figure 5.9. Plot of difference between $B(X)$ and $B(0.5)$ from one face center $(0, 1/2, 1/2)$ to the other $(1, 1/2, 1/2)$ versus position inside a cubical box (see Eq. (5.117) in the text). It is symmetric about the box-center. For this plot I took $n_\mu = 5.1$ and $a = 0.02$.

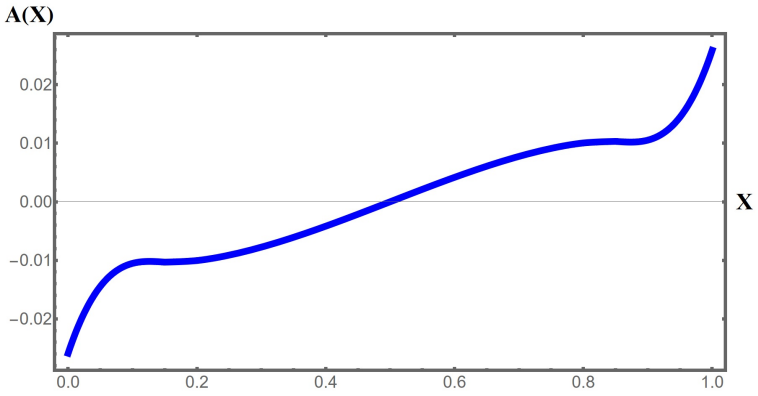

Figure 5.10. Plot $A(X)$ from one face center $(0, 1/2, 1/2)$ to the other $(1, 1/2, 1/2)$ versus position inside a cubical box (see Eq. (5.118) in the text). It vanishes and is anti-symmetric about the box-center. For this plot I took $n_\mu = 5.1$ and $a = 0.02$.

and the expression for the function $A(X)$ inside the box is as follows:

$$\begin{aligned} A(X) = \frac{8}{\pi^2} \sum_{n_{1x}, n_{2x}} \int_1^\infty dn_y \int_1^\infty dn_z \; I_{n_{1z}, n_{2z}}(Z) \sin(n_{1z}\pi Z) \sin(n_{2z}\pi Z) \\ \times \quad \left[\frac{n_F\Big(2a(n_{1x}^2 + n_y^2 + n_z^2 - n_\mu^2)\Big) - n_F\Big(2a(n_\mu^2 - n_{2x}^2 - n_y^2 - n_z^2)\Big)}{n_{1x}^2 + n_{2x}^2 + 2n_y^2 + 2n_z^2 - 2n_\mu^2} \right. \\ \left. - \quad \frac{1}{n_{1x}^2 + n_{2x}^2 + 2n_y^2 + 2n_z^2} \right] - \frac{1}{4\pi^2} \left[2Z - 1 + \tan^{-1}\left(\frac{1-Z}{Z}\right) + \tan^{-1}\left(\frac{Z}{Z-1}\right) \right], \end{aligned} \tag{5.118}$$

where $n^2 = n_x^2 + n_y^2 + n_z^2$. Note that I have summed over the indices in $\hat{x}$-direction and

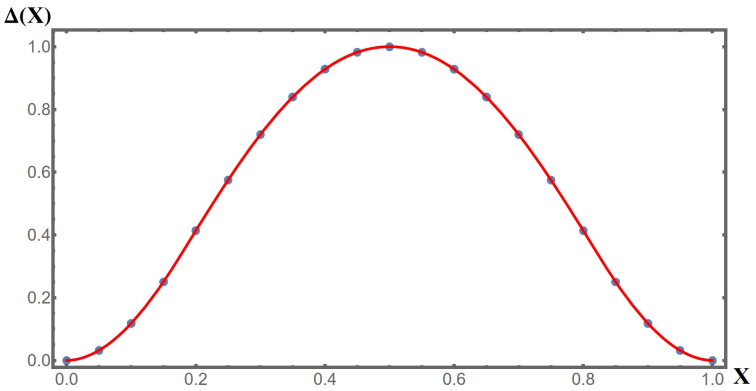

Figure 5.11. Plot of local pairing amplitude $\Delta(X)$ from one face center $(0, 1/2, 1/2)$ to the other $(1, 1/2, 1/2)$, versus position X inside a cubical box. The blue dots represent the solutions to the gap equation at various positions. For this plot I took $n_\mu = 5.1$ and $a = 0.02$. The red curve is our variational guess $\Delta(X) = 16 \cdot [X(1-X)]^2$ that fits the blue dots.

integrated indices in the $\hat{y}$ and $\hat{z}$-directions. In Fig. 5.9 and Fig. 5.10, I show the spatial profiles of the functions $B(X)$ and $\boldsymbol{A}(X)$ respectively. Following the previous subsection, to solve Eq. (5.116), I subtract off the same equation but evaluated at $X = 0.5$, i.e., the T_c equation, yielding:

$$B(X) - B(0.5) = A(X) \cdot \frac{d}{dx} \log \Delta(X), \tag{5.119}$$

which can now be solved to get the local pairing amplitude in the box along the path $\mathcal{P}$: $\boldsymbol{R} = \left(X, \frac{1}{2}, \frac{1}{2}\right)$:

$$\Delta(X) = e^{\int_0^X dX \left[\frac{B(X)-B(0.5)}{A(X)}\right]}, \tag{5.120}$$

which I have plotted in Fig.(5.11), which shows that the gap parameter vanishes at the edges $X = 0$ and $X = 1$, and has a spatial profile similar to $[X(1-X)]^2$, unlike the slab case where the exponent was 5.

To summarize, in this chapter I started with the Bogoliubov-de Gennes (BdG) Hamiltonian and modeled the interactions using the pseudopotential, which gave us a superfluid gap equation in the form of an integral eigenvalue equation. To solve this I Taylor

expanded the gap parameter to linear order, where the assumption is that $\Delta(\boldsymbol{R})$ varies slowly with respect to position. However, for a box-shaped trap I expect that the pairing vanishes at the edge (Dirichlet boundary condition) and should rise rapidly to some smooth value near the box center. This means that in order to correctly characterize the pairing near the edge an alternate approach needs to be found. Nonetheless, this Taylor expansion approach can be trusted near the box center and near the transition temperature regime.

CHAPTER 6. CONCLUDING REMARKS

In this thesis, I explored analogue inflationary particle creation in rapidly expanding toroidal Bose-Einstein condensates (BEC) and the associated entanglement properties, analogue Unruh effect and Takagi's statistics inversion in strained graphene, and how the properties of a superfluid change inside a box-shaped trap compared the standard BCS-theory for the bulk. Although, I discussed a wide variety of topics, there are some common themes between them. One such theme is the applicability of analogue gravity techniques to condensed matter setups that lead to spontaneous quasi-particle creation from the vacuum. For toroidal BEC and graphene I looked at this in detail, but I could have in principle applied it to the box trap, and depending on whether I put time dependence or some spatial disturbance, I would get quasi-particle generation there too. Another common theme, is that all these topics can be tested in cold atom setups. While this may be obvious for the toroidal BEC and the box-shaped trap, the strained honeycomb could in principle be constructed in optical lattices. In the coming subsections, I will provide concluding remarks and possible future work for each chapter.

6.1. Toroidal BEC

In Chapter 2, I have explored how an exponentially expanding thin toroidal Bose-Einstein condensate can reproduce the various features of primordial cosmological inflation. Our work was inspired by recent experimental and theoretical work by Eckel and collaborators who studied inflationary physics in a ring-shaped BEC [38]. These authors observed experimentally (and confirmed theoretically) the redshifting of phonons due to the

rapid expansion of this analogue 1D universe, a damping of phonon modes due to Hubble friction, and evidence of the preheating phenomena predicted to occur at the end of inflation.

A central finding of our work is that quantum pressure effects, even if they are quantitatively small, can have important implications for the dynamics of expanding toroidal BEC's. Such quantum pressure effects modify the Mukhanov-Sasaki equations for phonon modes in a fundamental way, with the resulting solutions exhibiting damping and redshift, just like in inflationary cosmology. I found that this damping is responsible for the change of the vacuum state of the fluctuations, which ultimately leads to the dynamical generation of phonons. This is the analogue of particle production in the early universe. As a result, if the perturbations start in a coherent state, the ring expansion forces them to bifurcate into two density waves that propagate opposite to each other, leading to a complex time-dependent density wave in the toroid. This phonon generation also manifests itself in the density-density noise correlations as a cusp-like feature that tracks the horizon size. Both of these results are clear signatures of particle creation and can be verified experimentally. However, it is important to note that, within the gravitational analogy viewpoint, the model I consider here is a very special one i.e. a quasi-one-dimensional toroidal BEC, the small width of which led us to consider the short-distance corrections due to quantum pressure. More general models could be realized experimentally that can give different results and interpretations [74].

I make note of two things. Firstly, a simple harmonic oscillator with a time dependent frequency [46], can also exhibit a change of vacuum states leading to particle creation. Secondly, the fact that no particle creation happens for $\gamma = 0$ is related to the

presence of an adiabatic invariant in 1D [38]. Unlike other settings where quantum pressure effects are unimportant for particle production (for example, the Sakharov oscillations measurements of Hung et al [24]), in the present case of a one-dimensional BEC, where I have assumed a time independent speed of sound c, it is essential to have a nonzero γ for the damping of modes. I emphasize that taking c to be constant is a simplifying approximation, and that a rapid time-dependent variation of c would also lead to phonon production. Within the preceding approximations, our work shows that quantum pressure is essential to achieve particle production, as seen from the form of Eq. (2.20) and its solution Eq. (2.21).

Such damping is also crucial within inflationary theory, where the horizon size is approximately fixed. During this period, some modes (which are due to spontaneously created particles) get stretched out of the horizon and thus freeze. However, other modes never exit the horizon and thus undergo damping. When inflation ends, the horizon again expands and starts enveloping these frozen modes, that re-enter the horizon and distribute the available matter and radiation. This way, inflation provides a mechanism through which vacuum fluctuations in the early universe manifest themselves later in the form of distribution of galaxies and the CMB anisotropies. In a BEC, the quantum pressure is essential for damping and particle creation. As a result, here too the same mechanism of horizon exit and freezing of modes is happening. In this sense, the quantum pressure terms provide us with an analogue of the inflationary mechanism in a BEC.

Future studies could look into other types of expansion rates like the ones arising from the quadratic or the Starobinsky models of inflation. A further possibility as mentioned in [38], could be to study how causally disconnected regions recombine. This could

potentially help cosmology experiments to observe physics beyond our current horizon. Another possibility as discussed in [54], is to see whether cold atomic systems can be used to study the trans-Planckian era that happened before inflation, which is believed to entail quantum effects of gravity.

6.2. Toroidal Entanglement

In Chapter 3, I revisited the setup of Chapter 2 in which a Bose-Einstein condensate (BEC) trapped inside a thin toroidal laser trap (effectively a one-dimensional ring), is rapidly expanded. Previous works such as [38, 73] have experimentally studied this system to show how the amplitude of the BEC fluctuations undergo damping due to the expansion of the ring which is an the analogue of cosmological redshift, and the mode wavelengths thus mimicking the gravitational redshift. In Chapter 2, I modeled this system using the Bogoliubov-de Gennes (BdG) Hamiltonian, which in the thin-ring limit yields the Mukhanov-Sasaki equation that describes how the azimuthal modes evolve in time. I divided the entire problem into three stages. The first stage is a static BEC with no phonons, which due to time-translation symmetry are described by plane wave modes in time and give us a notion of particles. The second phase is where the ring expands rapidly where the modes undergo damping due to the quantum pressure. When this expansion ends, I enter into the third phase of a static BEC with a larger ring radius. In the Heisenberg picture, the state of the system remains the same, but the quantum field operators described by density and phase modes evolve in time. Thus the notion of vacuum state changes and these field operators see the final BEC as filled with phonons. This is spontaneous particle creation leads to the phonons being generated in two-mode squeezed states

which manifests itself as a cusp (at zero temperature) or kink (finite temperature) like features in the density-density correlations.

Naturally then, one would like to know if these correlations are quantum or classical in nature, i.e., is there any entanglement present in this system in the sense of Einstein-Podolsky-Rosen (EPR). For this purpose, I then briefly reviewed the theory of Gaussian quantum continuous variables for bosons, wherein the state of the fluctuations (phonons) can be completely specified by the mean vector and the covariance matrix for a system of two modes n and $-n$. To discuss whether such states are entangled or not, I reviewed the PPT criterion which says that if the symplectic eigenvalues of the covariance matrix that is partially transposed with respect to one of the subsystems, are less than unity, then the state of such a phonon pair is entangled. I then employed this technique to the case of an initial static BEC prepared in the vacuum, thermally excited and single-mode squeezed states. I found that for an initial vacuum state, the entanglement is maximum for lowest energy modes $n = 1$, and decreases with increasing n in an oscillatory manner that is due to the presence of sonic horizon in the system. I then saw how thermal noise or the presence of imperfections in the detector (losses) can lead to entanglement degradation, whereas using states prepared with phonons squeezed in a single mode n, acts as a quantum resource and leads to the enhancement of entanglement. For a combination of such thermal and squeezed inputs, I found parameter spaces over which experiments could possibly detect such quantum correlations.

Finally, I ended our discussion by proposing a protocol that makes use of an angular version of the Hanbury-Brown and Twiss experiment. Here I aimed to measure the correlations in real space as they are easier to directly measure than the ones in the mode

space. I then discussed how a toroidal BEC cloud prepared any state and after expansion, can be split via laser Bragg diffraction into two parallel clouds with an tunable induced phase difference. Then one of the clouds is rotated and made to interfere with the non-rotated cloud which yields experimental data the atom density correlations. By varying the relative rotation angle and the induced phase, I showed how to extract from this data the phase-phase and density-density correlations of fluctuations in the BEC. Additionally, if the phase-phase correlations are measured as a function of time, then their time differential will yield the mixed correlations between phase and density. Thus, this procedure ends up giving us all types of real space correlations that can then be Fourier transformed to give the complete set of mode correlations. This way, the experimenter can build the covariance matrix and hence determine the amount of entanglement in the toroidal BEC.

As I discussed in the introduction, different inflaton potentials $V(\phi)$ in the early universe can give different expansion rates which could be mimicked in the toroidal setup, and and could thus result in different amounts of mode entanglement. A further possible direction could be to look at an expanding toroid of fermions (as in superfluids) where the due to Pauli's exclusion principle, the fermionic entanglement is maximum for a certain mode index, as was discussed in Refs. [72, 70]. Another possibility would be to extend the calculations in this paper to include non-gaussian processes [87] and non-classical correlations such as quantum discord [61].

6.3. Unruh Effect in Graphene

In Chapter 4, I have discussed how a honeycomb lattice that is strained inhomogenously can act as an arena where analogue Rindler physics associated with accelerating

observers can be realized. I broke this problem into two stages. The first stage is that of an unstrained flat graphene sheet that possesses (discrete) translation symmetry, and leads to an emergent Dirac equation for low energy modes. This mimics the evolution of fermions in flat Minkowski spacetime. I then solved the evolution equation to obtain the mode expansion in terms of plane waves in space and time. This choice helps us define a structure of ladder operators $\hat{a}_{\boldsymbol{k}}$ and $\hat{b}_{\boldsymbol{k}}$ which, when acting on the Minkowski or flat graphene vacuum state $|0_{\mathcal{M}}\rangle$, lead to excitation of electrons and holes that obey a linear in energy-momentum dispersion relation.

The second stage starts when I suddenly switch on strains to create a Rindler Hamiltonian with a spatially varying Fermi velocity $v(x) \simeq v_0 \frac{|x|}{\lambda}$ where the origin $x = 0$ acts as an analogue of Rindler horizon separating the $x < 0$ and $x > 0$ regions and forbidding low-energy and long-wavelength electrons to tunnel through. Thus the two disconnected sides of strained graphene mimic the causally disconnected left and right Rindler wedges. Then I solved the Dirac equation for right handed Weyl fermions and obtained the solutions in terms of Bessel functions that blow up at the horizon and asymptotically vanish at large x. Here the plane wave basis in Rindler time helps us choose the structure of Rindler creation and annihilation operators $\hat{c}_{k_y,\Omega}$ and $\hat{d}_{k_y,\Omega}$ for electrons and holes with respect to the Rindler vacuum state $|0_{\mathcal{R}}\rangle$. However, unlike the Minkowski case, here due to broken translation symmetry there is no band dispersion and the energy and momentum are decoupled.

Since the same quantum field operator has two different representations in the flat and strained regimes, by projecting one onto the other I find that the Minkowski vacuum $|0_{\mathcal{M}}\rangle$ appears to operators of the strained system as if it is at finite temperature, swarming

with Rindler particles. This can be understood in terms of the Heisenberg picture where the state of the system remains the same, whereas the operators evolve, and thus in the sudden approximation the original state is viewed as a linear combination of the eigenstates of the new Hamiltonian. In fact, the Minkowski vacuum state corresponding to the flat system can be expressed as a two-mode squeezed state with respect to the Rindler vacuum, since one side of the lattice is unavailable to the modes residing on the opposite side. Thus, expectation values on the right side effectively involve a trace over the left side, amounting to a mixed thermal density operator for the right side. This is similar to what happens in Rindler spacetime because when an observer picks a certain acceleration say $a > 0$, then they are naturally causally disconnected from the observers accelerating opposite to them. As a result of this, the Minkwoski vacuum averages of Rindler ladder operators pertaining to one side appear as thermal averages, which is known as the Fulling-Davies-Unruh effect.

After discussing this thermal-like creation of particles, I looked into the properties of the strained Green's functions which satisfy the KMS condition that ensures that if the analogue spacetime has a horizon in it, then the spectrum of particles it creates is bound to be thermal in nature. Another feature of these Green's functions was that the Huygens' principle gets violated due to graphene being a two-dimensional material and thus leads to a Bose-Einstein spectrum for electron-hole pairs created by strains, a manifestation of Takagi's statistics inversion.

I then discussed how the Unruh thermality (for low-energy and long wavelength modes) could be measured in photo-emission spectroscopy (PES) experiments and the inversion factor could be seen in scanning tunneling microscopy experiments that mea-

sure the density of states. In PES, shining photons on graphene would excite fermions to higher states according to a Bose distribution and therefore, in this sense, these experiments are related to the Unruh-DeWitt detectors that also get excited with a Bose-Einstein response when interacting with acceleration radiation. I also found that a similar thermal like behavior could be seen in measurements of the spatially averaged electronic conductivity of an isolated strained honeycomb lattice, which at low energies, exhibits a frequency dependence that is similar to that found in the case of a flat graphene sheet kept at finite environment temperature, hence signalling emergence of Unruh-like thermality. Finally, I ended our discussion with a calculation of the total system energy due to strains at finite environment temperature and found that it has a zero temperature portion which resembles the black body spectrum of photons thus signalling statistics inversion, and a finite temperature part whose contribution is negative. This is due to the fact that if I start with an initially excited (thermal) state in flat graphene, then strains lead to stimulated particle reduction due to the Pauli principle not allowing newly created fermions to occupy the energy levels already occupied by thermal fermions.

6.4. Superfluid in a Box-Shaped Trap

In Chapter 5, I discussed the properties of a superfluid that is confined to a box-shaped laser trap with vanishing boundary conditions. To study this theoretically, I with the Bogoliubov-de Gennes (BdG) Hamiltonian, where I first modeled the interactions using a Dirac delta function in one-dimension. Using the BCS-approximation, i.e. pairing is favored for modes of same energy, I found that the interaction function has a $1/L$ correction due to finite size of the box. As a result of this, the solution to the gap equation

gave us a level pairing that has a bulk contribution and a a $1/L$ correction dependent on the energy. Similar size correction also appeared when I solved the transition temperature equation to obtain T_c. However, this approach does not work for higher dimensions as the gap equaiton there is divergent, which does not cancel with divergence in the two-problem.

Thus for three dimensions, I considered the BdG Hamiltonian with pseudopotential interactions, which has regularization built into it, i.e., it cancels the divergence in the pairing when two fermions approach each other, thereby eliminating the need to invoke the two-body problem. At the transition temperature, I looked at the Green's function solution of the BdG Hamiltonian that led us to a superfluid gap equation in the form of an integral eigenvalue equation, where the kernel $\mathcal{K} = \mathcal{K}_0 + \mathcal{K}_1$ can be decomposed into a convergent piece (finite temperature part) $\mathcal{K}_1$ and a divergent piece (zero temperature part) $\mathcal{K}_0$. The pseudopotential then acts on $\mathcal{K}_0$ and eliminates the $1/r$-divergence. This procedure yields a well-behaved integral gap equation which in the bulk limit reproduces the standard transition temperature equation. To solve this integral eigenvalue problem, I Taylor expanded the gap parameter to linear order. This gave us a first order differential equation in $\Delta(\boldsymbol{R})$, which at the box center turns into a transition temperature equation with the first similar to the bulk case (except that the sum is over box eigenstates) and $1/L$ finite size correction. I solved this for various values of atom number in the box, and showed that in general the T_c in the box is lower than the bulk, and the lower the number atoms, the lower is T_c.

I then looked at the integral eigenvalue problem in the slab and cube cases. In the slab case, I took its height to be finite, and the length and breadth to be infinite. Therefor the sums in those two directions can be converted to integrals. This helped us obtain an

analytic expression for the zero-temperature part of the kernel $\mathcal{K}_0$. Employing the Taylor expansion of the gap parameter gave us first order differential whose solution gave us the local pairing amplitude in the slab along its height that vanishes on the edges. In the cube case, I chose to study pairing along a path that connects one face edge to the other, parallel to the cube's length. Thus integrals in the other two directions could be performed as the gap will vary only along the edge. This simplified the integral eigenvalue equation, where again the Taylor expansion method helped us find that the local pairing amplitude makes a bell-shape and vanishes at the box edge. I ended this chapter with a remark about the validity of the Taylor expansion approach which assumes that $\Delta(\boldsymbol{R})$ varies slowly with respect to position. As I saw in the plots for $\Delta(\boldsymbol{R})$, this is a valid assumption near the box center, but pairing rises rather rapidly as I go away from the edge, thereby contradicting our assumption. This suggests that I need to find a more general way of solving the eigenvalue problem that appropriately characterizes the near edge behavior of the pairing amplitude.

Future studies could look into the spin-imbalanced case and look for observable signatures of the Fulde-Ferrell-Larkin-Ovchinnikov (FFLO) phase. As I discussed in the introduction, in the bulk case the FFLO gap has the form $e^{i\boldsymbol{q}\cdot\boldsymbol{r}}$ which has been shown to be unstable [217] to arbitrarily small displacements in real space (Goldstone mode). The box however does not possess translation invariance because of a fixed boundary and thus there is a possibility that an FFLO gap of the form $\cos(\boldsymbol{q}\cdot\boldsymbol{r})$ will be stabilized for certain values of $\boldsymbol{q}$. Since experiments have been done on nano-films [218], I can extend our results for spin balanced Fermi gas in the thin film case to the spin imbalanced case. Another possible direction is to look at how Tan's contact density $C(\boldsymbol{r})$ [211] which has been

studied in the harmonic trap [214], gets modified the box-shaped trap.

APPENDIX A. DYNAMICS OF AN EXPANDING TOROIDAL BEC

In this section I study BEC's in the presence of an expanding toroidal-shaped trap given by Eq. (2.2). Our aim is to understand the background solution on which phonon excitations propagate. For this task I study the time-dependent Gross-Pitaevskii equation (GPE)

$$i\hbar\frac{\partial}{\partial t}\Phi_0(\boldsymbol{r},t) = -\frac{\hbar^2}{2M}\nabla^2\Phi_0(\boldsymbol{r},t) + \big(V(\boldsymbol{r},t)-\mu\big)\Phi_0(\boldsymbol{r},t) + U|\Phi_0(\boldsymbol{r})|^2\Phi_0(\boldsymbol{r},t). \tag{A.1}$$

Writing $\Phi_0(\boldsymbol{r},t) = \sqrt{n_0(\boldsymbol{r},t)}\mathrm{e}^{i\phi_0(\boldsymbol{r},t)}$, with n_0 the density and ϕ_0 the superfluid phase, I obtain:

$$-\hbar\partial_t\phi_0(\boldsymbol{r},t) = -\frac{\hbar^2}{2M\sqrt{n_0(\boldsymbol{r},t)}}\nabla^2\sqrt{n_0(\boldsymbol{r},t)} + \frac{\hbar^2}{2M}(\boldsymbol{\nabla}\phi_0(\boldsymbol{r},t))^2 + V(\boldsymbol{r},t) - \mu + Un_0(\boldsymbol{r},t), \tag{A.2}$$

$$\partial_t n_0(\boldsymbol{r},t) = -\frac{\hbar}{M}\boldsymbol{\nabla}\cdot\big(n_0(\boldsymbol{r},t)\boldsymbol{\nabla}\phi_0(\boldsymbol{r},t)\big), \tag{A.3}$$

A key question is whether the superfluid velocity, $\boldsymbol{v}(\boldsymbol{r},t) = \frac{\hbar}{M}\boldsymbol{\nabla}\phi_0(\boldsymbol{r},t)$, is equal to the radial ring velocity $\hat{\rho}\dot{R}(t)$. Before analyzing this, I recall the simpler case of a *homogeneously translated* trap moving at constant velocity $\boldsymbol{v}_T$. In this case, which can be described by a trapping potential $V(\boldsymbol{r},t) = V(\boldsymbol{r}-\boldsymbol{v}_T t)$, Galilean invariance [55] ensures that a solution to Eqs. (A.2) and Eqs. (A.3) always exists with superfluid velocity $\boldsymbol{v} = \boldsymbol{v}_T$ and density $n(\boldsymbol{r})$ static in the moving frame. That is, I can always boost to a moving reference frame in which the single-particle potential is static.

In the case of present interest, however, a toroidal expanding ring described by the trapping potential Eq. (2.2), the lack of Galilean invariance means that I cannot find such

a simple exact solution with $\boldsymbol{v} = \hat{\rho}\dot{R}(t)$. In the following, I investigate whether such a relation holds approximately under the conditions of the experiment. To do this, we take the gradient of both sides of Eq. (A.2), and use the definition of the superfluid velocity, to obtain the Euler equation:

$$-M\partial_t \boldsymbol{v} = \boldsymbol{\nabla}\Big[- \frac{\hbar^2}{2M\sqrt{n_0(\boldsymbol{r},t)}}\nabla^2\sqrt{n_0(\boldsymbol{r},t)} + \frac{1}{2}M\boldsymbol{v}^2 + V(\boldsymbol{r},t) - \mu + Un_0(\boldsymbol{r},t)\Big]. \tag{A.4}$$

I now invoke the Thomas-Fermi (TF) approximation [56] by neglecting the Laplacian term in square brackets on the right of Eq. (A.4). Then, I plug our assumed solution $\boldsymbol{v} = \hat{\rho}\dot{R}(t)$ into the left side, which leads to $-M\partial_t\boldsymbol{v} = -M\ddot{R}\hat{\rho}$, allowing us to find the following result for the TF density of a BEC in an expanding toroid:

$$n_0(\boldsymbol{r}) = \frac{1}{U}\Big(\mu(t) - \frac{1}{2}M\omega_z^2 z^2 - \lambda|\rho - R|^n - M\ddot{R}(\rho - R)\Big) \times\Theta\Big(\mu(t) - \frac{1}{2}M\omega_z^2 z^2 - \lambda|\rho - R|^n - M\ddot{R}(\rho - R)\Big), \tag{A.5}$$

obtained by integrating both sides of Eq. (A.4) with respect to ρ. Note I also plugged in $V(\boldsymbol{r},t)$ from Eq. (2.2), and an overall constant of integration was chosen so that the ρ dependence of Eq. (A.5) is via the combination $\rho - R(t)$ (although I suppressed the time argument in R for brevity).

The chemical potential in Eq. (A.5) is determined by satisfying the fixed number constraint $N = \int d^3r\, n_0(\boldsymbol{r})$, with N the total boson number. In this integration, the term proportional to $(\rho - R(t))$ will approximately vanish, with the other terms in Eq. (A.5)

determining the TF radii in the z and ρ directions, which are given by:

$$R_z = \sqrt{\frac{2\mu(t)}{M\omega_z^2}}, \tag{A.6}$$

$$R_\rho = \Big(\frac{\mu(t)}{\lambda}\Big)^{1/n}. \tag{A.7}$$

With these definitions, the density is given by:

$$n_0 \simeq \frac{\mu(t)}{U}\Big[1 - \frac{z^2}{R_z^2} - \frac{1}{R_\rho^n}|\rho - R|^n - \frac{M\ddot{R}}{\mu(t)}(\rho - R)\Big]$$
$$\times\Theta\Big(1 - \frac{z^2}{R_z^2} - \frac{1}{R_\rho^n}|\rho - R|^n - \frac{M\ddot{R}}{\mu(t)}(\rho - R)\Big), \tag{A.8}$$

describing a peak in the atom density that approximately follows the expanding ring. The large value of the exponent n implies a "flatness" to the density profile in the radial direction, i.e., a weak dependence of the density on ρ. I note that in the Eckel et al experiments the exponent $n \simeq 4$, although we'll keep it general in this section.

The system chemical potential $\mu(t)$ is determined by the requirement of a fixed total particle number N during expansion. Since the density at the center of the toroid (i.e. at $\rho = R(t)$ and $z = 0$) is proportional to $\mu(t)$ in Eq. (A.8), and the toroid volume is proportional to $R_z R_\rho R(t)$, then the fixed number constraint leads to the estimate

$$N \propto \mu(t) R_z R_\rho R(t) \propto \mu(t)^{\frac{3n+2}{2n}} R(t), \tag{A.9}$$

which implies the chemical potential satisfies

$$\mu(t) \propto R(t)^{-\frac{2n}{3n+2}}, \tag{A.10}$$

with exponent $\gamma \equiv \frac{2n}{3n+2} \simeq \frac{4}{7}$. Thus, during expansion, the chemical potential (and central density) decrease with increasing time. Note that since the sound velocity $c \propto \sqrt{n_0}$,

this result implies that the sound velocity scales with toroidal radius as $c \propto R(t)^{-\frac{1}{2}\gamma}$, or $R(t)^{-2/7}$ for the case of $n = 4$ [38].

I have found that a solution with $\boldsymbol{v} \simeq \dot{R}(t)\hat{\rho}$ can approximately satisfy the Euler equation and yields a time-dependent chemical potential in the number constraint equation. The next step is to examine the continuity equation, Eq. (A.3), which is:

$$\partial_t n_0 = -\boldsymbol{\nabla} n_0 \cdot \boldsymbol{v} - n_0 \boldsymbol{\nabla} \cdot \boldsymbol{v}. \tag{A.11}$$

I now analyze Eq. (A.11) without assuming $\boldsymbol{v} \simeq \dot{R}(t)\hat{\rho}$, but only the TF density profile result Eq. (A.5). To simplify the left side of Eq. (A.11), I note that Eq. (A.5) implies that the partial time derivative of n_0 satisfies:

$$\begin{aligned} \partial_t n_0 &= -\dot{R}(t)\hat{\rho} \cdot \boldsymbol{\nabla} n_0(\rho, z, t) \\ &+ \frac{1}{U}\Big(\partial_t \mu(t) - M(\rho - R(t))\,\dddot{R}(t)\Big). \end{aligned} \tag{A.12}$$

Henceforth I drop the final term on the right side, since it is small in the regime $\rho \to R(t)$. Plugging this into the left side of Eq. (A.11) gives

$$-\dot{R}(t)\hat{\rho} \cdot \boldsymbol{\nabla} n_0 + \frac{1}{U}\partial_t \mu(t) = -\boldsymbol{\nabla} n_0 \cdot \boldsymbol{v} - n_0 \boldsymbol{\nabla} \cdot \boldsymbol{v}. \tag{A.13}$$

I now analyze this equation in the regime of $\rho \simeq R(t)$. From Eq. (A.5), I find that the gradient of n_0 is a constant at $\rho \to R$ and is given by:

$$\hat{\rho} \cdot \boldsymbol{\nabla} n_0 \Big|_{\rho \to R(t)} = -\frac{M\ddot{R}(t)}{U}. \tag{A.14}$$

Plugging this in to the continuity equation, using our result for μ (which implies $\partial_t \mu = -\gamma \frac{\dot{R}}{R}\mu$), and cancelling an overall factor of $1/U$, I find:

$$M\dot{R}\ddot{R} - \mu\gamma\frac{\dot{R}}{R} = M\ddot{R}v - \mu \boldsymbol{\nabla} \cdot \boldsymbol{v}. \tag{A.15}$$

Now I take account of the fact that our system exhibits a rapid growth of R with increasing t. During this expansion, μ decreases slowly according to Eq. (A.10), while $\frac{\dot{R}}{R}$ is $\mathcal{O}(1)$ (e.g. for exponential growth). This implies that the first terms on the right and left sides of Eq. (A.15) are much larger than the second terms on the left and right sides. Dropping the subleading terms, I finally get:

$$M\dot{R}\ddot{R} = M\ddot{R}v, \tag{A.16}$$

or $v = \dot{R}$, consistent with our original assumption. This shows that, within the preceding approximations, a rapidly expanding toroidal BEC indeed exhibits a radial superfluid velocity $\boldsymbol{v} = \dot{R}\hat{\rho}$.

APPENDIX B. THE DIRAC EQUATION

In this section, I will investigate how fermionic quantum fields evolve in a $(2+1)$-dimensional spacetime equipped with the following line element:

$$ds^2 = -\left(1+\frac{|x|}{\lambda}\right)^2 c^2 dt^2 + dx^2 + dy^2, \tag{B.1}$$

which is written in some coordinates (t, x, y) whose interpretation depends on the choice of parameter λ. The limit in which it diverges, i.e. $\lambda \to \infty$, I recover the flat Minkowski metric expressed in inertial coordinates (t, x, y), which I could also re-label with (T, X, Y) as was done in (4.18):

$$\lim_{\lambda\to\infty} ds^2 = -c^2 dt^2 + dx^2 + dy^2, \tag{B.2}$$

whereas in the opposite limit where this parameter is small, i.e. $\lambda \to 0$, I recover the flat Minkowski metric written in terms of the Rindler coordinates (t, x, y):

$$\lim_{\lambda\to 0} ds^2 = -\frac{x^2}{\lambda^2} c^2 dt^2 + dx^2 + dy^2, \tag{B.3}$$

and thus here λ plays the role of $x_{\min} = \frac{c^2}{a}$ which is the closest distance of approach from the origin at $x = 0$, of a Rindler observer accelerating with a. To derive the Dirac equation in these two limits, I will write it using the most general metric (B.1). The Dirac equation describing the evolution for massless or Weyl fermions in arbitrary spacetime is as follows:

$$i\gamma^a e_a^\mu \nabla_\mu \hat{\psi}(x) = 0 \tag{B.4}$$

where $\psi(x)$ is the massless Dirac spinor (or Weyl spinor) and can be written as a two component spinor, which due to zero rest mass are decoupled from each other $\hat{\psi}^{\mathrm{T}}(x) =$

$\Big[\hat{\psi}_{\rm R}(x),\ \hat{\psi}_{\rm L}(x)\Big]$. Also, the covariant derivative is defined as $\nabla_\mu = \partial_\mu - \frac{i}{4}\omega_\mu^{ab}\sigma_{ab}$, where $\sigma_{ab} = \frac{i}{2}\big[\gamma_a, \gamma_b\big]$, where the Dirac matrices satisfy the Clifford algebra $\big\{\gamma^a, \gamma^b\big\} = 2\eta^{ab}$. From the line element in (B.1), I can write down the metric components as follows:

$$g_{\mu\nu} = \text{diag}\bigg[- c^2\bigg(1 + \frac{|x|}{\lambda}\bigg)^2, 1, 1\bigg], \tag{B.5}$$

which is diagonal and hence simplifies our derivation. Tetrads are objects that take us from an arbitrary metric to the local flat metric of the tangent space at a point. They are as defined as:

$$g_{\mu\nu} = e_\mu^a e_\nu^b \eta_{ab}, \quad \eta_{ab} = \begin{bmatrix} -1 & 0 & 0 & 0 \\ 0 & 1 & 0 & 0 \\ 0 & 0 & 1 & 0 \\ 0 & 0 & 0 & 1 \end{bmatrix}. \tag{B.6}$$

where η_{ab} is the Minkowski tensor. In our notation I make use of Greek $(\mu, \nu, ..)$ indices to denote curved spacetime labels such as (t, x, y), and Roman $(a, b, ..)$ indices signify that we are in the tangent space at a particular point in spacetime and therefore can take values $(0, 1, 2)$. By comparing (B.5) and (B.6) I get the following tetrads:

$$e_\mu^a = \text{diag}\bigg[c\bigg(1 + \frac{|x|}{\lambda}\bigg), 1, 1\bigg], \tag{B.7}$$

These tetrads can now be used to derive the spin connections ω_μ^{ab} which take into account the spin-precession of fermions due to the curvature of spacetime. They are defined as follows:

$$\begin{aligned} \omega_\mu^{ab} &= \frac{1}{2}e^{\nu a}\big(\partial_\mu e_\nu^b - \partial_\nu e_\mu^b\big) - \frac{1}{2}e^{\nu b}\big(\partial_\mu e_\nu^a - \partial_\nu e_\mu^a\big) \\ &- \frac{1}{2}e^{\rho a}e^{\sigma b}\big(\partial_\rho e_{\sigma c} - \partial_\sigma e_{\rho c}\big)e_\mu^c. \end{aligned} \tag{B.8}$$

which is manifestly anti-symmetric $\omega_\mu^{ab} = -\omega_\mu^{ba}$. The only surviving components of the spin connection in the metric of (B.1) are as follows:

$$\omega_t^{01} = -\omega_t^{10} = \frac{c}{\lambda}\text{sgn}(x), \tag{B.9}$$

where $\text{sgn}(x)$ is the signum function, i.e. it returns $+1$ for positive values and -1 for negative entries. Finally, I will be needing the Dirac matrices in the Weyl or Chiral representation:

$$\gamma^0 = \begin{bmatrix} 0 & -I_2 \\ -I_2 & 0 \end{bmatrix}, \quad \gamma^i = \begin{bmatrix} 0 & \sigma^i \\ -\sigma^i & 0 \end{bmatrix}, \quad \gamma^5 = \begin{bmatrix} I_2 & 0 \\ 0 & I_2 \end{bmatrix}, \tag{B.10}$$

where σ^i are the Pauli matrices:

$$\sigma^1 = \begin{bmatrix} 0 & 1 \\ 1 & 0 \end{bmatrix}, \quad \gamma^2 = \begin{bmatrix} 0 & -i \\ i & 0 \end{bmatrix}, \quad \sigma^3 = \begin{bmatrix} 1 & 0 \\ 0 & -1 \end{bmatrix}. \tag{B.11}$$

Plugging in the tetrads (B.7) and the spin-connection (B.9) pertaining to the metric (B.1) into the massless Dirac equation (B.4), I get two decoupled Weyl equations for the left and right handed fermions:

$$\begin{aligned} \partial_t \hat{\psi}_{\text{L}} &= c\left(1 + \frac{|x|}{\lambda}\right)\boldsymbol{\sigma}\cdot\boldsymbol{\nabla}\hat{\psi}_{\text{L}} + \frac{c\ \text{sgn}(x)}{2\lambda}\sigma^x\hat{\psi}_{\text{L}}, \\ \partial_t \hat{\psi}_{\text{R}} &= -c\left(1 + \frac{|x|}{\lambda}\right)\boldsymbol{\sigma}\cdot\boldsymbol{\nabla}\hat{\psi}_{\text{R}} - \frac{c\ \text{sgn}(x)}{2\lambda}\sigma^x\hat{\psi}_{\text{R}}. \end{aligned} \tag{B.12}$$

In the limit of $\lambda \to \infty$, the above set reduces to the Weyl equations for fermions in inertial frames (B.2):

$$\begin{aligned} \partial_t \hat{\psi}_{\text{L}} &= c\boldsymbol{\sigma}\cdot\boldsymbol{\nabla}\hat{\psi}_{\text{L}}, \\ \partial_t \hat{\psi}_{\text{R}} &= -c\boldsymbol{\sigma}\cdot\boldsymbol{\nabla}\hat{\psi}_{\text{R}}, \end{aligned} \tag{B.13}$$

which is the same as (4.17) describing massless fermions in a flat graphene sheet. In the opposite limit $\lambda \to 0$, I recover the Weyl equations for massless fermions in uniformly accelerating frames:

$$\begin{aligned} \partial_t \hat{\psi}_{\rm L} &= \frac{c|x|}{\lambda} \boldsymbol{\sigma} \cdot \boldsymbol{\nabla} \hat{\psi}_{\rm L} + \frac{c\ \mathrm{sgn}(x)}{2\lambda} \sigma^x \hat{\psi}_{\rm L}, \\ \partial_t \hat{\psi}_{\rm R} &= -\frac{c|x|}{\lambda} \boldsymbol{\sigma} \cdot \boldsymbol{\nabla} \hat{\psi}_{\rm R} - \frac{c\ \mathrm{sgn}(x)}{2\lambda} \sigma^x \hat{\psi}_{\rm R}, \end{aligned} \tag{B.14}$$

which is the same as Eq. (4.24) that describes how electrons and holes evolve in a Rindler strained graphene sheet.

APPENDIX C. BCS THEORY

To understand BCS theory, I will start with the following Hamiltonian $H = H_0 + H_1$ given in (5.1)-(5.2) which describes a Fermi gas kept in a spatial trap $V(\boldsymbol{r})$ and chemical potential μ:

$$H_0 = \sum_\sigma \int d^3r\ \Psi^\dagger_\sigma(\boldsymbol{r})\Big[\frac{\hat{p}^2}{2m} - \mu + V(\boldsymbol{r})\Big]\Psi_\sigma(\boldsymbol{r}), \tag{C.1}$$

$$H_1 = \lambda \int d^3r\ \Psi^\dagger_\uparrow(\boldsymbol{r})\Psi^\dagger_\downarrow(\boldsymbol{r})\Psi_\downarrow(\boldsymbol{r})\Psi_\uparrow(\boldsymbol{r}), \tag{C.2}$$

where H_0 is the kinetic part and H_1 is the interaction part made up of Delta potential $\hat{U}(\boldsymbol{r}_1, \boldsymbol{r}_2) = \lambda\delta(\boldsymbol{r}_1 - \boldsymbol{r}_2)$ which basically means that the interaction is largest when two fermions approach each other. $\Psi^\dagger_\sigma(\boldsymbol{r})$ and $\Psi_\sigma(\boldsymbol{r})$ are field operators that can create/annihilate fermions and σ represents spin. These field operators satisfy the anti-commutation relation: $\{\Psi_\sigma(\boldsymbol{r}), \Psi^\dagger_{\sigma'}(\boldsymbol{r'})\} = \delta^{(3)}_{\sigma\sigma'}\delta(\boldsymbol{r} - \boldsymbol{r'})$. They can be Fourier decomposed as:

$$\Psi_\sigma(\boldsymbol{r}) = \frac{1}{\sqrt{V}}\sum_{\boldsymbol{k}} e^{i\boldsymbol{k}\cdot\boldsymbol{r}} c_{\boldsymbol{k}\sigma}, \tag{C.3}$$

$$\Psi^\dagger_\sigma(\boldsymbol{r}) = \frac{1}{\sqrt{V}}\sum_{\boldsymbol{k}} e^{-i\boldsymbol{k}\cdot\boldsymbol{r}} c^\dagger_{\boldsymbol{k}\sigma}, \tag{C.4}$$

where $\frac{1}{\sqrt{V}}e^{i\boldsymbol{k}\cdot\boldsymbol{r}}$ are plane wave-functions that originate by assuming periodic boundary conditions. This is known as the Bulk case. $(c^\dagger_{\boldsymbol{k}\sigma}, c_{\boldsymbol{k}\sigma})$ are creation/annihilation operators for a fermion in a mode $\boldsymbol{k}$. Plugging (C.3)-(C.4) into (C.1)-(C.2) I get the Hamiltonian in $\boldsymbol{k}$-space

$$H = \sum_{\boldsymbol{k}\sigma} \xi_{\boldsymbol{k}} c^\dagger_{\boldsymbol{k}\sigma} c_{\boldsymbol{k}\sigma} + \lambda \sum_{\boldsymbol{k}_i} \delta^3(\boldsymbol{k_1} + \boldsymbol{k_2} - \boldsymbol{k_3} - \boldsymbol{k_4}) c^\dagger_{\boldsymbol{k}_1\uparrow} c^\dagger_{\boldsymbol{k}_2\downarrow} c_{\boldsymbol{k}_3\downarrow} c_{\boldsymbol{k}_4\uparrow}, \tag{C.5}$$

where $\boldsymbol{k}_i = (\boldsymbol{k_1}, \boldsymbol{k_2}, \boldsymbol{k_3}, \boldsymbol{k_4})$. Now I apply mean field theory to get the gap equation. To do this I start with a variational wavefunction $|\Psi\rangle = \prod_{\boldsymbol{k}}(u_{\boldsymbol{k}} + v_{\boldsymbol{k}} c^\dagger_{\boldsymbol{k}\uparrow} c^\dagger_{\boldsymbol{k}\downarrow})|0\rangle$ where $u_{\boldsymbol{k}}$ and $v_{\boldsymbol{k}}$

are the variational parameters. I use this ansatz to get the ground state energy defined as $E_G \equiv \langle\Psi|H|\Psi\rangle$ which gives:

$$E_G = \sum_{\boldsymbol{k}} \xi_{\boldsymbol{k}}(|v_{\boldsymbol{k}}|^2 - |u_{\boldsymbol{k}}|^2 + 1) + \lambda \sum_{\boldsymbol{k},\boldsymbol{k'}} v^*_{\boldsymbol{k}} u_{\boldsymbol{k}} v_{\boldsymbol{k'}} u^*_{\boldsymbol{k'}} + \sum_{\boldsymbol{k}} E_{\boldsymbol{k}}(|u_{\boldsymbol{k}}|^2 + |v_{\boldsymbol{k}}|^2 - 1), \tag{C.6}$$

where in the last line I put in the constraint $|u_{\boldsymbol{k}}|^2 + |v_{\boldsymbol{k}}|^2 = 1$ which comes from normalization condition $\langle\Psi|\Psi\rangle = 1$. Then I extremize this ground state energy with respect to the variational parameters that gives us the BdG equations:

$$\begin{bmatrix} \xi_{\boldsymbol{k}} & \Delta \\ \Delta^* & -\xi_{\boldsymbol{k}} \end{bmatrix} \begin{bmatrix} u_{\boldsymbol{k}} \\ v_{\boldsymbol{k}} \end{bmatrix} = E_{\boldsymbol{k}} \begin{bmatrix} u_{\boldsymbol{k}} \\ v_{\boldsymbol{k}} \end{bmatrix}, \tag{C.7}$$

where I have defined the quantity $\Delta \equiv -\lambda \sum_{\boldsymbol{k}} v^*_{\boldsymbol{k}} u_{\boldsymbol{k}}$ also called the level pairing amplitude or the gap parameter. The energy eigenvalues of this equation are $\pm E_k$ were $E_{\boldsymbol{k}} = \sqrt{\xi^2_{\boldsymbol{k}} + |\Delta|^2}$ and the variational parameters are $(u_{\boldsymbol{k}}, v_{\boldsymbol{k}}) = \left(\frac{1}{\sqrt{2}}\sqrt{1 + \frac{\xi_{\boldsymbol{k}}}{E_{\boldsymbol{k}}}}, \frac{1}{\sqrt{2}}\sqrt{1 - \frac{\xi_{\boldsymbol{k}}}{E_{\boldsymbol{k}}}}\right)$. Plugging these into the definition of the gap parameter I get the gap equation for zero temperature:

$$\Delta = -\lambda \sum_{\boldsymbol{k}} \frac{\Delta}{2E_k}, \tag{C.8}$$

where the sum on the right hand side is divergent.

I will renormalise this after I discuss its generalization to non-zero temperatures. I start with (C.5) and set the indices as $(\boldsymbol{k}_1 = \boldsymbol{k}, \boldsymbol{k}_2 = -\boldsymbol{k}, \boldsymbol{k}_3 = \boldsymbol{k}, \boldsymbol{k}_4 = -\boldsymbol{k})$ because pairing between two fermions with spins $\uparrow$ and $\downarrow$ is expected to be largest when they have equal and opposite momentum. Then I make the mean field approximation in the $\boldsymbol{k}$-space i.e. define the level pairing amplitude or gap as $\Delta = \lambda\langle c_{\boldsymbol{k}\uparrow} c_{-\boldsymbol{k}\downarrow}\rangle$ and its conjugate $\Delta^* =$

$\lambda\langle c^\dagger_{\boldsymbol{k}\uparrow} c^\dagger_{-\boldsymbol{k}\downarrow}\rangle$. This gives us:

$$
\begin{aligned}
H &= -\frac{|\Delta|^2}{\lambda} + \sum_{\boldsymbol{k}\sigma} \xi_{\boldsymbol{k}} c^\dagger_{\boldsymbol{k}\sigma} c_{\boldsymbol{k}\sigma} + \lambda \sum_{\boldsymbol{k}} (\Delta c_{-\boldsymbol{k}\downarrow} c_{\boldsymbol{k}\uparrow} + \Delta^* c^\dagger_{\boldsymbol{k}\uparrow} c^\dagger_{-\boldsymbol{k}\downarrow}), \qquad \text{(C.9)} \\
&= -\frac{|\Delta|^2}{\lambda} + \sum_{\boldsymbol{k}} \begin{bmatrix} c^\dagger_{\boldsymbol{k}\uparrow} & c_{-\boldsymbol{k}\downarrow} \end{bmatrix} \begin{bmatrix} \xi_{\boldsymbol{k}} & \Delta \\ \Delta^* & -\xi_{\boldsymbol{k}} \end{bmatrix} \begin{bmatrix} c_{\boldsymbol{k}\uparrow} \\ c^\dagger_{-\boldsymbol{k}\downarrow} \end{bmatrix}. \qquad \text{(C.10)}
\end{aligned}
$$

Diagonalizing this Hamiltonian gives us:

$$
H = -\frac{|\Delta|^2}{\lambda} + \sum_{\boldsymbol{k}} \left(\xi_{\boldsymbol{k}} - E_{\boldsymbol{k}}\right) + \sum_{\boldsymbol{k}\sigma} E_{\boldsymbol{k}} \alpha^\dagger_{\boldsymbol{k}\sigma} \alpha_{\boldsymbol{k}\sigma}, \qquad \text{(C.11)}
$$

where the new operators are defined as $\alpha_{\boldsymbol{k}\uparrow} \equiv u_{\boldsymbol{k}} c_{\boldsymbol{k}\uparrow} + v_{\boldsymbol{k}} c^\dagger_{-\boldsymbol{k}\downarrow}$ and $\alpha_{\boldsymbol{k}\downarrow} \equiv u_{\boldsymbol{k}} c_{-\boldsymbol{k}\downarrow} - v_{\boldsymbol{k}} c^\dagger_{\boldsymbol{k}\uparrow}$, and they follow anti-commutation relations $\{\alpha_{\boldsymbol{k}\sigma}, \alpha^\dagger_{\boldsymbol{k}'\sigma'}\} = \delta_{\boldsymbol{k}\boldsymbol{k}'}\delta_{\sigma\sigma'}$. Now to bring in temperature I need to minimize the grand free energy:

$$
\begin{aligned}
\Phi &= U - \mu N - TS, \\
&= \langle H\rangle - TS, \\
&= -\frac{|\Delta|^2}{\lambda} + \sum_{\boldsymbol{k}} \left(\xi_{\boldsymbol{k}} - E_{\boldsymbol{k}}\right) + \sum_{\boldsymbol{k}\sigma} E_{\boldsymbol{k}} \langle \alpha^\dagger_{\boldsymbol{k}\sigma} \alpha_{\boldsymbol{k}\sigma}\rangle - TS \\
&= -\frac{|\Delta|^2}{\lambda} + \sum_{\boldsymbol{k}} \left(\xi_{\boldsymbol{k}} - E_{\boldsymbol{k}}\right) + \sum_{\boldsymbol{k}} E_{\boldsymbol{k}} n_F(E_{\boldsymbol{k}}) \\
&+ 2k_B T \sum_{\boldsymbol{k}} \Big[n_F(E_{\boldsymbol{k}}) \ln(n_F(E_{\boldsymbol{k}})) + n_F(-E_{\boldsymbol{k}}) \ln(n_F(-E_{\boldsymbol{k}})) \Big] \qquad \text{(C.12)}
\end{aligned}
$$

where in the second line I have defined $\langle H\rangle \equiv U - \mu N$, U being the internal energy and N being the particle number. Then in the third line I have used (C.11) and in the fourth line I used for entropy $S = -2k_B \sum_{\boldsymbol{k}} \Big[n_F(E_{\boldsymbol{k}}) \ln(n_F(E_{\boldsymbol{k}})) + n_F(-E_{\boldsymbol{k}}) \ln(n_F(-E_{\boldsymbol{k}})) \Big]$, k_B being the Boltzmann constant. Now I will minimize (C.12) by setting its derivative zero i.e. $\frac{\partial \Phi}{\partial \Delta^*} = 0$, which upon simplifying gives us the gap equation at non-zero temperatures

(see Eq. 5.4):

$$\frac{1}{\lambda} = -\sum_{\boldsymbol{k}} \frac{\tanh \frac{E_k}{2T}}{2E_k}, \tag{C.13}$$

where E_k is the quasiparticle(Cooper pairs) energy dispersion relation and Δ is the gap parameter which quantifies the amount of pairing in the system.

APPENDIX D. PSEUDOPOTENTIAL

In this section, I first show why unlike the one-dimensional case, modeling interactions using delta function does not work for the three dimensional case. Then I will introduce the Fermi-Huang pseudopotential. To understand the problem with using delta function interactions in three-dimensions, let us look at the gap equation and the two-body scattering relation:

$$\Delta_{\boldsymbol{m}} = -\lambda \sum_{\boldsymbol{n}} \hat{\lambda}_{\boldsymbol{m},\boldsymbol{n}} \frac{\Delta_{\boldsymbol{n}}}{2E_{\boldsymbol{n}}}, \tag{D.1}$$

$$\frac{1}{\lambda} = \frac{m}{4\pi a_s} - \sum_{\boldsymbol{n}} \frac{1}{2\epsilon_{\boldsymbol{n}}}. \tag{D.2}$$

where $\hat{\lambda}_{\boldsymbol{m},\boldsymbol{n}} = \frac{1}{L}\big(1+\frac{1}{2}\delta_{m_x,n_x}\big)\big(1+\frac{1}{2}\delta_{m_y,n_y}\big)\big(1+\frac{1}{2}\delta_{m_z,n_z}\big)$. Multiplying Eq. (D.2) with $\Delta_{\boldsymbol{m}}$ and combining it with Eq. (D.1), I get:

$$\Delta_{\boldsymbol{m}}\bigg(-\frac{m}{4\pi a_s}+\sum_{\boldsymbol{n}}\frac{1}{2\epsilon_{\boldsymbol{n}}}\bigg) = \sum_{\boldsymbol{n}}\frac{\Delta_{\boldsymbol{n}}}{2E_{\boldsymbol{n}}} \tag{D.3}$$

The problem is that I cannot combine the sums since the gap $\Delta_{\boldsymbol{m}}$ is now level dependent. Also the sum on the left hand side is divergent and I do not know how to regularize it. Thus I see that modelling interactions by a delta function in a three dimensional box does not help us solve the gap equation.

Thus I will regularize in a different way by changing the form of the interaction potential to a pseudo-potential. In the bulk case, the pseudo-potential gives the same result as delta-function interaction. I will be following the discussion given in [195]. I start with the Schrodinger equation for two particles at positions $\boldsymbol{r}_1$ and $\boldsymbol{r_2}$ described by the wavefunction $\phi(\boldsymbol{r}_1,\boldsymbol{r}_2)$:

$$\bigg[-\frac{\hbar^2}{2m}\nabla_1^2 + -\frac{\hbar^2}{2m}\nabla_2^2 + V(\boldsymbol{r}_1,\boldsymbol{r}_2)\bigg]\phi(\boldsymbol{r}_1,\boldsymbol{r}_2) = E\phi(\boldsymbol{r}_1,\boldsymbol{r}_2), \tag{D.4}$$

interacting via a potential $V(\boldsymbol{r}_1, \boldsymbol{r}_2) = V(\boldsymbol{r}_1 - \boldsymbol{r}_2)$ which is a function only of the difference of particle coordinates or the radial coordinate. In scattering theory, at low energies the scattering of a particle by a potential does not depend on the shape of the potential, but depends only on a single parameter obtainable from the potential: the scattering length a. The total cross section at low energies is $4\pi a^2$. Hence a is the effective diameter of the potential i.e. at low energies the scattering from a potential looks like that from a hard sphere of diameter a. Thus I can use a hard sphere interaction to describe two particles scattering off each other. This system can have bound states or scattering states. The Schrodinger equation and the wavefunction can then be separated into centre of mass $\boldsymbol{R} = \frac{1}{2}(\boldsymbol{r}_1 + \boldsymbol{r}_2)$ and radial coordinates $\boldsymbol{r} = \boldsymbol{r}_2 - \boldsymbol{r}_1$ i.e.

$$(\nabla^2 + k^2)\psi(\boldsymbol{r}) = 0,\ r > a, \tag{D.5}$$

$$\psi(\boldsymbol{r}) = 0,\ r \leq a, \tag{D.6}$$

where $k = \sqrt{\frac{\mu(E_r - V)}{\hbar^2}}$ is the relative wave number, E_r is the radial part of energy eigenvalue, μ is the reduced mass and a is the scattering cross-section. Here I have used the hard sphere potential:

$$V(\boldsymbol{r}) = 0,\ r > a, \tag{D.7}$$

$$= \infty,\ r \leq a, \tag{D.8}$$

This form of potential means that it allows the wavefunction to take certain form outside a sphere of radius a but after that it is impenetrable. Thus it acts like a 'hard spherical wall' and thus at the surface it acts like a boundary condition.

For low energies however, this problem i.e. equation (D.5)-(D.6) can be recast into

a single differential equation with an inhomogeneous source term at $\boldsymbol{r} = 0$, which automatically incorporates the hard sphere boundary condition. This is what I mean by the method of pseudo-potentials first introduced by Fermi [193] and then later extended by Huang and Yang [194]. In order to understand this let us look at what equations (D.5)-(D.6) look like for low energies i.e. $k \to 0$:

$$\begin{aligned} \frac{1}{r^2}\frac{d}{dr}\left(r^2\frac{d\psi}{dr}\right) &= 0,\ r > a, \\ \psi(r) &= 0,\ r \leq a, \end{aligned}$$

whose solution is:

$$\psi(r) = \chi\Big(1 - \frac{a}{r}\Big),\ r > a, \tag{D.9}$$

$$\psi(r) = 0,\ r \leq a, \tag{D.10}$$

where χ is a constant which can be fixed either by normalizing the wavefunction or by using some boundary condition at $\boldsymbol{r} \to \infty$. Note that the wavefunction vanishes at $r = a$. I will now define a new wavefunction $\tilde{\psi}(r)$ such that it satisfies:

$$(\nabla^2 + k^2)\tilde{\psi}(r) = 0, \forall\ r \text{ except } r = 0, \tag{D.11}$$

$$\tilde{\psi}(a) = 0, \tag{D.12}$$

where (D.12) is the hard sphere boundary condition. Equation (D.11) is valid for all points except $r = 0$ since I expect singular behaviour($\sim \frac{1}{r}$) for radial wave-functions when the two particles are very close to each other($\boldsymbol{r} \to 0$), and thus the Laplacian acting on it should give us a Dirac delta instead of zero. Before I get to $r = 0$ I can see that the solution of (D.11) is simply $\tilde{\psi}(r) = \chi\Big(1 - \frac{a}{r}\Big)$. Note that this time I will determine the

constant χ by:

$$\chi = \frac{\partial}{\partial r}(r\tilde{\psi})\bigg|_{r=0}. \tag{D.13}$$

The advantage of doing this will be clear soon. Now to study the behaviour near the origin $r \to 0$, I will make the Laplacian act on the solution of (D.11) i.e. $\tilde{\psi}(r) = \chi\Big(1 - \frac{a}{r}\Big)$ and using (D.13):

$$\begin{aligned} \nabla^2\tilde{\psi}(r) &= 4\pi a\delta(\boldsymbol{r})\chi \\ &= 4\pi a\delta(\boldsymbol{r})\frac{\partial}{\partial r}(r\tilde{\psi})\bigg|_{r=0}. \end{aligned} \tag{D.14}$$

Now I can see that instead of writing a differential equation like (D.5) or (D.11) and then worrying about the various boundary conditions, one can simply concentrate on one differential equation which incorporates all the desired boundary conditions in the form of a pseudo-potential operator $\delta(\boldsymbol{r})\partial_r(r\cdot)$:

$$(\nabla^2 + k^2)\tilde{\psi}(r) = 4\pi a\delta(\boldsymbol{r})\frac{\partial}{\partial r}(r\tilde{\psi}). \tag{D.15}$$

For low energies and for $r > a$, $\tilde{\psi}$ satisfies the same equation and boundary conditions as ψ and thus I can say that $\tilde{\psi}$ safely captures the physics of ψ as long as we are looking outside the scattering length.

As I discussed in the last section, the pseudopotential is an alternate method of solving the two body problem by replacing the hard sphere interaction and its boundary condition by one Schrodinger equation involving a potential of the form $V(r)\psi(\boldsymbol{r}) \sim \partial_r(r\psi(\boldsymbol{r}))$. The argument of this potential is arranged in such a way that whatever singularity comes in the wavefunction i.e. $\phi(r) \to \frac{1}{r}$ as $r \to 0$, it will be removed upon multiplication by r and then applying the derivative ∂_r. It turns out that this way of regularization is useful and has given rise to universal relations (i.e. independent of the details of

the short-range interactions, except the scattering length a) for Fermi gases [211, 212, 213, 214, 215]. The first relation states that the internal energy E of a two-component Fermi gas as a function of its momentum distribution is given by [211]:

$$E = \frac{\hbar^2 \Omega C}{4\pi a m} + \sum_{\boldsymbol{k}\sigma} \frac{\hbar^2 k^2}{2m} \Big(n_{\boldsymbol{k}\sigma} - \frac{C}{k^4} \Big), \tag{D.16}$$

$$C \equiv \lim_{\boldsymbol{k}\to\infty} k^4 n_{\boldsymbol{k}\uparrow} = \lim_{\boldsymbol{k}\to\infty} k^4 n_{\boldsymbol{k}\downarrow}, \tag{D.17}$$

where the second line means that at high energies the tail of momentum distribution of fermions depends only on C, called Tan's contact [211, 212, 213], which is a universal number. Here Ω is the volume of space, $n_{\boldsymbol{k}\sigma}$ is the average number of fermions with wave vector $\boldsymbol{k}$ and spin σ, m is the mass of the fermions and a is the scattering length. The second relation [212] states that the contact C is proportional to the adiabatic derivative of the energy with respect to the reciprocal of the scattering length:

$$\frac{dE}{d(-1/a)} = \frac{\hbar^2 \Omega C}{4\pi a m} \tag{D.18}$$

This is called the 'adiabatic sweep theorem'. The third relation [212] is about the pressure of the uniform Fermi gas with large scattering length and equal populations of the two spin states, in thermal equilibrium:

$$P = \frac{2}{3}\rho_E + \frac{\hbar^2 C}{12\pi a m} \tag{D.19}$$

where $\rho_E \equiv E/\Omega$ is the energy density. These relations are independent of whether I have a few-body or many-body system, equilibrium or non-equilibrium, zero temperature or finite temperature, superfluid state or normal state, attractive or repulsive interactions and balanced or imbalanced spin populations. This contact C has now been measured [216]

and thus it confirms that such universal relation exist. However all this work on pseudopotentials has been done for the bulk case only and it would be interesting to see what happens to these universal relations when the Fermi gas is trapped in a box.

BIBLIOGRAPHY

[1] A. A. Starobinsky, *A New Type of Isotropic Cosmological Models Without Singularity*, Phys. Lett. B **91**, 99 (1980).

[2] A. H. Guth, *The Inflationary Universe: A Possible Solution to the Horizon and Flatness Problems*, Phys. Rev. D **23**, 347 (1981).

[3] A. Albrecht and P. J. Steinhardt, *Cosmology for Grand Unified Theories with Radiatively Induced Symmetry Breaking*, Phys. Rev. Lett. **48**, 1220 (1982).

[4] S. W. Hawking and I. G. Moss, *Supercooled Phase Transitions in the Very Early Universe*, Phys. Lett. **110B**, 35 (1982).

[5] A. D. Linde, *A New Inflationary Universe Scenario: A Possible Solution of the Horizon, Flatness, Homogeneity, Isotropy and Primordial Monopole Problems*, Phys. Lett. **108B**, 389 (1982).

[6] A. D. Linde, *Chaotic Inflation*, Phys. Lett. **129B**, 177 (1983).

[7] A. R. Liddle and D. H. Lyth, *Cosmological inflation and large scale structure*, Cambridge, UK: Univ. Pr. (2000).

[8] A. Ijjas and P. J. Steinhardt, *Bouncing Cosmology made simple*, Class. Quant. Grav. **35**, no. 13, 135004 (2018).

[9] P. A. R. Ade *et al.* [Planck Collaboration], *Planck 2015 results. XIII. Cosmological parameters*, Astron. Astrophys. **594**, A13 (2016).

[10] M. Tegmark *et al.* [SDSS Collaboration], *Cosmological parameters from SDSS and WMAP*, Phys. Rev. D **69**, 103501 (2004).

[11] J. E. Lidsey, A. R. Liddle, E. W. Kolb, E. J. Copeland, T. Barreiro and M. Abney, *Reconstructing the inflation potential : An overview*, Rev. Mod. Phys. **69**, 373 (1997).

[12] P. A. R. Ade *et al.* [Planck Collaboration], *Planck 2015 results. XX. Constraints on inflation*, Astron. Astrophys. **594**, A20 (2016).

[13] P. A. R. Ade *et al.* [Planck Collaboration], *Planck 2015 results. XVI. Isotropy and statistics of the CMB*, Astron. Astrophys. **594**, A16 (2016).

[14] C. Barcelo, S. Liberati and M. Visser, *Analogue gravity*, Living Rev. Rel. **14**, 3 (2011).

[15] W. G. Unruh, *Experimental black hole evaporation*, Phys. Rev. Lett. **46**, 1351 (1981).

[16] S. W. Hawking, *Black hole explosions*, Nature **248**, 30 (1974).

[17] S. W. Hawking, *Particle Creation by Black Holes*, Commun. Math. Phys. **43**, 199 (1975), Erratum: [Commun. Math. Phys. **46**, 206 (1976)].

[18] T. G. Philbin, C. Kuklewicz, S. Robertson, S. Hill, F. Konig and U. Leonhardt, *Fiber-optical analogue of the event horizon*, Science **319**, 1367 (2008).

[19] F. Belgiorno *et al.*, *Hawking radiation from ultrashort laser pulse filaments*, Phys. Rev. Lett. **105**, 203901 (2010).

[20] S. Weinfurtner, E. W. Tedford, M. C. J. Penrice, W. G. Unruh and G. A. Lawrence, *Measurement of stimulated Hawking emission in an analogue system*, Phys. Rev. Lett. **106**, 021302 (2011).

[21] J. Steinhauer, *Observation of quantum Hawking radiation and its entanglement in an analogue black hole*, Nature Phys. **12**, 959 (2016).

[22] T. Torres, S. Patrick, A. Coutant, M. Richartz, E. W. Tedford and S. Weinfurtner, *Rotational superradiant scattering in a vortex flow*, Nature Phys. **13**, 833 (2017).

[23] J.-C. Jaskula, G. B. Partridge, M. Bonneau, R. Lopes, J. Ruaudel, D. Boiron and C. I. Westbrook, *Acoustic analog to the dynamical Casimir effect in a Bose-Einstein condensate*, Phys. Rev. Lett. **109**, 220401 (2012).

[24] C. L. Hung, V. Gurarie and C. Chin, *From Cosmology to Cold Atoms: Observation of Sakharov Oscillations in Quenched Atomic Superfluids*, Science **341**, 1213 (2013).

[25] P. O. Fedichev and U. R. Fischer, *Gibbons-Hawking effect in the sonic de Sitter space-time of an expanding Bose-Einstein-condensed gas*, Phys. Rev. Lett. **91**, 240407 (2003).

[26] O. Fialko, B. Opanchuk, A. I. Sidorov, P. D. Drummond and J. Brand, *Fate of the false vacuum: towards realization with ultra-cold atoms*, EPL **110**, 56001 (2015).

[27] O. Fialko, B. Opanchuk, A. I. Sidorov, P. D. Drummond and J. Brand, *The universe on a table top: engineering quantum decay of a relativistic scalar field from a metastable vacuum*, J. Phys. B **50**, no. 2, 024003 (2017).

[28] J. Braden, M. C. Johnson, H. V. Peiris and S. Weinfurtner, *Towards the cold atom analog false vacuum*, JHEP **1807**, 014 (2018).

[29] T. P. Billam, R. Gregory, F. Michel and I. G. Moss, *Simulating seeded vacuum decay in a cold atom system*, Phys. Rev. D **100**, no. 6, 065016 (2019).

[30] J. Rodriguez-Laguna, L. Tarruell, M. Lewenstein and A. Celi, *Synthetic Unruh effect in cold atoms*, Phys. Rev. A **95**, no. 1, 013627 (2017).

[31] C. Barcelo, S. Liberati and M. Visser, *Probing semiclassical analog gravity in Bose-Einstein condensates with widely tunable interactions*, Phys. Rev. A **68**, 053613 (2003).

[32] P. O. Fedichev and U. R. Fischer, *'Cosmological' quasiparticle production in harmonically trapped superfluid gases*, Phys. Rev. A **69**, 033602 (2004)..

[33] U. R. Fischer and R. Schützhold, *Quantum simulation of cosmic inflation in two-component Bose-Einstein condensates*, Phys. Rev. A **70**, 063615 (2004).

[34] P. Jain, S. Weinfurtner, M. Visser and C. W. Gardiner, *Analog Model of a Friedmann-Robertson-Walker Universe in Bose-Einstein Condensates: Application of the Classical Field Method*, Phys. Rev. A **76**, 033616 (2007).

[35] A. Prain, S. Fagnocchi and S. Liberati, *Analogue Cosmological Particle Creation: Quantum Correlations in Expanding Bose Einstein Condensates*, Phys. Rev. D **82**, 105018 (2010).

[36] J. M. Gomez Llorente and J. Plata, *Expanding ring-shaped Bose-Einstein condensates as analogs of cosmological models: Analytical characterization of the inflationary dynamics*, Phys. Rev. A **100**, no. 4, 043613 (2019).

[37] Z. Fifer, T. Torres, S. Erne, A. Avgoustidis, R. J. A. Hill and S. Weinfurtner, *Analog cosmology with two-fluid systems in a strong gradient magnetic field*, Phys. Rev. E **99**, no. 3, 031101 (2019).

[38] S. Eckel, A. Kumar, T. Jacobson, I. B. Spielman and G. K. Campbell, *A rapidly expanding Bose-Einstein condensate: an expanding universe in the lab*, Phys. Rev. X **8**, no. 2, 021021 (2018).

[39] M. Wittemer, F. Hakelberg, P. Kiefer, J. P. Schröder, C. Fey, R. Schützhold, U. Warring and T. Schaetz, *Phonon Pair Creation by Inflating Quantum Fluctuations in an Ion Trap*, Phys. Rev. Lett. **123**, no. 18, 180502 (2019).

[40] M. Sasaki, *Gauge Invariant Scalar Perturbations in the New Inflationary Universe*, Prog. Theor. Phys. **70**, 394 (1983).

[41] H. Kodama and M. Sasaki, *Cosmological Perturbation Theory*, Prog. Theor. Phys. Suppl. **78**, 1 (1984).

[42] V. F. Mukhanov, *Quantum Theory of Gauge Invariant Cosmological Perturbations*, Sov. Phys. JETP **67**, 1297 (1988) [Zh. Eksp. Teor. Fiz. **94N7**, 1 (1988)].

[43] S. Weinberg, "Cosmology," Oxford, UK: Oxford Univ. Pr. (2008).

[44] P. J. E. Peebles, "Principles of physical cosmology," Princeton, USA: Univ. Pr. (1993).

[45] N. D. Birrell and P. C. W. Davies, *Quantum Fields in Curved Space*, Cambridge Univ. Pr. (1984).

[46] V. Mukhanov and S. Winitzki, *Introduction to quantum effects in gravity*, Cambridge Univ. Pr. (2007).

[47] L. Parker and D. Toms, *Quantum Field Theory in Curved Spacetime: Quantized Fields and Gravity*, Cambridge Univ. Pr. (2009).

[48] S. A. Fulling, *Aspects of Quantum Field Theory in Curved Space-time*, London Math. Soc. Student Texts **17**, 1 (1989).

[49] S. M. Carroll, "Spacetime and Geometry," San Francisco, USA: Addison-Wesley (2004).

[50] A. Imambekov, I. E. Mazets, D. S. Petrov, V. Gritsev, S. Manz, S. Hofferberth, T. Schumm, E. Demler, and J. Schmiedmayer, *Density ripples in expanding low-dimensional gases as a probe of correlations*, Phys. Rev. A **80**, 033604 (2009).

[51] I. Carusotto, S. Fagnocchi, A. Recati, R. Balbinot and A. Fabbri, *Numerical observation of Hawking radiation from acoustic black holes in atomic BECs*, New J. Phys. **10**, 103001 (2008).

[52] M. Naraschewski and R. J. Glauber, *Spatial coherence and density correlations of trapped Bose gases*, Phys. Rev. A **59**, 4595 (1999).

[53] M. Schellekens, R. Hoppeler, A. Perrin, J. Viana Gomes, D. Boiron, A. Aspect, C. I. Westbrook, *Hanbury Brown Twiss Effect for Ultracold Quantum Gases*, Science **310**, 648 (2005).

[54] S. Y. Chä and U. R. Fischer, *Probing the scale invariance of the inflationary power spectrum in expanding quasi-two-dimensional dipolar condensates*, Phys. Rev. Lett. **118**, no. 13, 130404 (2017), Addendum: [Phys. Rev. Lett. **118**, no. 17, 179901 (2017)].

[55] V.I. Yukalov, *Theory of cold atoms: Bose-Einstein statistics*, Laser Physics **26**, 062001 (2016).

[56] G. Baym and C.J. Pethick, *Ground-State Properties of Magnetically Trapped Bose-Condensed Rubidium Gas*, Phys. Rev. Lett. **76**, 6 (1996).

[57] E. Schrodinger, *The proper vibrations of the expanding universe*, Physica **6**, 899 (1939).

[58] L. Parker, *The Creation of Particles in an Expanding Universe*, Ph.D. thesis, Harvard University (1966).

[59] L. Parker, *Particle creation in expanding universes*, Phys. Rev. Lett. **21**, 562 (1968).

[60] R. de Putter and O. Doré, *In search of an observational quantum signature of the primordial perturbations in slow-roll and ultraslow-roll inflation*, Phys. Rev. D **101**, 043511 (2020).

[61] J. Martin and V. Vennin, *Quantum Discord of Cosmic Inflation: Can I Show that CMB Anisotropies are of Quantum-Mechanical Origin?*, Phys. Rev. D **93**, 023505 (2016).

[62] J. Martin and V. Vennin, *Obstructions to Bell CMB Experiments*, Phys. Rev. D **96**, 063501 (2017).

[63] D. Campo and R. Parentani, *Inflationary spectra and violations of Bell inequalities*, Phys. Rev. D **74**, 025001 (2006).

[64] J. Maldacena, *A model with cosmological Bell inequalities*, Fortsch. Phys. **64**, 10 (2016).

[65] S. Kanno and J. Soda, *Infinite violation of Bell inequalities in inflation*, Phys. Rev. D **96**, 083501 (2017).

[66] S. Choudhury, S. Panda and R. Singh, *Bell violation in the Sky*, Eur. Phys. J. C **77**, 60 (2017).

[67] J. Martin and V. Vennin, *Real-space entanglement in the Cosmic Microwave Background*, JCAP **10**, 036 (2021).

[68] A. Ashtekar, A. Corichi and A. Kesavan, *Emergence of classical behavior in the early universe*, Phys. Rev. D **102**, 023512 (2020).

[69] I. Agullo, B. Bonga and P. R. Metidieri, *Does inflation squeeze cosmological perturbations?*, arXiv:2203.07066 [gr-qc].

[70] E. Martin-Martinez and N. C. Menicucci, *Cosmological quantum entanglement*, Class. Quant. Grav. **29**, 224003 (2012).

[71] J.-T. Hsiang, and B.-L. Hu, *No Intrinsic Decoherence of Inflationary Cosmological Perturbations*, arXiv:2112.04092 [gr-qc].

[72] I. Fuentes, R. B. Mann, E. Martin-Martinez and S. Moradi, *'Entanglement of Dirac fields in an expanding spacetime*, Phys. Rev. D **82**, 045030 (2010).

[73] S. Banik, M. Gutierrez Galan, H. Sosa-Martinez, M. Anderson, S. Eckel, I. B. Spielman and G. K. Campbell, *Accurate Determination of Hubble Attenuation and Amplification in Expanding and Contracting Cold-Atom Universes*, Phys. Rev. Lett. **128**, 090401 (2022).

[74] M. Wittemer, F. Hakelberg, P. Kiefer, J. P. Schröder, C. Fey, R. Schützhold, U. Warring and T. Schaetz, *Phonon Pair Creation by Inflating Quantum Fluctuations in an Ion Trap*, Phys. Rev. Lett. **123**, 180502 (2019).

[75] J. Steinhauer, M. Abuzarli, T. Aladjidi, T. Bienaimé, C. Piekarski, W. Liu, E. Giacobino, A. Bramati and Q. Glorieux, *Analogue cosmological particle creation in an ultracold quantum fluid of light*, Nature Commun. **13**, 2890 (2022).

[76] A. Bhardwaj, D. Vaido and D. E. Sheehy, *Inflationary Dynamics and Particle Production in a Toroidal Bose-Einstein Condensate*, Phys. Rev. A **103**, 023322 (2021).

[77] S. Eckel and T. Jacobson, *Phonon redshift and Hubble friction in an expanding BEC*, SciPost Phys. **10**, 064 (2021).

[78] D. E. Bruschi, N. Friis, I. Fuentes and S. Weinfurtner, *On the robustness of entanglement in analogue gravity systems*, New J. Phys. **15**, 113016 (2013).

[79] A. Finke, P. Jain and S. Weinfurtner, *On the observation of nonclassical excitations in Bose–Einstein condensates*, New J. Phys. **18**, 113017 (2016).

[80] C. A. Chen, S. Khlebnikov and C. L. Hung, *Observation of Quasiparticle Pair Production and Quantum Entanglement in Atomic Quantum Gases Quenched to an Attractive Interaction*, Phys. Rev. Lett. **127**, 060404 (2021).

[81] I. Agullo, A. J. Brady and D. Kranas, *Quantum Aspects of Stimulated Hawking Radiation in an Optical Analog White-Black Hole Pair*, Phys. Rev. Lett. **128**, 091301 (2022).

[82] J. R. Muñoz de Nova, K. Golubkov, V. I. Kolobov and J. Steinhauer, *Observation of thermal Hawking radiation and its temperature in an analogue black hole*, Nature **569**, 688 (2019).

[83] X. Busch and R. Parentani, *Quantum entanglement in analogue Hawking radiation: When is the final state nonseparable?*, Phys. Rev. D **89**, 105024 (2014).

[84] S. Finazzi and I. Carusotto, *Entangled phonons in atomic Bose-Einstein condensates*, Phys. Rev. A **90**, 033607 (2014).

[85] F. Kiałka, M. Ahmadi and A. Dragan, *Spatial entanglement of nonvacuum Gaussian states*, Phys. Rev. D **93**, 125003 (2016).

[86] M. Isoard, N. Milazzo, N. Pavloff and O. Giraud, *Bipartite and tripartite entanglement in a Bose-Einstein acoustic black hole*, Phys. Rev. A **104**, 063302 (2021).

[87] A. Serafini, *Quantum Continuous Variables: A Primer of Theoretical Methods* (CRC Press, 2017).

[88] A. Einstein, B. Podolsky and N. Rosen, *Can quantum mechanical description of physical reality be considered complete?*, Phys. Rev. **47**, 777 (1935).

[89] D. Hellweg, L. Cacciapuoti, M. Kottke, T. Schulte, K. Sengstock, W. Ertmer, and J. J. Arlt, *Measurement of the Spatial Correlation Function of Phase Fluctuating Bose-Einstein Condensates*, Phys. Rev. Lett. **91**, 010406 (2003).

[90] T. S. Bunch and P. C. W. Davies, *Quantum Field Theory in de Sitter Space: Renormalization by Point Splitting*, Proc. Roy. Soc. Lond. A **360**, 117 (1978).

[91] A. E. Leanhardt, T. A. Pasquini, M. Saba, A. Schirotzek, Y. Shin, D. Kielpinski, D. E. Pritchard, W. Ketterle, *Cooling Bose-Einstein Condensates Below 500 Picokelvin*, Science **301, 5639 (2003).**

[92] T. Kovachy, J. M. Hogan, A. Sugarbaker, S. M. Dickerson, C. A. Donnelly, C. Overstreet, and M. A. Kasevich, *Matter Wave Lensing to Picokelvin Temperatures*, Phys. Rev. Lett. **114**, 143004 (2015).

[93] Christian Deppner et al, *Collective-Mode Enhanced Matter-Wave Optics*, Phys. Rev. Lett. **127**, 100401 (2021).

[94] R. H. Brown and R. Q. Twiss, *A new type of interferometer for use in radio astronomy*, Philosophical Magazine. 45 (366): 663 (1954).

[95] R. H. Brown and R. Q. Twiss, *Correlation between Photons in two Coherent Beams of Light*, Nature **177**, 27 (1956).

[96] R. H. Brown and R. Q. Twiss, *A Test Of A New Type Of Stellar Interferometer On Sirius*, Nature. **178**: 1046 (1956).

[97] W. Greiner and J. Reinhardt, *Field quantization* (Springer 1997).

[98] M. M. Glenz and L. Parker, *Study of the Spectrum of Inflaton Perturbations*, Phys. Rev. D **80**, 063534 (2009).

[99] R. M. Wald, *Quantum Field Theory in Curved Space-Time and Black Hole Thermo-*

dynamics, University of Chicago Press (1994).

[100] A. Fabbri and J. Navarro-Salas, *Modeling black hole evaporation*, Imperial College Press (2005).

[101] W. Rindler, *Kruskal Space and the Uniformly Accelerated Frame*, Am. J. Phys. **34**, 1174 (1966).

[102] S. A. Fulling, *Nonuniqueness of canonical field quantization in Riemannian space-time*, Phys. Rev. D **7**, 2850 (1973).

[103] P. C. W. Davies, *Scalar particle production in Schwarzschild and Rindler metrics*, J. Phys. A **8**, 609 (1975).

[104] W. G. Unruh, *Notes on black hole evaporation*, Phys. Rev. D **14**, 870 (1976).

[105] R. Kubo, *Statistical-mechanics theory of irreversible processes. I. General theory and simple application to magnetic and conduction problems*, J. Phys. Soc. Jpn. **12**, 570, (1957).

[106] P. C. Martin, and J. Schwinger, *Theory of many-particle systems. I*, Phys. Rev. **115**, 1342 (1959).

[107] G. W. Gibbons and S. W. Hawking, *Cosmological Event Horizons, Thermodynamics, and Particle Creation*, Phys. Rev. D **15**, 2738 (1977).

[108] S. Takagi, *Vacuum Noise and Stress Induced by Uniform Acceleration: Hawking-Unruh Effect in Rindler Manifold of Arbitrary Dimension*, Prog. Theor. Phys. Suppl. **88**, 1 (1986).

[109] H. Ooguri, *Spectrum of Hawking Radiation and Huygens' Principle*, Phys. Rev. D **33**, 3573 (1986).

[110] W. G. Unruh, *Accelerated Monopole Detector in Odd Space-time Dimensions*, Phys. Rev. D **34**, 1222 (1986).

[111] H. Terashima, *Fluctuation dissipation theorem and the Unruh effect of scalar and Dirac fields*, Phys. Rev. D **60**, 084001 (1999).

[112] L. Sriramkumar, *Odd statistics in odd dimensions for odd couplings*, Mod. Phys. Lett. A **17**, 1059 (2002).

[113] L. Sriramkumar, *Interpolating between the Bose-Einstein and the Fermi-Dirac distributions in odd dimensions*, Gen. Rel. Grav. **35**, 1699 (2003).

[114] S. Pascazio, F. V. Pepe, and J. M. Pérez-Pardo, "Huygens' principle and Dirac-Weyl equation", Eur. Phys. J. Plus **132**, 287 (2017).

[115] J. Arrechea, C. Barceló, L. J. Garay and G. García-Moreno, *Inversion of statistics and thermalization in the Unruh effect*, Phys. Rev. D **104**, 065004 (2021).

[116] L. C. B. Crispino, A. Higuchi and G. E. A. Matsas, *The Unruh effect and its applications*, Rev. Mod. Phys. **80**, 787 (2008).

[117] E. Martin-Martinez, I. Fuentes and R. B. Mann, *Using Berry's phase to detect the Unruh effect at lower accelerations*, Phys. Rev. Lett. **107**, 131301 (2011).

[118] P. D. Nation, J. R. Johansson, M. P. BlencoI and F. Nori, *Stimulating Uncertainty: Amplifying the Quantum Vacuum with Superconducting Circuits*, Rev. Mod. Phys. **84**, 1 (2012).

[119] C. Gooding, S. Biermann, S. Erne, J. Louko, W. G. Unruh, J. Schmiedmayer and S. Weinfurtner, *Interferometric Unruh detectors for Bose-Einstein condensates*, Phys. Rev. Lett. **125**, 213603 (2020).

[120] A. Retzker, J. I. Cirac, M. B. Plenio, and B. Reznik, *Methods for Detecting Acceleration Radiation in a Bose-Einstein Condensate*, Phys. Rev. Lett. **101**, 110402 (2008).

[121] J. Hu, L. Feng, Z. Zhang and C. Chin, *Quantum simulation of Unruh radiation*, Nature Phys. **15**, 785 (2019).

[122] A. Kosior, M. Lewenstein and A. Celi, *Unruh effect for interacting particles with ultracold atoms*, SciPost Phys. **5**, 061 (2018).

[123] O. Boada, A. Celi, J. I. Latorre and M. Lewenstein, *Dirac Equation For Cold Atoms In Artificial Curved Spacetimes*, New J. Phys. **13**, 035002 (2011).

[124] A. Iorio and G. Lambiase, *The Hawking-Unruh phenomenon on graphene*, Phys. Lett. B **716**, 334 (2012).

[125] M. Cvetic and G. W. Gibbons, *Graphene and the Zermelo Optical Metric of the BTZ Black Hole*, Annals of Phys. **327**, 2617 (2012).

[126] A. Iorio and G. Lambiase, *Quantum field theory in curved graphene spacetimes, Lobachevsky geometry, Weyl symmetry, Hawking effect, and all that*, Phys. Rev. D **90**, 025006 (2014).

[127] S. S. Hegde, V. Subramanyan, B. Bradlyn and S. Vishveshwara, *Quasinormal Modes and the Hawking-Unruh Effect in Quantum Hall Systems: Lessons from Black Hole Phenomena*, Phys. Rev. Lett. **123**, 156802 (2019).

[128] V. Subramanyan, S. S. Hegde, S. Vishveshwara and B. Bradlyn, *Physics of the Inverted Harmonic Oscillator: From the lowest Landau level to event horizons*, Annals Phys. **435**, 168470 (2021).

[129] G. E. Volovik, *Black hole and Hawking radiation by type-II Weyl fermions*, JETP Lett. **104**, (2016)

[130] P. R. Wallace, *The Band Theory of Graphite*, Phys. Rev. **71**, 622 (1947).

[131] G. W. Semenoff, *Condensed-Matter Simulation of a Three-Dimensional Anomaly*, Phys. Rev. Lett. **53**, 2449 (1984).

[132] K. S. Novoselov, A. K. Geim, S. V. Morozov, D. Jiang, Y. Zhang, S. V. Dubonos, I. V. Grigorieva, and A. A. Firsov , *Electric Field Effect in Atomically Thin Carbon Films*, Science **306**, 666, (2004).

[133] K. S. Novoselov, A. K. Geim, S. V.Morozov, D. Jiang, M. I. Katsnelson, I. V. Grigorieva, S. V. Dubonos & A. A. Firsov, *Two-dimensional gas of massless Dirac fermions in graphene*, Nature **438**, 197 (2005)

[134] K. L. Lee, B. Gremaud, R. Han, B. Englert and C. Miniatura, *Ultracold fermions in a graphene-type optical lattice*, Phys. Rev. A **80**, 043411 (2009).

[135] P. Soltan-Panahi, J. Struck, P. Hauke, A. Bick, W. Plenkers, G. Meineke, C. Becker, P. Windpassinger, M. Lewenstein & K. Sengstock, *Multi-component quantum gases in spin-dependent hexagonal lattices*, Nature Phys. **7**, 434 (2011).

[136] P. Soltan-Panahi, D.-S. Lühmann, J. Struck, P. Windpassinger, & K. Sengstock, *Quantum phase transition to unconventional multi-orbital superfluidity in optical lattices*, Nature Phys. **8**, 71 (2012).

[137] L. Tarruell, D. Greif, T. Uehlinger, G. Jotzu and T. Esslinger, *Creating, moving and merging Dirac points with a Fermi gas in a tunable honeycomb lattice*, Nature **483**, 302 (2012).

[138] J. Li, W. Huang, B. Shteynas, S. Burchesky, F. Çağrı Top, E. Su, J. Lee, A. Jamison, and W. Ketterle, *Spin-Orbit Coupling and Spin Textures in Optical Superlattices*, Phys. Rev. Lett. **117**, 185301 (2016).

[139] R. R. Nair, P. Blake, A. N. Grigorenko, K. S. Novoselov, T. J. Booth, T. Stauber, N. M. R. Peres, A. K. Geim, *Fine Structure Constant Defines Visual Transparency of Graphene*, Science **320**, 1308 (2008).

[140] E. G. Mishchenko, *Minimal conductivity in graphene: Interaction corrections and ultraviolet anomaly*, Europhys. Lett. **83**, 17005 (2008).

[141] D. E. Sheehy, J. Schmalian, *Optical transparency of graphene as determined by the fine-structure constant*, Phys. Rev. B **80**, 193411 (2009).

[142] J. M. Link, P. P. Orth, D. E. Sheehy, and J. Schmalian, *Universal collisionless transport of graphene*, Phys. Rev. B **93**, 235447 (2016).

[143] F. de Juan, M. Sturla and M. A. H. Vozmediano, *Space dependent Fermi velocity in strained graphene*, Phys. Rev. Lett. **108**, 227205 (2012).

[144] A. H. Castro Neto, F. Guinea, N. M. R. Peres, K. S. Novoselov, A.K. Geim, *The electronic properties of graphene*, Rev. Mod. Phys. **81**, 109 (2009).

[145] A. Das, *Lectures on quantum field theory*, World Scientific Publishing Company (2008).

[146] C. W. Misner, K. S. Thorne and J. A. Wheeler, *Gravitation*, Princeton University Press (1972).

[147] R. M. Wald, *General Relativity*, University of Chicago Press (1984).

[148] W. Rindler, *Relativity: Special, general, and cosmological*, Oxford University Press (2006)

[149] W. G. Unruh, *Alternative Fock Quantization of Neutrinos in Flat Space-Time*, Proc. Roy. Soc. Lond. Series A, Mathematical and Physical Sciences **338**, (1974): 517.

[150] P. Candelas and D. Deutsch, *Fermion Fields in Accelerated States*, Proc. Roy. Soc. Lond. A **362**, 251 (1978).

[151] M. Soffel, B. Muller and W. Greiner, *Dirac Particles in Rindler Space*, Phys. Rev. D **22**, 1935 (1980).

[152] R. J. Hughes, *Uniform Acceleration and the Quantum Field Theory Vacuum. 1*, Annals of Phys. **162**, 1 (1985).

[153] B. R. Iyer, *Dirac equation in Kasner spacetime with local rotational symmetry*, Phys. Lett. A **112**, 313 (1985).

[154] R. Jáuregui, M. Torres and S. Hacyan, *Dirac vacuum: Acceleration and external field effects*, Phys. Rev. D **43**, 3979 (1991).

[155] I. S. Gradshteyn, I. M. Ryzhik, Alan Jeffrey, and Daniel Zwillinger, *Table of Integrals, Series, and Products*, Academic Press; 6th edition (2000).

[156] P. M. Alsing, I. Fuentes-Schuller, R. B. Mann and T. E. Tessier, *Entanglement of*

Dirac fields in non-inertial frames, Phys. Rev. A **74**, 032326 (2006).

[157] J. Leon and E. Martin-Martinez, *Spin and occupation number entanglement of Dirac fields for noninertial observers*, Phys. Rev. A **80**, 012314 (2009).

[158] J. Bardeen, L. N. Cooper, and J. R. Schrieffer, *Microscopic Theory of Superconductivity*, Phys. Rev. **106**, 162 (1957).

[159] J. Bardeen, L. N. Cooper, and J. R. Schrieffer, *Theory of Superconductivity*, Phys. Rev. **108**, 1175 (1957).

[160] Leon N. Cooper, *Bound Electron Pairs in a Degenerate Fermi Gas*, Phys. Rev. **104**, 1189 (1956).

[161] B. S. DeWitt, *Quantum gravity: the new synthesis*, in General relativity: an Einstein centenary survey, S.W. Hawking and W. Israel eds., Cambridge University Press, Cambridge U.K. (1979), pg. 680.

[162] Piers Coleman, *Introduction to Many-Body Physics*, Cambridge University Press; 1st edition (February 1, 2016) .

[163] T. Matsubara, *A New approach to quantum statistical mechanics*, Prog. Theor. Phys. **14**, 351 (1955).

[164] L. Boltzmann, *Lectures on gas theory*, Berkeley, CA, USA: U. of California Press, (1964).

[165] R. C. Tolman, *The Principles of Statistical Mechanics*, Oxford University Press, London, UK, (1938).

[166] A. Einstein, Zur Quantentheorie der Strahlung [*On the quantum theory of radiation*], Physikalische Zeitschrift 18 (1917), 121-128. English translation: D. ter Haar (1967): The Old Quantum Theory. Pergamon Press, pp. 167.

[167] J. Rammer and H. Smith, *Quantum field-theoretical methods in transport theory of metals*, Rev. Mod. Phys. **58**, 323 (1986).

[168] R. Courant and D. Hilbert (1962), *Methods of Mathematical Physics*, Interscience Publishers, vol. II .

[169] G. D. Mahan, *Many Particle Physics, Plenum*, New York, (1990).

[170] T. Stauber, N. M. R. Peres, and A. K. Geim, *Optical conductivity of graphene in the visible region of the spectrum*, Phys. Rev. B **78**, 085432 (2008).

[171] L. Parker, *Quantized fields and particle creation in expanding universes. 2*, Phys. Rev. D **3**, 346 (1971).

[172] B. L. Hu and D. Pavon, *Intrinsic Measures of Field Entropy in Cosmological Particle Creation*, Phys. Lett. B **180**, 329 (1986).

[173] B. L. Hu and H. E. Kandrup, *Entropy Generation in Cosmological Particle Creation and Interactions: A Statistical Subdynamics Analysis*, Phys. Rev. D **35**, 1776 (1987).

[174] H. E. Kandrup, *Entropy Generation, Particle Creation, and Quantum Field Theory in a Cosmological Space-time: When Do Number and Entropy Increase?*, Phys. Rev. D **37**, 3505 (1988).

[175] Anderson, M. H., J. R. Ensher, M. R. Matthews, C. E. Wieman and E. A. Cornell, *Observation of Bose-Einstein Condensation in a Dilute Atomic Vapor*, Science 269, 198 (1995).

[176] Davis, K. B., M.-O. Mewes, M. R. Andrews, N. J. van Druten, D. S. Durfee, D. M. Kurn, and W. Ketterle, *Bose-Einstein Condensation in a Gas of Sodium Atoms*, Phys. Rev. Lett. 75, 3969 (1995).

[177] Giorgini, S., Pitaevskii, L. P., Stringari, S., *Theory of ultracold atomic Fermi gases*, Rev. Mod. Phys. 80, 1215 (2008).

[178] Bloch, I., Dalibard, J., Zwerger, W., *Many-body physics with ultracold gases*, Rev. Mod. Phys. 80, 884 (2008).

[179] Ketterle, W., Zwierlein, M. W., *Making, probing and understanding ultracold Fermi gases*, arXiv:0801.2500 [cond-mat.other] (2008).

[180] De Marco, L., Valtolina, G., Matsuda, K., Tobias, W. G., Covey, J. P., Ye, J., *A degenerate Fermi gas of polar molecules*, Science 363, 6429 (2019).

[181] Morsch, O., and M. Oberthaler, *Dynamics of Bose-Einstein condensates in optical lattices*, Rev. Mod. Phys. 78, 179 (2006).

[182] Orso, G., and G. V. Shlyapnikov, *Superfluid Fermi Gas in a 1D Optical Lattice*, Phys. Rev. Lett. 95, 260402 (2005).

[183] Werner, F., O. Parcollet, A. Georges, and S. R. Hassan, *Interaction-Induced Adiabatic Cooling and Antiferromagnetism of Cold Fermions in Optical Lattices*, Phys. Rev. Lett. 95, 056401 (2005).

[184] Gaunt, A. L., Schmidutz, T.F., Gotlibovych, I., Smith, R. P., Hadzibabic, Z., *Bose-Einstein Condensation of Atoms in a Uniform Potential*, Phys. Rev. Lett. 110,

200406 (2013).

[185] Mukherjee, B., Yan, Z., Patel, P.B., Hadzibabic, Z., Yefsah, T., Struck, J., Zwierlein, M.W., *Homogeneous Atomic Fermi Gases*, Phys. Rev. Lett. 118, 123401 (2017).

[186] Hueck, K., Luick, N., Sobirey, L., Siegl, J., Lompe, T., Moritz, H., *Two-Dimensional Homogeneous Fermi Gases*, Phys. Rev. Lett. 120, 060402 (2018).

[187] Fulde, P., Ferrell, R. A., *Superconductivity in a Strong Spin-Exchange Field*, Phys. Rev. 135, A550-A563 (1964).

[188] Larkin, A.I., Ovchinnikov, Yu.N., *Nonuniform state of superconductors*, Sov. Phys. JETP 20, 762-769 (1965).

[189] Sheehy, D.E., Radzihovsky, L., *BEC–BCS crossover, phase transitions and phase separation in polarized resonantly-paired superfluids* Ann. of Phys. 322, 1790 (2007).

[190] Mahan, G. D., *Many-Particle Physics*, (Springer, Boston, MA, 2000).

[191] Ku, M. J. H., Mukherjee, B., Yefsah, T., Zwierlein, M.W., *Cascade of Solitonic Excitations in a Superfluid Fermi gas: From Planar Solitons to Vortex Rings and Lines*, Phys. Rev. Lett. 116, 045304 (2016).

[192] Bruun, G., Castin, Y., Dum, R., Burnett, K., *BCS theory for trapped ultracold fermions*, Eur. Phys. J. D 7, 433-439 (1999).

[193] Fermi, E., Ricerca Sci. 7, 13 (1936).

[194] Huang, K., Yang, C. N., *Quantum-Mechanical Many-Body Problem with Hard-Sphere Interaction*, Phys. Rev. 105, 767 (1957).

[195] Huang, K., *Statistical Mechanics*, (Wiley, New York) 1987

[196] Onnes, H. K., *The Superconductivity of Mercury*, Commun. Phys. Lab. Univ. Leiden 120b (April 1911), reprinted in Proc. K. Ned. Akad. Wet. 13, 1274 (1911).

[197] Meissner, W.; Ochsenfeld, R., *A new effect when superconductivity occurs*, Naturwissenschaften (1933), 21 (44): 787–788.

[198] Kapitza, P., *Viscosity of Liquid Helium below the λ-Point*, Nature 141 74 (1938).

[199] Allen, J.F., Misener, A. D., *Flow of Liquid Helium II*, Nature 141, 75 (1938).

[200] Bose, S. N., (1924), *Planck's law and light quantum hypothesis*, Zeitschrift für Physik. 26 (1): 178–181.

[201] Einstein, A., (1925), *Quantum theory of the monatomic ideal gas*, Sitzungsberichte der Preussischen Akademie der Wissenschaften. 1: 3.

[202] Bardeen, J., Cooper, L. N., Schrieffer, J. R., *Microscopic Theory of Superconductivity*, Physical Review. 106 (1): 162–164 (1957).

[203] Bardeen, J. Cooper, L. N., Schrieffer, J. R., *Theory of Superconductivity*, Physical Review. 108 (5): 1175–1204 (1957).

[204] Marini, M., Pistolesi, F., Strinati, G.C., *Evolution from BCS superconductivity to Bose condensation: analytic results for the crossover in three dimensions*, Eur. Phys. J. 1, 151 (1998).

[205] Radzihovsky, L., Sheehy, D. E., *Imbalanced Feshbach-resonant Fermi gases*, Rep. Prog. Phys. 73 (2010) 076501.

[206] Blatt, J.M., Thompson, C.J., *Shape Resonances in Superconducting Thin Films*, Phys. Rev. Lett. 10, 332 (1963).

[207] Paskin A., Singh, A.D., *Boundary Conditions and Quantum Effects in Thin Superconducting Films*, Phys. Rev. 140, A1965 (1965).

[208] Valentinis, D., van der Marel, D., Berthod, C., *Rise and fall of shape resonances in thin films of BCS superconductors*, Phys. Rev. B 94 054516 (2016).

[209] Simonucci, S., Strinati, G.C., *Equation for the superfluid gap obtained by coarse graining the Bogoliubov–de Gennes equations throughout the BCS-BEC crossover*, Phys. Rev. B 89, 054511 (2014).

[210] Lacroix-A-Chez-Toine, B., Le Doussal, P., Majumdar, S. N., Schehr, G., *Statistics of fermions in a d-dimensional box near a hard wall*, EPL 120 10006 (2017).

[211] Tan, S., *Energetics of a strongly correlated Fermi gas*, Annals of Physics 323 (2008) 2952–2970.

[212] Tan, S., *Large momentum part of a strongly correlated Fermi gas*, Annals of Physics 323 (2008) 2971–2986.

[213] Tan, S., *Generalized virial theorem and pressure relation for a strongly correlated Fermi gas*, Annals of Physics 323 (2008) 2987–2990.

[214] Werner, F., Castin, Y., *General relations for quantum gases in two and three dimensions: Two-component fermions*, Phys. Rev. A 86, 013626 (2012).

[215] Valiente, M., *Tan's distributions and Fermi-Huang pseudopotential in momentum*

space, Phys. Rev. A 85, 014701 (2012).

[216] Stewart, J. T., Gaebler, J. P., Drake, T. E., Jin, D. S., *Tan's distributions and Fermi-Huang pseudopotential in momentum space*, Phys. Rev. Lett. 104, 235301 (2010).

[217] Radzihovsky, L., *Fluctuations and phase transitions in Larkin-Ovchinnikov liquid-crystal states of a population-imbalanced resonant Fermi gas*, Phys. Rev. A 84, 023611.

[218] Wojcik, P., Zegrodnik, M., *Interplay between quantum confinement and Fulde–Ferrell–Larkin–Ovchinnikov phase in superconducting nanofilms*, Physica E 83, 442-449 (2016).

VITA

Anshuman Bhardwaj was born in the year 1991. After attending school in New Delhi, in 2009, he joined the Indian Institute of Technology Roorkee to pursue an Integrated M.Sc. Programme in Physics. He received his Integrated M.Sc. degree on September 20, 2014. He then enrolled in two masters courses at the University of Nottingham. In 2015, he received his M.Sc. in Gravity, Particles and Fields, and in 2017, he received his M. Res. in Physics. Subsequently, he joined Louisiana State University to pursue his doctoral studies in the Condensed Matter Group with Dr. Daniel E. Sheehy as his advisor. He plans to graduate in May 2023, and in June 2023, he will be joining the University of Texas at Dallas as a postdoctoral research associate under the supervision of Dr. Chuanwei Zhang.